



Reactive adsorption of molecules and radicals on surfaces under plasma exposure

Daniil Marinov

► To cite this version:

Daniil Marinov. Reactive adsorption of molecules and radicals on surfaces under plasma exposure. Plasma Physics [physics.plasm-ph]. Ecole Polytechnique X, 2012. English. NNT: . pastel-00752987

HAL Id: pastel-00752987

<https://pastel.hal.science/pastel-00752987>

Submitted on 16 Nov 2012

HAL is a multi-disciplinary open access archive for the deposit and dissemination of scientific research documents, whether they are published or not. The documents may come from teaching and research institutions in France or abroad, or from public or private research centers.

L'archive ouverte pluridisciplinaire **HAL**, est destinée au dépôt et à la diffusion de documents scientifiques de niveau recherche, publiés ou non, émanant des établissements d'enseignement et de recherche français ou étrangers, des laboratoires publics ou privés.

Thèse présentée pour obtenir le grade de
DOCTEUR DE L'ÉCOLE POLYTECHNIQUE

Spécialité :
Physique des Plasmas

Présentée par
Daniil Marinov

Reactive adsorption of Molecules and Radicals on Surfaces under Plasma Exposure

Thèse soutenue le 19 Octobre 2012

Jury composé de :

Gilles Cartry, Rapporteur

MC, PIIM, U Provence

Richard Engeln, Rapporteur

Assistant Professeur, TU Eindhoven

Antoine Rousseau, Directeur

DR, CNRS-LPP, Ecole Polytechnique

Olivier Guaitella, Co-directeur

IR, LPP, Ecole Polytechnique

Achim von Keudell

Professeur, RUB Bochum

Vasco Guerra

Assistant Professeur, IST Lisbon

Khaled Hassouni, President

Professeur, LIMHP, U Paris XIII

Acknowledgements

First of all I would like to thank Antoine Rousseau for giving me the chance to pursue my PhD in France and Olivier Guaitella for co-supervising this thesis. Antoine, Olivier, I thank you for offering me an exciting topic on which I have been working during these three years. I sincerely appreciate your confidence in me, your patience, your availability and continuous encouragement. While working on this thesis I have enjoyed the freedom to test different ideas but I have always felt your support. I would like to thank you for giving me many occasions to present my work at international conferences where I could meet other members of plasma physics community and also discover beautiful places all around the world.

I would like to thank Yuri Ionikh who introduced me to the world of plasma physics and showed me the right direction to follow. I also appreciate his support and valuable advice during my work on the thesis.

I thank Gilles Cartry and Richard Engeln for reporting my thesis and also Vasco Guerra, Achim von Keudell and Khaled Hassouni for their agreement to participate in the jury.

Many of the results presented in this manuscript are obtained in collaboration with people from different laboratories as well as with the members of LPP. I thank Jean-Paul Booth and Nishant Sirse for teaching me the secrets of TALIF. I thank Vasco Guerra for sharing with me his knowledge on kinetic modeling. I thank Achim von Keudell, Carles Corbella and Teresa de los Arcos for XPS measurements which have changed my vision of atomic recombination on surfaces. I thank Juergen Roepke and his group at INP Greifswald for intense and fruitful experimental campaigns with quantum cascade lasers. Special thanks to Marko Huebner and Dmitri Lopatik from INP for long hours spent in the lab and for showing me the hints of measurements with QCLs. I also thank Paul Gravejat for enlightening discussions on the mechanisms of surface processes (but also nganga, and la problematique de la véracité) and for the help with catalytic film deposition.

I thank all the LPP researchers and especially Pascal Chabert, Ane Aanesland and Svetlana Starikovskaya from low temperature plasma team for many informal discussions that have shown me new horizons. Thanks to Jean Guillon, Mickael and Jonathan for technical support of the experiment. I wish to thank Cathy, Elodie, Catherine, Edouard, Olivier, Philippe, Bruno and Nicolas for their help with administrative and IT questions.

Of course, I thank all the PhD students and post-docs who made LPP the most enjoyable place to work in: Jerome, Lara, Christelle, Ilya, Jaime, Andrei, Malik, Sergey, Lorenzo, Pierre-Alexandre, Noureddine, Claudia, Ana, Emilie, Paul, Laurent, Joseph, Sedina, Eugenio, Binjie. In the continuation of this list I wish to thank again Olivier who has been not only my supervisor but also a good friend.

I wish to thank my parents and my sister for their support during all the years of my studies and for making a long trip from Saint-Petersburg to assist at my defense. I warmly

thank my brother Ilya who decided to move to France and do a PhD in plasma physics at the same time as me. That is great that we have been sharing everything! Ilya, thank you for organizing lots of amazing “sorties culturelles” and fantastic trips. And finally, very special thanks to Anna for bringing new bright colors in my (parisian) life and for her support and patience during the writing of this thesis.

Contents

I. Introduction	7
I.1 Plasma-surface interactions: historical overview	7
I.2 Context of the study	8
I.3 Organization of the thesis	9
1. Chapter I: Surface reactivity in N₂/O₂ plasmas	11
1.1 Interaction of radicals with surfaces: basic concepts	11
1.1.1 Adsorption	11
1.1.1.1 Physisorption	12
1.1.1.2 Chemisorption	13
1.1.2 Mechanisms of surface reactions	14
1.1.3 Surface reactions: thermodynamic viewpoint	15
1.2 Modelling of surface reactivity in plasmas	16
1.3 Mesoscopic modelling of atomic recombination on surfaces	17
1.3.1 Surface kinetics in N ₂ /O ₂ mixtures	20
1.3.2 Role of plasma exposure	20
1.4 Surface reactions in N ₂ /O ₂ plasmas: review of experimental studies	21
1.4.1 Recombination of O and N atoms on surfaces	21
1.4.2 Molecule production/conversion on surfaces	22
1.5 Research questions	23
1.6 Research strategy	24
1.7 Definitions and notations	25
2. Chapter II: Experimental setup and diagnostic techniques	27
2.1 Discharge setup	27
2.1.1 Reactor and gas system	27
2.1.2 Pulsed discharge systems	28
2.1.2.1 Direct current glow discharge	28
2.1.2.2 Radiofrequency capacitive discharge	30
2.2 Diagnostics employed	31
2.2.1 Tuneable diode laser absorption spectroscopy in mid-infrared range	31
2.2.1.1 Principles of laser absorption spectroscopy	31
2.2.1.2 Advantages of laser absorption measurements	32

Contents

2.2.1.3	<i>Pitfalls of laser absorption measurements</i>	32
2.2.1.4	<i>Diode laser spectrometer</i>	33
2.2.1.5	<i>Three-channel quantum cascade laser spectrometer</i>	35
2.2.2	Time resolved emission and absorption spectroscopy in UV-Vis range.	38
2.2.2.1	<i>Optical emission spectroscopy for gas temperature determination</i>	39
2.2.2.2	<i>OES setup and data treatment</i>	40
2.2.2.3	<i>Time resolved measurements of ozone concentration</i>	42
2.2.3	TALIF measurements of atomic oxygen.	43
2.2.3.1	<i>Principles and calibration of O TALIF measurements</i>	43
2.2.3.2	<i>Laser setup</i>	44
2.2.4	Mass spectrometric gas analysis	46
2.2.5	XPS surface diagnostics	47
2.2.6	Summary on used diagnostics	48
3.	Chapter III: Adsorption and reactivity of N atoms on silica surface under plasma exposure	49
3.1	Introduction	49
3.1.1	Experimental procedures	49
3.2	Determination of the coverage of N_{ads} : XPS study	51
3.2.1	Dynamics of N adsorption on SiO_2	51
3.2.2	Species responsible for nitridation: ions or neutrals?	54
3.2.3	Reactivity of SiO_xN_y under plasma exposure	54
3.2.4	Conclusions on XPS study	56
3.3	Reactivity of N_{ads} : Isotopic study	57
3.3.1	Experimental details	57
3.3.2	Characterization of the discharge: measurements of N_2 dissociation degree... 59	
3.3.2.1	<i>Dissociation of N_2 in pulsed dc discharge</i>	59
3.3.2.2	<i>Dissociation in pulsed rf discharge</i>	62
3.3.2.3	<i>Estimation of atomic nitrogen exposure on the surface</i>	63
3.3.3	^{14}N adsorption on SiO_2 under $^{28}N_2$ plasma exposure	64
3.3.4	Reactivity of grafted ^{14}N atoms under $^{30}N_2$ plasma exposure	67
3.3.4.1	<i>Evidence for a distribution of reactivity of N_{ads}</i>	67
3.3.4.2	<i>Do N_{ads} participate in surface recombination of N atoms?</i>	69
3.3.5	Conclusions on the isotopic study	71

3.4	Recombination of N_{ads} with O atoms.....	71
3.4.1	Experimental details.....	71
3.4.2	Kinetics of NO production on the surface.....	73
3.4.2.1	<i>Proof of recombination mechanism $N_{ads} + O \rightarrow NO$</i>	73
3.4.2.2	<i>Kinetics of NOx in the probe discharge</i>	74
3.4.2.3	<i>Estimation of the coverage of N_{ads} that produce NO</i>	75
3.4.2.4	<i>NO production on the surface under continuous O_2 plasma exposure</i>	77
3.4.3	Investigation of adsorption and reactivity of N using measurements of NO production on the surface.....	78
3.4.3.1	<i>Kinetics of adsorption</i>	78
3.4.3.2	<i>Are N_{ads}^* active for recombination of N on the surface?</i>	80
3.5	Discussion and conclusions	82
3.5.1	Summary and conclusions on used diagnostics	85
4.	Chapter IV: Adsorption and reactivity of oxygen atoms on oxide surfaces under plasma exposure.....	87
4.1	Introduction.....	87
4.1.1	Experimental procedures.....	88
4.2	Chemisorption of O on silica-like surfaces: isotopic study	88
4.2.1	Experimental details.....	88
4.2.2	Do O atoms of the material participate in surface reactivity?.....	90
4.2.3	^{16}O adsorption on the surface under $^{32}O_2$ plasma exposure	92
4.2.4	Conclusions on the isotopic study	94
4.3	Adsorption of atomic oxygen on Pyrex and related reactivity towards NO... 94	
4.3.1	Experimental details.....	95
4.3.2	Evidence of NO oxidation by adsorbed O atoms.....	96
4.3.3	Determination of the surface coverage of adsorbed O atoms	97
4.3.4	Evidence of a distribution of reactivity adsorbed O atoms	98
4.3.5	Conclusions on the study of O_{ads} reactivity on Pyrex	99
4.4	On the role of O_{ads} for VOC oxidation.....	99
4.4.1	Context of the study: influence of the chemical nature of the surface on the reactivity of O_{ads}	100
4.4.2	C_2H_2 oxidation by adsorbed oxygen atoms on TiO_2	101
4.4.2.1	<i>Experimental details</i>	101
4.4.2.2	<i>Kinetics of C_2H_2 destruction on pretreated TiO_2 surface</i>	102

Contents

4.4.2.3	<i>Oxidation of adsorbed reaction intermediates</i>	103
4.4.3	Discussion and conclusions on the study of O_{ads} reactivity on TiO_2	105
4.5	Investigation of ozone formation on surfaces.....	106
4.5.1	Experimental details.....	107
4.5.2	Ozone production in bare silica tube.....	107
4.5.3	Ozone production in the presence of high specific surface material.....	111
4.5.3.1	<i>Influence of gas pressure and surface pretreatment</i>	113
4.5.4	Modelling of ozone production in bare silica tube.....	114
4.5.5	Conclusions on the ozone production study.....	117
4.6	Conclusions.....	118
5.	Chapter V: Study of surface vibrational relaxation of N_2	121
5.1	Introduction.....	121
5.2	Kinetics of vibrationally excited nitrogen	121
5.2.1	Role played by $N_2(v)$ in nitrogen containing plasmas.....	121
5.2.2	Electron impact excitation/de-excitation of $N_2(v)$	122
5.2.3	Vibrational relaxation of $N_2(v)$ in the gas phase	124
5.2.4	Vibrational relaxation on surfaces: motivation of the study	125
5.3	Study of $N_2(v)$ relaxation using infrared titration	127
5.3.1	Principles of the infrared titration technique.....	127
5.3.2	Experimental procedure	127
5.3.3	Validity of the diagnostics.....	128
5.3.3.1	<i>Gas temperature and its influence on the relaxation measurements</i>	130
5.3.3.2	<i>Dissociation and re-association of titrating molecules</i>	131
5.3.3.3	<i>Vibrational excitation of titrating molecules</i>	132
5.4	Modeling of vibrational kinetics in N_2 - CO_2	133
5.4.1	Relevant relaxation processes	133
5.4.2	Model description.....	135
5.4.2.1	<i>Gas phase processes</i>	135
5.4.2.2	<i>Heterogeneous processes</i>	136
5.4.2.3	<i>Numerical solution</i>	137
5.4.3	Validation of the model.....	137
5.4.4	On the possibility of experimental determination of γ_{N_2} dependence on v	138
5.4.5	Modeling results in $N_2 - CO_2$ mixtures.....	140

5.4.6	Determination of γ_{N_2} for silica. The influence of CO_2 admixture.....	142
5.4.7	Conclusions on the study of the $N_2 - CO_2$ system	145
5.4.8	Data analysis using characteristic relaxation times.....	145
5.5	Application of the IR titration for γ_{N_2} determination on catalytic and plasma-pretreated surfaces	149
5.5.1	The effect of plasma pretreatment.....	149
5.5.2	Vibrational relaxation on TiO_2	152
5.5.3	Vibrational relaxation on other catalytic surfaces.....	154
5.5.4	Vibrational relaxation on silica surface in air plasma.....	155
5.6	Infrared titration as a plasma diagnostics tool: determination of the vibrational temperature of N_2	155
5.6.1	Formulation of the method and its application to the $N_2 - CO_2$ system	155
5.6.2	On the vibrational temperature measurements in $N_2 - N_2O$ and $N_2 - CO$	156
5.7	Conclusions.....	158
6.	Chapter VI: General conclusions and outlook	161
6.1	General conclusions	161
6.2	Summary of the main results	162
6.3	Implication for modelling of surface recombination	163
6.4	Future work.....	164
6.5	New diagnostic techniques	166
7.	References	167

I. Introduction

I.1 Plasma-surface interactions: historical overview

The word plasma was introduced in 1928 by Irving Langmuir [1] who was struck by the analogy between blood plasma that transports red and white corpuscles and a discharge column acting as a sub-stratum carrying molecules, ions and electrons. It is interesting to note that Langmuir got the Nobel Prize in Chemistry in 1932 for his achievements in surface science. Langmuir clarified the true nature of surface adsorption and established the existence of monolayers as two-dimensional structures on the surface. Therefore, it wouldn't be exaggerating to say that both plasma science and surface science as we know them today were started by the same person almost a century ago.

The importance of surface catalyzed processes in reactive plasmas has been recognized since the early 1920s. Low pressure glow discharges in glass tubes were used in those times as a source of molecular and atomic spectra. In 1920 Wood made an observation of recombination of atomic hydrogen on glass surface in his study of Balmer series in a long discharge tube [2]. In the following, recombination of atomic hydrogen on different catalytic surfaces in a broad temperature range was thoroughly studied and the first models describing the recombination process were proposed [3,4] by the end of 1940s.

Following the advent of numerous techniques for detection of atomic species (catalytic probes, mass-spectrometry, optical emission spectroscopy, electron paramagnetic resonance), the number of studies of the surface catalyzed recombination of atoms has rapidly increased in 1950 – 1960s ([5] and references therein). In those times interaction between radicals and catalytic surfaces was investigated by the catalysis community and many ideas coming from classical heterogeneous catalysis with stable molecules were adopted in order to explain reaction mechanisms. In the majority of works, recombination of atoms was studied in flow-tube experiments in the post-discharge zone. Thus, plasma was used only as a source of radicals and there was no direct interaction between the plasma and the studied surface.

Plasma-surface interactions became an expanding field of research in 1970s when the potential of plasmas for material processing was realized. Unique properties of etching reactive plasmas used for microelectronics applications were investigated in details. In the classical work [6] a synergetic effect between Ar^+ ions and reactive XeF_2 molecules for poly-Si etching was discovered in beam experiments. It was found that when Si surface is exposed to both Ar^+ and XeF_2 the etch rate is not simply a sum of the etch rates obtained under ion bombardment or neutral gas flow but increases by an order of magnitude. Later on, synergetic effects between charged and neutral species were observed in the process of film growth in low temperature plasmas [7]. Therefore, it was finally realized that the unique property of reactive plasmas is that they produce at once flows of radicals, excited species and ions on the surface.

Introduction

Today study of plasma-surface interactions is a growing field of research which is driven by a great number of applications. Plasma processing of surfaces is widely used for microelectronics, material science, thin films and coatings. Plasma surface interactions play a key role in nuclear fusion, atmospheric re-entry and plasma medicine.

In the space, reactions of radicals and formation of molecules on solid surfaces is one of the most important problematic of astrochemistry. In the interstellar medium reactions between gas phase species are very rare and the chemistry takes place on the surface of dust particles.

Regardless a long lasting history of research on surface processes in reactive molecular plasmas this field is still barely studied and poorly understood, especially compared to the present knowledge of the mechanisms of gas phase reactions. Surface is still the “terra incognita” for plasma science. This can be clearly observed in the kinetic modelling of low pressure discharges. State of the art discharge models include dozens of gas phase reactions between stable and excited species taking into account individual electronic and vibrational levels. However, surface processes are often introduced using effective reaction coefficients that are not known *a-priori* and used as tuning parameters. These adjustable parameters reduce the accuracy and predictive capability of the models. Therefore, there is a real need for a deeper understanding of mechanisms of surface processes in reactive plasmas.

I.2 Context of the study

One of the promising applications of low temperature plasmas is the destruction of air pollutants. High reactivity and low gas temperature of non-equilibrium plasmas are very attractive for low energy cost oxidation of volatile organic compounds (COV). A combination of low temperature plasmas with heterogeneous catalyst was proposed in 1990s in order to improve the efficiency and selectivity of pollutant destruction [8][9][10][11][12].

The research activity on plasma-catalyst coupling for VOC abatement has started at the Laboratory of Plasma Physics in the beginning of 2000s with the PhD works of Olivier Guaitella, Frederic Thevenet and Lina Gatilova. It was shown that introduction of a porous catalytic material (SiO_2 or TiO_2) in atmospheric pressure dielectric barrier discharge (DBD) increases the efficiency of oxidation of C_2H_2 (which was selected as a model pollutant). Improvement of CO_2/CO selectivity was also observed. Increase of the lifetime of atomic oxygen due to its stabilization on the surface of the catalyst was proposed as an explanation of observed synergetic effects. However, the mechanisms of plasma-catalyst interaction in DBDs are very difficult to study due the complexity of the discharge phenomena at atmospheric pressure.

The originality of the approach developed at LPP consisted in the utilization of a low pressure (~ 1 mbar) dc discharge for investigation of elementary processes on the surface of real catalytic materials that were previously studied in atmospheric pressure DBDs. The use of pulsed dc discharge allowed much better control over the plasma parameters and various in-situ and time resolved diagnostics were applied. Similar synergetic effects in C_2H_2 destruction by plasma-catalyst combination were observed at low pressures [13]. In parallel the

elementary kinetics of air plasmas at mbar pressures was studied. Production of O atoms, NO and NO₂ molecules, and electronically excited species N₂(B³Π, C³Π) was measured and modelled in [14][15][16].

This effort resulted in quite a complete understanding of the gas phase kinetics in pulsed dc discharge in air and air/C₂H₂ mixtures. However, surface processes were still barely understood although it was shown that they play a very important role in low pressure conditions. How radicals are lost and molecules are formed and how vibrational energy is relaxed on surfaces under plasma exposure remained unclear even for such simple non-catalytic reactor wall materials as silica or Pyrex, to say nothing about real high specific surface catalysts.

Understanding of surface processes in N₂/O₂ containing plasmas at mbar pressures was therefore the aim of my thesis. The interest of this work is more general than just air pollution control. The research questions that will be addressed are relevant to any application where N₂/O₂ plasmas meet the surface.

Plasmas containing N₂ and O₂ play an important role for a great number of applications. Many of these applications rely on the processes that take place on surfaces in contact with the plasma. In addition to air pollution control mentioned above we can name nitridation [17], deposition of thin films [18], treatment of polymers [19], and thermal protection on re-usable space vehicles [20]. In some cases plasma-surface interactions are inevitable; they arise from the presence of reactor walls and influence the kinetics of the plasma. This is the case of atomic sources [21] as well as any type of low pressure plasmas in N₂/O₂ mixtures [22].

I.3 Organization of the thesis

In Chapter 1 of this thesis we give an outlook on the present understanding of reaction mechanisms of radicals on surfaces. Theoretical and experimental approaches to the study of surface reactions in N₂/O₂ containing plasmas are reviewed. The open questions concerning the role of chemisorbed atoms in surface catalyzed processes are outlined. Finally, we formulate our objectives and research strategy. We propose the approach which consists in the pretreatment of the surface by N₂ or O₂ plasma followed by probing of the coverage and reactivity of adsorbed atoms.

In Chapter 2 the experimental setup and the used diagnostics are presented.

In Chapter 3 we investigate adsorption and reactivity of N atoms on silica surface under N₂ plasma exposure. We apply surface diagnostics such as XPS in order to determine the coverage of adsorbed N atoms and follow the modification of the chemical composition of the surface by plasma. Production of N₂ and NO molecules on the surface catalysed by adsorbed nitrogen atoms is studied by mass spectrometry and laser absorption spectroscopy in order to get insight in the reactivity of N_{ads}. Different methods of titration of N_{ads} are compared.

In Chapter 4 we study adsorption and reactivity of oxygen atoms on oxide surfaces (silica, Pyrex, TiO₂) under O₂ plasma exposure. Reactivity of adsorbed O towards stable molecules

Introduction

(NO, C₂H₂) and radicals (¹⁸O) is investigated using laser absorption spectroscopy and mass spectrometry. In order to get insight into the reactivity of weakly bonded oxygen atoms, we study ozone production from recombination (O+O₂)_{wall} on silica surface.

In Chapter 5 we study relaxation of vibrationally excited nitrogen molecules on the surface using a new infra red (IR) titration technique. A short dc discharge pulse is used to excite a mixture containing a small amount of CO₂, N₂O or CO in N₂. Due to a very efficient vibrational energy transfer between N₂ and IR tracers, their vibrational excitation is an image of the vibrational excitation of N₂. In the afterglow, the vibrational relaxation of titrating molecules is monitored *in-situ* using quantum cascade laser absorption spectroscopy (QCLAS). Relaxation measurements have been interpreted in terms of a numerical model of non-equilibrium vibrational kinetics. Probability of N₂ vibrational quantum loss (γ_{N_2}) on the surface has been determined from the best agreement between the experiment and the model.

1. Chapter I: Surface reactivity in N_2/O_2 plasmas

1.1 Interaction of radicals with surfaces: basic concepts

Interaction between gas phase species and surfaces is a general problem that has been studied with relation to a number of applications ranging from supersonic flights to heterogeneous catalysis. Today, the global picture of gas-surface interactions is well established and can be found in textbooks [23]. In this section we introduce the basic concepts required for description of surface reactions of radicals. One particular case, which is central for our study – interaction of O and N atoms with silica like surfaces is considered as an example.

1.1.1 Adsorption

What happens when gas phase atoms arrive on a surface? The first step is the adsorption, i.e. formation of a bond between atoms and the surface. Depending on the nature of this bond, two cases are distinguished – *physical* and *chemical* adsorption, schematically these cases are represented in Figure 1. 1.

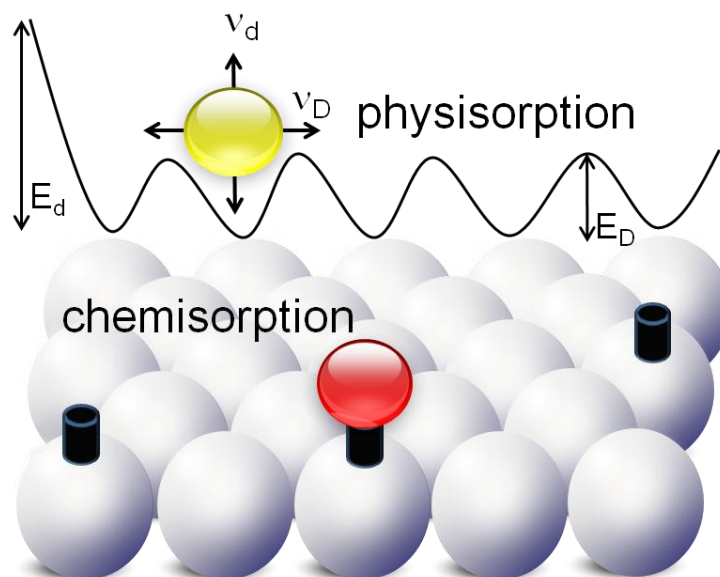


Figure 1. 1 Schematic representation of physisorption and chemisorption of atoms on the surface.

Surface reactivity in N₂/O₂ plasmas

1.1.1.1 Physisorption

Physisorption is a result of the Van der Waals interaction between gas phase species and the surface. Van der Waals forces originate from the attraction between induced electric dipoles and therefore physical adsorption is a collective effect of interaction between impinging species and atoms of the surface. Figure 1. 1 shows schematically the potential energy of this interaction which is modulated following the position of surface atoms. These periodic potential wells are called physisorption sites. The depth of the potential wells in the direction perpendicular to the surface is the energy of desorption; typically it is found in the range $E_d \sim 0.01 - 0.2$ eV per particle [23]. Apart from being desorbed, physisorbed species may also move (diffuse) in the direction parallel to the surface. The energy barrier that atoms need to overcome in order to hop between neighbouring physisorption sites is obviously smaller than the energy of desorption.

In order to describe physisorption of atoms on silica-like surfaces several parameters have to be considered:

- **The surface density of physisorption sites [F].** The value of [F] coincides with the number of atoms on the surface (typically $\sim 10^{15} \text{ cm}^{-2}$). It is usually supposed in the models that all the physisorption sites are identical, i.e. the surface is homogeneous.
- **The fractional coverage of physisorption sites θ_F .** This parameter is simply the ratio of the number of occupied physisorption sites to the total number of physisorption sites.
- **The energies of desorption E_d and diffusion E_D .** These parameters represent the depths of potential wells in the direction perpendicular (E_d) and parallel (E_D) to the surface. Typically, in the models $E_d \sim 0.5$ eV [5]. The activation energy for diffusion E_D is supposed to be a fraction of the activation energy for desorption E_d , according to [24] on glass surfaces $E_D/E_d \sim 0.5$.
- **The characteristic frequencies of desorption (ν_d) and diffusion (ν_D).** For illustration purposes, one can imagine that physisorbed atoms oscillate in the potential wells. The frequency of these oscillations in perpendicular (ν_d) and parallel (ν_D) directions is the frequency at which an atom attempts to leave the surface or hop on the neighbouring physisorption site. The characteristic residence time of an atom on a physisorption site with respect to desorption (τ_d) and surface diffusion (τ_D) can be written as follows [25]:

$$\tau_{d(D)} = 1/\nu_{d(D)} \exp(E_{d(D)}/kT_{wall}) \quad (1. 1)$$

Typically, for atoms adsorbed on silica-like materials $\nu_d \sim 10^{15} \text{ s}^{-1}$ and $\nu_D \sim 10^{13} \text{ s}^{-1}$ [5]. In (1. 1) the dependence of the characteristic times on T_{wall} is exponential. Therefore, the temperature of the surface is a very important parameter for processes involving physisorbed atoms.

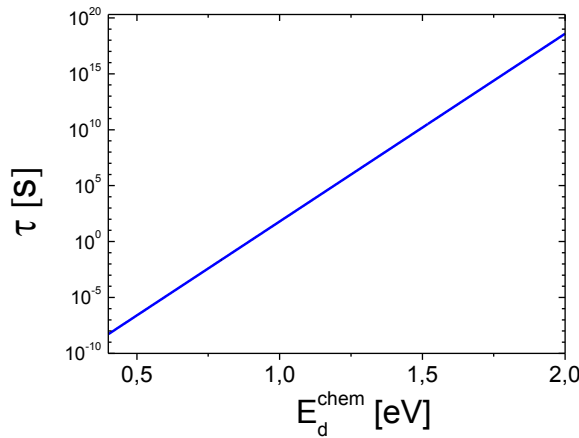
- **Sticking coefficient s .** This parameter accounts for the probability of an atom to be physisorbed in a single collision with the surface. The value of s depends on the surface coverage, $s = s_0(1 - \theta_F)$ where s_0 is the sticking coefficient on clean surface. Usually, in the models of surface atomic recombination it is supposed that $s_0 = 1$. However, as mentioned in [26] this assumption may break down when the kinetic energy of impinging species is increased.

1.1.1.2 Chemisorption

Oxygen and nitrogen atoms have unpaired electrons and therefore they may efficiently form a chemical bond (ionic or covalent) with the surface. In contrast to physisorption, formation of this chemical bond is possible only on specific places on the surface which are called chemisorption sites. The binding energy in the case of chemisorption is typically found in the range $E_d^{chem} \sim 0.4 - 8$ eV [23] per particle.

Are chemisorbed atoms necessarily stable?

Generally speaking, words “chemisorbed” and “stable” shouldn’t be used as synonyms. The lifetime of chemisorbed species can be calculated using (1. 1); result of calculation with a typical value of $\nu_d \sim 10^{15} \text{ s}^{-1}$ [25] at room temperature is shown in the graph:



One can see that for E_d^{chem} in the range 0.4 – 2 eV the value of τ changes over 25 orders of magnitude. Species with $E_d^{chem} \leq 1$ eV have the lifetime on the surface of the order of 1 minute and less; therefore, they can’t be considered as absolutely stable. In order to be able speak about the stability of adsorbed species, their lifetime on the surface should be compared with other characteristic times in the system.

Parameters required for description of chemisorption on silica-like surfaces are similar to those considered above for the case of physisorption:

Surface reactivity in N₂/O₂ plasmas

- **The surface density of chemisorption sites [S].** The density of chemisorption sites [S] is always smaller than the density of physisorption sites [F]. For silica-like surfaces, the literature values of [S]/[F] are scattered in the range $10^{-3} - 10^{-1}$ [5] [22] [26] [27][28]. One of the reasons of such a big uncertainty is rather fundamental – in fact, the nature of chemisorption sites is not yet clear. It is believed that chemisorption sites are associated with non-saturated Si atoms, impurities and surface defects. But to the best of our knowledge the density of chemisorption sites has never been measured directly. As in the case of physisorption, in the models all the chemisorption sites are supposed to be identical and homogeneously distributed on the surface.
- **The fractional coverage of chemisorption sites θ_s .** This is the ratio of the number of occupied chemisorption sites to the total number of chemisorption sites.
- **The energy of desorption E_d^{chem} .** As the nature of chemisorption sites on silica-like surfaces is not well understood, the value of E_d^{chem} is generally an unknown parameter. In the models, chemisorbed atoms are supposed to be irreversibly trapped by surface sites. In [5] the value $E_d^{chem} \sim 3$ eV was found for both O and N chemisorbed on fused silica. Due to this high desorption energy, thermal desorption and diffusion of chemisorbed atoms is discarded in the models when surface temperature is not too high.
- **Activation energy for chemisorption.** Usually it is supposed that adsorption of atoms on vacant chemisorption sites proceeds with zero activation energy, i.e. there is no potential barrier for chemisorption.

1.1.2 Mechanisms of surface reactions

As we have seen above, chemisorbed atoms are trapped by active sites, while physisorbed species may diffuse along the surface. Due to the existence of these mobile species there exist two mechanisms of surface processes: i) Eley-Rideal (E-R) according to which reaction takes place in a direct impact between gas phase species and adsorbed species ii) Langmuir-Hinshelwood (L-H) that proceeds via diffusion on the surface. Schematically, E-R and L-H mechanisms are shown in Figure 1. 2. Occupation of free adsorption sites, recombination of atoms and chemical reactions on the surface may proceed according to one of these two mechanisms. Surface diffusion and L-H reactions become pronounced at lower temperatures when physisorbed species spend more time on the surface. At higher temperatures direct E-R mechanism is dominating.

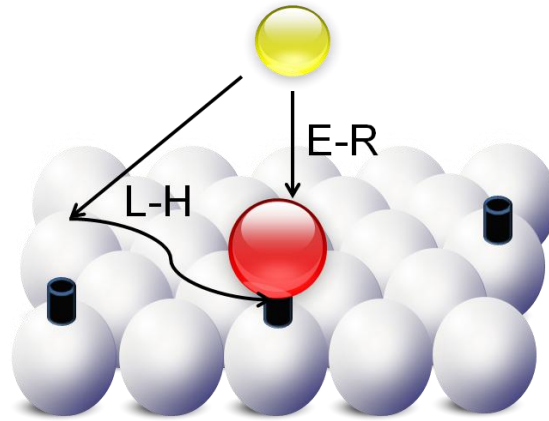


Figure 1. 2 Schematics of Langmuir-Hinshelwood and Eley-Rideal mechanisms.

An important parameter for description of atomic recombination on surfaces is **the activation energy of recombination** E_{rec} . Recombination of atoms A on the surface



where S states for a chemisorption site is similar to the chemical reaction $BC + D \rightarrow B + CD$. According to [29], if this exchange reaction is exothermic, its activation energy can be estimated as $0.055D(B-C)$ where $D(B-C)$ is the bond strength in the molecule BC.

Nitrogen and oxygen atoms chemisorbed on silica-like surfaces are strongly bound with the bond energy E_d^{chem} of few electron volts. Therefore, the recombination process should have the energy barrier of the order of $E_{rec} \sim 0.2$ eV [5]. It is supposed in the models that E_{rec} is the same for both L-H and E-R recombination mechanisms. The value of E_{rec} determines the temperature dependence of the reaction rate of (1. 2):

$$k = k^0 \exp(-E_{rec}/kT_{wall}) \quad (1. 3)$$

where k^0 is a so-called steric factor.

1.1.3 Surface reactions: thermodynamic viewpoint

As any other type of chemical reactions, reactions on the surface in equilibrium conditions are determined by the laws of thermodynamics. According to the classical thermodynamics, at constant temperature and pressure spontaneous chemical reactions proceed with a reduction of Gibbs free energy ($\Delta G < 0$), where $G = H - TS$ (H – enthalpy, S – entropy and T – temperature of the system). Following this general rule, let us consider a recombination reaction between adsorbed species A_{ads} and species B coming from the gas phase. Product AB is supposed to leave the surface. As an example of such reaction one may consider recombination of atoms ($O+O_{ads}$, $O+N_{ads}$, $N+N_{ads}$) or production of molecules on the surface ($NO+O_{ads}$, O_2+O_{ads}). Reaction $A_{ads} + B \rightarrow AB$ will be thermodynamically favourable if

Surface reactivity in N₂/O₂ plasmas

$$\Delta G = (H_{AB} - H_A - H_B) - T(S_{AB} - S_A - S_B) < 0 \quad (1.4)$$

Condition (1. 4) signifies that depending on the nature of the reaction partner B different species A_{ads} may be potentially involved. Let's consider for example two recombination reactions: (i) O+O_{ads}→O₂ and (ii) O₂+O_{ads}→O₃. Standard enthalpies of formation and absolute entropies of reacting species are listed in Table 1. 1 [30].

	ΔH_f (kJ/mol)	S^0 (kJ/mol·K)
O	249	0.161
O ₂	0	0.205
O ₃	142,7	0.239

Table 1. 1 Thermodynamic data for O, O₂ and O₃ [30].

For reaction (i) calculation using (1. 4) at 300 K yields $\Delta G = H_{Oads} - 498 \text{ kJ/mol} - 300 \cdot (0.44 \text{ kJ/(mol K)} - S_{Oads})$ and for reaction (ii) $\Delta G = H_{Oads} - 106 \text{ kJ/mol} - 300 \cdot (0.44 \text{ kJ/(mol K)} - S_{Oads})$, where H_{Oads} is the heat of adsorption of O. The value of S_{Oads} is not known, typically in condensed phase absolute entropy is found in the range 0.02 – 0.1 kJ/(mol K). Therefore, the maximum uncertainty related to the entropy term is rather small, only of the order of $\pm 10 \text{ kJ/mol}$ (or $\pm 0.1 \text{ eV}$). The physical meaning of the condition $\Delta G < 0$ in this case is very simple – the adsorption energy of O_{ads} at the surface should be smaller than the bond energy of O in the product molecules. For (i) this means that $E_d^{chem}(\text{O}_{ads}) < D(\text{O}_2) \approx 5 \text{ eV}$ and for (ii) $E_d^{chem}(\text{O}_{ads}) < D(\text{O}_3) \approx 1 \text{ eV}$.

This example demonstrates that the binding energy of adsorbed species is the key parameter that determines surface reactivity.

1.2 Modelling of surface reactivity in plasmas

Processes introduced in the previous section play a role of elementary steps in surface reactions. What we call a **mechanism** of surface reaction is in fact a sequence of elementary steps by which products are formed. From the theoretical viewpoint we can distinguish three levels of description of surface reactions in reactive plasmas.

- “*Macroscopic*” level. The elementary reaction mechanisms in this case are ignored and surface reactions are characterized using effective probabilities (γ). An example of this approach can be found in [31][32][33]. Values of γ and their dependencies on the conditions are usually unknown and they are adjusted in order to reach the best agreement with the experiment. From a perspective of plasma modelling the predictive power of this approach is very limited.

- *Mesosopic level.* In this case the kinetics of surface reactions is described in terms of the fractional coverage of active sites governed by a set of differential equations. Elementary processes on the surface (adsorption, desorption, diffusion, recombination) are supposed to occur with defined rates. A great number of mesoscopic models was developed in the past in order to explain recombination of atoms in low pressure plasmas and afterglows [5][22][26][27][28] and in the conditions relevant to the atmospheric re-entry [34][35][36]. Mesoscopic description may be considered on a more microscopic scale by using Monte-Carlo technique as it was done in [37]. Monte-Carlo methods allow inclusion of the effects of local interactions between adsorbed species.
- *Simulation on the atomic level.* This approach gives a complete picture of surface reactivity from the first principles without introduction of any empirical parameters. It has been developed over the past 10 years in [35][38][39][40] for description of O and N atoms recombination on SiO₂ surfaces. *Ab-initio* modelling of surface recombination is split in two parts. First, using density functional theory (DFT) computation the electronic structure of the crystalline solid interacting with incoming gas phase species is calculated. This gives a gas-surface interaction potential and a spectrum of lattice phonons that are used for semi-classical molecular dynamics simulation of the recombination process. In addition to calculation of recombination probability, ab-initio calculations provide information about energy accommodation between recombining species and the surface. Although this approach is very promising, so far it has been applied only to adsorption and recombination of atoms on model SiO₂ clusters composed of less than 100 atoms. Extrapolation to real conditions is not straightforward due to the complexity of real disordered surfaces containing various defects and impurities. Effects of plasma exposure is yet another complication in real systems.

We conclude that at present mesoscopic approach presents the most useful and reliable way to describe and predict surface reactivity in plasmas.

1.3 Mesoscopic modelling of atomic recombination on surfaces

We have described a number of elementary processes that come into play when atoms interact with surfaces. The overall result of this interaction that is observable in the experiment is the loss of gas phase atoms which can be characterized by the **recombination probability** γ . By definition γ is the probability that impinging gas phase atoms A will recombine on the surface with the formation of volatile molecular species A₂. It shouldn't be mixed with the effective loss probability β that takes into account all the processes leading to losses of atoms on the surface (adsorption and recombination). Values of γ for N and O atoms on silica-like surfaces have been intensively measured experimentally. The aim of the modelling is to reproduce experimental results based on the defined set of elementary processes.

Surface reactivity in N₂/O₂ plasmas

Here we will sum up the main results of the models of atomic recombination on silica-like surfaces developed in [5][26][27][28]. In these models only recombination in the post-discharge is described.

- When the surface is exposed to a flux of atoms, chemisorption sites become almost fully occupied, i.e. $\theta_s \approx 1$. This is explained by the fact that chemisorbed atoms leave the surface only via recombination which is a thermally activated process. Population of chemisorption sites is faster (it has no energy barrier) and it compensates losses of chemisorbed atoms.
- Surface recombination takes place between chemisorbed atoms and impinging gas phase atoms (E-R) or diffusing physisorbed atoms (L-H). Recombination between two physisorbed atoms is usually discarded because of a low fractional coverage of physisorption sites. This result breaks down and requires special treatment at very low surface temperatures as it is mentioned in [26].

The exact values of the parameters of elementary surface processes ($[S]$, E_d , E_D , E_{rec} , ν_d , ν_D , steric factors for chemisorption and recombination) are not known *a-priori*. With an appropriate adjustment of these parameters measured in the experiment, temperature dependence of γ may be reasonably well reproduced by models. For example, variation of the recombination probability γ_O of atomic oxygen on pyrex as a function $1000/T_{wall}$ measured and modelled in [28] is shown in Figure 1. 3. One can see that γ exhibits a complex non-monotonous temperature dependence. Similar results were obtained in [5] for O and N recombination on silica. The high-temperature branch of the γ_O dependence on SiO₂ was studied in [34][35] in conditions relevant to the atmospheric re-entry.

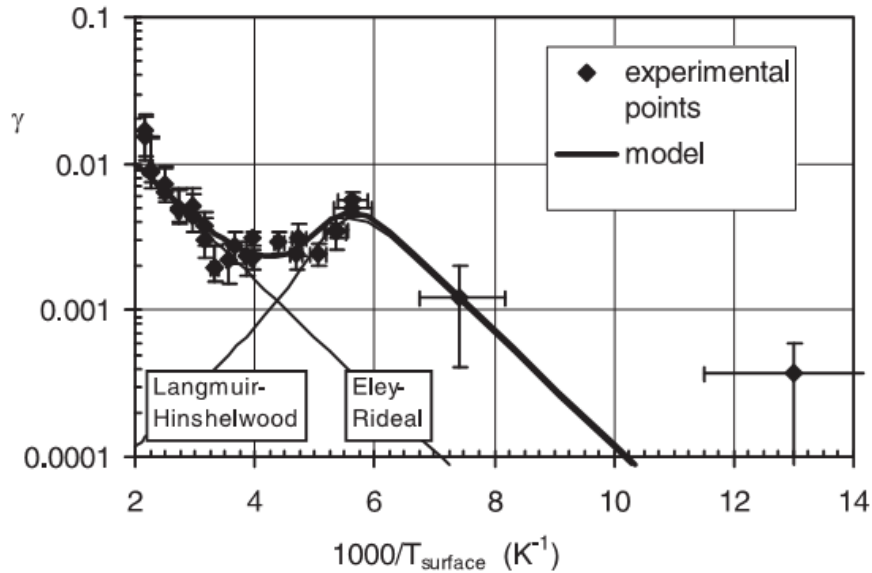


Figure 1. 3 Measured and modelled in [28] recombination probability of O atoms on pyrex at different surface temperatures.

Three characteristic temperature regions were distinguished in [28]:

- High temperatures ($T_{wall} > 330$ K): desorption of atoms from physisorption sites is faster than surface diffusion. Only E-R mechanism is efficient. The slope of the dependence of γ versus $1000/T_{wall}$ is determined by the activation energy of E-R recombination.
- Intermediate temperatures ($160 \text{ K} < T_{wall} < 330 \text{ K}$) where both E-R and L-H mechanisms have comparable efficiency.
- Low temperatures ($T_{wall} < 160$ K). Physisorbed atoms have sufficiently long residence time on the surface and L-H mechanism is dominating. The decrease of the value of γ with decreasing the temperature is determined by the activation energy of L-H recombination.

We can see that the measured variation of γ_O is reproduced reasonably well. But a question may arise: does the model describe the **reality** or it is just an effective way to **fit** the evolution of γ_O observed in the experiment? Another question which is related to the first one – is the set of parameters of elementary processes obtained from the best agreement with the experiment **unique**? Regardless a huge number of published experimental and theoretical studies these questions are still open. The reason for this is that the recombination of atoms on the surface is a result of an interplay between many elementary processes. The rates of these processes are generally unknown. Deduction of several parameters from one measured quantity (γ) is an ill-posed problem from both physical and mathematical viewpoints.

Let us show to what extent the fitting procedure is “unstable” and dependent on the assumptions made about the parameters of the model. Consider for example the high temperature part of γ_O in Figure 1. 3. It is well established that at high temperatures only E-R recombination is efficient because physisorbed atoms are immediately desorbed back into the gas phase. This has been recently confirmed by molecular dynamic simulations [35]. The γ_O dependence on $1/T_{wall}$ can be well fitted with

$$\gamma_O = a \cdot \exp(-b/T_{wall}) \quad (1.5)$$

In the mesoscopic model of Kim&Boudart [5], coefficient b is interpreted as an activation energy of ER recombination. In later work of Bedra *et.al* [35] this coefficient is vaguely called “the total recombination activation energy” and *ab-initio* calculations performed in the same study show that ER recombination process itself has no energy barrier. Similar barrierless behaviour of recombination reactions $O_{ads}+O$ and $O_{ads}+N$ was found in *ab-initio* calculations performed in [40]. It is evident that there is a conflict between mesoscopic and microscopic interpretation of the activation barrier for recombination.

Understanding of the pre-exponential factor a is not much better. According to [5], $a = [S] \cdot k_{ER}^0$ where k_{ER}^0 is the steric factor for E-R recombination (see expression (1. 3)). In principle, both k_{ER}^0 and $[S]$ are unknown. If we suppose that $k_{ER}^0=1$ as it was done in [5], expression (1. 5) immediately gives the density of chemisorption sites $[S] = a$. However, if we assume $k_{ER}^0 \cong 0.1$ as in [27] or [41], higher value of $[S]$ would be estimated. The value of $[S]$

Surface reactivity in N₂/O₂ plasmas

obtained from the high temperature measurements influences in turn the best fit parameters of L-H processes that come into play at intermediate and low temperatures.

We can see that the description of recombination of one sort of atoms in a gas containing only one sort of molecules is already a difficult task with many unknown parameters. The complexity increases manyfold when we just mix N₂ and O₂!

1.3.1 Surface kinetics in N₂/O₂ mixtures

Extension of models for pure gases to mixtures has been done for Pyrex [22], silica-based thermal protection systems [42] and metallic surfaces [43]. According to these models N and O atoms may compete for active sites or even occupy different types of sites. Recombination pathways include formation of O₂ and N₂ as in pure gases but also NO in association between O and N. NO produced on the surface may undergo further heterogeneous reactions forming NO₂ or N₂O. Theoretical description of the ensemble of these processes requires introduction of a great number of parameters.

1.3.2 Role of plasma exposure

The picture of surface reactivity discussed so far doesn't take into account any effect of plasma exposure. So what is the possible influence of charged and excited species produced in the plasma on the surface reactivity? In low pressure plasmas, positive ions are accelerated towards reactor walls in the near wall sheath [44] and gain kinetic energy which easily exceeds ~10 eV. This energy is enough to break chemical bonds formed between the surface and chemisorbed species and even between atoms of the material (in quartz bond energy of oxygen atoms is of the order of 5 eV [45]). Therefore, ion bombardment may remove atoms from occupied active sites, create new sites (by creating defects) or even modify structure of the surface. Moreover, ions may activate chemical reaction due to a local supply of thermal energy to the surface. Similar effects are expected from exposure to UV photons and excited species carrying few electron volts of energy.

These examples clearly demonstrate that there is a need for further studies that would limit the number of unknowns and shed light on the role of plasma exposure for mesoscopic description of surface reactivity in N₂/O₂ plasmas.

Let's see what types of experimental investigations have been performed so far.

1.4 Surface reactions in N₂/O₂ plasmas: review of experimental studies

A great number of studies of surface catalyzed reactions in N₂/O₂ containing plasmas is available in the literature. Two main groups of processes under investigation may be distinguished:

- Recombination of N and O atoms on surfaces.
- Production/conversion of molecules on the surface.

Most of the studies were performed at low pressures ($p \sim 1$ mbar) because in low pressure conditions surface processes dominate the overall chemical kinetics of the plasma and the mechanisms of heterogeneous reaction may be investigated in details.

1.4.1 Recombination of O and N atoms on surfaces

Recombination probabilities of oxygen (γ_O) and nitrogen (γ_N) atoms on different surfaces have been measured by many authors. As a general rule, the value of γ depends on:

- Type of recombining atoms.
- Type of the material. For the same chemical composition of the material there is a dependence on the crystalline structure and surface morphology.
- Pretreatment history.
- Surface temperature.
- Plasma exposure on the surface and conditions in the plasma (pressure, gas mixture).

Catalytic properties of silica-based materials (silica, Pyrex, various glasses) have been studied intensively in connection with atomic sources and thermal protection systems on reusable space vehicles. Several experimental techniques for γ determination were employed:

- *Spatial post discharge.* Atoms produced in a discharge are transported by the gas flow outside the plasmas zone and the value of γ is deduced from the measured profiles of atomic concentrations. Using this technique recombination probability of O atoms (γ_O) was determined on silica [33][46] and Pyrex [47] at 300 K and as a function of the wall temperature between 194 K and 1250 K on silica [5][48]; γ_N was measured on silica [5][33][49] and Pyrex [50] at different temperatures.
- *Temporal post discharge.* The value of γ is deduced from the time evolution of atomic concentrations in a pulsed discharge during plasma OFF phase. Recombination of atoms takes places on the surface that was exposed to the discharge during plasma ON. This technique was used for γ_O determination on silica [21][27] and Pyrex [28] [51].
- *Stationary discharge.* Under continuous plasma exposure recombination probabilities are found from the measured gradients of atomic concentration in front of the studied surface or by means of global modelling. This technique was employed for γ_O

Surface reactivity in N₂/O₂ plasmas

measurements on silica at high temperatures relevant for re-entry conditions [34][35] [20] and at 300K [52] as well as on Pyrex [22][53] at various temperatures.

- *Spinning wall technique:* Recently, a so-called spinning wall technique for the study of surface catalyzed processes in reactive plasmas has been developed by the group of V. Donnelly [54]. With this method, a cylindrical section of the wall of the plasma reactor is rotated and periodically exposed to the plasma and then to a differentially pumped mass spectrometer. Using spinning wall technique the products of L-H recombination may be detected 0.5 – 40 ms after plasma exposure. This information is complementary to the measurements of the total recombination probability. Recombination of atomic oxygen on stainless steel, anodized aluminium and SiO₂ using the spinning wall technique was investigated in [54][55].

A summary of the published measurements of γ_N can be found in a recent review [56]; comparison of the values of γ_O determined by different authors is done in [46]. Analysis of the results for silica and Pyrex reveals a significant scatter of the published values depending on the experimental conditions and notably on the technique that was employed for γ determination. For the same material the values of γ measured in stationary discharges or temporal post discharges are systematically higher (by at least one order of magnitude) than those found in the flowing post discharge where there is no contact between the plasma and the studied surface.

In [27] it was shown that the effect of plasma exposure on the value of γ_O may persist during many minutes after the end of the wall treatment by a discharge. In [57] the effect of O₂ and N₂ plasma pretreatment on the recombination of atomic oxygen on silica and Pyrex surface was studied and interpreted in terms of population and depopulation of surface active sites under plasma exposure. It was suggested that ion bombardment “clean” active sites and increase therefore catalytic activity of the surface, while O atoms passive the surface when they stick to chemisorption sites.

1.4.2 Molecule production/conversion on surfaces

While heterogeneous atomic recombination is a “classical” process that has been studied for several decades, only recently the role of the surface as a source of new molecules in reactive plasmas has been recognized. New molecules may be produced in surface reactions of atoms, for example $(O+N)_{\text{wall}} \rightarrow NO$ or $(O+NO)_{\text{wall}} \rightarrow NO_2$. Therefore, losses of atoms and production of new molecules are closely coupled. However, investigation of molecule formation on surfaces requires a special approach because surface terms have to be separated from production of molecules in the gas phase. This is usually done by a combination of measurements of species concentrations with kinetic modelling.

In [43][58][59] formation of NO, NO₂ and N₂O in recombining N₂ – O₂ plasmas in a stainless steel vessel at a pressure ~ 0.1 – 1 mbar was investigated. Measured concentrations of N_xO_y were compared with the results of a kinetic model. The evidence of NO, NO₂ and N₂O production on the surface was demonstrated. It was shown that molecules are formed in

recombination between mobile adsorbed O, N and NO and impinging gas phase species. A set of sticking coefficients and activation energies for different surface reactions was obtained from the best fit between measured and calculated concentrations.

In [31][32][60][61] molecule formation was studied in a hollow-cathode discharge with NO, NO₂, N₂O and N₂/O₂ used as precursors at a pressure $p \sim 1$ mbar. An important role of N_xO_y production reactions on the stainless steel cathode surface was demonstrated. Probabilities of heterogeneous NO, NO₂ and N₂O formation were obtained from the best agreement between measurements and kinetic modelling.

Recently production of NO from surface recombination of N and O atoms on silica has been evidenced in [33][62]. Measurements of O, N and NO concentrations were performed in a side arm reactor with the wall temperature ranging between 300 K and 1200 K. It was found that the reaction rate of $(N+O)_{\text{wall}} \rightarrow \text{NO}$ is comparable in magnitude to $(N+N)_{\text{wall}} \rightarrow \text{N}_2$ and $(O+O)_{\text{wall}} \rightarrow \text{O}_2$ in the whole temperature range.

Here we conclude that the fact of production and conversion of molecules on the surface in low pressure N₂/O₂/N_xO_y plasmas is well established. However, mechanisms of surface reactions in such complex environment are far from being fully understood. First, due to a great number of different elementary processes that take place simultaneously (in [43] 17 recombination reactions on the surface were considered). And second, the rates of surface reactions in cited works are not measured directly but obtained from the best agreement between experiment and simulations. Gas phase kinetics in N₂/O₂ plasmas itself is very complex. For example, in order to describe NO production in air discharge a number of reactions with electronically and vibrationally excited N₂ has to be considered [16][63]. The rates of these reactions are not known with a good precision. Therefore, the “formula”

$$[\text{Surface Production}] = [\text{Measured Production}] - [\text{Modelled Gas Phase Production}]$$

is limited in accuracy, although it allows in many cases to evidence the importance of surfaces for molecule production.

1.5 Research questions

In order to get insight into elementary processes in N₂/O₂ plasma – surface interactions simple systems with reduced number of relevant reactions (on the surface as well as in the gas phase) should be studied. Ideally, it would be desirable to isolate and investigate one surface reaction at a time. The objective of this thesis is to investigate chemisorption and reactivity of N and O atoms on oxide surfaces (silica, Pyrex, TiO₂) under plasma exposure. The following question will be addressed:

- *Can atoms be chemisorbed?* Although introduced in the models, chemisorbed N and O atoms on silica-like surfaces have never been observed experimentally, so this question is the first to be answered.
- *What is the coverage of these atoms?*

Surface reactivity in N₂/O₂ plasmas

- *What are the main processes of adsorption and desorption?*
- *How chemisorbed atoms catalyse production of molecules on the surface and participate in surface recombination of atoms?*

1.6 Research strategy

In this thesis we will study adsorbed atoms that are sufficiently **stable** and have a lifetime on the surface of at least few minutes. Therefore, once being adsorbed these atoms remain attached to the surface even after the end of plasma/atomic flux exposure. This opens a way to separate in time the adsorption step and the study of grafted species. We propose the approach which consists in the pretreatment of the surface by N₂ or O₂ plasma followed by probing of the density and reactivity of adsorbed atoms. We must acknowledge that the idea of this approach was inspired by work of G. Cartry [57], dosing experiments of R. Zijlmans [43] and fruitful discussions with Prof. D. Schram.

The role of the studied surface in our experiments is played by the inner wall of the discharge tube which can be made of silica, Pyrex or silica with a sol-gel film of an oxide catalyst (TiO₂). For ex-situ surface diagnostics, small samples of the same materials are treated in the discharge in the same conditions as employed for the pretreatment of the reactor surface. Schematically the experimental sequence is shown in Figure 1. 4.

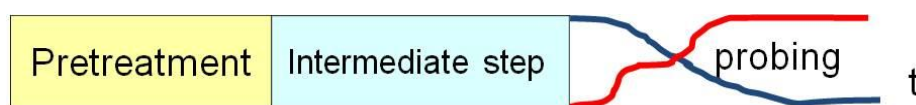


Figure 1. 4 Schematic of the experimental procedure.

The so-called “intermediate step” may be just pumping of the reactor or exposure of the pretreated surface to elevated temperatures, UV light or Ar plasma in order to investigate the stability of adsorbed atoms. During the third step the surface is probed in three possible ways:

- *Ex-situ x-ray photoelectron spectroscopy (XPS) analysis.* This diagnostics is mainly applied after N₂ plasma exposure in order to monitor nitridation of SiO₂.
- *Reactivity of adsorbed atoms under plasma exposure:* after the pretreatment the discharge tube is filled with an alternative gas (for example O₂ after N₂ plasma treatment or ³⁶O₂ after ³²O₂ plasma treatment) and a discharge is started in closed reactor. Molecules produced on the surface in recombination between gas phase and adsorbed atoms are detected using laser absorption spectroscopy or mass spectrometric diagnostics.
- *Reactivity of adsorbed atoms in the post discharge:* after plasma pretreatment a controlled amount of probe molecules (NO, NO₂, C₂H₂) is admitted in the reactor. Losses of these molecules and production of new species on the reactor walls

catalyzed by adsorbed atoms are monitored by laser absorption and mass spectrometric diagnostics.

In the following chapters we will separately investigate adsorption and reactivity of nitrogen (Chapter 3) and oxygen (Chapter 4) atoms on various surfaces using proposed experimental methods.

1.7 Definitions and notations

In the following chapters we will see that different types of O and N atoms on the studied surface may exist. Here we will give some definitions:

We denote \mathbf{N}_{ads} and \mathbf{O}_{ads} – adsorbed atoms that have a residence time on the surface at least $\sim 10^3$ s, so they can be detected in the experimental sequence shown in Figure 1. 4.

We will find that in some conditions there exist sub-groups of stable adsorbed atoms \mathbf{N}_{ads} and \mathbf{O}_{ads} that are more reactive; we will use $\mathbf{N}_{\text{ads}}^*$ and $\mathbf{O}_{\text{ads}}^*$ to denote these atoms.

For atoms that leave the surface during the pumping of the reactor after the pretreatment we use \mathbf{N}^{weak} and \mathbf{O}^{weak} . These atoms may be either physisorbed or weakly chemisorbed.

And finally we will see that oxygen atoms belonging to the crystalline network of oxide materials (such as silica or Pyrex) may also contribute to surface reactivity. But we will not use any special notation for these atoms.

2. Chapter II: Experimental setup and diagnostic techniques

2.1 Discharge setup

2.1.1 Reactor and gas system

A dedicated experimental setup for investigation of interaction between low pressure plasmas and catalytic surfaces has been created in the Low Temperature Plasmas group during the PhD works of Olivier Guaitella [64] and Lina Gatilova[65]. With some further modifications and addition of new diagnostics the same setup is used in this study.

Figure 2. 1 shows the view of the setup. Plasma is ignited in a cylindrical reactor of 2 cm inner diameter and 60 cm full length. Discharge tube consists of three parts. Central part has a length of 40 cm and it is installed between two Pyrex sections using specially designed vacuum connections. This part can be easily dismantled. Therefore, reactors made of different materials or containing different catalysts can be studied without any modification of the system. In the present geometry plasma is in contact only with the studied surface what significantly simplifies the analysis of the results. Two fast pneumatic valves isolate the reactor from the rest of the system in order to perform experiments in static conditions with no gas flow. With the low leak rate ($3 \cdot 10^{-5}$ sccm) adsorption/desorption reactions on the catalytic surfaces may be followed during hours without a strong influence of the atmospheric impurities. KBr windows are fixed on each end of the tube allowing infrared laser absorption diagnostics inside the reactor.

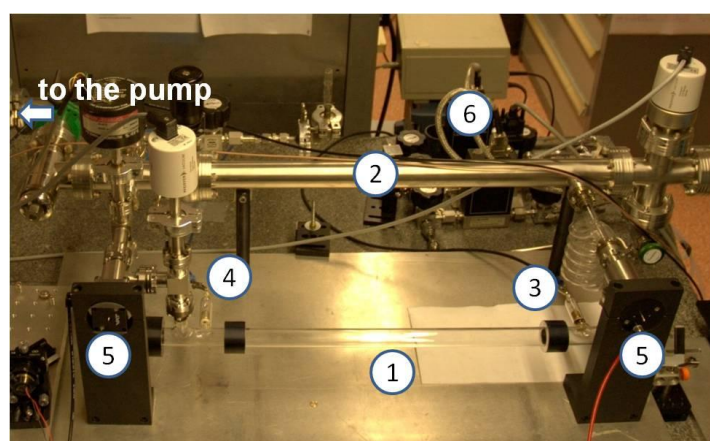


Figure 2. 1 Experimental setup (1) – interchangeable discharge tube section, (2) – buffer volume, (3) – high voltage electrode, (4) – grounded electrode, (5) – pneumatic valves, (6) – mass-flow controllers

Experimental setup and diagnostic techniques

The vacuum system is pumped using an oil-free scroll pump (Edwards XDS10) to a base pressure of 0.1 Pa. Introduction of working gases is performed using 3 mass flow controllers (10, 100 and 500 sccm). When working in flowing conditions, gas pressure is adjusted by changing the pumping rate using a valve at the reactor outlet. Pure gases Ar, N₂, O₂ with the typical level of impurities <3 ppm and prefabricated gas mixtures containing 1% of NO, NO₂, N₂O, CO, CO₂ or C₂H₂ diluted in argon or N₂ are employed in the experiments.

When reactivity of plasma-pretreated surfaces is studied, it is essential to introduce in the reactor a gas mixture containing a well defined number of probe molecules. The buffer volume is used to prepare the desirable gas mixtures and rapidly inject them in the reactor using the pneumatic valves. Then the valves are closed again and the evolution of the gas phase species may be followed by different *in-situ* diagnostics. Due to the operation in static conditions with precise dosing of reactive gases we are able to perform experiments with specially pretreated surfaces in which kinetics of gas phase species in a single discharge pulse is investigated.

2.1.2 Pulsed discharge systems

The focus of this thesis is the investigation of surface processes in low pressure N₂/O₂ plasmas. From the view point of the discharge type our objective was to create the plasma in the most simple and well controlled way. For this reason direct current (dc) glow discharge and radiofrequency (rf) capacitively coupled discharge are selected. In this study, pulsed discharge technique is used in order to investigate kinetic processes in plasmas. The advantage of pulsed discharges compared to continuous ones is that processes having different characteristic timescales (electronic excitation, vibrational excitation, dissociation, gas heating, etc..) may be easily controlled and separated by an appropriate selection of the discharge pulse duration.

2.1.2.1 Direct current glow discharge

A pulsed dc glow discharge is ignited by applying a high voltage to a pair of electrodes via a ballast resistor. The schematic of the discharge setup is shown in Figure 2. 2. Power supply consists of a capacitance bank charged by a continuous (0-30 kV) power supply, high voltage pulses are formed using a triggered solid state switch. Positive pulses with the rise time of 1 μs and up to 10 kV in amplitude are obtained. The maximum pulse duration is limited by the energy stored in the capacitance and by the amplitude of the desired discharge current. Discharge current is adjusted by choosing the value of the ballast resistor ($R_b=15-70\text{ k}\Omega$) and the applied high voltage.

Electrical diagnostics of the dc discharge consists in the measurements of current and voltage waveforms. The discharge voltage is measured with a high voltage probe (LeCroy PPE20kV). The discharge current is deduced from the voltage drop on an $R_m=18.4\text{ }\Omega$ series resistor placed between the cathode and the ground. Both current and voltage signals are digitalized

using an oscilloscope (LeCroy 44Xi, 400 MHz). Typical voltage and current waveforms are shown in Figure 2. 3.

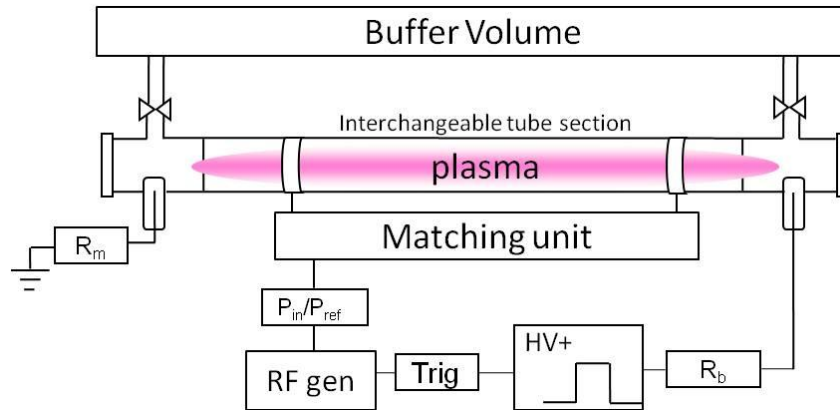


Figure 2. 2 Schematic of the experimental setup. Both dc and rf discharge power supplies are shown.

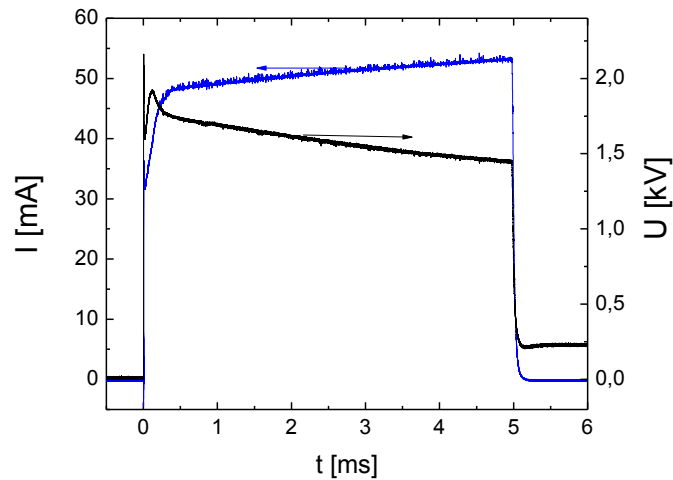


Figure 2. 3 Discharge voltage and current waveforms, N_2 $p=133$ Pa.

The main advantages of using a pulsed dc discharge for investigation of plasma-surface interactions are the following:

- Easy control of the discharge parameters (discharge current, pulse duration).
- Discharge column is homogeneous along the reactor axis – different parts of the discharge tube undergo the same plasma exposure.
- Easy in-situ diagnostics. Homogeneity of the discharge column allows for a number of quantitative *in-situ* diagnostics (laser absorption, UV absorption). Local species concentrations may be obtained from measurements averaged along the discharge axis.
- Very well studied discharge type. The pulsed dc discharge system used in this work was characterized in the PhD works of O. Guaitella [64] and L. Gatilova[65]. Kinetics of dc discharges in N_2 [66], O_2 [67] and their mixtures [16][63] similar to one used in this study have been intensively investigated in the past and several numerical models

Experimental setup and diagnostic techniques

were created. With these models all the discharge properties may be predicted with a good precision based on four input parameters: i) discharge tube radius, r ii) gas pressure, p iii) gas mixture iv) discharge current, I . Results of different studies may be compared due to the existence of scaling laws for dc glow discharges [68].

The conditions of dc discharge operation used in this study and typical plasma parameters (according to previous studies [63][65][66][67]) are listed in Table 2. 1.

Gas	p , [mbar]	i [mA]	τ [ms]	E/N [Td]	n_e [cm^{-3}]	T_e [eV]	P^1 [W/cm^3]
N_2	0.53	100	5	120	$1.7 \cdot 10^{10}$	3	0.4
N_2	1.3	50	5	80	$1.1 \cdot 10^{10}$	1.7	0.3
O_2	0.53	100	10	60	$1.9 \cdot 10^{10}$	3.8	0.17
O_2	1.3	100	10	50	$2.2 \cdot 10^{10}$	3.6	0.35

¹P – power density

Table 2. 1 Typical dc discharge conditions used in this study.

2.1.2.2 Radiofrequency capacitive discharge

A capacitive rf discharge is ignited in the same discharge tube. Two copper ring electrodes are placed on the tube outer surface and driven symmetrically by a 13.56 MHz generator (Sairem 300W) through a specially designed push-pull matching network. The discharge is operated in either pulsed or continuous mode. Typically, the rf discharge is operated in the same pressure and gas flow conditions as the dc one. The length of visually homogeneous rf discharge column is 40 cm and it occupies entirely the interchangeable section of the discharge tube. The total length of rf plasma column is 50 cm, i.e. the same as in the case of the dc discharge. The use of a rf discharge in addition to the dc discharge is motivated by several reasons:

- When surface cleaning by plasma is performed it is desirable to use relatively high power coupled to the discharge in order to get reproducible results with reasonable pretreatment times. Increase of the dc discharge power would inevitably lead to the erosion of the electrodes and pollution of the studied surfaces.
- In the experiments on molecules oxidation on plasma pretreated surfaces it was found that some molecules react on the metallic dc electrodes. In this case a dedicated discharge tube with rf excitation using external electrodes only has to be used.
- The length of the rf discharge column can be easily changed by moving the ring electrodes along the discharge tube. Therefore the studied surfaces may be exposed directly to the discharge or to the flowing afterglow. This allows discrimination between the roles of ions and neutral radicals in surface reactivity.

Our discharge system is not adapted for detailed electric diagnostics. Grounded surfaces in the vicinity of the discharge column introduced uncontrolled stray capacitance and the determination of the rf current flowing in the plasma is not possible. Therefore, the discharge is characterized by the power absorbed in the plasma. Incident and reflected rf powers are measured by an in-line power meter placed between the rf generator and the matchbox. In

order to measure the power absorbed by plasma, losses in the matching circuit should be taken into account. This was done using the subtraction method [69]. First, incident (P_i^0) and reflected (P_r^0) powers as well as the voltage (U_{RF}^0) on the electrodes are measured without plasma (at a pressure too high for the discharge ignition). Without the discharge the difference $P_i^0 - P_r^0$ represents the losses on the active resistance of the matcher and electrical contacts and therefore it is proportional to $(U_{RF}^0)^2$. When the discharge is ignited, power dissipation in the plasma is calculated as follows:

$$P_{pl} = (P_i^1 - P_r^1) - (P_i^0 - P_r^0) \left(\frac{U_{RF}^1}{U_{RF}^0} \right)^2 \quad (2.1)$$

Index “1” corresponds to the measurements with plasma ON, “0” – plasma OFF. Typically, the P_{pl} is in the range 10-30 W what corresponds to injected power density 0.06 – 0.2 W/cm³. It was found that P_{pl} accounts for about 50% of the value of $(P_i^1 - P_r^1)$. Therefore, power losses in the matcher cannot be neglected.

2.2 Diagnostics employed

In this work reactivity of different catalytic surfaces under plasma exposure is studied. We analyze primarily gas phase products of surface catalyzed reactions. Therefore, a number of gas analysis techniques are employed, namely tunable diode laser absorption spectroscopy (TDLAS), ultra-violet (UV) absorption spectroscopy and mass spectrometry (MS). Plasma ON phase is characterized by optical emission spectroscopy (OES) and the production of atomic oxygen in the discharge is studied using two photon absorption laser induced fluorescence (TALIF). Chemical analysis of the surface after plasma exposure is performed using x-ray photoelectron spectroscopy (XPS).

In this section the principles and the experimental implementation of these techniques will be described.

2.2.1 Tuneable diode laser absorption spectroscopy in mid-infrared range

2.2.1.1 Principles of laser absorption spectroscopy

Numerous molecules and radicals exhibit strong absorption features in mid-infrared range ($\lambda=2.5-25 \mu\text{m}$) corresponding to roto-vibrational transitions within the same electronic state. Availability of tunable lasers and sensitive fast detectors working in mid-IR make laser absorption spectroscopy a powerful tool for *in-situ* time resolved gas sensing [70][71].

The basic principle of the absorption technique is expressed in the Beer-Lambert law:

$$\int \ln \left(\frac{I_v(L)}{I_v(0)} \right) dv = - \int \int_0^L k_v N(z) dz dv = -k \langle N \rangle L \quad (2.2)$$

Experimental setup and diagnostic techniques

where $I_\nu(0)$ and $I_\nu(L)$ signify the intensity of the incident and transmitted laser radiation at frequency ν passing through the absorbing medium having the length L ; N is the concentration of absorbing molecules per cm^3 . Spectral integration is performed over the complete absorption line profile. Spectrally integrated absorption cross section k can be expressed as follows:

$$k = \frac{h\nu_{ik}}{c} B_{ik} \frac{g_i e^{-\frac{E_i}{kT}}}{Q_{rot}(T)} \left(1 - \frac{g_i n_k}{g_k n_i} \right) \quad (2.3)$$

where B_{ik} and ν_{ik} are the Einstein coefficient and the frequency of the observed transition, n_i (n_k), g_i (g_k) are the population and the statistical weight of the lower (upper) level, E_i is the energy of the lower level and $Q_{rot}(T)$ is the rotational partition function. From equation (2.5) it follows that the concentration averaged over the absorbing length is actually measured.

In this work, laser absorption measurements are performed *directly* in the discharge tube. Thus, the absorbing volume has a length of 60 cm, allowing for the detection limits of the order of 10^{12} molecules cm^{-3} (depending, of course, on the measured species) with a single laser pass inside the reactor. Due to the homogeneity of the discharge along the tube axis, average quantities measured by laser absorption may be considered as a good approximation for the local values of species concentrations.

2.2.1.2 Advantages of laser absorption measurements

Combination of high sensitivity, high time resolution (down to few μs) and possibility of fast acquisition of a sequence of absorption spectra without signal accumulation make tunable laser absorption spectroscopy a unique tool for kinetic studies. It is the only gas sensing technique allowing time resolved *in-situ* measurements in a *single* plasma pulse.

2.2.1.3 Pitfalls of laser absorption measurements

When absorption spectroscopy with diode lasers is employed, individual roto-vibrational levels of absorbing molecules are probed (n_i). In order to deduce the total concentration N , the vibrational and rotational distributions of absorbing molecules have to be taken into account. In thermal equilibrium, these distributions are always Boltzmann with the same temperature equal to the kinetic temperature of the gas (T_g). In non-equilibrium conditions which are typical for low temperature plasmas the following ordering of the characteristic temperatures is usually established $T_g = T_{rot} \leq T_{vibr}$. Even at low pressures (~ 1 mbar) fast rotational-translational relaxation leads to the equilibrium between rotational and translational degrees of freedom. Formation of non-equilibrium vibrational distributions is observed when vibrations are efficiently excited and the vibrational-translational relaxation is slow.

In order to perform correct measurements during plasma ON phase, the knowledge of the gas temperature is required. An additional complication arises from the fact that temperature

gradients are established between the axis of the discharge and the reactor walls. At constant gas pressure, temperature gradients result in the gradients of the neutral gas density what makes accurate absorption measurements a very difficult task.

In the present study in order to get rid of the undesirable distortions we combine the pulsed discharge technique with time resolved laser absorption measurements. In Figure 2. 4 a schematic of a typical behaviour of the laser absorption signal in the presence of gas cooling and vibrational relaxation effects is shown. For correct interpretation of absorption measurements, in every particular case the analysis of the characteristic times of different processes (chemical reactions, gas cooling, vibrational relaxation) should be performed.

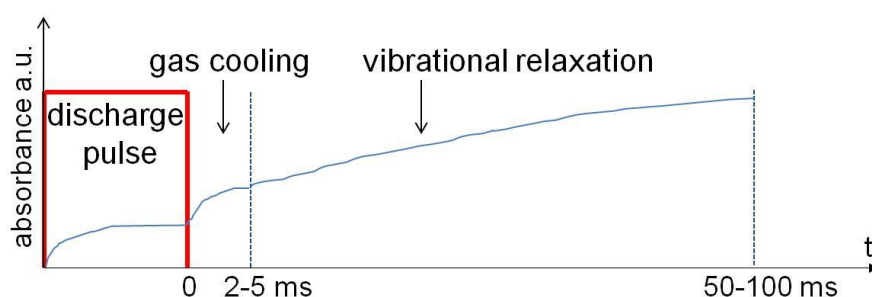


Figure 2. 4 A typical behaviour of the absorption signal in a pulsed discharge in the presence of gas cooling and vibrational relaxation effects.

2.2.1.4 Diode laser spectrometer

A commercial laser spectrometer (LaserComponents) is used for *in-situ* monitoring of species in the reactor. A schematic of the laser system is shown in Figure 2. 5. The main components of the spectrometer are:

- A **cold head** in which four PbSe diodes cooled by a closed-cycle helium refrigerator are installed. The diodes are kept at a pressure of 10^{-7} mbar and cooled down to 10K. Typical operating temperature of the diodes lies in the range 50-120K and it is adjusted by a resistive heating of the copper support on which the diodes are mounted.
- The temperature of the lasers and the driving current flowing through the diodes are adjusted by a PC operated **controller**.
- Typically, led salt diodes are multimode, whereas for quantitative absorption measurements a single mode operation is required. A grating **monochromator** is used to select the desired emission mode of the laser.
- After passing through the reactor the intensity of the laser radiation is measured by a liquid nitrogen cooled **detector** (JudsonJ15D16).
- The detector signal is amplified and then transferred to the PC via a 2 MHz acquisition card (NI PCI 6111). Then the signals are analysed by the **TDL Wintel**

Experimental setup and diagnostic techniques

software that performs fitting of the absorption spectra for concentration determination.

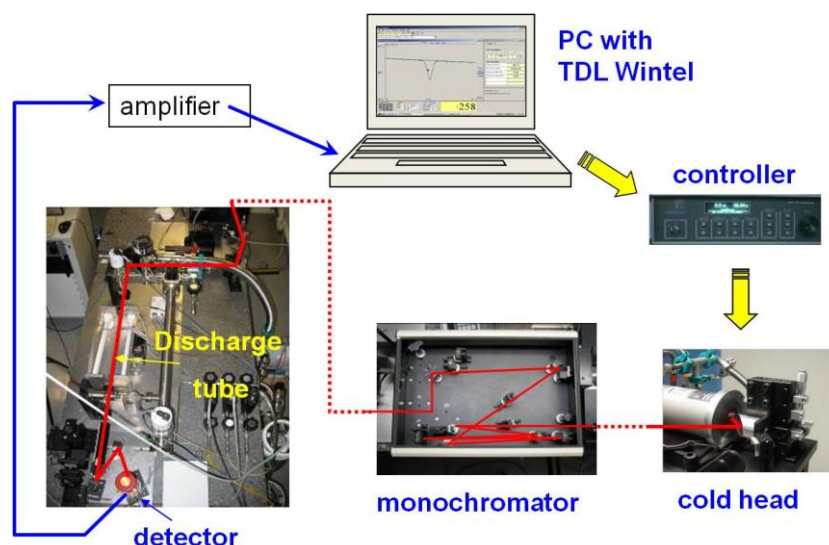


Figure 2. 5 Schematic of the tuneable laser system.

Chirped laser radiation is emitted when a current ramp ($\sim 300\text{--}600\text{ mA}$) is applied to the diode. Coarse tuning of the laser frequency is performed by the temperature adjustment ($4\text{ cm}^{-1}/\text{K}$) and fine tuning is achieved by setting the current (less than $0.1\text{ cm}^{-1}/\text{mA}$). Typical tuning range of each laser is of the order of 20 cm^{-1} and output laser power is $0.1\text{--}1\text{ mW}$. Commercially available lasers cover the spectral range of $660\text{--}3250\text{ cm}^{-1}$. In order to achieve the best detection limits the diodes are selected to match with the most intense absorption features of the species of interest. Therefore, usually for each molecule a specific diode has to be used.

In Figure 2. 6 an example of a diode laser operation for NO detection around 1900 cm^{-1} is shown. The laser is tuned over approximately 0.2 cm^{-1} during the current ramp of a total duration of $380\text{ }\mu\text{s}$. The $20\text{ }\mu\text{s}$ off phase is used to estimate the baseline of the detector. The total pulse repetition frequency is 2.5 kHz (the duty cycle ratio is 95%) what set the limit for the time resolution of the measurements. Several successive laser pulses may be averaged by the TDL Wintel software in order to improve the signal to noise ratio. As a rule, improvement of the detection limits is always performed at the expense of the time resolution. In practice, for NO measurements a typical time resolution was set to $5\text{--}20\text{ ms}$ depending on the experimental conditions.

The transmission spectrum of a germanium Fabry-Perot etalon with a known 0.047 cm^{-1} fringe spacing allows conversion of the time scale of the current ramp (upper panel) into the frequency scale of the absorption spectra (lower panel). The TDL Wintel software performs fitting and integration of the absorption line and the values of the concentration are automatically calculated using the molecular parameters from the HITRAN database [72].

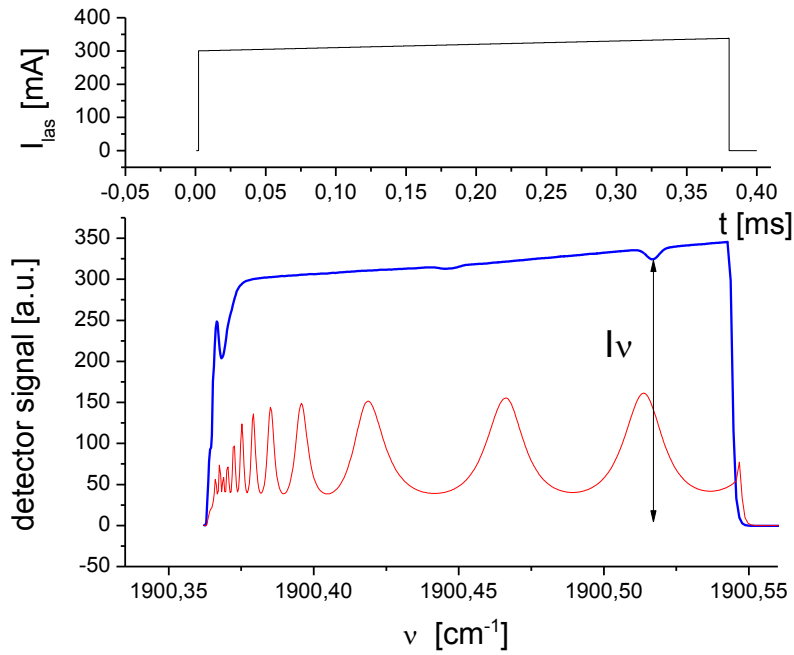


Figure 2. 6 Example of a diode laser operation around 1900 cm^{-1} . The upper panel shows the waveform of the laser driving current. The lower panel shows the absorption spectrum of NO and the signal of a germanium Fabry-Perot etalon with 0.047 cm^{-1} fringe spacing.

2.2.1.5 Three-channel quantum cascade laser spectrometer

Quantum cascade laser (QCL) is a new type of semiconductor lasers that was theoretically predicted in 1970s in USSR [73] and implemented in 1994 in Bell Laboratories [74]. The laser active region of QCL comprises a periodic series of thin layers of different materials (a so-called super-lattice). A single electron moving through the QCL active region emits a photon every time it travels the distance equal to the period of the super-lattice. Therefore, photons are emitted in a cascade-like manner what gave the name to this type of lasers.

Compared to classical TDLAS quantum cascade laser absorption spectroscopy (QCLAS) has a number of advantages:

- QCLs do not require cryogenic cooling and can operate at $(-30..+30)\text{ }^{\circ}\text{C}$ with thermoelectric cooling. This reduces significantly the size and the cost of the laser system. Compact size permits combination of several lasers in one system for simultaneous multi species detection.
- Due to the cascade photon emission mechanism the quantum efficiency and hence the output power of QCLs is much higher. This allows utilisation of fast thermoelectrically cooled detectors.
- QCLs emit one single mode and therefore can be used without any mode selectors.
- The pulse repetition frequency of QCLs may reach few hundred kilohertz allowing for μs time resolution.

Experimental setup and diagnostic techniques

Regardless their invention about 20 years ago, only recently QCLs have been recognized as a promising tool for plasma diagnostics [71]. The group of Prof. Roepke at INP Greifswald are among the first who started design and production of dedicated QCL spectrometers for species concentration measurements in plasmas. A 3-channel TRIPLE Q [75] system developed at INP Greifswald is used in this work. The schematic of the TRIPLE Q spectrometer and its optical layout is shown in Figure 2. 7. Compared to led salt diodes QCLs have even smaller tuning range ($\sim 7 \text{ cm}^{-1}$), therefore with three laser system 3 different species can be simultaneously measured. Overlapping of absorption features of some species (CO and N_2O @ 2200 cm^{-1} , C_2H_2 and CH_4 @ 1300 cm^{-1}) allowed detection of 5 and more different molecules in some cases.

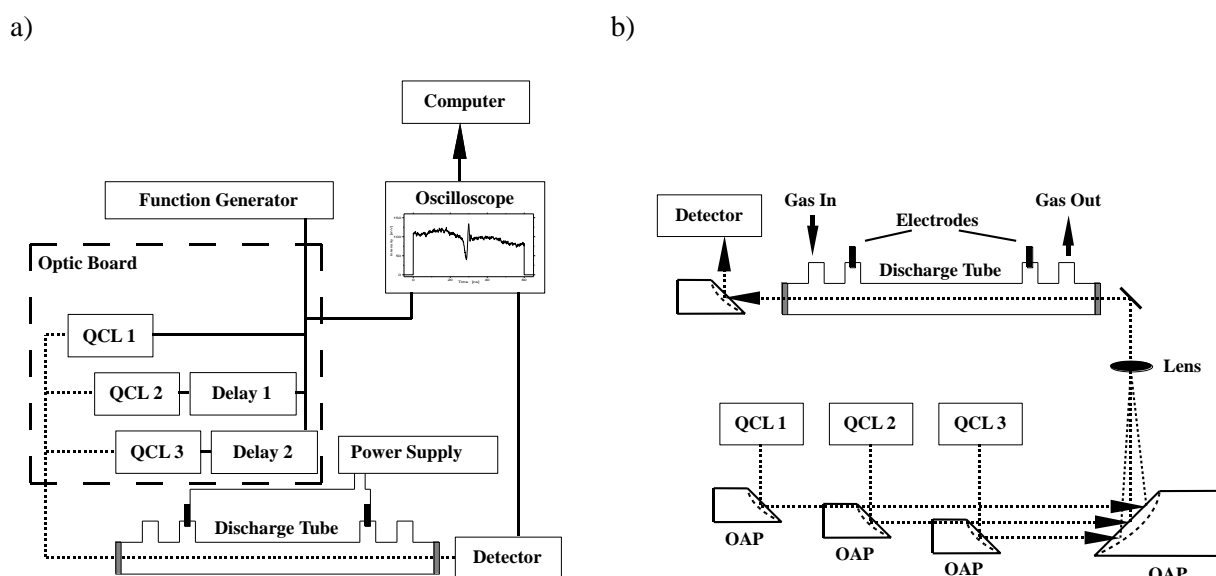


Figure 2. 7 Principle scheme of the TRIPLE Q spectrometer a) control signals b) optical arrangement (OAP – off-axis parabolic mirror).

QCLs are housed in temperature-stabilised laser heads and operated by pulsed laser drivers (Q-MACS Basic, neoplas control). The divergent laser radiation is collimated using off-axis parabolic mirrors (OAP) and combined in a single laser beam by a telescopic system. This beam is then directed three times through the discharge tube and finally focused onto a fast detector (IRDM-600, neoplas control). The detector module contains a temperature controller specifically adjusted to the detector element (VIGO, PDI-2TE-10/12) and pre-amplifier (bandwidth: 600 MHz, rise time: 2 ns).

The QCLs are operated in a so-called *intra-pulse* mode, i.e. the laser frequency is scanned during a short (100-200 ns) current ramp. In

Figure 2. 8 an example of the absorption spectrum of CO_2 around 2325 cm^{-1} is shown. The QCL chirp rate is about $0.02 \text{ cm}^{-1}/\text{ns}$ and therefore it is tuned over the absorption features of CO_2 in $\sim 5 \text{ ns}$. Apart from the fast detector, a high-end digital oscilloscope (1 GHz bandwidth, 10 GS/s sampling rate) has to be used for acquisition of such rapidly changing signals. In the TRIPLE Q arrangement, the 3 lasers are triggered using a combination of pulse generators in such a way that laser pulses arrive on the same detector delayed in time. In

Figure 2. 8 a sequence of 3 laser pulses is shown. The maximum time resolution achieved by the TRIPLE Q system is limited by the duty cycle ratio of the QCLs which should not exceed 2% according to the manufacturer specification. Therefore with 100 ns pulse duration, 200 kHz repetition rate (5 μ s time resolution) may be reached. For time resolved measurements a train of consecutive pulses is saved in the oscilloscope memory and then analysed on a PC.

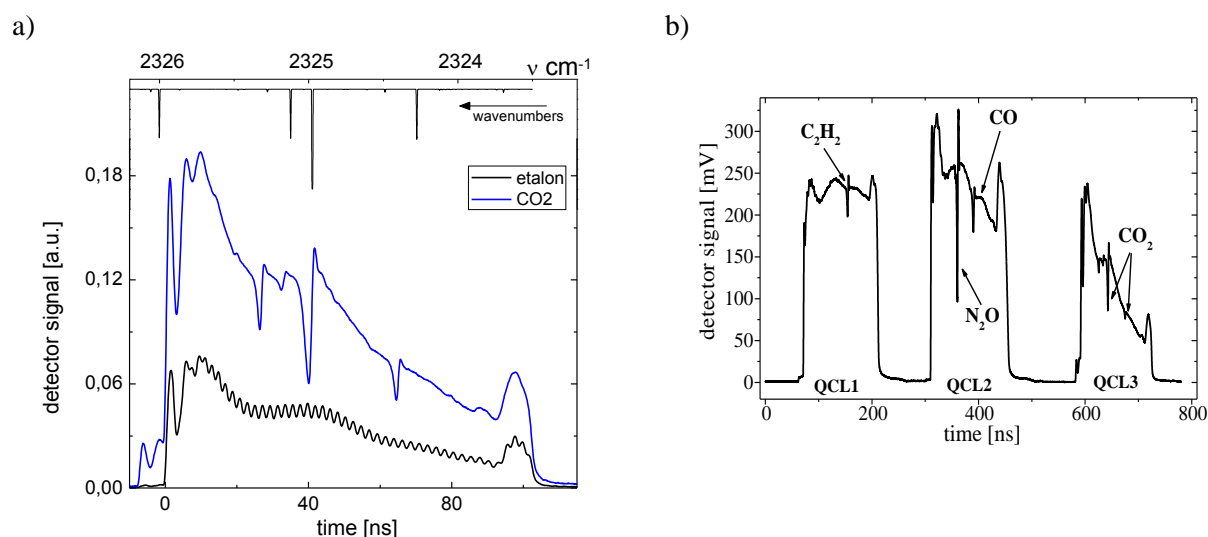
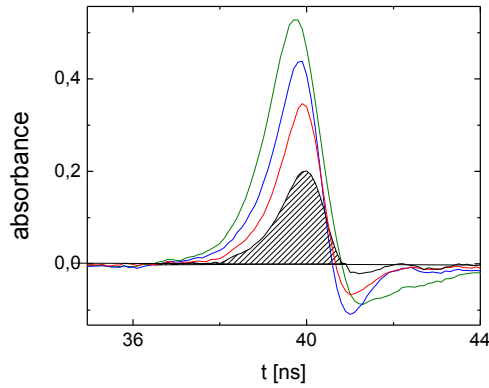


Figure 2. 8 a) Absorption spectrum of CO_2 around 2325 cm^{-1} and the etalon spectrum (0.047 cm^{-1} fringe spacing) obtained using a QCL. CO_2 spectrum from HITRAN is also shown. b) A sequence of 3 laser pulses of the TRIPLE Q system designed for C_2H_2 , CO_2 , CO and N_2O detection.

Due to the fast chirp rate of the QCLs, a number of non-linear effects in absorption of laser radiation may be observed [76,77]. Manifestation of the *rapid passage effect* in the overshoot of the absorption signals of CO_2 can be seen on Figure 2. 8 a). Rapid passage effect is established when the interaction time between the chirped radiation and a pair of molecular levels is shorter than the relaxation time of the upper level [71]; it vanishes at higher pressures when collisional quenching becomes fast enough. Deformation of absorption lines at low pressure (~ 10 mbar) makes a direct application of the Beer-Lambert law impossible in QCLAS. Calibration procedure is thus required. In this work, we are interested in the kinetics of small stable molecules having distinct absorption features in mid-IR (NO , NO_2 , N_2O , CO , CO_2 , C_2H_2). Therefore, following the procedure described in [71][78] the intensity of single distorted absorption lines as a function of species concentration is performed by introducing a known amount of molecules in the reactor. Absorption signals are integrated until the point where absorbance turns negative. In Figure 2. 9 the absorption line integration procedure and the result of the calibration for CO_2 are shown. Similar procedure is done for CO , C_2H_2 , N_2O , NO , NO_2 .

Experimental setup and diagnostic techniques

a)



b)

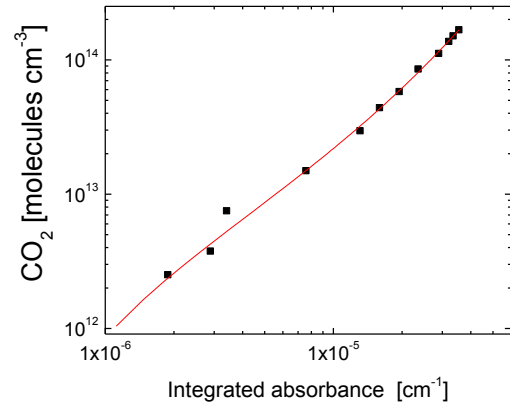


Figure 2. 9 a) Absorbance ($\ln(I_0/I_v)$) for different concentrations of CO_2 . b) Calibration curve: points – experiment, line – approximation by a third order polynomial.

Table 2. 2 shows a complete list of lasers and detection limits for corresponding species.

Molecule	Laser type	Spectral position (cm^{-1})	Detection limit (molecules cm^{-3})
NO	PbSe diode	1900	10^{12}
	QCL	1897	10^{13}
NO_2	PbSe diode	1629	10^{12}
	QCL	1612	10^{13}
N_2O	QCL	2208	10^{12}
C_2H_2	QCL	1370	10^{13}
CO	QCL	2209	10^{13}
CO_2	QCL	2325	10^{12}

Table 2. 2 The list of tuneable lasers used in this work.

2.2.2 Time resolved emission and absorption spectroscopy in UV-Vis range.

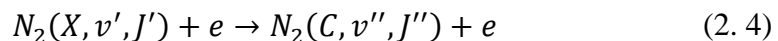
Optical emission spectroscopy (OES) and broad band absorption spectroscopy are among the most well established techniques for plasma diagnostics. With the advent of multi-element intensified light detectors (iCCD) optical diagnostics of kinetic processes in pulsed discharges with time resolution in the nanosecond scale became a routine and very powerful tool. In this work we use a grating monochromator (Andor Shamrok SR-303i) coupled with a fast intensified CCD camera (Andor iStar) for gas temperature measurements in N_2/O_2 pulsed DC discharge from the rotational structure of the N_2^+ system emission. The same spectrometer is used in combination with a broad band UV source for time resolved ozone concentration measurements.

2.2.2.1 Optical emission spectroscopy for gas temperature determination

In the previous sections it was shown that the knowledge of the gas temperature is crucial for correct interpretation of laser absorption measurements in pulsed plasmas. Sometimes variation of laser absorption signals in time may be used for temperature estimation as in [78][79]. However, an independent method for T_g measurements is desirable; one possibility is the analysis of the rotational structure of the $N_2\ 2^+$ system ($N_2(C^3\Pi) \rightarrow N_2(B^3\Pi)$) [80].

Determination of the kinetic gas temperature from the rotational structure of molecular emission in plasmas is a well known technique that has been applied to the bands of H_2 [81], O_2 [82], N_2 [83], N_2^+ [84], OH [85], NO [86] and many other molecules and radicals. As we have discussed above, the rotational temperature of the ground state of all the stable species in plasmas is equal to the temperature of the gas even in low pressure conditions. Typically, few collisions are enough to equilibrate rotational and translational temperatures [87]. Therefore, if a molecule has a lifetime in plasma which is longer than the rotational-translational relaxation (R - T) time T_g and T_{rot} will be in equilibrium. Molecular emission in plasmas originate from the excited electronic states, which have a radiative lifetime ranging from a few tens nanoseconds (for radiative states) up to seconds (for metastable states). If before the emission of a photon an electronically excited state hasn't suffered enough R - T collisions, the structure of the emission will retain the information about how this state was excited. As a rule, at elevated pressures the rotational distribution of electronically excited states has the same temperature as the temperature of the gas. Recently, a spectacular exception to this rule has been discovered in H_2O containing plasmas [88]. It has been shown that even at atmospheric pressure the rotational distribution of $OH(A)$ is not an image of the kinetic gas temperature but it reflects the formation processes. An extremely fast quenching of $OH(A)$ by water molecules has been proposed to explain this effect. Thus, even at atmospheric pressure the creation and loss processes of molecular excited states have to be carefully analyzed for correct T_g determination.

At low pressures the R - T relaxation times become of the same order and even greater than the radiative lifetimes. For example, in N_2 at 1 mbar the $\tau_{RT} \sim 8 \cdot 10^{-7}$ s while the radiative lifetime of $N_2(C^3\Pi)$ is $\tau_{rad} = 4 \cdot 10^{-8}$ s. Therefore, the rotational structure of the $N_2\ 2^+$ system at 1 mbar is an image of the excitation processes. It has been shown in [83] that even in low pressure conditions the temperature of the gas may be deduced from the rotational structure of the 2^+ system if the radiating state is excited predominantly by direct electronic impact. It is argued that light-weight electrons are not able to transfer a significant rotational momentum to a heavy N_2 molecule during the excitation process.



Therefore, transitions with a small change of angular momentum are dominant and the rotational distribution of the lower state is copied to the radiative state upon the excitation. Other population processes such as pooling or cascades from higher electronic states lead to

Experimental setup and diagnostic techniques

complex non-Boltzmann distributions of the rotational levels of $N_2(C^3\Pi)$ and make spectroscopic determination of T_g impossible. Thus, the validity of the spectroscopic technique should be carefully checked in every particular case.

2.2.2.2 OES setup and data treatment.

Depending on the spectral resolution of the optical system two strategies for spectroscopic data analysis may be used:

- If individual roto-vibrational lines are resolved, T_{rot}^C is deduced from a Boltzmann plot of the relative populations of the rotational levels of $N_2(C^3\Pi)$ [83][89].
- If the rotational structure is not resolved, the experimental spectra are compared with synthetic ones calculated for different T_{rot}^C and then the best-fit value of T_{rot}^C is deduced.

In our case the second possibility is employed and spectral modeling is performed using Specair [90] software package. The schematic of the experimental setup is shown in Figure 2. 10. The spectra are acquired using a 303 mm focal length spectrograph (Andor Shamrok SR-303i) with an 1800 l/mm holographic grating and an entrance slit of 100 μm . The spectral window that can be recorded without moving the grating is 20 nm and the spectral resolution is 0.2 nm. The most intense 2^+ (0-0) band at 337 nm is used.

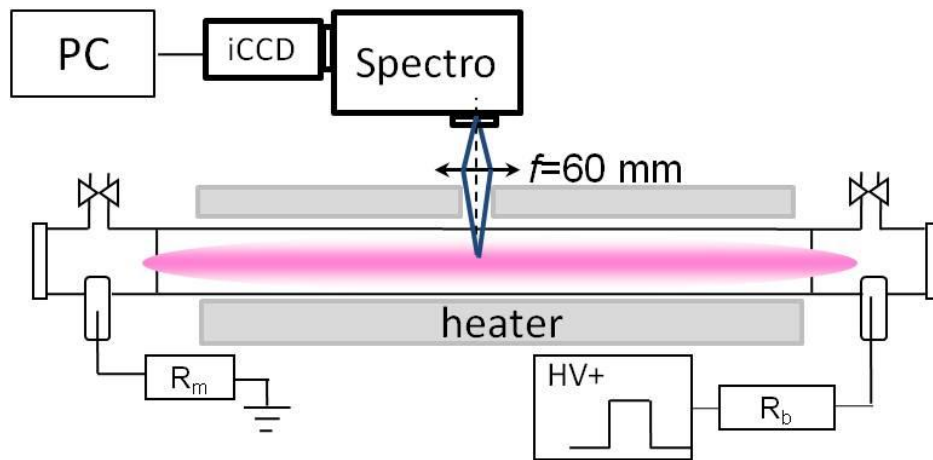


Figure 2. 10 Spectroscopic setup for T_{rot}^C determination in the pulsed DC discharge.

Discharge emission is collected by a 60 mm focal length fused silica lens. Time resolved measurements in the pulsed DC discharge are performed by setting the delay of the iCCD gate with respect to the beginning of the discharge. In order to measure the T_g kinetics in the post-discharge, plasma-induced fluorescence (PIF) technique is employed [21]. Short additional discharge pulses are applied after the end of the main pulse in order to re-excite the 2^+ emission. Figure 2. 11 illustrates the principle of time-resolved measurements during the main discharge pulse and in the afterglow.

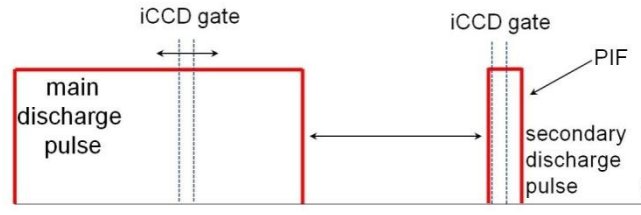


Figure 2. 11 Discharge and iCCD triggering during the main plasma pulse and in the post-discharge (PIF).

Observation of the discharge emission perpendicular to the tube axis in front of its midpoint is required for PIF measurements. When the gas temperature is decreased after the end of the main pulse, a simultaneous contraction of the volume of the afterglow column takes place due to the constant pressure condition; a fresh cold gas is then pushed in the reactor. Therefore, in the afterglow of the main pulse the gas in the reactor is stratified and when it is re-excited by the secondary pulses emission from the “hot” part only should be collected. The main disadvantage of the radial observation compared to the axial one is that the light from different radial positions is collected and an effective average value of the temperature is measured.

A tubular heater shown in Figure 2. 10 is used for experimental validation of the spectroscopic gas temperature determination technique in the conditions of this work. The discharge tube is heated at 300 – 700 K and the gas (pure N₂ or N₂/O₂=4/1 at 1.33 mbar) is excited by short (30 μs) discharge pulses; no significant perturbation of the gas temperature could occur on such a short timescale. Using Specair a set of synthetic spectra is calculated for T_{rot}^C in the range 300 – 700 K with 10 K step. Then the best fit value of T_{rot}^C is found using the least-squares method. The uncertainty of the fitting procedure is estimated to be ± 30 K.

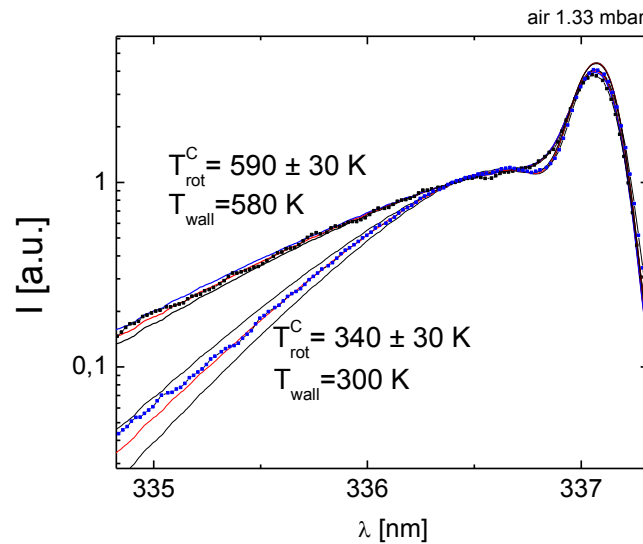


Figure 2. 12 Fitting of experimental spectra using Specair for two different temperatures of the reactor walls. The uncertainty of the T_{rot}^C determination is estimated to be ± 30 K.

Experimental setup and diagnostic techniques

In Figure 2. 13 values of T_{rot}^C are compared with the experimentally measured temperatures of the discharge tube walls. One can see that a good general agreement is obtained, especially for $T_{wall} > 400$ K. For lower temperatures an overestimation by about 50 K can be seen. Nevertheless, we conclude that in the conditions of our pulsed DC discharge at mbar pressure T_{rot}^C gives a good estimation of the neutral gas temperature.

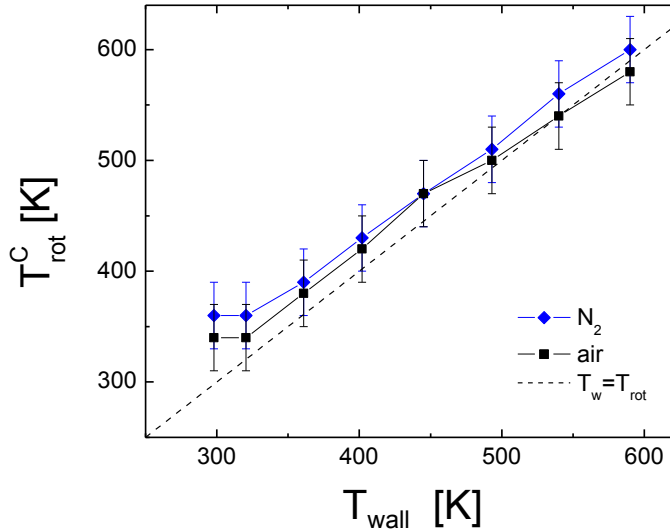


Figure 2. 13 Comparison between the rotational temperature of $N_2(C)$ obtained using the Specair fitting and the temperature of the reactor walls. The gas mixture in the reactor is pure nitrogen or air at 1.33 mbar, discharge pulse duration is 30 μ s.

2.2.2.3 Time resolved measurements of ozone concentration

The same spectroscopic system is employed for time resolved *in-situ* measurements of ozone concentration by absorption in Hartley band centred at 253,7 nm. This time a 600 l/mm grating is used allowing for a spectral interval of 70 nm to be recorded by the iCCD. Fused silica windows are fixed on each end of the tube and a deuterium tungsten halogen lamp (Ocean Optics DH-2000) is used as a broad-band UV source. Measurements are performed in the afterglow of a pulsed discharge and ozone kinetics is studied by setting the iCCD gate with respect to the discharge end. For every given delay absorption spectra are averaged over 100 discharge pulses.

The absorption cross section of ozone is taken from [91] and $[O_3]$ is deduced from the fitting of experimental spectra. In Figure 2. 14 an example of the fit for $[O_3]=2.65 \cdot 10^{14} \text{ cm}^{-3}$ is shown. Minimum detectable absorbance in this experiment is ~ 0.001 which corresponds to the O_3 detection limit of the order of 10^{12} cm^{-3} .

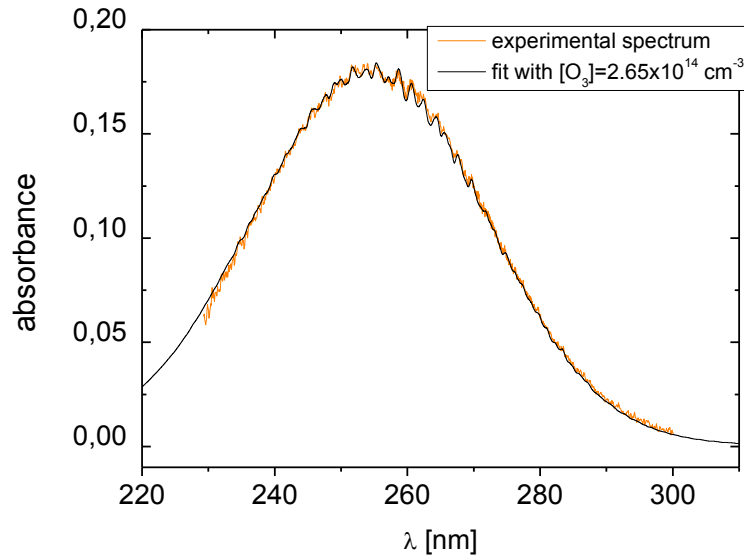


Figure 2. 14 Comparison between calculated and measured absorbance of O_3 . Deduced value of $[O_3]$ is $2.65 \cdot 10^{14} \text{ cm}^{-3}$.

2.2.3 TALIF measurements of atomic oxygen.

Laser induced fluorescence techniques are widely employed for time and space resolved measurements of absolute species concentrations in plasmas [92][93][94][95]. For LIF detection of atomic ground states (O, N, H, etc) VUV photons are required, what present a big complication from the experimental view point. Consequently, a non-linear two photon absorption laser induced fluorescence (TALIF) technique is usually used. The efficiency of 2-photon absorption is relatively small and excitation with focused laser radiation should be performed in most cases. This implies a good space resolution which is limited by the dimensions of the focus. Absolute calibration of TALIF measurements using noble gases has been proposed in [93].

2.2.3.1 Principles and calibration of O TALIF measurements.

The scheme of the 2-photon excitation and subsequent emission for O and Xe atoms is shown in Figure 2. 15. Calibration is based on the reference measurements with a known concentration of Xe. TALIF signals of both O and Xe should be measured with the same spatial and temporal intensity distribution of the laser radiation. This condition is best satisfied when the 2-photon transitions are spectrally as close as possible what determines the choice of the calibration partner.

In normal conditions the intensity of the fluorescence scales as a square of the excitation laser intensity. However, a number of non-linear effects [96] (step-wise ionization, depletion of the ground state population and stimulated emission) may significantly alter the normal behaviour

Experimental setup and diagnostic techniques

when the laser intensity is increased. Therefore, for calibration the laser power should be kept as low as possible.

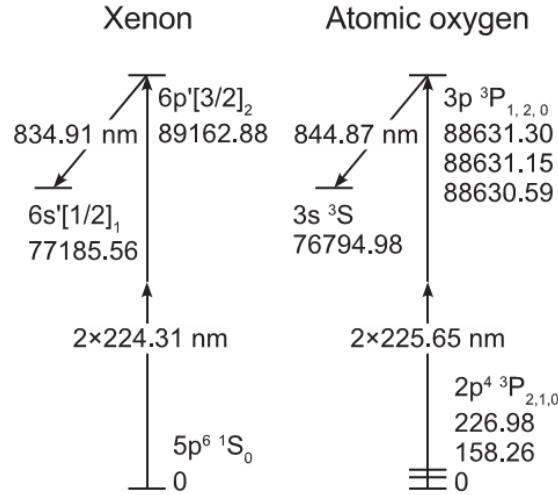


Figure 2. 15 TALIF excitation scheme of O and Xe atoms.

If all the required conditions are fulfilled the concentration of atomic oxygen (n_O) may be calculated using the following formula [93]:

$$n_O = s \frac{\gamma_{Xe}}{\gamma_O} \frac{A_{ik}(Xe)}{A_i(Xe) + Q(Xe)} \frac{A_i(O) + Q(O)}{A_{ik}(O)} \frac{\sigma^2(Xe)}{\sigma^2(O)} \frac{I_F(O)}{I_F(Xe)} n_{Xe} \quad (2.5)$$

where s is the statistical factor accounting for the splitting of the O ground state, γ is the relative detection efficiency of the optical system at the corresponding fluorescence wavelength. A_{ik} , A_i and Q – stand for the Einstein coefficient of the fluorescence transition, spontaneous emission and quenching rate of the excited state. σ^2 – 2-photon excitation cross section and I_F is the temporally and spectrally integrated fluorescence intensity. All the required atomic data can be found in the literature [92].

2.2.3.2 Laser setup

The schematic of the laser setup is shown in Figure 2. 16. Tuneable laser radiation at 225 nm is generated by frequency doubling the 450 nm output of a dye laser (Sirah, Coumarin 2 dye) pumped by the third harmonic of a pulsed Nd:YAG laser (Quanta-Ray). Up to 1.5 mJ with pulse duration of 5 ns at a repetition rate of 10 Hz are obtained. The laser energy is monitored by a pyroelectric detector equipped with a signal amplifier. The laser beam is focused into the discharge tube by an $f=300$ mm fused silica lens. Oxygen and xenon fluorescence signals are collected by an $f=60$ mm lens on a Hamamatsu R3896 photomultiplier equipped with an interference filter centred at 840 nm. The PMT signal is digitalized by an oscilloscope

(LeCroy Weverunner, 1GHz) and analyzed on a PC by a LabView routine. Time resolved fluorescence signals of Xe (0.13 mbar) and O are shown in Figure 2. 17.

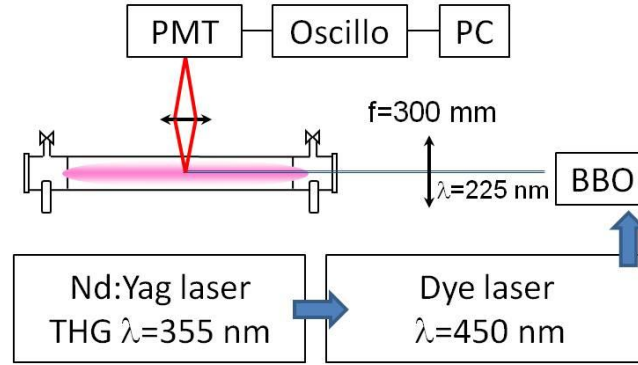


Figure 2. 16 Schematic of the TALIF setup.

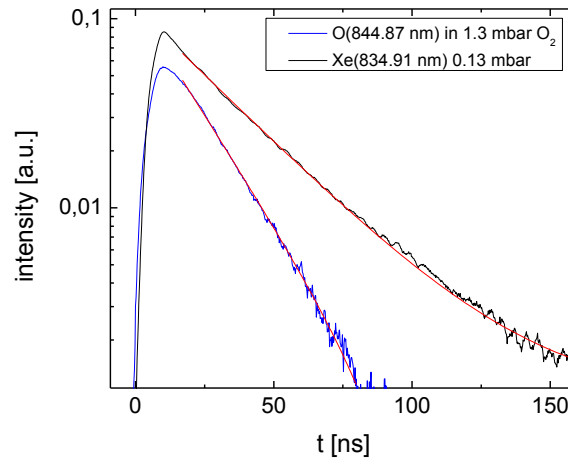


Figure 2. 17 Time-resolved fluorescence signals of Xe and O.

Two types of TALIF measurements are typically performed. When the absolute concentration of atomic oxygen is measured, the frequency of the laser is scanned over the two-photon excitation resonance and time-integrated fluorescence signals are recorded for each spectral position of the laser. Two-photon excitation line profiles of O and Xe recorded in such way are shown in Figure 2. 18. The value of I_F is obtained by spectral integration of the lines. Using the described technique the absolute calibration of TALIF measurements is performed with the laser energy of 17 $\mu\text{J}/\text{pulse}$. According to literature data [92] (where similar laser focusing optics was used) we expect that at 17 $\mu\text{J}/\text{pulse}$ both Xe and O TALIF signals are in normal excitation regime and saturation effects are negligible.

Experimental setup and diagnostic techniques

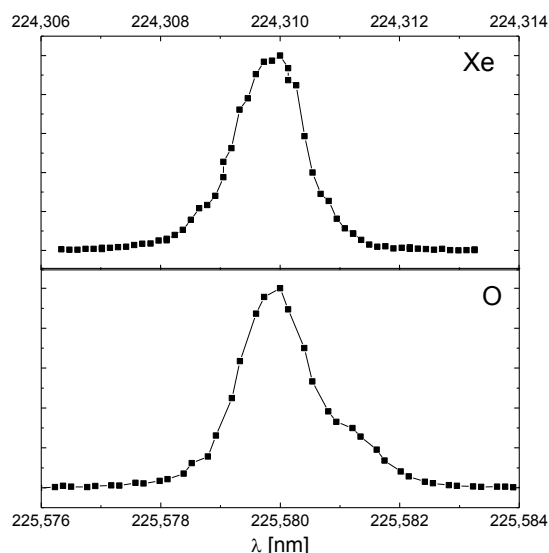


Figure 2. 18 Two-photon excitation line profiles of O and Xe.

Once the calibration is performed, the relative measurements of the O density with respect to the calibration conditions are done with higher laser energy (typically 100-200 $\mu\text{J}/\text{pulse}$). This allows better detection limits due to the increase of the fluorescence intensity. In [92] it is shown that the saturation effects in two-photon excitation of O start to play a role starting from the laser energy of the order of 150 $\mu\text{J}/\text{pulse}$ in conditions similar to ours. Anyhow, the relative measurements may be performed even when the saturation effects are important. The essential is that the TALIF intensity is linearly proportional to the concentration of O, which holds true in a broad range of laser energies [94]. The relative error of absolute O concentration measurements was estimated to be 30%.

For kinetic measurements of [O], the wavelength of the laser is set to the maximum of the excitation line profile. Then the time integrated intensity of the fluorescence is measured with variable delay between the discharge beginning/end and the laser pulse. This technique allows, for example, measurements of the O lifetime in the afterglow of a pulsed DC discharge in O_2 .

2.2.4 Mass spectrometric gas analysis

One of the disadvantages of the laser absorption technique described in the previous sections is that the species that can be monitored are exclusively molecules having dipole allowed transitions in mid-IR. In addition the number of simultaneously detected molecules is limited due to the narrow tuning range of the lasers. In order to get information about the complete gas composition in the reactor including atomic and homonuclear gases, a quadrupole mass spectrometer (QMS) is used in this work.

A quadrupole residual gas analyzer Pfeiffer PrismaPlus 0-100 a.m.u. equipped with an open ion source and a secondary electrons multiplier is mounted on a separate vacuum vessel

pumped down to 10^{-9} mbar by a turbo molecular pump. Using this simple system, species having the mass difference $\Delta m=1$ a.m.u. can be easily distinguished. The optimum operating pressure of the MS is 10^{-6} – 10^{-5} mbar; a leak valve (UDV 040) is used in order to introduce the gases from the reactor into the MS chamber. For absolute measurements of stable species concentrations a calibration of the MS is performed using gas mixtures having a known composition. Concentrations are always measured with respect to the number density of the carrier gas (Ar, N₂ or O₂). The limit of detection for different species depends strongly on the carrier gas and mutual mass interferences, typically it is found in the range 10-100 ppm.

In Figure 2. 19 mass spectra and a calibration graph for C₂H₂ are shown. After the correction of the MS background the calibration is described by a straight line going through the origin.

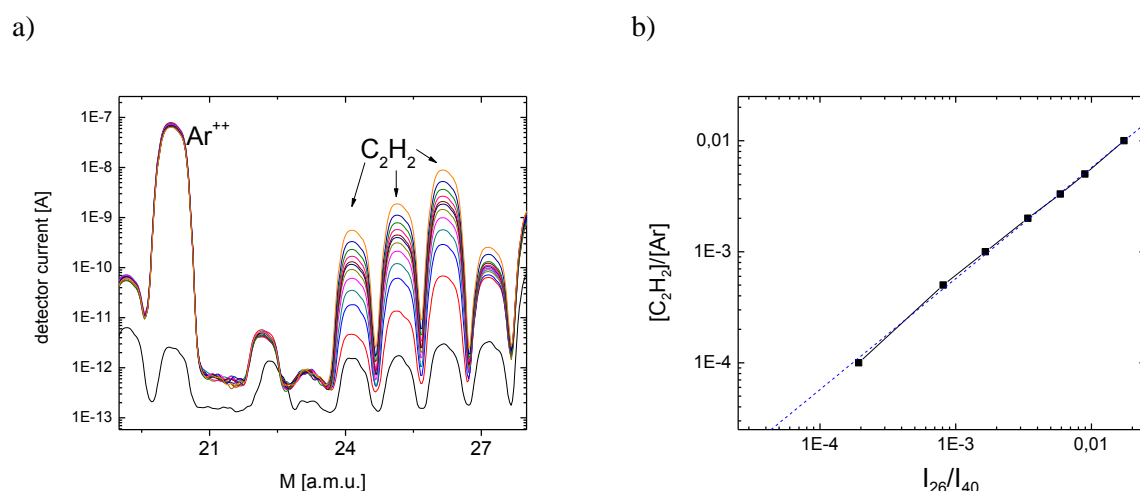


Figure 2. 19 a) Mass spectra of C₂H₂ in Ar for (0.01 – 1)% C₂H₂ b) calibration graph showing the number density ratio $[C_2H_2]/[Ar]$ as a function of the ratio of MS signals at $m=26$ and 40 a.m.u respectively.

Time resolution of the mass spectrometric measurements is limited by the time of the gas sampling through a 3 mm i.d. tube that connects the reactor with the inlet valve of the MS, which was of the order of 10 s. However, for investigation of processes that take place in the gas phase and on the surface, much better effective time resolution can be achieved by using a pulsed dc discharge. Typically in our experiments, we apply a short (few milliseconds long) discharge pulse to a gas mixture in static conditions and then perform measurements with the mass spectrometer. This approach doesn't allow a distinction between processes that take place during plasma ON and in the post discharge. But we will see that it permits to follow the kinetics of adsorption and desorption of atoms on the surface under plasma exposure.

2.2.5 XPS surface diagnostics

X-ray photoelectron spectroscopy (XPS) is a quantitative technique for probing the elemental composition and the bonding of different materials. XPS spectra are obtained by irradiating a material with a beam of monochromatic x-rays. The kinetic energy and the flux of electrons that escape from the material surface layer are measured in ultra high vacuum conditions.

Experimental setup and diagnostic techniques

In this work we use the XPS facility of the Ruhr University of Bochum for the analysis of silica surface exposed to different low pressure plasmas. XPS analysis is performed using a Versaprobe spectrometer from Physical Electronics (PHI 5000 VersaP-robe) with monochromatic Al K α (1486.6 eV) radiation and spectral resolution of 0.35 eV. In order to avoid positive charge build up in case of non-conducting samples, a low energy electron and Ar⁺ beams are directed on the analysed surface. The detection limit of the XPS system is typically of the order of 0.1 at. % and the depth of the probed surface layer is ~ 2 nm.

2.2.6 Summary on used diagnostics

In this study we employ essentially diagnostics for probing gas phase species which are summarized in Table 2. 3.

Technique	Species	Time resolution	Detection limit [cm ⁻³]	In-situ
TDLAS	NO, NO ₂	5 ms	10 ¹²	Yes
QCLAS	C ₂ H ₂ , CO, CO ₂ , N ₂ O	5 μ s	10 ¹² - 10 ¹³	Yes
UV-abs	O ₃	2 ms	10 ¹²	Yes
TALIF	O	200 ns	10 ¹³ -10 ¹⁴	Yes
QMS	all stable m=1 – 100 amu	~ few ms	10 ¹³ -10 ¹⁴	No

Table 2. 3 Summary on used diagnostics

3. Chapter III: Adsorption and reactivity of N atoms on silica surface under plasma exposure

3.1 Introduction

At present the information on the mechanisms of interaction between nitrogen atoms and silica-like surfaces is obtained from the studies of N losses on the surface. Regardless a great number of works devoted to the investigation of atomic recombination there is still a lot of uncertainty. Recombination probabilities of atomic nitrogen on silica-like surfaces measured by different authors span over 5 orders of magnitude $\gamma_N = 5 \cdot 10^{-8} - 2 \cdot 10^{-3}$ [56][97]! Even the kinetic order of the recombination reaction is not well established, in different studies the first [5] [98] or the second [99] [100] order in N density is proposed. The role of plasma exposure is also barely understood, it is only known that treatment of the surface by N₂ plasma enhances the value of γ_N by about an order of magnitude [97] [101].

The approach developed in this chapter is complementary to the recombination studies. We investigate stable N atoms that are adsorbed on the surface. According to existing models of surface recombination[5][26], chemisorbed N atoms are the main sites for N recombination on silica-like surfaces. Therefore, by characterizing the **coverage** and the **reactivity** of N_{ads} we can get an insight in the mechanism of atomic recombination on the surface.

Speaking more generally, our aim in this chapter is to understand how N_{ads} participate in the **production of molecules** on silica-like surfaces in contact with N₂/O₂ plasmas and afterglows. We will investigate therefore formation of N₂ on the surface in recombination process N_{ads} + N and formation of NO in reaction N_{ads} + O.

3.1.1 Experimental procedures

Here we employ the experimental approach outlined in Chapter 1 that consists in the pretreatment of silica surface by N₂ plasma followed by the study of grafted N species. Typically, the pretreatment is performed using a rf discharge in flowing nitrogen. Standard discharge parameters during the pretreatment are shown in Table 3.1. In the same table standard conditions for treatment with O₂ and Ar plasmas are listed.

Adsorption and reactivity of N atoms

	N ₂	O ₂	Ar
Pressure (mbar)	0.53	0.53	0.27
Gas flow (sccm)	10	10	10
P _{pl} ¹ (W)	17	16	13

¹power dissipated in plasma

Table 3.1 Standard discharge conditions for N₂, O₂ and Ar plasma pretreatments.

After the pretreatment we probe the surface trying to answer the following questions:

- What is the coverage of adsorbed N atoms?
- What is their role in surface recombination of N?
- What is their role in production of NO on the surface?

Three types of experimental techniques were employed:

- *XPS analysis.* Small silica samples were placed on the inner surface of the discharge tube and pretreated in standard conditions for different time intervals. Pretreated samples were removed from the reactor and analyzed *ex-situ* using x-ray photoelectron spectrometer at Ruhr University Bochum. The samples are made of the same material as silica discharge tube and they experience the same plasma pretreatment. Therefore, with this experiment we investigate the modification of the chemical composition of the inner surface of silica discharge tube after different plasma exposures and determine the number of N atoms grafted to the surface.
- *Reactivity of N_{ads} under ³⁰N₂ plasma exposure.* XPS diagnostics gives insight into the density and binding configuration of adsorbed species, but not about their ability to produce molecules on the surface. To investigate the reactivity of N_{ads} we should look at the products of surface catalyzed reactions. In the first instance silica surface pretreated by ²⁸N₂ plasma was exposed to a discharge in heavy nitrogen isotope ³⁰N₂. Molecules ¹⁴N¹⁵N produced on the surface and detected in the gas phase by a mass spectrometer carry information about surface recombination processes in N₂ plasma. By measuring the absolute density of ¹⁴N¹⁵N in the gas phase we determine the initial coverage of ¹⁴N_{ads}.
- *Reactivity of N_{ads} under O₂ plasma exposure.* The pretreated surface containing N_{ads} was exposed to a pulsed discharge in O₂. Production of NO molecules from surface recombination (O+N_{ads})_{wall} was monitored using laser absorption spectroscopy. This experiment provides two types of information: (i) first, NO production is an alternative way to probe the density and reactivity of N atoms adsorbed on SiO₂ under N₂ plasma exposure (ii) second, kinetics of NO formation in recombination between O and N_{ads} gives an insight in the mechanism of NO production on the surface in N₂/O₂ plasmas.

3.2 Determination of the coverage of N_{ads} : XPS study

3.2.1 Dynamics of N adsorption on SiO_2

Small ($10\text{mm} \times 10\text{mm} \times 5\text{ mm}$) silica samples were placed on the inner surface of silica discharge tube. First they were cleaned by rf O_2 plasma at $p=0.53\text{ mbar}$ and $P_{pl}=16\text{ W}$ and then by Ar plasma at $p=0.26\text{ mbar}$ and $P_{pl}=13\text{ W}$. As we will see later, after this cleaning procedure the surface is free from adsorbed nitrogen and oxygen atoms. This is the standard initial condition for surface pretreatment with N_2 plasma. Clean samples were treated during 1 – 360 min by a flowing capacitive rf discharge in N_2 in standard conditions.

For each sample a low resolution survey XPS spectrum was taken to determine the most important elements. Survey spectra of just cleaned sample and samples treated during 1, 25 and 360 minutes are shown in Figure 3. 1. One can see the peaks corresponding to silicon $Si(2s, 2p)$ and oxygen $O(1s)$ coming from SiO_2 structure. Appearance of carbon $C(1s)$ is due to the pollution during the exposure to the ambient air before analysis and nitrogen $N(1s)$ appears due to N_2 plasma exposure.

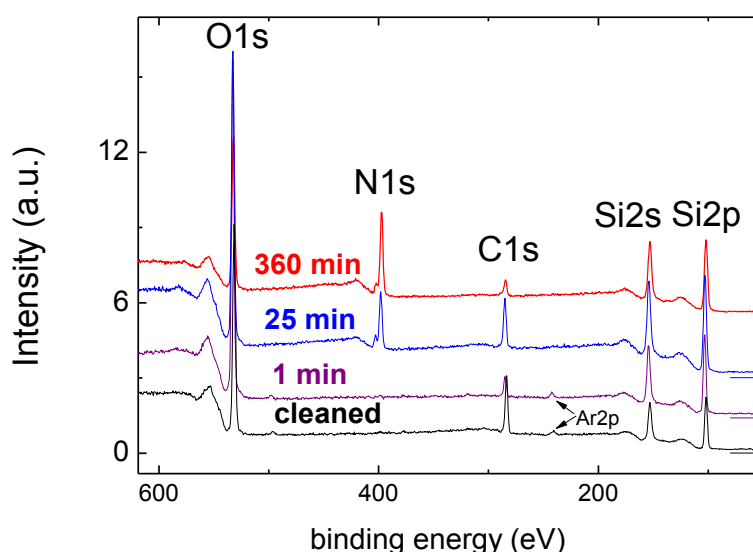


Figure 3. 1 Survey XPS spectra of SiO_2 samples just cleaned and treated by N_2 plasma in standard conditions during 1, 25 and 360 minutes.

For relative concentration measurements high resolution XPS spectra (0.35 eV resolution) of the main peaks were recorded. Figure 3. 2 shows high resolution spectra of $Si2p$, $O1s$, $N1s$ and $C1s$ in the sample that was treated by N_2 plasma during 25 minutes. Spectra were analysed using Unifit software and the relative concentrations of species were obtained from integrated peak areas using known sensitivity of the XPS spectrometer.

Adsorption and reactivity of N atoms

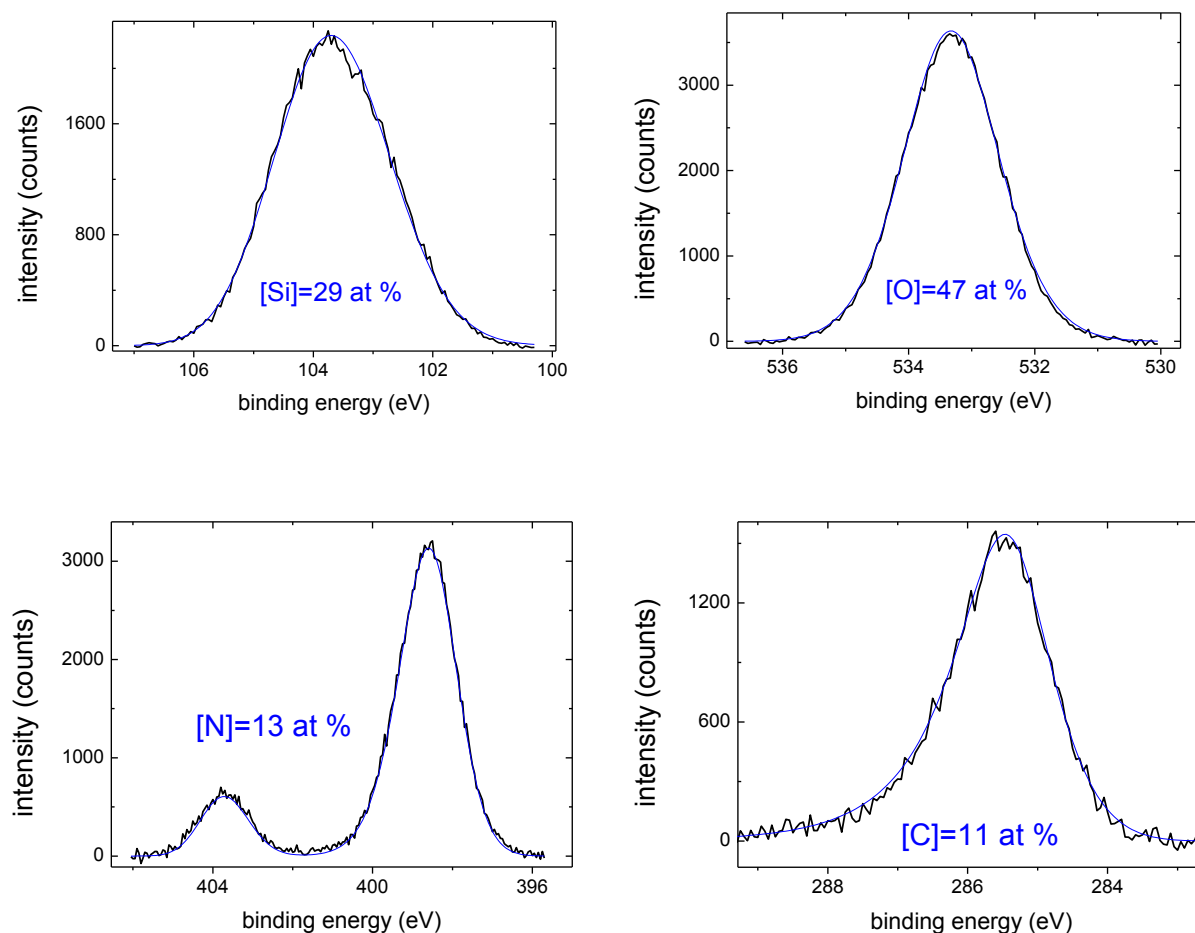


Figure 3. 2 High resolution XPS spectra of silica sample treated during 25 min by N_2 plasma in standard conditions. Four panels show the main peaks – Si(2p), O(1s), N(1s) and C(1s). Blue curves represent the result of fitting using Unifit software. Concentrations of elements in relative atomic percent are inscribed on the graphs.

One can see that N(1s) consists of two peaks at 398.7 eV and 403.7 eV. Similar double-peak structure of N(1s) has been previously observed in [17][102] in nitrided SiO_2 thin films. The peak at 398.7 eV is usually assigned to Si_3N_4 configuration in which every N atom is bonded with three silicon atoms, such as in Si_3N_4 [17][102]. According to [102] the second peak at 403.7 eV may be assigned to Si- NO_2 binding configuration; but in [103] this peak was attributed to free molecular-like N_2 in the SiO_2 lattice. Whatever is the exact binding structure of nitrogen on the surface, spectra shown in Figure 3. 2 prove that N atoms are not simply chemisorbed on SiO_2 , but **nitridation** of silica surface takes place under N_2 plasma exposure. Nitridation of SiO_2 thin films in N_2 plasma is a known phenomenon from microelectronics technology [17] but it is completely overlooked in studies of atomic recombination on the surface.

Figure 3. 3 shows the evolution of relative atomic concentrations of Si, O and N as a function of the pretreatment duration. After 1 minute of N_2 plasma treatment no detectable incorporation of N is observed and the measured composition of the sample is the same as in

pure SiO_2 ($[\text{Si}]/[\text{O}]=1/2$) within the experimental uncertainty. For longer pretreatment times the concentration of nitrogen increases and the composition of the surface layer can be approximately described by the formula $\text{SiO}_{2-x}\text{N}_x$. This means that nitrogen atoms replace oxygen on the surface while the concentration of silicon stays constant. After 6 hours of plasma exposure $x \approx 1$, i.e. approximately 50% of O atoms in the layer probed by XPS are replaced by N. According to [17], the escape depth of photoelectrons in SiO_2 is $\lambda_{\text{SiO}_2}=24.2 \text{ \AA}$. This means that the measured composition is an average over several atomic layers and it is quite probable that the outmost layer may be composed of pure Si_3N_4 containing no oxygen at all.

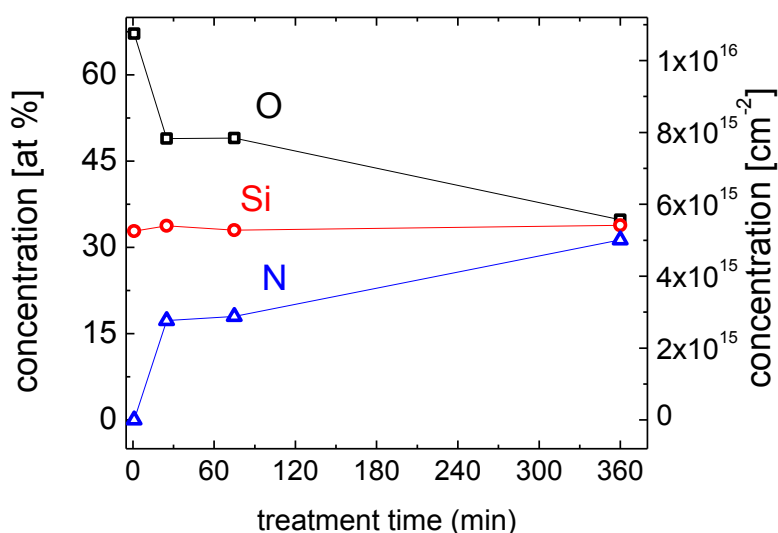


Figure 3. 3 Relative atomic concentrations of O, Si and N in SiO_2 sample after different duration of N_2 plasma treatment. The right axis gives an estimation of the absolute surface densities of species (for more details see the text).

One can see that the rate of nitridation varies a lot during the plasma exposure. Within the first 25 minutes the same amount of N is incorporated in the surface as during the following 330 minutes. This may be explained by a fast nitridation of the superficial layer followed by much slower penetration of N deeper under the surface.

Using the data from [17] the absolute surface density of N in the silicon oxynitride layer may be estimated based on the XPS measurements. With the known concentration of atomic oxygen in SiO_2 ($[\text{O}]=4.4 \cdot 10^{22} \text{ cm}^{-3}$) and the escape depth of photoelectrons $\lambda_{\text{SiO}_2}=24.2 \text{ \AA}$ the surface density of oxygen atoms in the layer probed by x-rays was estimated to be $[\text{O}]=1.06 \cdot 10^{16} \text{ cm}^{-2}$. This allowed the absolute calibration of the atomic concentrations measured by XPS. The right hand axis in Figure 3. 3 represents absolute atomic concentrations obtained in this way.

It should be noted that absolute calibration is justified only for smooth surfaces and it may give some error for real rough samples.

Adsorption and reactivity of N atoms

3.2.2 Species responsible for nitridation: ions or neutrals?

In order to estimate the relative role of ions/neutrals in the nitridation process a silica sample was placed in the flowing post discharge zone. The gas transit time between the end of the discharge zone and the position of the sample was ~ 50 ms. This time is shorter than the typical lifetime of N with respect to surface recombination on silica (~ 200 ms) [5]. Therefore, significant fraction of atomic nitrogen is still remaining in the position where SiO_2 sample is placed. Vibrationally excited N_2 molecules having the lifetime of the order of 100 ms in our conditions may also be present.

After 75 minutes of the post discharge exposure the measured concentration of N in the sample was only 0.2 at % while under direct plasma exposure the same duration of the pretreatment gave $[\text{N}] = 18$ at %. Therefore, bombardment with ions and short lived excited species is mainly responsible for nitridation of SiO_2 . Nitrogen atoms alone are inefficient for nitridation. This result is in agreement with observations of [17], where it was shown that the density of N atoms in the N_2 plasma nitrided SiO_2 is proportional to the number of incident nitrogen ions.

Silica samples were pre-treated in the positive column of the rf discharge, far from electrode zones. Thus, only low energy ions (with energies of the order of ~ 10 eV) are expected to arrive on the surface [44]. However, even in such mild conditions ion bombardment has a strong impact on the surface. This is confirmed by observed nitridation of SiO_2 .

Another striking observation was made in a SiO_2 sample just treated by Ar plasma. In the XPS spectrum of this sample shown in Figure 3. 1 a peak around 240 eV can be seen, which is assigned to Ar(2p) [104]. Argon atoms do not form chemical bond with SiO_2 , what means that they are implanted in the sample under Ar plasma exposure. Implantation of noble gases under ion beam bombardment is well documented, but for ion energies in the range of keV [105]. Observation of Ar implantation confirms previous conclusion about the important role of ion bombardment of SiO_2 surface in the conditions of this study.

3.2.3 Reactivity of SiO_xN_y under plasma exposure

Here using XPS diagnostics we investigate stability and reactivity of silicon oxynitride layer under plasma exposure. First, silica samples were pre-treated in standard conditions by N_2 plasma during 75 minutes. On the second step the samples were exposed to oxygen or argon plasma in standard conditions (see Table 3.1) for various time duration. The results of XPS measurements of relative atomic concentration of nitrogen after different sequences are summarized in Table 3. 2. One can see that 1 hour of O_2 or Ar plasma is enough to remove SiO_xN_y layer almost completely. Concentrations $\sim 0.4 - 0.5$ at % measured after long cleaning periods are close to the detection limit of the XPS spectrometer.

Gas	Duration	[N] at %
just pre-treated by N ₂ plasma		18
O ₂	1 min	4.4
O ₂	60 min	0.4
O ₂	120 min	0.4
Ar	60 min	0.5

Table 3. 2 Concentration of atomic N in silica samples treated by N₂ plasma during 75 minutes followed by O₂ or Ar plasma exposure for different time intervals.

Figure 3. 4 shows high resolution XPS spectra of N(1s) in samples that were exposed to O₂ plasma during 1 and 60 minutes after 75 minutes of N₂ plasma pretreatment. According to the absolute calibration shown in Figure 3. 3 during 1 minute of O₂ plasma exposure about $2 \cdot 10^{15}$ nitrogen atoms per cm⁻² are removed from the surface. This proves that N atoms that form SiO_xN_y layer are reactive when exposed to O₂ or argon plasma.

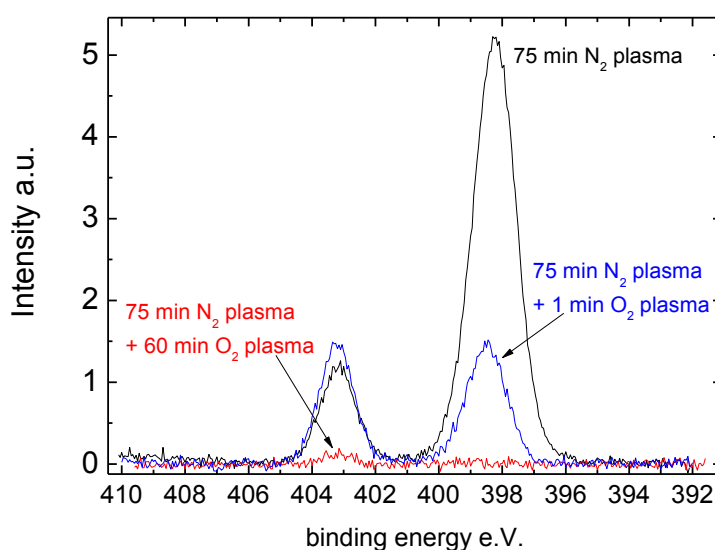


Figure 3. 4 XPS spectra of N(1s) doublet in SiO₂ samples pre-treated by N₂ plasma during 75 min (—) followed by 1 min (—) and 60 min (—) of O₂ plasma.

It is interesting to note that the peak at 398.7 eV disappears much faster than the one at 403.7 eV. After 60 minutes of O₂ only this high energy peak is observed. Therefore, N atoms corresponding to the low energy peak are more reactive. This observation is coherent with the assignment of the peaks that was made above. Superficial nitrogen that forms Si₃N₄ on the surface (398.7 eV peak) is more reactive than molecular-like nitrogen trapped in the SiO₂ lattice (403.7 eV peak).

Adsorption and reactivity of N atoms

The mechanism of SiO_xN_y layer removal under Ar plasma exposure is not clear. It may be due to argon ion bombardment or due to reactions with oxygen atoms coming from trace (~ 1 ppm) amounts of O_2 and H_2O in argon gas.

We have seen that SiO_xN_y formed by N_2 plasma pretreatment is reactive under O_2 plasma exposure. It is interesting to check what happens if both N_2 and O_2 are present in the discharge simultaneously. A pretreatment of silica sample by air ($\text{N}_2/\text{O}_2 = 80/20$) plasma during 75 min at $p=0.53$ mbar and $P_{\text{pl}}=16\text{W}$ was performed. The concentration of N measured in this case was rather low $[\text{N}]=0.5$ at % and only high energy peak at 403.7 eV was observed. Therefore, the presence of oxygen in plasma inhibits formation of the Si_3N_4 layer on SiO_2 surface. However, some minor incorporation of molecular-like N_2 still takes place due to the bombardment by nitrogen ions.

3.2.4 Conclusions on XPS study

In this section we have applied ex-situ XPS diagnostics in order to investigate the state of the surface of silica discharge tube after different plasma exposures. We have found that:

- Under N_2 plasma exposure nitridation of SiO_2 takes place. Nitrogen atoms replace oxygen atoms on the SiO_2 surface and SiO_xN_y layer is formed. The surface density of N atoms in SiO_xN_y layer after 60 min of N_2 plasma pretreatment is $3 \cdot 10^{15} \text{ cm}^{-2}$, i.e. of the order of one full monolayer,
- The nitridation is driven by ion bombardment and it doesn't take place when SiO_2 is exposed to a neutral flow containing N atoms (or at least it is much less efficient). At present we cannot specify the exact role of ions; bombardment with N_2^+ ions may either directly lead to nitridation of SiO_2 or just activate the incorporation of N atoms. To distinguish between these pathways experiments with independent ion and atomic beams should be performed.
- Silicon oxynitride layer is removed when it is exposed to O_2 or Ar plasma. Nitrogen atoms that are more reactive under O_2 plasma contribute to the characteristic peak at 398.7 eV in the XPS spectrum which is usually assigned to Si_3N_4 structure.

Our results demonstrate that the simplified vision of recombination of N atoms on a “static” SiO_2 surface is not applicable in the case of direct N_2 plasma exposure. In reality the outmost surface layer is continuously modified due to bombardment with ions and N atoms. Nitrogen atoms are not chemisorbed on sparse active sites, but form a SiO_xN_y layer that after long exposure time may contain equal amounts of N and O atoms.

Generally speaking, in the case of SiO_xN_y formation the term “chemisorption” has to be clarified. Can we consider N atoms in the SiO_xN_y layer as chemisorbed? On the one hand, the answer is positive, because these atoms are chemically bonded with the atoms of the surface. On the other hand it is known from the literature [17] that on SiO_2 the thickness of the layer nitrided by N_2 plasma may reach 2-3 nm. It would be unjustified to use the term “chemisorbed” for N atoms implanted in the material; by definition chemisorption takes place on the surface, but not in the material bulk.

Probably, the most appropriate term that should be used in this case is **sorption** which includes surface adsorption and incorporation of atoms. Nevertheless, we could not find in the literature any example of the use of this term in relation to surface reactivity in plasmas. In order to avoid any misleading of the readers we will continue to use the word **adsorption** but keeping in mind that it may also infer incorporation of N atoms within 2-3 nm layer on the SiO₂ surface. We will use terms **grafted or adsorbed N atoms** to describe all the stable nitrogen atoms present on the silica surface treated by N₂ plasma.

3.3 Reactivity of N_{ads}: Isotopic study

In the previous section we have evidenced adsorption of nitrogen atoms on SiO₂ using XPS diagnostics. Do these atoms participate in surface-catalyzed reactions in N₂ plasma? To answer this question, N_{ads} should be characterized from the viewpoint of their **reactivity**. XPS diagnostics is not sensitive to the reactivity of adsorbed species; therefore, in addition to a classical surface diagnostics a different technique capable of probing the reactivity of N_{ads} has to be applied. In this section we develop a new experimental approach that uses the isotopic exchange $^{14}\text{N} \leftrightarrow ^{15}\text{N}$ on the surface under plasma exposure. With this method we detect in the gas phase the products of surface reactions catalyzed by adsorbed N atoms and thus get information about the reactivity of N_{ads}.

3.3.1 Experimental details

The employed experimental procedure is shown schematically in Figure 3. 5. First, the silica discharge tube was pre-treated by ²⁸N₂ plasma in standard conditions. Then the reactor was pumped during 10 minutes to remove gas phase ²⁸N₂ and to let the wall cool down to the room temperature. Then the tube was filled with ³⁰N₂ (Sigma-Aldrich, 98 at % ¹⁵N) at 0.53 mbar and an rf discharge (probe discharge) with standard parameters was started in closed reactor for various time duration. Grafted ¹⁴N atoms react under ³⁰N₂ plasma exposure leading to appearance of ²⁹N₂ and ²⁸N₂ in the gas phase. Mass spectrometer was used to detect these products in the probe discharge. The response time of the gas inlet system of the mass spectrometer was not enough to follow production of molecules *in-situ* in real time. Therefore, the kinetic measurements were performed by stopping the probe discharge after a certain exposure time.

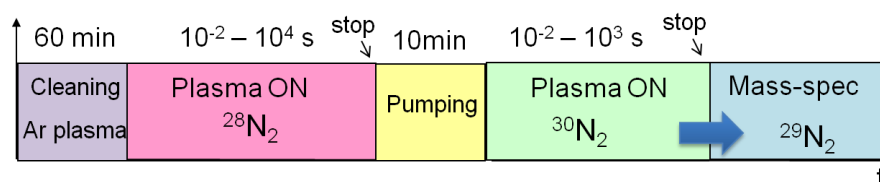


Figure 3. 5 Experimental procedure of the isotopic study.

Adsorption and reactivity of N atoms

Two types of experiments were performed:

- *Investigation of adsorption kinetics:* the pretreatment duration was varied while the length of the probe discharge was fixed. Before each experiment the tube was cleaned by argon plasma in order to have the same state of the surface in the beginning of N_2 plasma pretreatment.
- *Investigation of the reactivity of grafted nitrogen:* the pretreatment duration was fixed, while the probe discharge duration was varied. Typically, we used rf discharge for pretreatment and probing the reactivity of $^{14}N_{ads}$. For more precise dosing of atomic nitrogen in some experiments we used dc discharge with pulse duration of 5 ms.

With the mass spectrometer relative concentrations of three nitrogen isotopologues ($^{30}N_2$, $^{29}N_2$, $^{28}N_2$) were determined. An example of mass-spectrometric measurements is shown in Figure 3. 6. Normalized by the total intensity of three mass peaks spectra are taken after different probe $^{30}N_2$ discharge durations in the reactor pretreated by $^{28}N_2$ plasma. One can see peaks corresponding to $^{28}N_2$ and $^{29}N_2$ that appear due to surface reactions with $^{14}N_{ads}$. Nitrogen molecules are continuously dissociated and re-associated in the probe discharge what results in a statistical distribution of ^{14}N over $^{29}N_2$ and $^{28}N_2$. Both $m=28$ and $m=29$ peaks were integrated to determine the number of $^{14}N_{ads}$ that were picked up from the surface under plasma exposure.

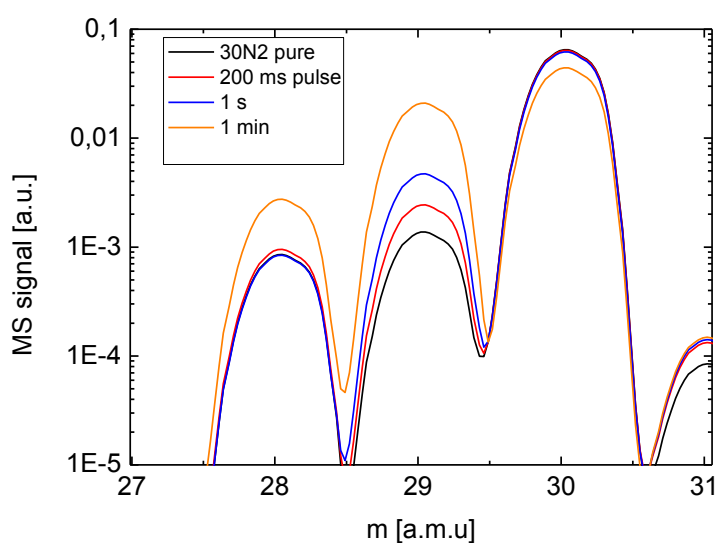


Figure 3. 6 Normalized mass spectra measured after different $^{30}N_2$ probe discharge durations in the reactor pretreated by $^{28}N_2$ plasma

Absolute concentrations of gas phase species were obtained based on relative QMS measurements using the known gas pressure in the reactor. Every ^{14}N atom measured in the gas phase is picked up from the surface. This allows determination of the surface density of ^{14}N from gas phase measurements using volume to surface ratio of the reactor:

$$[^{14}\text{N}]_{surf} = [^{14}\text{N}]_{gas} \frac{V}{S} \quad (3.1)$$

where $S = 314 \text{ cm}^2$ is the area of the pretreated part of the discharge tube (the length of the rf discharge column was 50 cm and the total length of the tube was 60 cm). And $V = 306 \text{ cm}^3$ is the total volume of the reactor between two closing pneumatic valves. In (3.1) the roughness of the tube material is not taken into account and $[^{14}\text{N}]_{surf}$ is related to the geometric and not to the real surface area.

The sensitivity of the diagnostics was limited by the stability of relative MS signals and by eventual leaks in the system (^{14}N coming from the leak distorts the measurements of ^{14}N coming from the surface). It was estimated to be $2 \cdot 10^{13} \text{ }^{14}\text{N}$ atoms per cm^2 .

3.3.2 Characterization of the discharge: measurements of N_2 dissociation degree

For quantitative investigation of surface reactions in N_2 plasma the number of molecules produced on the surface has to be compared with incoming radical fluxes. It is important, therefore, to characterize the discharge that is used for surface treatment or probing. We have measured the degree of dissociation of N_2 molecules in pulsed dc discharge and in pulsed rf discharge using the isotopic exchange technique. The idea of this technique is based on a simple fact: if a discharge is ignited in a mixture containing $^{28}\text{N}_2$ and $^{30}\text{N}_2$, due to dissociation and re-association of molecules, $^{29}\text{N}_2$ will be produced and the rate of $^{29}\text{N}_2$ production will depend on the rate of dissociation of initial molecules.

3.3.2.1 Dissociation of N_2 in pulsed dc discharge

A mixture containing approximately 50/50 $^{28}\text{N}_2/^{30}\text{N}_2$ was introduced in the reactor at 0.53 mbar in static conditions. Then dc discharge pulses with the current $i = 100 \text{ mA}$ and duration $\tau = 5 \text{ ms}$ were applied. Relative concentrations of $^{28}\text{N}_2$, $^{29}\text{N}_2$ and $^{30}\text{N}_2$ were measured with the mass spectrometer. Figure 3.7 shows the evolution of measured concentrations as a function of the number of applied discharge pulses. One can see that $^{29}\text{N}_2$ is produced at the expense of $^{28}\text{N}_2$ and $^{30}\text{N}_2$ and after 200 pulses a stationary state is reached. The cumulated discharge duration after 200 pulses is only 1 second, it is sufficiently short to neglect the nitridation of SiO_2 . Therefore, losses of N atoms due to adsorption on the surface may be ignored in the overall mass balance.

Adsorption and reactivity of N atoms

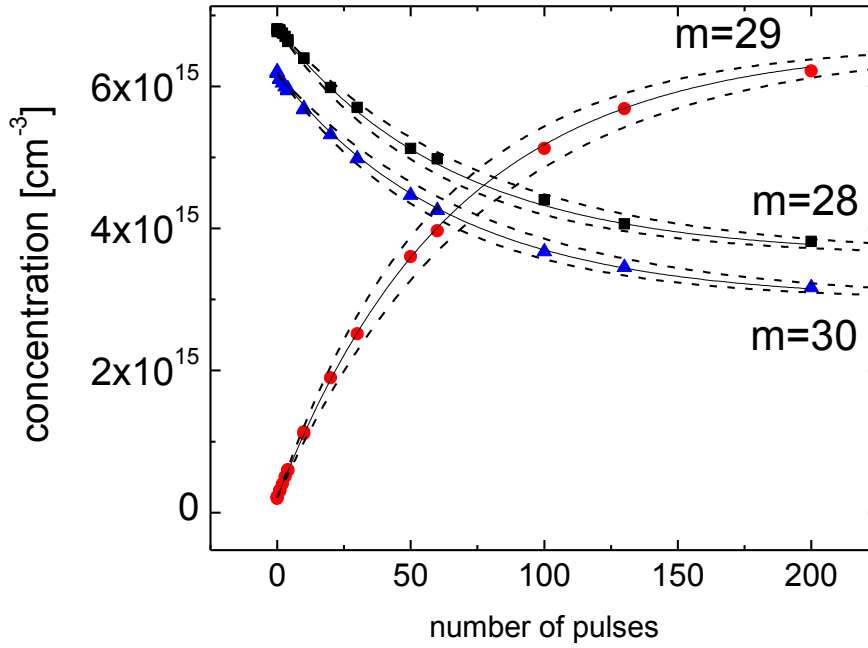


Figure 3. 7 Concentrations of three nitrogen isotopologues as a function of the number of applied dc discharge pulses. DC discharge parameters were $p=0.53$ mbar, $i=100$ mA, $\tau=5$ ms, static conditions. Solid lines are calculated assuming that 2.8% of N_2 molecules are dissociated per pulse. Dashed lines are calculated with $\delta = 2.4\%$ and $\delta = 3.1\%$, they demonstrate the relative accuracy of the δ determination method of the order of 10%.

There are two processes that can contribute to observed isotopic exchange:

- Dissociation of N_2 followed by surface recombination of N atoms. Gas phase recombination in our conditions is slow.
- Exchange reactions between atoms and molecules in the gas phase, for example:



However, in [106] it was shown that process (3. 2) and similar reactions are very slow due to a high dissociation energy of N_2 . Therefore, dissociation followed by surface recombination is the only relevant mechanism of isotopic exchange. This condition is prerequisite for validity of the method.

In order to deduce the dissociation rate of N_2 in the discharge from measurements shown in Figure 3. 7 a numerical model was applied. For simplicity, we supposed that all the isotopologues of nitrogen are dissociated in the discharge with an identical rate and then produced ^{14}N and ^{15}N atoms recombine randomly on the surface. Let δ_1 be the fraction of N_2 molecules dissociated in the reactor during the discharge pulse. Concentrations of produced atoms are given by the following expressions:

$$\begin{aligned} [^{14}\text{N}]_{pulse} &= \delta_1(2[^{28}\text{N}_2] + [^{29}\text{N}_2]) \equiv a \\ [^{15}\text{N}]_{pulse} &= \delta_1(2[^{30}\text{N}_2] + [^{29}\text{N}_2]) \equiv b \end{aligned} \quad (3.3)$$

The mixing of isotopes due to dissociation and re-association after a certain number of discharge pulses doesn't change the values of a and b because the total number of atoms of each type is conserved. Concentrations of N_2 isotopologues formed as a result of random recombination of produced atoms can be calculated as follows:

$$\begin{aligned} \Delta[^{28}\text{N}_2] &= \frac{a^2}{2(a+b)} \\ \Delta[^{29}\text{N}_2] &= \frac{ab}{(a+b)} \\ \Delta[^{30}\text{N}_2] &= \frac{b^2}{2(a+b)} \end{aligned} \quad (3.4)$$

Therefore, the evolution of concentrations of three isotopologues of N_2 as a function of the pulse number i can be described by a recurrent system:

$$\begin{aligned} [^{28}\text{N}_2]_i &= (1 - \delta_1)[^{28}\text{N}_2]_{i-1} + \frac{a^2}{2(a+b)} \\ [^{29}\text{N}_2]_i &= (1 - \delta_1)[^{29}\text{N}_2]_{i-1} + \frac{ab}{(a+b)} \\ [^{30}\text{N}_2]_i &= (1 - \delta_1)[^{30}\text{N}_2]_{i-1} + \frac{b^2}{2(a+b)} \end{aligned} \quad (3.5)$$

Using (3.5) the evolution of concentrations of three nitrogen isotopologues was calculated numerically with initial concentrations taken from the experiment. The only unknown parameter in the model was the fraction of N_2 molecules dissociated per discharge pulse (δ_1). The value of δ_1 was varied to reach an agreement with the experiment. In our experiments the volume of the discharge column ($V_{disch}=166 \text{ cm}^3$) is smaller than the volume of the reactor ($V_{reactor}=306 \text{ cm}^3$). Dissociation takes place only in the plasma column; therefore in order to obtain the fraction of dissociated molecules in the discharge (δ), the best-fit value of δ_1 should be corrected $\delta = \delta_1 \cdot V_{reactor}/V_{disch}$. In the following discussion we will use the value of δ to describe N_2 dissociation in plasma.

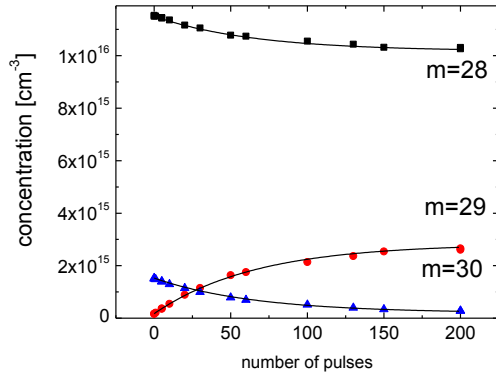
In Figure 3.7 results of the model calculation are compared with the experiment. An excellent agreement is obtained with $\delta=2.8\%$. Calculations with $\delta=2.4\%$ and $\delta=3.1\%$ demonstrate the accuracy of the technique. The relative error of δ determination was estimated to be 10%. Obtained result is in a good agreement with the theoretical calculations performed by V. Guerra and C. Pintassilgo. For the conditions of this work in the modelling it was found $\delta=3.5\%$. This proves the validity of our new method for N_2 dissociation measurements.

Measurements with different initial concentrations of $^{28}\text{N}_2$ and $^{30}\text{N}_2$ were performed. In Figure 3.8 results of measurements and calculations for $^{28}\text{N}_2/^{30}\text{N}_2=87/13$ and $^{28}\text{N}_2/^{30}\text{N}_2=13/87$ are shown. With the same value $\delta=2.8\%$ all the results are well reproduced by the model. This

Adsorption and reactivity of N atoms

proves the validity of our assumption concerning the identity of different nitrogen isotopes from the viewpoint of dissociation and surface recombination. If there was a difference in dissociation and/or recombination rates of different nitrogen isotopes, results with different initial mixture compositions wouldn't be reproduced by our simple model with the same value of δ .

a)



b)

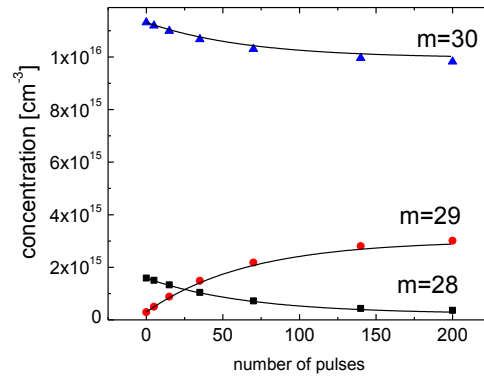


Figure 3. 8 Concentrations of three nitrogen isotopologues as a function of the number of applied dc discharge pulses. DC discharge parameters were $p=0.53$ mbar, $i=100$ mA, $\tau=5$ ms. Initial composition of the mixture was a) $^{28}\text{N}_2/^{30}\text{N}_2=87/13$ b) $^{28}\text{N}_2/^{30}\text{N}_2=13/87$. Solid line is the result of calculation with $\delta=2.8\%$

The advantage of the isotopic exchange technique is that it allows direct determination of the dissociation rate of N_2 in the discharge. Usually in the experiments the density of atomic nitrogen $[\text{N}]$ in the gas phase is measured. But $[\text{N}]$ depends on the balance between dissociation of N_2 and losses of N . When the losses take place on the surface and the value of γ_{N} is not known, the dissociation rate cannot be determined from measured value of $[\text{N}]$.

It is interesting to note that this method wouldn't work for oxygen. In O_2 isotopic exchange between atoms and molecules in the gas phase is very efficient [107] and one oxygen atom can trigger a chain of exchange reactions like $^{16}\text{O} + ^{18}\text{O}^{18}\text{O} \rightarrow ^{18}\text{O} + ^{18}\text{O}^{16}\text{O}$, $^{18}\text{O} + ^{16}\text{O}^{16}\text{O} \rightarrow ^{16}\text{O} + ^{18}\text{O}^{16}\text{O}$ and so on. Therefore, statistical distribution of isotopologues is reached very fast and the initial dissociation degree cannot be deduced. The difference between O_2 and N_2 may be explained by the attractive potential in $\text{O} - \text{O}_2$ collisions due to the existence of a stable complex O_3 . Similar stable molecule N_3 doesn't exist.

3.3.2.2 Dissociation in pulsed rf discharge

The same procedure was applied to measure the rate of N_2 dissociation in an rf discharge at $p=0.53$ mbar in standard conditions. The reactor was filled with a mixture $^{28}\text{N}_2/^{30}\text{N}_2 \approx 50/50$ and $\tau=40$ ms discharge pulses were applied. Figure 3. 9 shows the results of measurements and calculations with $\delta=7.4\%$. Therefore, $1.95 \cdot 10^{15} \text{ cm}^{-3}$ N atoms are produced during 40 ms rf discharge pulse. This gives the rate of atomic nitrogen production in N_2 rf discharge in standard pretreatment conditions $d[\text{N}]/dt = (5 \pm 1) \cdot 10^{16} \text{ cm}^{-3} \text{ s}^{-1}$.

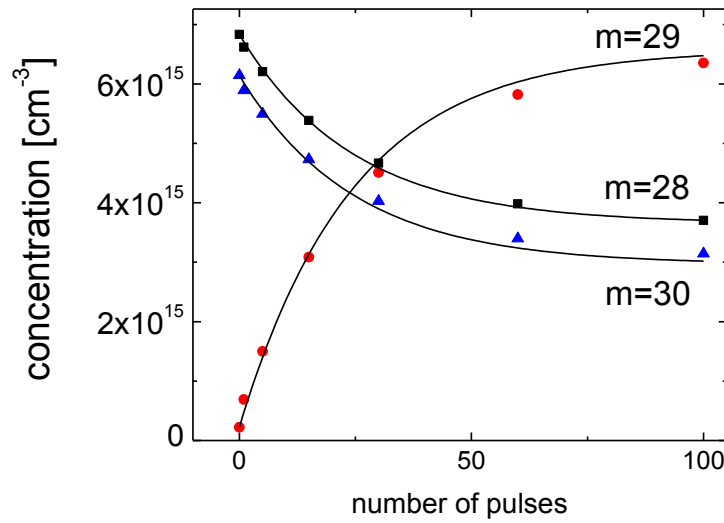


Figure 3.9 Relative concentrations of three nitrogen isotopologues as a function of the number of applied rf discharge pulses. RF discharge parameters were $p=0.53$ mbar, $P=17$ W, $\tau=40$ ms, static conditions. Solid lines are the result of model calculation with $\delta=7.4\%$.

3.3.2.3 Estimation of atomic nitrogen exposure on the surface

The flux of nitrogen atoms on the surface can be easily calculated if the concentration of atomic nitrogen is known: $f_N = \frac{1}{4}[N]v_N$ where v_N is the thermal velocity of atoms. Above we have determined the dissociation rate in two types of probe discharges used in this study. But atomic concentration depends on the balance between dissociation of N_2 and losses of N atoms and in case of pulsed discharge it is also changing with time. Therefore, the number of collisions of N atoms with the surface per unit time or per probe discharge pulse is difficult to determine from our measurements.

However, we can introduce another quantity to characterize the exposure of N atoms on the surface – the flux of N atoms **lost** on the surface (due to recombination and adsorption), which can be expressed using the effective atomic loss probability β : $f_{lost}^N = \frac{1}{4}[N]v_N\beta$. Due to the fact that volume recombination is negligible at low pressure used in this study, the number of produced nitrogen atoms is always balanced by the number of N lost on the surface. In stationary conditions, this balance is established at any moment of time. In pulsed discharges, all atoms eventually end up on the surface after the end of the discharge pulse. Therefore, the balance is valid in time-integrated sense.

From the dissociation fractions determined above we find that:

- In the pulsed dc discharge ($p=0.53$ mbar, $i=100$ mA, $\tau=5$ ms) the atomic exposure on the surface is $2 \cdot 10^{14}$ lost N atoms per cm^2 per **pulse**.

Adsorption and reactivity of N atoms

- In the continuous rf discharge ($p=0.53$ mbar, $P_{pl}=17$ W) the atomic exposure on the surface is $2.5 \cdot 10^{16}$ lost N atoms per cm^2 per **second**.

It should be noted that atomic exposure is determined with respect to the geometric surface of the discharge tube without taking into account surface roughness. We have shown that dissociation rate doesn't depend on the isotopologue, hence obtained values are applicable to probe discharges in $^{28}\text{N}_2$ as well as in $^{30}\text{N}_2$.

Now, when our discharges are characterized we can apply them for probing surface reactivity of SiO_2 under N_2 plasma exposure.

3.3.3 ^{14}N adsorption on SiO_2 under $^{28}\text{N}_2$ plasma exposure

First, we investigate the adsorption of ^{14}N on SiO_2 under plasma exposure. The following experimental parameters were used for cleaning, pretreatment and probing of silica discharge tube:

- Cleaning: Ar plasma $3.6 \cdot 10^3$ s (standard flowing rf discharge).
- Pretreatment: $^{28}\text{N}_2$ plasma $0.1 - 3.6 \cdot 10^3$ s (standard flowing rf discharge).
- Probing: $^{30}\text{N}_2$ 600 s (standard static rf discharge).

The wall temperature increased in the course of the pretreatment reaching $T_w \sim 380$ K after approximately 100 s of plasma exposure. For short pretreatment times (< 10 s) the wall temperature was equal to $T_w \sim 300$ K.

A question may arise if all the $^{14}\text{N}_{\text{ads}}$ are probed by 600 s $^{30}\text{N}_2$ discharge? To check if there are still some $^{14}\text{N}_{\text{ads}}$ left on the surface after the probe discharge, the reactor was refilled with fresh $^{30}\text{N}_2$ and a discharge was repeated again. This procedure showed that the exchange during the first probe discharge is complete within 10% if the $^{28}\text{N}_2$ pretreatment duration is 600 s and shorter. However for longer pretreatments, 600 s of $^{30}\text{N}_2$ discharge is clearly not enough to probe all the $^{14}\text{N}_{\text{ads}}$. For example, after 60 min pretreatment 3 successive fillings with $^{30}\text{N}_2$ were required to exchange all the $^{14}\text{N}_{\text{ads}}$. Obtained result is rather logical because:

- With increasing the duration of $^{28}\text{N}_2$ pretreatment ^{14}N atoms penetrate deeper in the material and longer exposure time is required for their extraction during the probe discharge in $^{30}\text{N}_2$.
- When the concentration of ^{14}N atoms in the probe discharge becomes relatively high they may be re-adsorbed on the surface leading to an equilibrium distribution between the surface and the gas phase.

Figure 3. 10 shows the density of $^{14}\text{N}_{\text{ads}}$ as a function of the duration of $^{28}\text{N}_2$ plasma treatment. Due to a better sensitivity of the isotopic diagnostics compared to XPS we were able to follow adsorption kinetics for pretreatment duration as short as 100 ms. For 60 min pretreatment the concentration of $^{14}\text{N}_{\text{ads}}$ was obtained using three successive probe discharges in $^{30}\text{N}_2$. Looking at Figure 3. 10 we can conclude:

- Nitrogen atoms are indeed grafted to the surface of SiO₂ under ²⁸N₂ plasma exposure.
- These atoms are reactive in the sense that they may be removed from the surface by the probe discharge in ³⁰N₂.

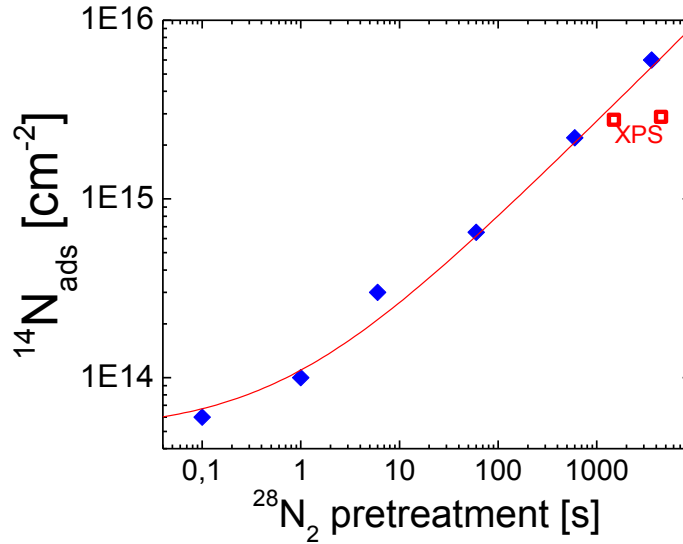


Figure 3. 10 ♦ surface density of ¹⁴N_{ads} as a function of the duration of ²⁸N₂ plasma pretreatment. Probe ³⁰N₂ discharge duration 600 s, ■ results of XPS measurements from Figure 3. 3. Data points are fitted with a power function $N_{ads} = 5 \cdot 10^{13} + 6 \cdot 10^{13} \cdot t^{0.55}$.

The ¹⁴N_{ads} coverage found after 60 min pretreatment [¹⁴N_{ads}]_{isotopes} = 6 · 10¹⁵ cm⁻² is two times higher than the result of XPS measurements after 75 min pretreatment [¹⁴N_{ads}]_{XPS} ≈ 3 · 10¹⁵ cm⁻². As it was mentioned before, with isotopic exchange technique we obtain the ¹⁴N_{ads} coverage with respect to the geometric surface of the tube. XPS measurements give surface concentrations related to real surface of the sample. The roughness factor of silica is ~ 2 [5] what may explain the 2-fold difference between two diagnostics. Obtained agreement is encouraging and it confirms the validity of both techniques for determination of the density of ¹⁴N_{ads} on the surface of the discharge tube.

Adsorption kinetics

Data points shown in Figure 3. 10 can be well approximated by a power function: $N_{ads} = 5 \cdot 10^{13} + 6 \cdot 10^{13} \cdot t^{0.55}$ where t is the pretreatment time. We have found that during the first second of plasmas exposure the rate of adsorption is maximal and it reaches ≈ 10¹⁴ atoms cm⁻²s⁻¹. After 100 s of pretreatment adsorption slows down by two orders of magnitude. This may be explained by fast top-surface nitridation followed by much slower penetration of N atoms deeper in the bulk.

It is interesting to compare the rate of ¹⁴N adsorption with the fluxes of atoms and ions on the surface. In § 3.3.2.3 the flux of recombining N atoms was measured to be 2.5 · 10¹⁶ atoms cm⁻²

Adsorption and reactivity of N atoms

$2s^{-1}$ which is 2 orders of magnitude higher than the maximum rate of adsorption. Therefore, adsorption of N is a slow process in comparison with surface recombination.

An order of magnitude estimation of the ion flux can be done assuming that $n_e \sim 10^9 \text{ cm}^{-3}$ and $T_e \sim 3 \text{ eV}$ which is reasonable for the conditions of this study according to [108]. Calculation using standard expression for collisionless sheath gives [44]:

$$j_+ \cong n_+ \sqrt{\frac{kT_e}{M_+}} \cong 3 \cdot 10^{14} \text{ ions cm}^{-2} \text{ s}^{-1} \quad (3.6)$$

Therefore, the initial rate of N adsorption is comparable with the flux of ions on the surface. Similar ordering between the number of incident ions and the density of N grafted to the surface was obtained in plasma nitridation of thin SiO_2 films [17]. However, as it was mentioned in § 3.2.2 we are unable to determine the exact role of ions because in N_2 plasma the surface is exposed to atomic and ion fluxes simultaneously.

Do ions remove N_{ads} under continuous N_2 plasma exposure?

We have seen that ion bombardment is essential for the formation of SiO_xN_y layer. But what is the role of ions for the conditions on the surface of this layer? In [57] Cartry evidence the possibility of desorption of oxygen atoms adsorbed on SiO_2 by ion bombardment in O_2 dc discharge at 0.3 torr. Our case is similar to one described in [57] with the only difference that the surface is SiO_xN_y and the discharge is in N_2 . In order to see if ion bombardment liberates adsorption sites two pretreatment procedures have been compared:

- Standard pretreatment with rf discharge in N_2 during 60 min.
- Standard pretreatment followed by 100 short dc pulses in N_2 (0.53 mbar, $i=100 \text{ mA}$, $\tau=5 \text{ ms}$).

Using (3.6) we have estimated the number of N_2^+ ions incident on the surface during the dc pulse to be $\approx 3 \cdot 10^{13} \text{ cm}^{-2}$. Which is one order of magnitude smaller than the number of N atoms lost on the surface (measured in § 3.3.2.3 to be $3 \cdot 10^{14} \text{ cm}^{-2}$ per discharge pulse). Hence, with the dc pulses the surface is exposed mostly to the atomic flux. If there are some free adsorption sites left on the surface after rf treatment, they can be occupied by N atoms. But we have found that addition of dc pulsed doesn't change the number of N adsorbed on the surface. This proves that under standard pretreatment conditions eventual desorption of $^{14}\text{N}_{\text{ads}}$ by ion bombardment is less efficient than re-adsorption of atomic nitrogen and all the adsorption sites are normally occupied.

^{14}N adsorption: role of O_2 admixture in the discharge

With XPS measurements we have seen that addition of 20% O_2 into N_2 discharge inhibits formation of SiO_xN_y on silica surface. This effect was explained by removal of N_{ads} in reactions with O atoms. Using isotopic exchange technique we have investigated pretreatment of silica surface by rf discharge in a mixture containing 0.1 % of oxygen in N_2 . Even such a

small addition of O₂ in the discharge results in ~10 fold reduction of the density of grafted ¹⁴N! The surface density [¹⁴N_{ads}]=4·10¹⁴ cm⁻² was measured in this case. This example shows how strongly the state of the surface in contact with N₂/O₂ plasmas is dependent on the gas composition.

Is adsorption of nitrogen atoms isotope - dependent?

It was interesting to check if both nitrogen isotopes are adsorbed on silica surface in the same manner. A series of experiments with ³⁰N₂ plasma pretreatment was performed. In this case discharge was ignited in a closed reactor without a gas flow. Measured concentrations [¹⁵N_{ads}] were systematically ~ 2 times lower than [¹⁴N_{ads}] after the same pretreatment time in ²⁸N₂. This could be in principle interpreted as an isotope-dependent adsorption of nitrogen atoms on SiO₂. However as we have mentioned above, adsorption of N atoms on SiO₂ is very sensitive to the presence of oxygen additions in N₂. Therefore, more plausible explanation for this effect would be a higher level of impurities (such as O₂ or H₂O) in the ³⁰N₂ gas used.

3.3.4 Reactivity of grafted ¹⁴N atoms under ³⁰N₂ plasma exposure

XPS and isotopic exchange diagnostics have both shown that the surface of SiO₂ pretreated by low pressure N₂ plasma is saturated with N atoms. We know that these atoms can be removed from the surface by ³⁰N₂ plasma, i.e. they are reactive under plasma exposure. Our objective now is to understand if these adsorbed nitrogen atoms play a role of active sites for recombination of N on the surface. In other words, if adsorbed atoms that we have detected in our experiments are those “chemisorbed” atoms that are so widely used in the models?

We use a probe discharge in ³⁰N₂ to send a controlled amount of ¹⁵N atoms on the surface previously pretreated by ²⁸N₂ plasma. Comparison between the number of lost ¹⁵N and the number of ¹⁴N picked up from the surface will give the answer to formulated questions.

3.3.4.1 Evidence for a distribution of reactivity of N_{ads}

In order to investigate the reactivity of ¹⁴N_{ads}, silica surface was pretreated by ²⁸N₂ plasma during 60 minutes in standard conditions and then probed by ³⁰N₂ discharge with duration varied in the range 5·10⁻² – 10³ s in closed reactor. Figure 3. 11 shows the evolution of the number of adsorbed atoms picked up from the surface as a function of the probe discharge duration (¹⁴N_{des}).

One can note that for long probe discharge durations the concentration of ¹⁴N atoms in the gas phase becomes non-negligible in comparison with the concentration of ¹⁵N. For example after t_{probe} = 10³ s, relative atomic concentration of ¹⁴N is 25%. This means that ¹⁴N from the gas phase may be re-adsorbed on the surface and thus the value of ¹⁴N_{des} is underestimated. Accurate correction of the measurements for the re-absorption effect is difficult. As we will see, different groups of N atoms on the surface have different characteristic times of isotopic exchange with the gas phase under plasma exposure. If equilibrium between the plasma and the reactor wall is attained, the relative concentration of ¹⁴N should be the same in the gas

Adsorption and reactivity of N atoms

phase and in the probed part of the SiO_xN_y layer. Therefore, the underestimation of the value of $^{14}\text{N}_{\text{des}}$ for $t_{\text{probe}} = 10^3$ s is $\sim 25\%$. For $t_{\text{probe}} \leq 10^2$ s this correction is always smaller than 10% and it can be neglected.

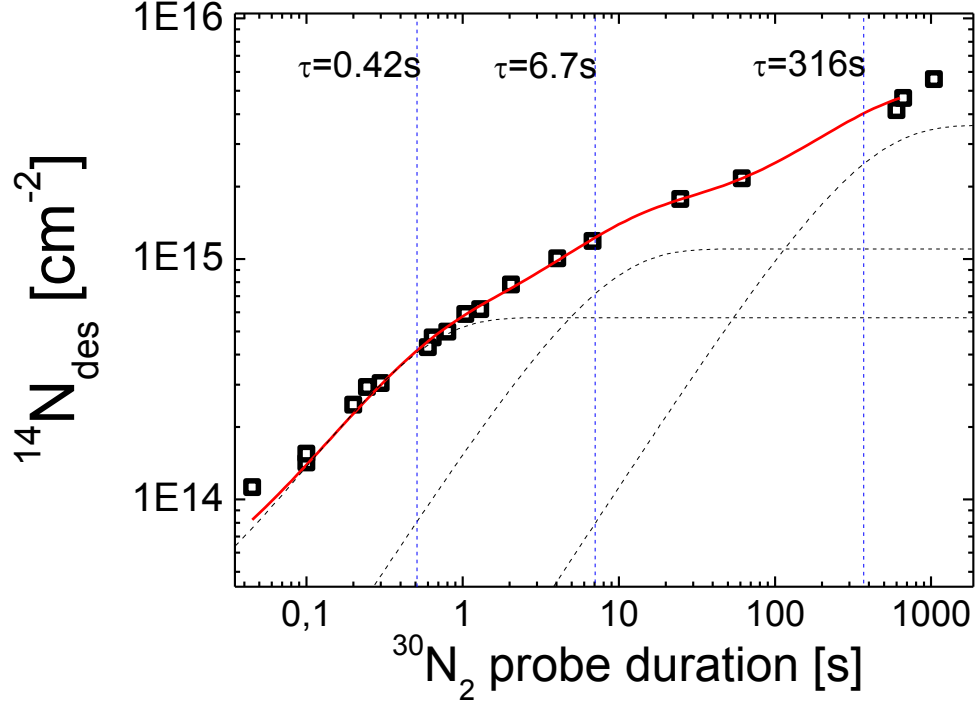


Figure 3. 11 Evolution of the density of $^{14}\text{N}_{\text{ads}}$ atoms picked up from the surface as a function of the probe rf discharge duration in $^{30}\text{N}_2$. Silica discharge tube was pre-treated by $^{28}\text{N}_2$ plasma during 60 minutes. Multi-exponential fit with $a - \sum_{i=1..3} a_i e^{-t/\tau_i}$ is shown by a solid line. Three components of the fit are shown by dashed lines.

We can see that the value of $^{14}\text{N}_{\text{des}}$ gradually increases when the duration of probe discharge is varied by 4 orders of magnitude. This observation points to the presence on the surface of different groups of $^{14}\text{N}_{\text{ads}}$ that have different probability to react and to be desorbed in the gas phase during the probe discharge. If all the adsorbed atoms had the same reactivity, the evolution of $^{14}\text{N}_{\text{des}}$ would be described by single-exponential time dependence $[N_{\text{des}}] = a(1 - e^{-t/\tau})$. But in order to reproduce experimental data we had to use a combination of three exponential functions $[N_{\text{des}}] = a - \sum_{i=1..3} a_i e^{-t/\tau_i}$ with following parameters:

i	$a_i [\text{cm}^{-2}]$	$\tau_i [\text{s}]$
1	$5.5 \cdot 10^{14}$	0.42
2	$1.1 \cdot 10^{15}$	6.7
3	$3.6 \cdot 10^{15}$	316

Table 3. 3 Parameters of multi-exponential fit of the data shown in Figure 3. 11.

Different reactivity of groups of atoms with $i=1$ and $i=2$ may be related to the difference in their binding energy [54]. The total coverage of the most reactive N_{ads} $a_1 + a_2$ is of the order

of one monolayer. It would be reasonable to suggest that these atoms occupy the outmost layer on the surface of SiO_xN_y and they are directly exposed to the plasma. When the surface is pretreated by an rf discharge in N_2 in standard conditions, these superficial atoms are continuously replaced with the characteristic turnover time ~ 7 s.

According to [17] in plasma nitrided SiO_2 thin films, N atoms are incorporated within a ~ 3 nm thick surface layer. Atoms belonging to the third group may be distributed in the SiO_xN_y layer beneath the surface what would explain their slow desorption rate.

It is evident that only the most reactive N_{ads} significantly contribute to the recombination of nitrogen atoms on the surface in the discharge.

3.3.4.2 Do N_{ads} participate in surface recombination of N atoms?

Up to now we haven't yet discussed the mechanism of ^{14}N removal from the surface under $^{30}\text{N}_2$ plasma exposure. Several processes may take place simultaneously:

- Recombination with ^{15}N :



- Ion bombardment
- Desorption by photons and fluxes of excited species

At present we don't have any evidence of the contribution of photons and excited molecules, but we are confident that ions play an important role. The fact that nitridation of SiO_2 takes place only under direct plasma exposure proves that ion bombardment in our conditions may significantly modify the outmost surface layer. Therefore, desorption of $^{14}\text{N}_{\text{ads}}$ by ions cannot be ruled out.

In the first instance we will assume that atomic recombination is the only relevant reaction for N_{ads} removal and we will neglect all the other processes. This will allow an estimation of the upper limit for the efficiency of recombination between adsorbed $^{14}\text{N}_{\text{ads}}$ and impinging ^{15}N .

In order to see the effect of the most active $^{14}\text{N}_{\text{ads}}$ that react in the very beginning of the probe discharge, the exposure to the flux of ^{15}N should be as small as possible. Our pulsed rf discharge was not adapted for working with short single discharge pulses. For this reason we used a dc probe discharge with pulse duration $\tau=5$ ms and current $i=100$ mA at $p=0.53$ mbar. According to the measurements presented in § 3.3.2.3, in every dc pulse the number ^{15}N atoms lost per cm^2 of the tube surface is $2 \cdot 10^{14}$. As we have estimated in § 0, the number of incident N_2^+ ions in the same conditions is about one order of magnitude smaller.

Silica discharge tube was pretreated by $^{28}\text{N}_2$ plasma in standard conditions during 60 min and then probe pulsed discharge in $^{30}\text{N}_2$ was applied. In Figure 3. 12, the number of $^{14}\text{N}_{\text{ads}}$ picked up from the surface ($\phi_{14\text{N}}$) is plotted as a function of the number of ^{15}N lost ($\phi_{15\text{N}}$). Results obtained with dc and rf probe discharges (from Figure 3. 11) are compared.

Adsorption and reactivity of N atoms

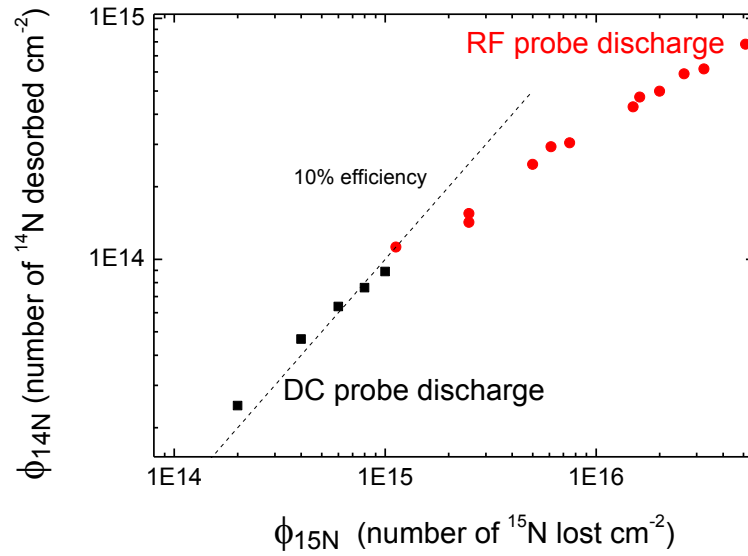


Figure 3. 12 The density of $^{14}\text{N}_{\text{ads}}$ atoms picked up from the surface as a function of the number of lost ^{15}N . Results obtained with dc and rf probe discharges are shown. Dashed line depicts $\phi_{14\text{N}} \approx 0.1 \cdot \phi_{15\text{N}}$, i.e. 1 out of 10 ^{15}N atoms is lost in recombination with $^{14}\text{N}_{\text{ads}}$.

One can see that for $\phi_{15\text{N}} < 10^{15} \text{ cm}^{-2}$, the number of desorbed ^{14}N atoms is directly proportional to the number of lost ^{15}N and $\phi_{14\text{N}} \approx 0.1 \cdot \phi_{15\text{N}}$. This means that only 1 out of 10 ^{15}N is lost in recombination with $^{14}\text{N}_{\text{ads}}$. If we assume that one more ^{15}N atom is consumed to occupy the place of removed ^{14}N we obtain that the *maximum* contribution of strongly bonding sites (i.e. sites where stable ^{14}N are adsorbed) into surface recombination of ^{15}N is only 20 %.

Where recombine remaining 80% of ^{15}N ? Two hypotheses may be proposed:

- Recombination of ^{15}N takes place on **weakly bonding** active sites.
- Only a **small fraction** $^{14}\text{N}_{\text{ads}}$ are active for recombination of ^{15}N . Upon the exposure of the surface to pulsed discharge in $^{30}\text{N}_2$, there is a fast turnover of ^{15}N on these active sites that doesn't lead to the production of $^{29}\text{N}_2$. The detection limit of mass spectrometer is equivalent to $\sim 2 \cdot 10^{13}$ atoms per cm^2 . If the coverage of active atoms is of the order of 10^{13} cm^{-2} their contribution to the production of $^{29}\text{N}_2$ on the surface in experiments shown in Figure 3. 12 cannot be measured.

Physically both hypotheses mean that on the surface there exists a **distribution** of binding energy and/or reactivity of adsorbed N atoms.

3.3.5 Conclusions on the isotopic study

In this section we have developed isotope exchange technique for investigation of interaction between SiO₂ surface and low pressure N₂ plasma. This technique allowed us to characterize the coverage and reactivity of N_{ads} on SiO₂. Let us outline the main results:

- It has been confirmed that a SiO_xN_y layer is formed on SiO₂ under plasma exposure. We were able to follow dynamics of SiO₂ nitridation and the concentration of ¹⁴N atoms on the surface after 60 minutes of ²⁸N₂ plasma treatment [¹⁴N_{ads}] = 6·10¹⁵ cm⁻² was found to be in a good agreement with previous XPS measurements.
- Formation of SiO_xN_y layer is very sensitive to the presence of O₂ admixtures in N₂ plasma. Addition of 0.1% of O₂ into N₂ reduces the number of grafted N atoms by a factor of 10.
- ¹⁴N_{ads} exhibit a distribution of reactivity when pretreated surface is exposed to ³⁰N₂ plasma.
- Recombination with ¹⁴N_{ads} accounts at maximum for 20% of surface losses of nitrogen atoms on SiO_xN_y.
- We suppose that 80% of heterogeneous losses of N takes place on either weakly bonding active sites or with participation of a small fraction of N_{ads}.

In order to choose between these two hypotheses the limit of detection of N_{ads} should be improved. In the following section we will develop a technique capable of detecting coverage of N_{ads} of the order of 10¹² cm⁻².

3.4 Recombination of N_{ads} with O atoms

We have seen that ¹⁴N_{ads} can recombine with ¹⁵N producing ²⁹N₂. In this section we will investigate recombination reaction N_{ads} + O → NO. Thus, after the pretreatment of silica surface by N₂ plasma we ignite in the reactor a discharge in pure oxygen. Nitric oxide (NO) molecules produced on the surface are detected *in-situ* using tuneable laser diagnostics with millisecond time resolution. High sensitivity and time resolution of TDLAS open a possibility to follow kinetics of recombination process and to separate production of NO during the probe discharge pulse and in the afterglow. Detection of NO production on the surface is an alternative way to probe the reactivity of N_{ads}, so we will be interested in the mechanism of NO formation as well as in the properties of reactive N_{ads}.

3.4.1 Experimental details

Experimental procedure consists in several steps, schematically shown in Figure 3. 13. First the silica discharge tube was pretreated by N₂ plasma in standard conditions (see Table 3.1) during 60 minutes. Then the reactor was pumped out during 10 minutes in order to remove gas phase N₂ and let the surface cool down to the room temperature. On the next step the discharge tube was filled with pure O₂ and a single discharge pulse (dc or rf) was ignited in

Adsorption and reactivity of N atoms

closed reactor. Production of NO was monitored *in-situ* using TDL spectrometer with typical time resolution of 10 ms. It is essential that in experiments with pretreated surface the complete time evolution of NO concentration was measured in a single probe discharge. In our conditions no data accumulation is possible because the next probe pulse can be applied only after 70 minutes when the surface is pretreated again.

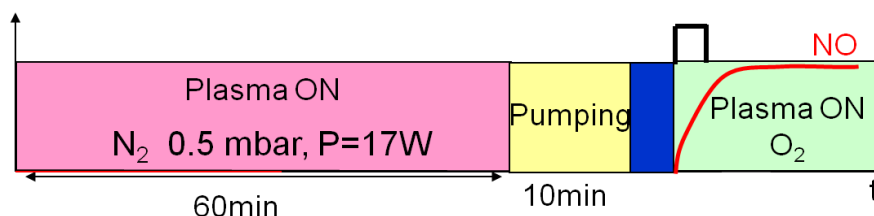


Figure 3. 13 Experimental procedure used for investigation of NO formation on the surface.

Within the same emission mode of the laser we were able to detect absorption features of two isotopologues of nitric oxide - ^{14}NO and ^{15}NO with approximately the same line strengths. Therefore, kinetics of both species was followed simultaneously. Figure 3. 14 shows an absorption spectrum of a gas mixture containing both isotopologues of NO.

The detection limit of NO measurements using TDLAS was $\sim 10^{12} \text{ cm}^{-3}$. In terms of surface coverage of N atoms (if we assume that NO is produced from recombination of N_{ads} and O) this correspond to $\sim 5 \cdot 10^{11} \text{ cm}^{-2}$, i.e. less than 10^{-3} of a monolayer. Hence using NO production as a probe, we can detect much smaller surface coverage of N_{ads} in comparison with XPS and isotopic exchange technique.

The absolute concentration of O atoms in the probed O_2 discharge is measured using TALIF.

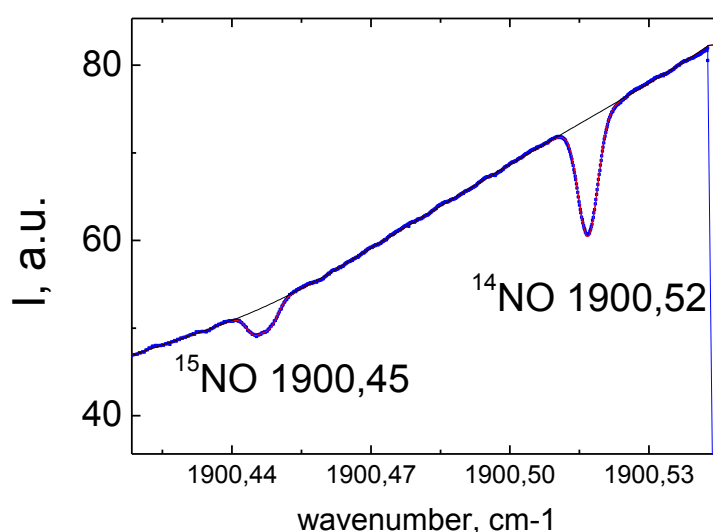


Figure 3. 14 Absorption spectrum of a mixture containing ^{14}NO and ^{15}NO recorder with TDL spectrometer.

3.4.2 Kinetics of NO production on the surface

Figure 3. 15 shows time evolution of NO concentration measured in a probe discharge pulse ($i=100$ mA, $\tau=10$ ms) at three different O_2 pressures, $p = 0.53$, 1.3 and 5.3 mbar. First of all we see that NO production on the surface is possible. We use pure O_2 so NO can come only from reactions on the surface.

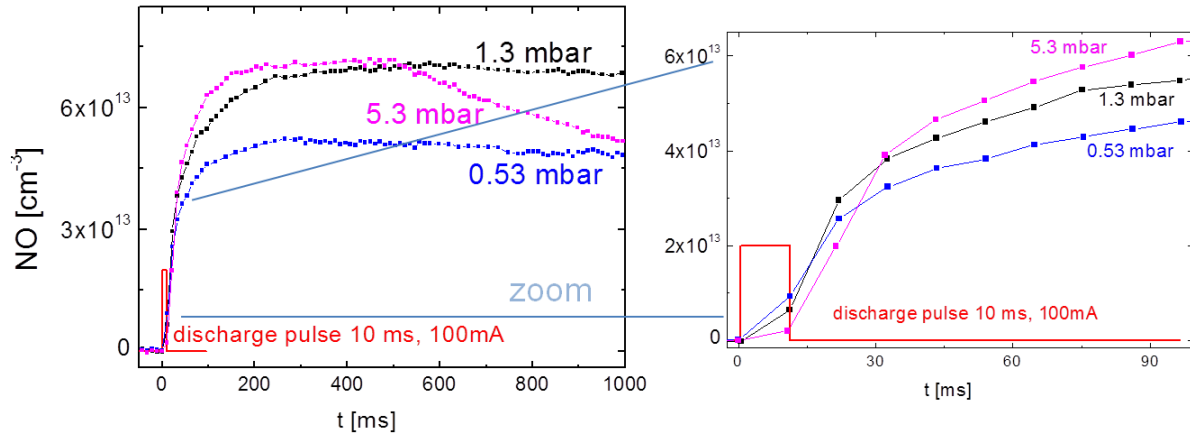


Figure 3. 15 NO production in probe dc discharge pulses ($i=100$ mA, $\tau=10$ ms) at different pressures of O_2 $p=0.53$, 1.3, 5.3 mbar. Silica discharge tube was pretreated by N_2 plasma in standard conditions during 60 minutes. Zoom on the first 100 ms of the acquisition is also shown, $t=0$ corresponds to the beginning of the probe pulse.

Measurements of NO can provide information about the mechanism of recombination reaction ($O+N_{ads} \rightarrow NO$) only if two conditions are satisfied:

- ($O+N_{ads} \rightarrow NO$) is indeed the main channel of NO production in the probe discharge.
- Losses and conversion of NO are negligible.

Below we will show that in experiments shown in Figure 3. 15 both conditions are fulfilled.

3.4.2.1 Proof of recombination mechanism $N_{ads} + O \rightarrow NO$

In principle, NO can be produced on the surface in reactions with ions and electronically excited species. But the lifetime of these species is short and they can contribute to NO production only during the probe discharge. In Figure 3. 15, concentration of nitric oxide just after the end of plasma pulse is less than 10% of the maximum measured NO concentration. Therefore, we can neglect the reactivity of short-lived species as a source of NO in this experiment.

Production of NO persists during ~ 200 ms in the post discharge. Among all active oxygen species only $O_2(a^1\Delta)$ and O atoms have comparable lifetimes in our conditions [109]. But

Adsorption and reactivity of N atoms

molecular singlet oxygen has very low excitation energy ($\sim 1\text{eV}$) and it would be reasonable to suggest that it is much less reactive than O. This means that atomic oxygen is the only relevant reaction partner for NO production.

We have also tested a possible role of adsorbed N_2 molecules for production of NO. When the reactor was pretreated with neutral N_2 flow, no formation of NO was detected in the probe discharge. Therefore, adsorbed nitrogen molecules have no contribution to NO production on the surface in our conditions.

We conclude that in experiments shown in Figure 3. 15 NO is produced mainly from recombination between N_{ads} and atomic oxygen.

3.4.2.2 Kinetics of NOx in the probe discharge

If we want to use NO as a marker of surface reactions, it should not be destroyed or converted after being produced on the surface. It is known that in N_2/O_2 containing plasmas different nitrogen oxides are formed in the gas phase and on the surface [43][32]. In our oxygen-rich conditions NO_2 is the most plausible product of NO conversion. Let's consider the most important reactions that may influence kinetics of NO in the afterglow of the probe discharge.

	Reaction	Rate constant	Ref
R1	$\text{O} + \text{N}_{\text{ads}} \rightarrow \text{NO}$	//	
R2	$\text{NO}_2 + \text{O} \rightarrow \text{NO} + \text{O}_2$	$k_2 = 9.3 \cdot 10^{-12} \text{ cm}^3 \text{ s}^{-1}$	[16]
R3	$\text{NO} + \text{O} + \text{M} \rightarrow \text{NO}_2 + \text{M}$	$k_3 = 8.6 \cdot 10^{-32} \text{ cm}^6 \text{ s}^{-1}$	[16]
R4	$\text{NO} + \text{O}_3 \rightarrow \text{NO}_2 + \text{O}_2$	$k_4 = 1.8 \cdot 10^{-12} \text{ e}^{-1370/T} \text{ cm}^3 \text{ s}^{-1}$	[16]
R5	$\text{NO} + \text{O}_{\text{ads}} \rightarrow \text{NO}_2$	//	

Table 3. 4 Relevant NO production and loss mechanisms in the afterglow of the probe discharge.

We see that NO can be converted into NO_2 in reactions R3-R5, but the reverse reaction R2 is rather fast and in it tends to recover NO_2 into NO. The probability of reaction R5 just after the end of the probe discharge when atomic oxygen is still present in the gas phase is not known. In the next chapter we will see that on Pyrex surface in the late post-discharge this reaction has a probability $\gamma \sim 10^{-6}$, i.e. it is rather slow. Let's make an estimation of the efficiency of NO conversion in NO_2 for O_2 pressure 1.3 mbar. In § 4.5.2 we show that at $p=1.3$ mbar concentration of O_3 produced in the discharge is smaller than 10^{13} cm^{-3} , thus reaction R4 can be neglected. If we neglect R5, the balance between production and losses of NO_2 in reactions R2 and R3 in quasi steady is independent of the concentration of O:

$$\frac{[\text{NO}_2]}{[\text{NO}]} = \frac{k_3 [\text{M}]}{k_2} \sim 10^{-4} \quad (3. 8)$$

Therefore, while the concentration of atomic oxygen is not too small, concentration of NO_2 is negligible because it is destroyed in reaction R2. When all oxygen atoms recombine on the surface, reactions R4 and R5 may become important. This is clearly seen in Figure 3. 15 for

p=5.3 mbar; 500 ms after the end of the probe discharge [NO] starts to decrease. This may be explained by reaction R4 with ozone which is efficiently produced at elevated O₂ pressure. As we will show in § 4.5.2, concentration of ozone reaches $\sim 10^{14} \text{ cm}^{-3}$ at 5 mbar in similar conditions.

Here we conclude that in experiments shown in Figure 3. 15 NO conversion in NO₂ may be neglected (at least for t<500 ms in the afterglow of the probe discharge).

3.4.2.3 Estimation of the coverage of N_{ads} that produce NO

We have proven that NO is produced from recombination between N_{ads} and O and every NO molecules measured in the gas phase corresponds to one N_{ads} picked up from the surface due to negligible losses of NO. This allows estimation of the coverage of N_{ads} that took part in recombination using volume (V) to surface (S) ratio of the discharge tube

$$[N_{\text{ads}}] = [\text{NO}] \frac{V}{S} \quad (3. 9)$$

But what is the maximum amount of N_{ads} that can react with O?

In Figure 3. 15 we can see that the maximum concentration of produced NO increases with increasing the pressure from 0.53 to 1.3 mbar and then it stays the same for O₂ pressure 5.3 mbar. In order to understand this behaviour we have measured NO production with different probe pulse durations at p = 1.3 mbar. In addition the concentration of atomic oxygen at the end of the probe discharge was measured using TALIF.

Table 3. 5 shows results of the measurements of the concentration of atomic oxygen and corresponding number of O atoms lost per cm² of the tube surface per probe discharge pulse. The probe pulse duration is much shorter than the typical lifetime of atomic oxygen in our conditions (see § 4.5.2); therefore, the number of lost O atoms is simply proportional to the concentration of atomic oxygen at the end of the pulse $[O_{\text{lost}}] = [O] \frac{V}{S}$.

Conditions	p mbar	[O] cm ⁻³	[O _{lost}] cm ⁻²
i=100 mA, τ=0.5 ms	1.3	$1 \cdot 10^{14}$	$5 \cdot 10^{13}$
i=100 mA, τ=2 ms	1.3	$4.5 \cdot 10^{14}$	$2.2 \cdot 10^{14}$
i=100 mA, τ=10 ms	0.53	$9 \cdot 10^{14}$	$4.5 \cdot 10^{14}$
i=100 mA, τ=10 ms	1.3	$2 \cdot 10^{15}$	$1 \cdot 10^{15}$
i=100 mA, τ=10 ms	5.3	$6 \cdot 10^{15}$	$3 \cdot 10^{15}$

Table 3. 5 Concentration of atomic oxygen at the end of the probe discharge measured using TALIF and corresponding exposure of the surface to atomic oxygen measured in atoms lost per cm² of the tube surface.

In Figure 3. 16 the maximum concentration of formed nitric oxide $[\text{NO}]_{\text{max}}$ is plotted as a function of $[O_{\text{lost}}]$; $[\text{NO}]_{\text{max}}$ is proportional to $[O_{\text{lost}}]$ for $[O_{\text{lost}}] \leq 5 \cdot 10^{14} \text{ cm}^{-2}$ and then it

Adsorption and reactivity of N atoms

reaches saturation. These measurements show that for low values of $[O_{\text{lost}}]$, NO production is limited by the amount of available atomic oxygen. Saturation can be explained by the limited number of reactive N_{ads} on the surface. We have seen in § 3.4.2.2 that losses of NO are not increased with increasing the density of atomic oxygen; hence, saturation of $[NO]_{\text{max}}$ is not related to the conversion of NO into NO_2 .

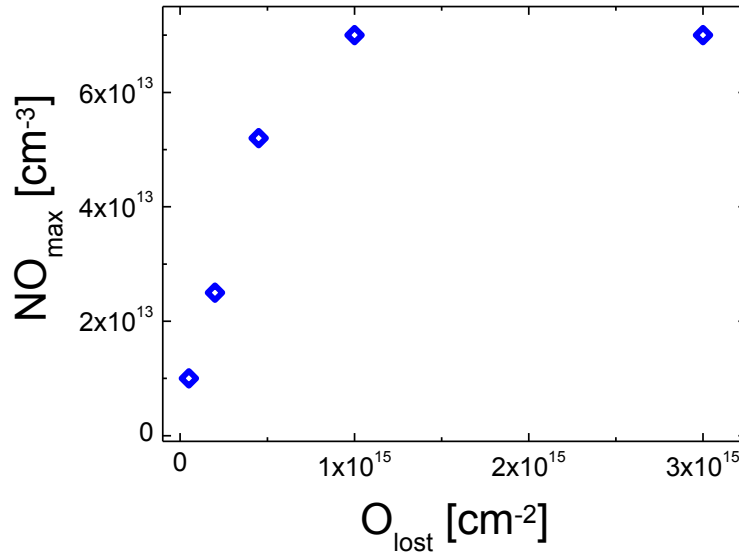


Figure 3. 16 Maximum concentration of NO produced on the surface as a function of the number of O atoms lost on the surface of after the probe discharge. Surface pretreatment conditions are the same as in Figure 3. 15.

Comparison between the number of O lost on the surface and the amount of produced NO clearly shows that recombination with N_{ads} is not the main loss mechanism of atomic oxygen on the surface. From the initial linear part of the dependence shown in Figure 3. 16 we deduce that only ~5% of O atoms recombine with the production of NO.

Saturation level $[NO]_{\text{max}} = 7 \cdot 10^{13} \text{ cm}^{-3}$ corresponds to the total coverage of N_{ads} after the pretreatment $[N_{\text{ads}}] = 3.5 \cdot 10^{13} \text{ cm}^{-2}$. Obtained coverage is two orders of magnitude smaller than the density of N_{ads} measured with XPS or isotopic exchange. This means that only a small fraction of nitrogen atoms on the surface can participate in NO formation under the flux of atomic oxygen in the post-discharge. In order to distinguish these very reactive atoms from the rest of N_{ads} , in the following discussion we will denote them N_{ads}^* .

We don't know exactly what differs N_{ads}^* from other adsorbed N atoms on the surface. Probably, they have smaller binding energy what determines their reactivity towards O.

3.4.2.4 NO production on the surface under continuous O₂ plasma exposure

Results discussed so far are obtained in a temporal post discharge where O atoms are the only active species. Now we will investigate how NO is produced when the pretreated surface it is exposed to a continuous O₂ plasma where ion and atom fluxes are present simultaneously. In Figure 3. 17 a) kinetics of NO production in a probe rf discharge in standard conditions is shown. We can see that NO is rapidly formed when rf discharge is ignited and then a slight increase of the NO concentration is observed during the following 60 seconds. In Figure 3. 17 b) results obtained using dc and rf probe discharges are compared. Surprisingly, characteristic production time and absolute concentration of NO are identical in both cases.

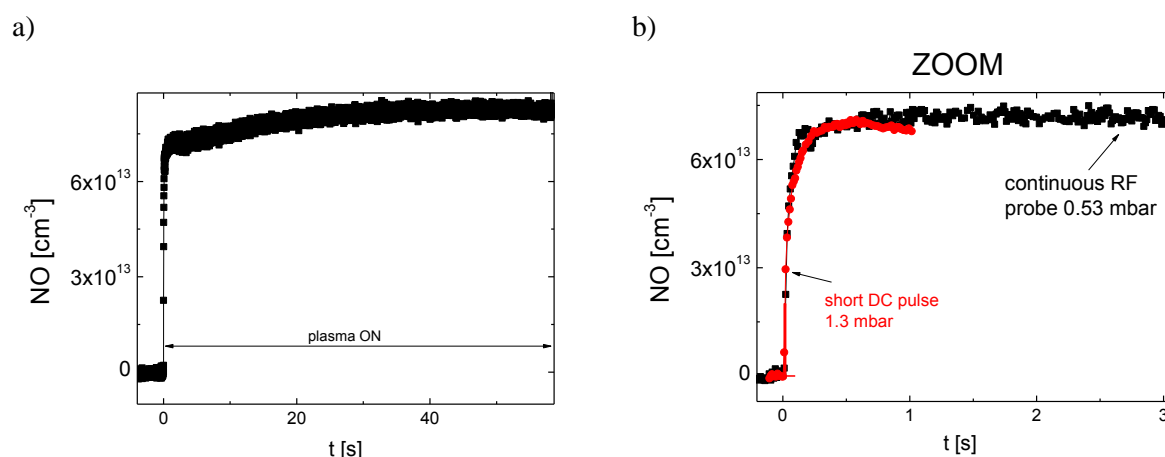


Figure 3. 17 Production of NO in an O₂ rf discharge in standard conditions. Silica discharge tube was pretreated by N₂ plasma during 60 minutes. For comparison results obtained using a dc probe discharge at 1.3 mbar are shown. Right panel shows a comparison between rf and dc probes during the first 3 seconds of plasma exposure.

According to our XPS measurements shown in Figure 3. 4, after 1min of O₂ plasma exposure in standard conditions about $2 \cdot 10^{15}$ nitrogen atoms per cm² are removed from the surface. Concentration of NO measured after 1 minute of rf probe discharge corresponds to only $4 \cdot 10^{13}$ of N_{ads} per cm². Therefore, the balance of nitrogen atoms based on NO measurements in the continuous rf probe discharge is incomplete.

Mass spectrometric measurements have shown that in addition to NO significant amount of N₂ is produced. After 1 minute of probe discharge we have found $[N_2] = 1 \cdot 10^{15}$ cm⁻³, that corresponds to $2 \cdot 10^{15}$ cm⁻² nitrogen atoms picked up from the surface. This result agrees well with XPS and isotopic exchange measurements presented in § 3.2.3 and § 3.3.3 .Thus, most of N_{ads} that react under continuous O₂ plasma exposure end up in the form of N₂; NO represents only a small fraction of the N atoms balance in the probe discharge.

Table 3. 6 shows a list of gas phase reactions that may explain observed production of N₂. In continuous rf probe discharge NO molecules are dissociated by electron impact (R6). Produced N atoms may either re-associate on the surface into NO or react further with NO in very efficient reaction R7 that forms N₂. Nitrogen molecules in turn participate in the production of NO in gas phase reactions R8-R10. Concentrations of NO and N₂ that are

Adsorption and reactivity of N atoms

established in the probe discharge arise from the balance between processes of NO destruction and production.

Reaction	Rate constant	Ref
R6 $e + NO \rightarrow N + O$	//	
R7 $N + NO \rightarrow N_2 + O$	$k_6 = 1.8 \cdot 10^{-11} \text{ cm}^3 \text{ s}^{-1}$	[63]
R8 $N_2(A) + O \rightarrow NO + N(^2D)$	$k_7 = 7 \cdot 10^{-12} \text{ cm}^3 \text{ s}^{-1}$	[63]
R9 $N_2(v>12) + O \rightarrow NO + N(^4S)$	$k_8 = 10^{-11} \text{ cm}^3 \text{ s}^{-1}$	[63]
R10 $N(^2D) + O_2 \rightarrow NO + O$	$k_9 = 5.2 \cdot 10^{-12} \text{ cm}^3 \text{ s}^{-1}$	[63]

Table 3. 6 Gas phase reactions relevant to NO kinetics during the probe discharge.

We conclude that under continuous O_2 plasma exposure NO is not a good marker for probing surface reactivity because it is rapidly transformed into N_2 . Remarkable coincidence of results obtained using dc and rf probe discharge shown in Figure 3. 17 is accidental and should not be misinterpreted. In the dc pulsed discharge saturation of NO concentration is reached when O atoms recombine with all the available N_{ads}^* while in the rf discharge saturation originates from the balance between production and destruction of NO.

3.4.3 Investigation of adsorption and reactivity of N using measurements of NO production on the surface

Based on the results obtained with pulsed and continuous O_2 probe discharges we can distinguish two types of N atoms on silica surface pretreated by N_2 plasma.

- N_{ads}^* that are available for recombination with O atoms in the afterglow of a pulsed O_2 discharge. The coverage of these atoms $[N_{\text{ads}}^*] = 3.5 \cdot 10^{13} \text{ cm}^{-2}$.
- The rest of N_{ads} atoms in SiO_xN_y layer. These atoms are less reactive and they can be removed from the surface under continuous O_2 plasma exposure where ion and atomic fluxes are present simultaneously. The coverage of these atoms $[N_{\text{ads}}] \sim 5 \cdot 10^{15} \text{ cm}^{-2}$ after 60 minutes of standard N_2 rf discharge pretreatment.

N_{ads}^* are active for recombination with O atoms. What if N_{ads}^* efficiently recombine with N? In § 3.3.4.2 we have suggested that recombination of nitrogen atoms on the surface may take place on a small fraction of strongly bonded but reactive N_{ads} . The coverage of N_{ads}^* is comparable with the detection limit of mass spectrometric diagnostics, so they could have been missed in experiments shown in Figure 3. 12. Measurements of NO production on the surface allows for much better detection limits of adsorbed nitrogen atoms. Below using NO as a probe, we investigate adsorption kinetics and reactivity of N_{ads}^* trying to understand if they indeed play a role of active sites for recombination of N on the surface.

3.4.3.1 Kinetics of adsorption

Silica discharge tube was first cleaned by argon plasma in standard conditions during 60 min and then exposed to N_2 rf discharge for time duration in the range $10^{-2} - 10^4$ s. Then the

density of N_{ads}^* was probed by a pulsed dc discharge in O_2 in closed reactor ($p=5.3$ mbar, $i=100$ mA, $\tau=10$ ms). Figure 3. 18 shows the evolution of the coverage of N_{ads}^* as a function of the pretreatment duration. The upper abscissa axis represents the number of N atoms lost on the surface during the pretreatment (see the estimation made in §3.3.2.3).

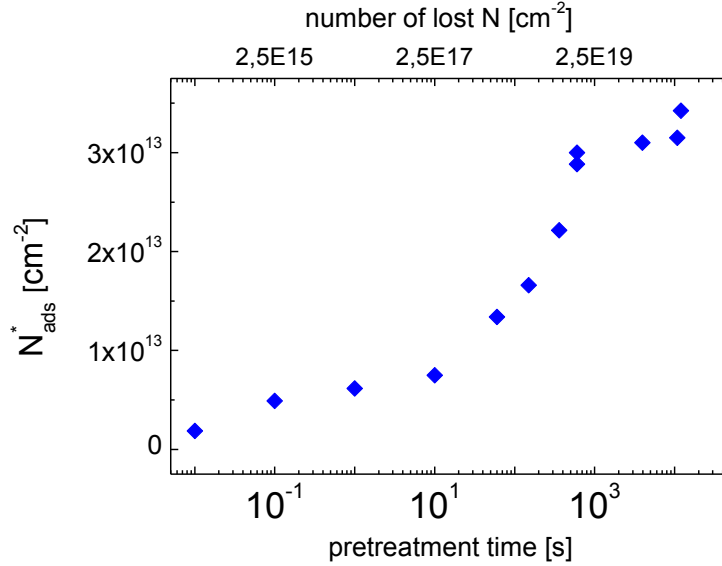


Figure 3. 18 The density of N_{ads}^* grafted to the surface of silica discharge tube as a function of N_2 plasma pretreatment duration. The upper abscissa axis represents the number of N atoms lost on the surface during the N_2 plasma pretreatment.

One can see that the coverage of N_{ads}^* increases when the duration of N_2 plasma is increased and it reaches saturation at $t \sim 10^3$ s. Comparison between the density of grafted atoms and the number of N lost on the surface shows that most of N atoms produced in the discharge during the pretreatment recombine without being adsorbed as N_{ads}^* . In other words, building up of the coverage N_{ads}^* is a slow process compared to the recombination of N on the surface. It is interesting to note that the time required to reach a saturating coverage of N_{ads}^* is equal to the time of formation of a SiO_xN_y layer containing $2 \cdot 10^{15}$ nitrogen atoms per cm^2 .

In order to check if nitrogen atoms alone can be adsorbed on silica surface, pretreatment by a flowing afterglow was studied. First, the reactor was cleaned by a discharge in argon as before and then N_2 plasma pretreatment was performed by a half of the standard length (25 cm long) discharge column placed either in the upstream or in the downstream configuration during 60 minutes (see Figure 3. 19). Nitrogen pressure and flow were the same as in standard conditions. After this sequence a dc probe discharge ($p=5.3$ mbar, $i=100$ mA, $\tau=10$ ms) in O_2 was applied.

Figure 3. 19 shows NO production in the probe discharge after upstream, downstream and standard (full length) N_2 plasma pretreatment. One can note that half size pretreatment yields

Adsorption and reactivity of N atoms

approximately two times less production of nitric oxide and that both upstream and downstream configurations result in almost the same amount of NO. If the adsorption sites for N_{ads}^* on SiO_2 were available after argon plasma cleaning, N atoms produced in the upstream configuration would be transported by the gas flow and adsorbed in the downstream region. But this adsorption is not observed within the uncertainty of the measurements which was $\sim 2 \cdot 10^{12}$ N atoms per cm^2 .

This means that adsorption of neutral nitrogen atoms on neat SiO_2 is very weak. Significant amount of N_{ads}^* is grafted to the surface only under direct N_2 plasma exposure and as we have seen adsorption is slow so a SiO_xN_y layer has enough time to be formed. In other words, N_{ads}^* represent a reactive superficial nitrogen atoms on the SiO_xN_y layer formed on SiO_2 under N_2 plasma exposure.

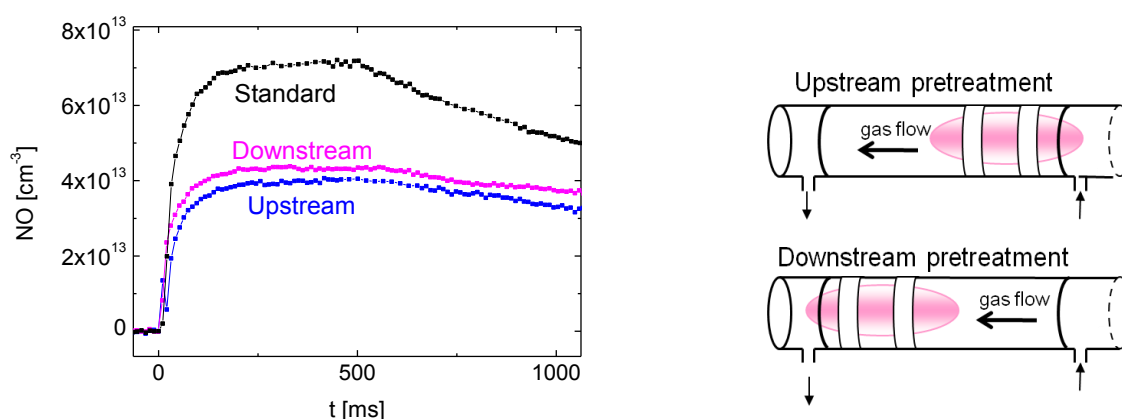


Figure 3. 19 Comparison of NO production in the probe discharge after three different pretreatment configurations.

3.4.3.2 Are N_{ads}^* active for recombination of N on the surface?

Once the SiO_xN_y layer is formed and the coverage of N_{ads}^* has reached the saturation, do these reactive atoms participate in surface recombination of N? To answer this question we use again isotopic exchange under $^{30}N_2$ plasma exposure. But in order to improve the sensitivity instead of measuring $^{29}N_2$ produced on the surface we detect isotopologues of NO in the probe discharge in O_2 .

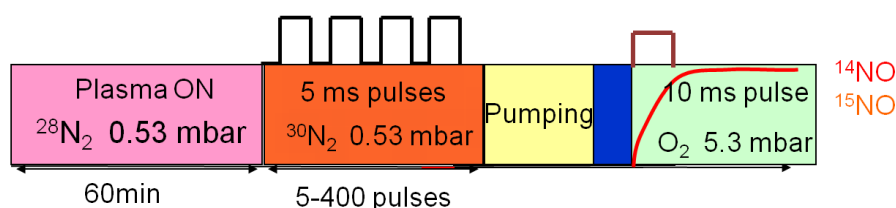


Figure 3. 20 Experimental procedure for investigation of isotopic exchange with TDLAS diagnostics.

Schematics of the experimental procedure is shown in Figure 3. 20. First, silica discharge tube was pretreated by N₂ plasma in standard conditions during 60 minutes. Then it was pumped and filled with ³⁰N₂ at p=0.53 mbar and pulsed dc discharge was applied in closed reactor (i=100 mA, τ=5 ms). Then the reactor was pumped again and filled with O₂ at 5.3 mbar and a single probe pulse (i=100 mA, τ=10 ms) was applied. Production of ¹⁵NO and ¹⁴NO in the probe discharge was detected *in-situ* using TDL spectrometer. Surface coverage of ¹⁴N_{ads}^{*} and ¹⁵N_{ads}^{*} was calculated based on the maximum measured concentrations of ¹⁵NO and ¹⁴NO.

Figure 3. 21 a) shows an example of simultaneous time resolved measurements of ¹⁵NO and ¹⁴NO production on the surface in the probe discharge. In panel b) the coverage of ¹⁴N_{ads}^{*} and ¹⁵N_{ads}^{*} as a function of the number of discharge pulses in ³⁰N₂ is shown. One can see that atoms ¹⁴N are replaced by ¹⁵N while the total coverage stays constant. The rate of ¹⁴N ↔ ¹⁵N exchange should be compared with the number of ¹⁵N lost on the surface (see the estimation made in § 3.3.2.3). The fastest exchange rate was observed during the first discharge pulses in ³⁰N₂. After five dc pulses in ³⁰N₂ the coverage of ¹⁴N_{ads}^{*} replaced by ¹⁵N_{ads}^{*} is 1.2 · 10¹³ cm⁻² but the number of ¹⁵N lost on the surface is 10¹⁵ cm⁻². This means that only a small fraction of ¹⁵N (approximately 2%) recombine with ¹⁴N_{ads}^{*}. This experiments show that even the most reactive N_{ads} on the surface – ¹⁴N_{ads}^{*} are not efficient for surface recombination of ¹⁵N.

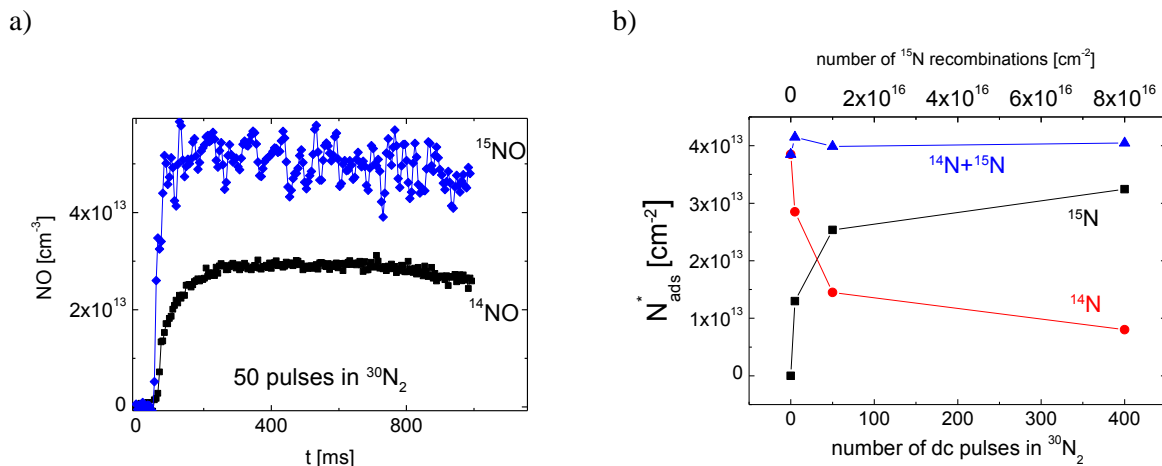


Figure 3. 21 a) Time resolved measurements of ¹⁴NO and ¹⁵NO in a 10 ms, 100 mA probe discharge in O₂ at p=5.3 mbar after standard pretreatment with ²⁸N₂ rf discharge followed by 50 dc discharge pulses in ³⁰N₂ b) Coverage of ¹⁴N_{ads}^{*} and ¹⁵N_{ads}^{*} as a function of the number of dc pulses in ³⁰N₂ measured using TDLAS.

Even using diagnostics capable of detecting surface coverage of N_{ads} of the order of 10¹² cm⁻² we haven't found N_{ads} that are active for N recombination on the surface. We think that hypothesis (i) proposed in § 3.3.4.2 is more plausible, recombination of nitrogen atoms on the surface takes place on **weakly bonding** active sites. Atoms adsorbed on these sites are not stable, they leave the surface shortly after the end of plasma exposure that is why they are not detected in the probe discharge.

Adsorption and reactivity of N atoms

3.5 Discussion and conclusions

To the best of our knowledge nitrogen atoms chemisorbed on the surface of SiO₂ have never been observed experimentally. Thus, our starting point was the model description of atomic recombination of Kim&Boudart [5] and similar [22][26][110]. We expected that after N₂ plasma exposure the surface of silica would be covered with chemisorbed N atoms having the density of the order of 10¹³ - 10¹⁴ cm⁻². According to [5] chemisorbed atoms effectively recombine with N coming from the gas phase and play the role of the main active sites for atomic recombination on the surface.

The real picture of interaction between N₂ plasma and silica surface turned out to be more complex. Here are the main results of this chapter.

Adsorption of N

- Under N₂ plasma exposure silicon oxynitride layer is formed on the surface of silica discharge tube. In our standard pretreatment conditions the density of N_{ads} is increasing as a square root of the pretreatment duration; [N_{ads}](1s) = 1·10¹⁴ cm⁻² and [N_{ads}](3600s) = 6·10¹⁵ cm⁻².
- Nitridation is driven by ion bombardment and it takes place only under direct N₂ plasma exposure. When silica surface is exposed to a flowing post-discharge nitridation is negligible. Therefore, material of the surface in discharge and flowing post-discharge zones is completely different (SiO_xN_y in plasma zone and SiO₂ in the post-discharge zone). This may partially explain the enhancement of γ_N under direct plasma exposure reported in [101].
- Formation of SiO_xN_y layer is very sensitive to the presence of O₂ admixtures in N₂ plasma. Addition of 0.1% of O₂ into N₂ reduces the number of grafted N atoms by a factor of 10. Therefore, condition of the reactor surface is strongly dependent on the composition of the gas mixture.

Reactivity of N_{ads}

- Under N₂ plasma exposure, N_{ads} are continuously replaced. We have found two groups of N_{ads}: i) first with a characteristic turnover time ~ 10 s in our standard rf discharge conditions ii) second having the characteristic replacement time ~ 300 s. The first group was assigned to N on the outmost surface layer and the second one to N distributed in the SiO_xN_y layer. Our results demonstrate that under direct N₂ plasma exposure the surface is not static, it is continuously modified due to the exposure to ion and atomic fluxes.
- Nitrogen atoms on the surface of SiO_xN_y exhibit a distribution of reactivity. We have found a small fraction of N_{ads} (having a coverage [N_{ads}^{*}]=3.5·10¹³ cm⁻²) that readily recombine with atomic oxygen producing NO molecules.

- N_{ads} participate in recombination of N on the surface, but recombination with these atoms cannot explain the rate of N losses on the surface. We suppose therefore that recombination of N atoms takes place on **weakly bonding** active sites.

What is the nature of these weakly bonded atoms that are active for recombination? They may be either (i) physisorbed or (ii) chemisorbed but with a relatively small binding energy.

Models of surface recombination [5][26] predict that at room temperature the coverage of physisorbed atoms on silica-like surfaces is small and LH recombination between two physisorbed atoms or ER recombination between physisorbed and gas phase atoms is negligible. We think that hypothesis (ii) is more plausible. According to the estimation made in § 1.1.1.2 atoms with binding energy smaller than approximately 1 eV are weakly chemisorbed. Existence N^{weak} signifies that on the surface there exists a **distribution** of chemisorption sites with different adsorption energies. Real silica surface is not perfectly smooth and homogeneous, as one can clearly see on a microscope image of quartz shown in Figure 3.22 (the image is taken from [20]). Therefore different adsorption configurations of N may exist leading to the presence of relatively weakly bonded chemisorbed species that efficiently participate in surface recombination.

Recently, distribution of binding energies of O atoms on different surfaces has been demonstrated in spinning wall experiments of Donnelly *et al.* [54]. Similarly to the results of this section, authors [54] show that stable strongly bonded O atoms are not efficient for LH recombination on the surface of the rotating substrate. According to [54], O_{ads} that participate in surface recombination have the lifetime on the surface of the order of few milliseconds.

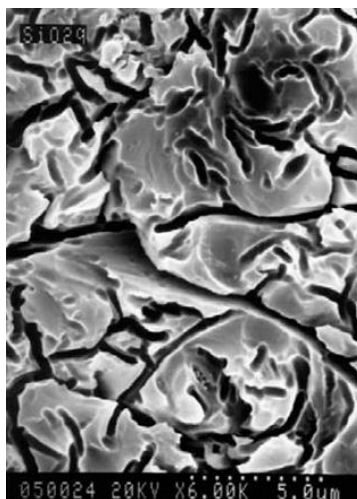


Figure 3.22 Microscope image of quartz published in [20].

It is interesting to note that even ideal crystalline SiO_2 surface may possess different types of adsorption sites. A recent *ab-initio* study of O and N adsorption on β -cristobalite [40] has revealed adsorption configurations with binding energies in the range 0.2 – 6 eV. Therefore, distribution of binding energy of atoms on real surfaces is a general phenomenon and it should be taken into account in the modelling of surface atomic recombination.

Adsorption and reactivity of N atoms

Based on the observations made in this chapter we conclude that the mechanism of N recombination on the surface of SiO_2 under plasma exposure differs from simplified picture used in mesoscopic models. Three types of N atoms on SiO_2 surface exposed to N_2 plasma can be distinguished:

- Atoms incorporated in SiO_xN_y . These atoms are distributed in the 2-3 nm thick surface layer, they compose the material of the surface and their contribution to recombination of N is negligible.
- Stable N atoms on the surface of SiO_xN_y . Reactions with these atoms account for maximum 20% of atomic nitrogen losses on the surface. Among these atoms we have found a small fraction of reactive N_{ads}^* that produce NO in reactions with atomic oxygen.
- Weakly bonded N atoms with binding energy inferior to ≈ 1 eV. Surface recombination proceeds mainly via reactions of these unstable atoms.

Schematically different groups of N atoms are shown in Figure 3. 23. In the first figure the spatial distribution of N on the surface is shown. In the second case we tentatively arrange different groups as a function of their binding energy on the surface.

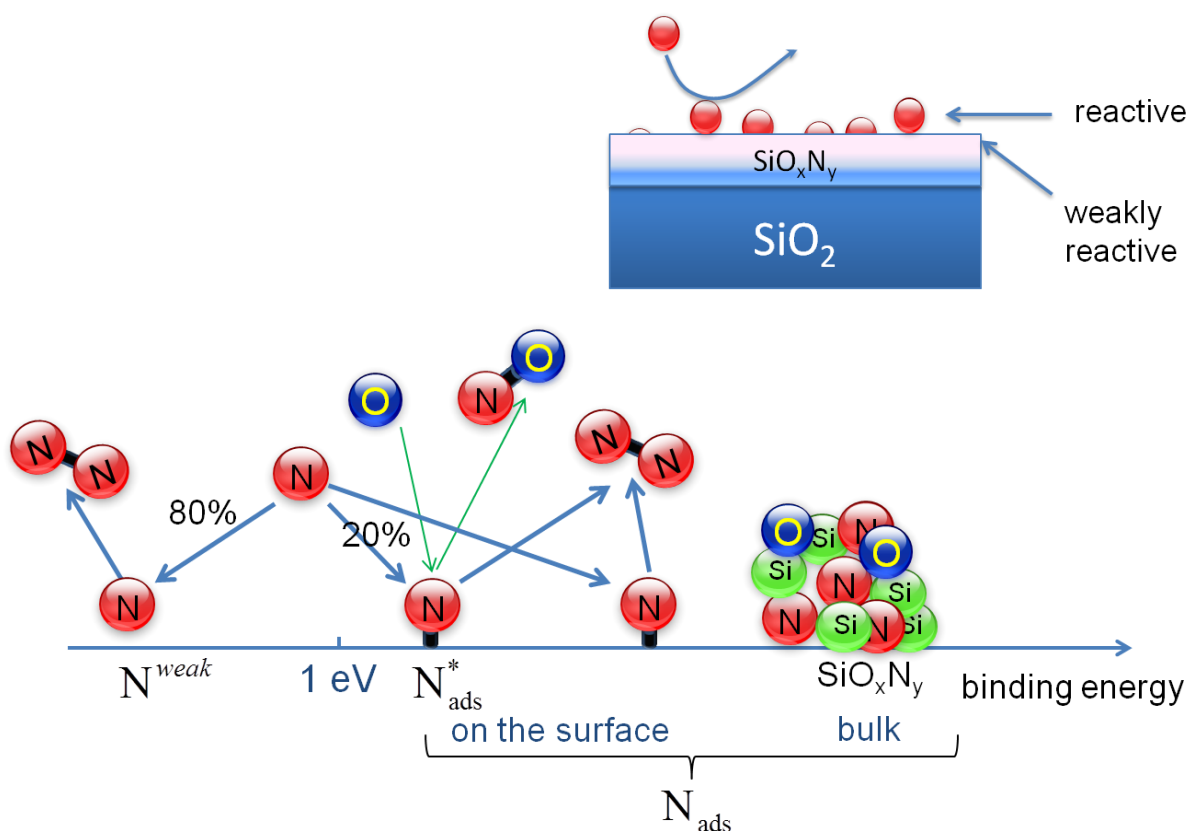


Figure 3. 23 Schematic representation of different group of N atoms on silica surface.

3.5.1 Summary and conclusions on used diagnostics

In this section we have employed three different techniques in order to probe the coverage and reactivity of nitrogen atoms on SiO₂ pretreated by N₂ plasma. Apart from XPS which is a classical diagnostics for surface analysis, two other methods were developed and validated in this work. Here we list the main advantages and limitations of the used experimental techniques.

XPS:

- ✓ Real surface diagnostics – gives information about binding configurations of species on the surface.
- ✓ Absolute measurements of surface concentrations are possible.
- ✗ Not sensitive to the reactivity of adsorbed species.
- ✗ Ex-situ. Samples may be modified when exposed to air.
- ✗ Bad sensitivity ($[N_{\text{ads}}] \sim 10^{14} \text{ cm}^{-2}$).

Isotopic exchange:

- ✓ Gives information about reactivity of adsorbed N atoms.
- ✓ Absolute measurements of surface concentrations are possible.
- ✓ Rather sensitive, detection limit is of the order of 10^{13} cm^{-2} .
- ✓ In-situ.
- ✗ It is not possible to follow the kinetics of surface reactions in real time.

Titration with NO:

- ✓ Gives information about reactivity of adsorbed N atoms.
- ✓ Very sensitive, detection limit 10^{12} cm^{-2} .
- ✓ In-situ.
- ✓ Time-resolved measurements of the kinetics of surface recombination.
- ✗ Absolute measurements of surface concentrations are difficult because produced NO further reacts on the surface and in the gas phase.

Table 3. 7 summarizes the characteristics of the diagnostics used to probe the coverage and reactivity of N on the surface.

	binding config.	sensitive to react.	abs. coverage	in-situ	detection limits	time resolution
XPS	✓	✗	✓	✗	10^{14} cm^{-2}	10^2 s
Isotopic exchange	✗	✓	✓	✓	10^{13} cm^{-2}	0.1 s
NO production	✗	✓	✗	✓	10^{12} cm^{-2}	10^{-3} s

Table 3. 7 Summary on the diagnostics used to probe the coverage and reactivity of N on the surface.

Adsorption and reactivity of N atoms

4. Chapter IV: Adsorption and reactivity of oxygen atoms on oxide surfaces under plasma exposure

4.1 Introduction

Fundamentally, interaction between O atoms and silica-like surfaces is analogous to the case of N-SiO₂ that we have studied in the previous chapter. For example, in Kim&Boudart [5] model parameters (activation energy, active site density, etc.) found for O and N recombination on silica are identical. Similarly to γ_N , the values of γ_O published in the literature exhibit a strong scatter [21][46]. According to [21][110] the value γ_O on the surface in direct contact with the plasma is systematically higher than on unexposed surface.

In spite of named similarities, several particular features of interaction between O₂ plasma and silica-like (and more generally oxide) surfaces can be outlined:

- Oxide materials such as silica, Pyrex or TiO₂ are already composed of atomic oxygen. Therefore, under O₂ plasma exposure the chemical nature of oxide materials will not be changed in contrast to oxynitride formation observed in experiments with N₂ plasma.
- We have found that N_{ads} are particularly stable and weakly reactive. Several test experiments have been done (not mentioned in the previous chapter) showing that N_{ads} do not react with stable molecules such as NO, NO₂, N₂O, CO₂, CO, C₂H₂. Atomic oxygen is a strong oxidizing agent, in [8] it has been shown that stable O adsorbed on catalyst materials under plasma exposure are capable of oxidizing CO into CO₂. Therefore, in case of O_{ads} we will specially focus on the reactivity of O_{ads} towards stable molecules.
- In recombination of atomic oxygen on the surface two channels are possible: (O+O)_w→O₂ and (O+O₂)_w→O₃. The second mechanism is usually overlooked, but recently it has been shown that it may be an important source of ozone as well as an efficient loss mechanism of atomic oxygen in O₂ plasmas [107][111]. As it was discussed in § 1.1.3, the bond strength of O in ozone $D(O-O_2)=1.04$ eV and only O with binding energy smaller than 1.04 eV may participate in O₃ formation on the surface. Therefore, formation of ozone takes place in reactions of O^{weak}.

Our aim in this chapter is to understand how oxygen atoms are adsorbed on oxide surfaces under O₂ plasma exposure and to evaluate their role in surface-catalyzed reactions of stable molecules and radicals.

Adsorption and reactivity of O atoms

4.1.1 Experimental procedures

In this study we use the approach described in Chapter 1 that consists in the pretreatment of the surface by O_2 plasma followed by the study of grafted O species. Three different materials are investigated: silica, Pyrex and TiO_2 . The pretreatment is performed using a flowing rf discharge in O_2 in standard conditions (see Table 3.1). Then we probe the pretreated surface in order to answer the following questions:

- *What is the coverage of O_{ads} ?*
- *What is their role in surface recombination of O?*
- *How O_{ads} participate in surface oxidation of stable molecules such as NO and C_2H_2 ?*

It should be noted, that we work with oxide catalysts that already contain oxygen atoms. This makes difficult the detection of adsorbed O species by surface analysis techniques (such as XPS). Therefore, the following experiments have been performed:

- *Reactivity of $^{16}O_{ads}$ under $^{36}O_2$ plasma exposure:* the surface pretreated by rf discharge in $^{32}O_2$ is exposed to plasma in $^{36}O_2$. Molecules $^{18}O^{16}O$ produced on the surface are then detected using the mass spectrometer. Procedure with inverted order is also employed – first $^{36}O_2$ plasma pretreatment and then $^{32}O_2$ probe discharge.
- *Reactivity of O_{ads} in the post discharge:* a controlled amount of probe molecules (NO, NO_2 , C_2H_2) is introduced in the pretreated reactor in static conditions. Then the kinetics of surface reactions is followed using laser absorption spectroscopy or mass-spectrometry.
- In order to get insight in the reactivity of O^{weak} we investigate ozone formation on the surface in a pulsed dc discharge in O_2 . Time resolved measurements of O and O_3 concentrations are performed using TALIF and UV absorption spectroscopy.

4.2 Chemisorption of O on silica-like surfaces: isotopic study

In experiments with heavy nitrogen isotopes we have seen that isotopic exchange on the surface under plasma exposure allows characterization of the coverage and reactivity of adsorbed atoms and their role for surface atomic recombination. In this section we use $^{16}O \leftrightarrow ^{18}O$ exchange coupled with mass spectrometric diagnostics in order to investigate adsorption and reactivity of O atoms on the surface of silica and Pyrex.

4.2.1 Experimental details

Typical experimental procedure is shown in Figure 4. 1. First, the discharge tube made of silica or Pyrex was cleaned by an rf discharge in argon during 30 min in standard conditions (see Table 3.1). Then $^{36}O_2$ gas (Icon Isotope Services 99 at. % of ^{18}O) was introduced in the reactor at $p=0.53$ mbar and standard rf discharge (see Table 3.1) was started in static

conditions for time duration in the range $10^{-1} - 10^3$ s. Then the reactor was pumped and an identical rf discharge in $^{32}\text{O}_2$ at $p=0.53$ mbar was applied in order to probe adsorbed ^{18}O left on the surface after the first step. Oxygen gas was sampled to the quadrupole mass spectrometer (QMS) after each plasma step.

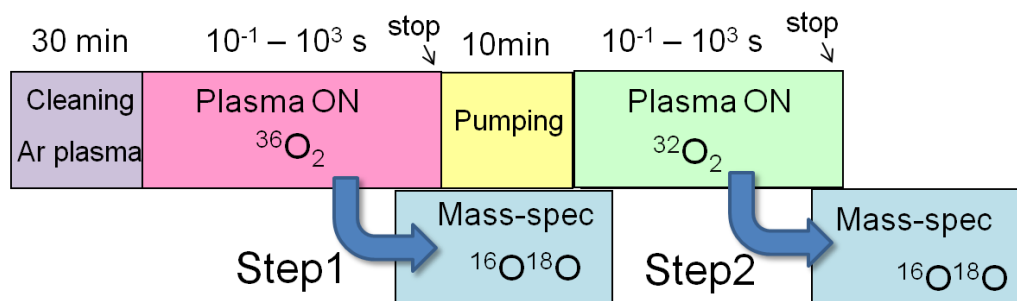


Figure 4. 1 Schematics of the experimental procedure.

In oxygen, exchange reactions like $^{18}\text{O} + ^{16}\text{O}^{16}\text{O} \leftrightarrow ^{16}\text{O} + ^{18}\text{O}^{16}\text{O}$ are very fast [107]. Thus in the discharge, a statistical isotopic distribution of three O_2 isotopologues is always established. The signals at $m=32$, 34 and 36 a.m.u. were measured with the QMS in order to determine the number of oxygen atoms that were picked up from the surface. Figure 4. 2 shows an example of the mass-spectrometric measurements performed on the “Step 1”. Mass peaks at $m=32$ and $m=34$ a.m.u. appear with increasing the duration of the discharge in $^{36}\text{O}_2$.

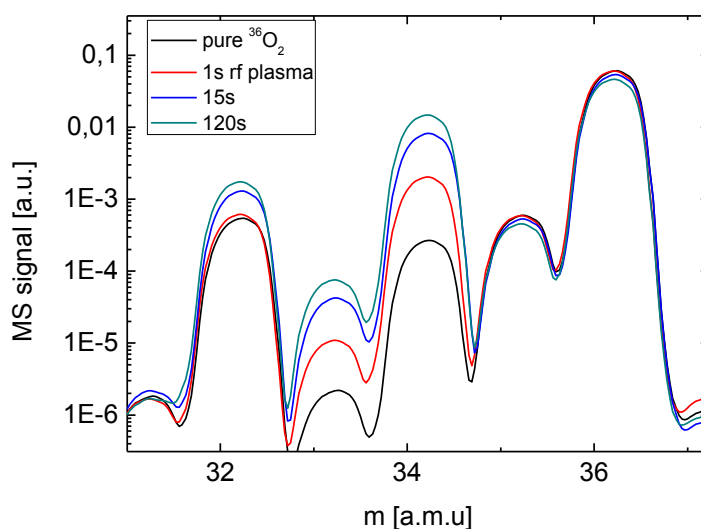


Figure 4. 2 Mass spectra obtained after various duration of rf discharge in $^{36}\text{O}_2$ in Pyrex discharge tube. Reactor was initially cleaned by argon plasma during 30 min.

Relative measurements of the isotopic composition were converted in absolute gas phase concentrations using the known value of the gas pressure. The coverage of O_{ads} was

Adsorption and reactivity of O atoms

determined using the surface to volume ratio of the reactor as in § 3.3.1. The detection limit of O_{ads} was estimated to be approximately 10^{13} cm^{-2} .

4.2.2 Do O atoms of the material participate in surface reactivity?

First we investigate the Step 1 shown in Figure 4. 1. As we will see in the following sections, after argon plasma cleaning the surface is free from adsorbed oxygen atoms. The appearance of ^{16}O in the gas phase under $^{36}\text{O}_2$ plasma exposure may be ascribed only to the reactivity of oxygen from the crystalline network of silica or Pyrex. In Figure 4. 3 the surface density of ^{16}O atoms picked-up from the surface is shown as a function of the duration of $^{36}\text{O}_2$ plasma exposure in the range 0.1 – 480 s.

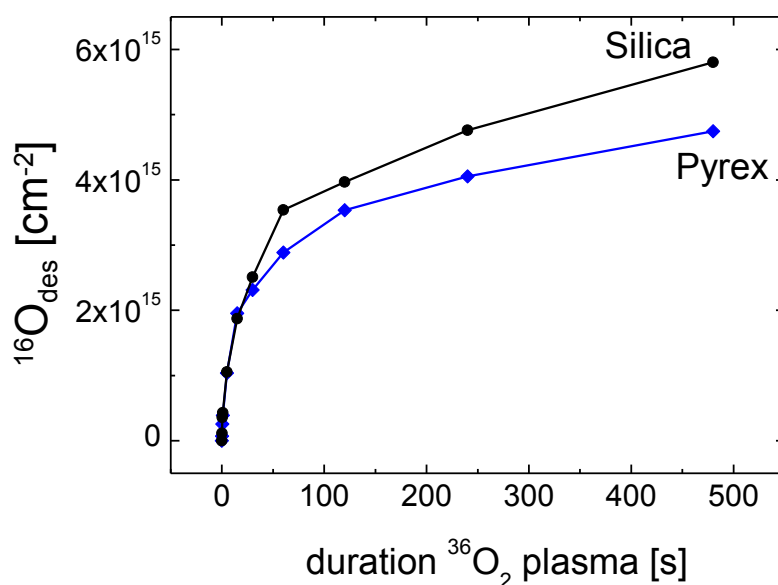


Figure 4. 3 Evolution of the density of ^{16}O atoms picked up from the surface as a function of the probe discharge duration in $^{36}\text{O}_2$. Silica and Pyrex discharge tubes were pre-treated by Ar plasma during 30 minutes.

The coverage of ^{16}O atoms that were picked up from the surface reaches $(5-6) \cdot 10^{15} \text{ cm}^{-2}$ after 480 s of $^{36}\text{O}_2$ plasma exposure. The coverage of $^{16}\text{O}_{des}$ is measured with respect to the geometric surface area of the tube without taking into account surface roughness. According to literature data [26][27] obtained value of $^{16}\text{O}_{des}$ is comparable to one full monolayer on silica-like surface. The initial rate of ^{16}O desorption is $5 \cdot 10^{14} \text{ atoms s}^{-1} \text{ cm}^{-2}$ and it decreases to $5 \cdot 10^{12} \text{ atoms s}^{-1} \text{ cm}^{-2}$ after 400 s of $^{36}\text{O}_2$ plasma exposure. This may be explained by a fast removal of superficial oxygen followed by much slower extraction of atoms from sub-surface layers. It is interesting to note that results obtained with silica and Pyrex are almost identical. This means that the density and binding of O atoms in these materials are similar.

In the $^{36}\text{O}_2$ discharge, ^{16}O atoms removed from the surface are replaced by ^{18}O . This was verified on the “Step 2” of the experiment. After the $^{36}\text{O}_2$ plasma exposure, the reactor was refilled with $^{32}\text{O}_2$ and a 240 s rf discharge was applied in static conditions. In Figure 4. 4, the

coverage of ^{18}O desorbed from silica surface during $^{32}\text{O}_2$ discharge is plotted as a function of the $^{36}\text{O}_2$ discharge duration. For comparison the coverage of ^{16}O desorbed from the surface during the Step 1 is also shown.

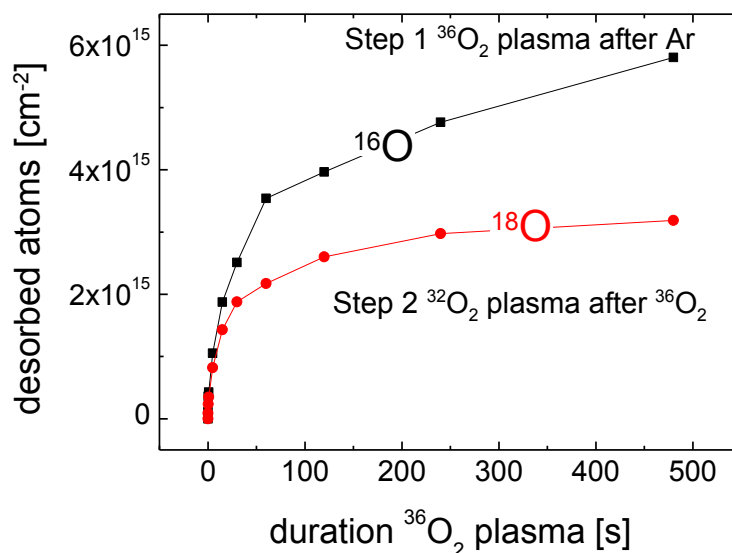


Figure 4. 4 Evolution of the coverage of ^{16}O desorbed from the surface of silica discharge tube under $^{36}\text{O}_2$ plasma exposure (Step 1) as in Figure 4. 3. On the second step ^{18}O was desorbed from the surface by a discharge in $^{32}\text{O}_2$ during 240 s.

One can see that the coverage of desorbed ^{18}O atoms is always smaller than the amount of desorbed ^{16}O . From the first glance this result seems counterintuitive because we would expect that $^{36}\text{O}_2$ plasma grafts some extra ^{18}O atoms to the surface compared to Ar cleaning performed before the Step 1. Observed effect can be explained by the diffusion of ^{18}O into the bulk of SiO_2 , atoms that diffuse inside the material are no longer accessible to the probe discharge in $^{32}\text{O}_2$. The diffusion of O in the SiO_2 network has been observed experimentally at moderate temperatures in [112]. Local surface heating and ion bombardment under direct $^{36}\text{O}_2$ plasma exposure may further promote the diffusion of ^{18}O from the surface.

In addition for relatively long $^{36}\text{O}_2$ pretreatment times, 240 s of $^{32}\text{O}_2$ probe discharge may be not enough to desorb all the available ^{18}O . That explains the saturation of ^{18}O desorption shown in Figure 4. 4 while ^{16}O is still increasing with increasing the $^{36}\text{O}_2$ exposure time.

Our results demonstrate that under direct O_2 plasma exposure oxygen atoms of silica-like materials are continuously exchanged. Therefore, the surface is constantly **re-structured** and it cannot be considered as a static system.

It is interesting to compare the kinetics of ^{16}O desorption from silica surface under $^{36}\text{O}_2$ plasma (shown in Figure 4. 4) with the analogous measurements of ^{14}N desorption performed in $^{30}\text{N}_2$ discharge after $^{28}\text{N}_2$ plasma pretreatment of silica surface (from Figure 3. 11). Surprisingly, the kinetic curves superimposed in Figure 4. 5 are almost **identical** regardless the difference in the plasma forming gas and the chemical nature of the surface. The only

Adsorption and reactivity of O atoms

parameters which were kept the same in two experiments are the gas pressure and the injected power.

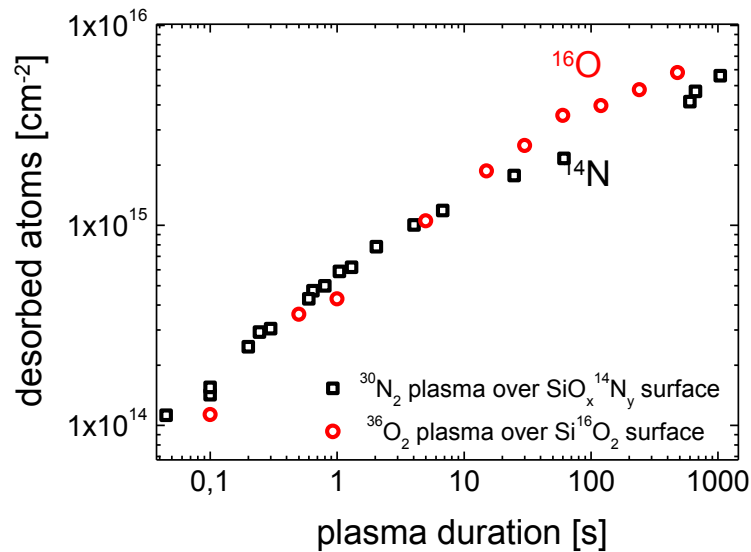


Figure 4. 5 Comparison of the kinetics of desorption of atoms from the surface under plasma exposure. In the first case we observe desorption of ^{14}N under $^{30}\text{N}_2$ plasma exposure from silica surface pretreated by $^{28}\text{N}_2$ discharge (data from Figure 3. 11). In the second case we observe desorption of ^{16}O from silica under $^{36}\text{O}_2$ plasma exposure (data from Figure 4. 4).

Observed result points to the similarity of the mechanism of removal of atoms from the surface in both cases. With the same power injected in the discharge, the dissociation rate in nitrogen is much lower than in oxygen. In [113] authors show that the energy cost of N_2 dissociation in electrical discharges (~ 100 eV per produced atom) is typically 10 times higher than in the case of O_2 (~ 10 eV per produced atom). This is explained by higher dissociation threshold in N_2 . Therefore, atomic fluxes on the surface in the experiments shown in Figure 4. 5 are expected to be quite different. On the contrary, ion flux on the surface is proportional to the density of electrons which is controlled by the injected power. Therefore, ion fluxes in O_2 and N_2 should be comparable. We suppose that ion bombardment plays an important role in the observed isotopic exchange of N and O atoms on the surface.

We don't know yet if ions themselves participate in the exchange of surface atoms or there is a synergetic effect between the ions and neutral atoms. Experiments in which the surface is exposed to independent atomic and ion beams should be performed in order to separate different contributions.

4.2.3 ^{16}O adsorption on the surface under $^{32}\text{O}_2$ plasma exposure

In this experiment we investigate if O atoms can be grafted to the surface under O_2 plasma exposure. Experimental procedure is shown schematically in Figure 4. 6. The surface is probed by a rf discharge in $^{36}\text{O}_2$ in standard conditions and we compare desorption of ^{16}O

from the surface after argon plasma cleaning (“Step 1” in Figure 4. 1) and after $^{32}\text{O}_2$ plasma pretreatment during 20 minutes in standard conditions.

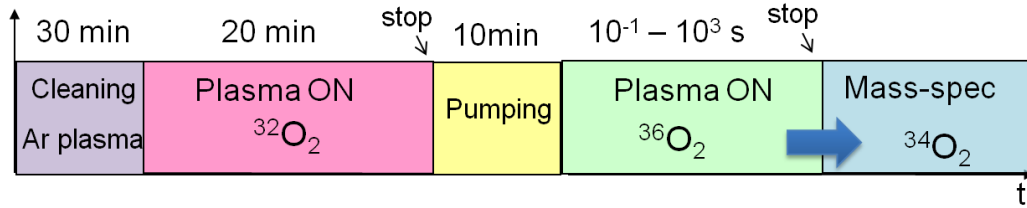


Figure 4. 6 Experimental procedure.

In Figure 4. 7 desorption kinetics of ^{16}O after argon and $^{32}\text{O}_2$ plasma pretreatment are compared. One can see that for both silica and Pyrex $^{32}\text{O}_2$ pretreatment yields somewhat higher desorption of ^{16}O . This indicates that some extra ^{16}O were grafted to the surface by $^{32}\text{O}_2$ plasma. The desorption curves almost coincide during the first 60 s of $^{36}\text{O}_2$ plasma exposure for silica and 20 s for Pyrex.

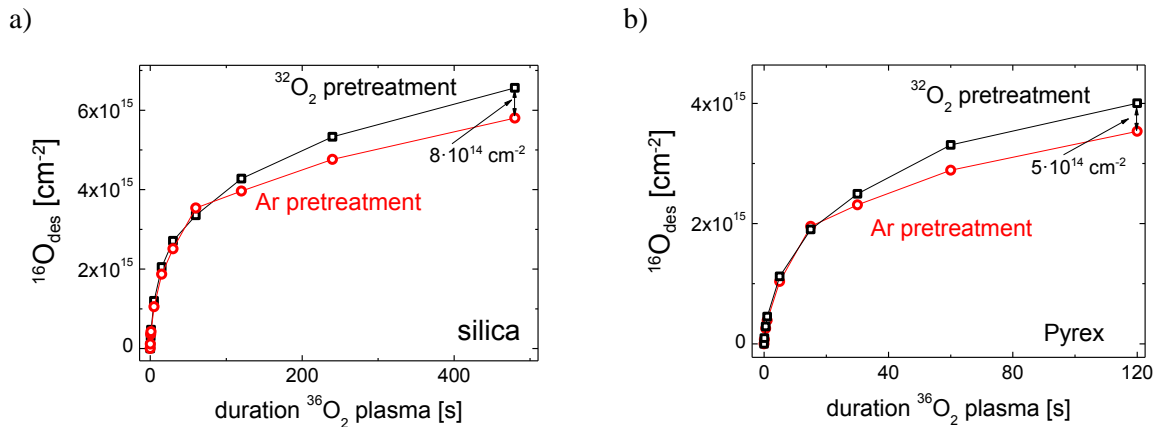


Figure 4. 7 Comparison of ^{16}O desorption from silica (left panel) and Pyrex surface (right panel) under $^{36}\text{O}_2$ plasma exposure after argon plasma pretreatment and $^{32}\text{O}_2$ plasma pretreatment.

If adsorbed oxygen atoms were active for surface recombination, we would expect to observe a fast desorption of ^{16}O in the beginning of $^{36}\text{O}_2$ probe discharge corresponding to grafted ^{16}O ; followed by a parallel evolution of two curves due to the exchange of ^{16}O belonging to the material. Two possible hypotheses may be proposed in order to explain the slow increase of the difference between the desorption curves shown in Figure 4. 7 a) and b):

- ^{16}O grafted to the surface by $^{32}\text{O}_2$ plasma are **weakly reactive**.
- After argon cleaning the state of the surface is **modified** so a direct comparison between Ar and $^{32}\text{O}_2$ pretreatments is not meaningful. In fact, when we compare the results obtained after two different surface pretreatments we suppose that the effect of argon plasma is just “cleaning” and removal of adsorbed O. In [114] it is shown that argon plasma exposure leads to a modification of SiO_2 structure and creation of loose

Adsorption and reactivity of O atoms

and broken bonds. Therefore, argon plasma treatment may coarsen the surface and increase the number of ^{16}O immediately available for exchange under $^{36}\text{O}_2$ plasma exposure. Therefore, the difference between ^{16}O desorption after Ar and $^{32}\text{O}_2$ pretreatments is not ascribed exclusively to the presence of adsorbed ^{16}O .

More work is required in order to verify which hypothesis is correct. In order to probe the reactivity of adsorbed O atoms it would be desirable to get rid from the reactivity of O of the material. For this, ion bombardment on the surface in the probe discharge should be reduced. Therefore, pulsed probe discharge as in § 3.3.4.2 should be used.

4.2.4 Conclusions on the isotopic study

In this section we have applied the isotopic exchange technique in order to investigate interaction between low pressure O_2 plasma and silica-like surfaces (silica, Pyrex). We have found that:

- Under direct O_2 plasma exposure, oxygen atoms that compose the outmost layer of studied materials are exchanged with O atoms and ions from the gas phase. The surface density of O atoms that can be exchanged during $5 \cdot 10^2$ s in our standard pretreatment conditions is of the order of one monolayer $(5-6) \cdot 10^{15} \text{ cm}^{-2}$. Our results show that under O_2 plasma exposure the surface of silica-like materials can't be considered as a static system, it is continuously modified due to ion and atomic exposures.
- Results obtained with silica and Pyrex are very close what indicates that the density and binding of oxygen atoms on the surface of these materials is similar.
- Due to the reactivity of O atoms of the material we were unable to detect unambiguously ^{16}O atoms adsorbed on the surface after $^{32}\text{O}_2$ plasma treatment and evaluate their role in surface recombination of O. Experiment with short dc pulses in $^{36}\text{O}_2$ (similar to one done with $^{30}\text{N}_2$) should be performed in the future.

4.3 Adsorption of atomic oxygen on Pyrex and related reactivity towards NO

We have seen in the previous section that O atoms that compose the crystalline network of silica or Pyrex participate in surface reactivity under $^{36}\text{O}_2$ plasma exposure. Therefore, it is difficult to make a distinction between adsorbed O atoms and atoms of the material when the surface is probed by a continuous discharge.

Following the logic of the Chapter III we have tried to observe the formation of NO in surface recombination $(\text{N} + \text{O}_{\text{ads}})_{\text{wall}}$. But no nitric oxide production was observed in a pulsed dc discharge in N_2 after O_2 plasma pretreatment of the reactor. The main obstacle for detection of surface production of NO in a N_2 discharge is the fast reaction $\text{N} + \text{NO} \rightarrow \text{N}_2 + \text{O}$ that may completely destroy all the produced NO molecules.

In this section we use an alternative way to probe O_{ads} on Pyrex, namely we follow the oxidation of NO in the reaction:



Absolute measurements of NO and NO_2 give the information about the coverage and the reactivity of O_{ads} .

What atoms on the surface are potentially detectable by titration with NO? As it was discussed in § 1.1.3, the reaction ($NO + O_{ads}$) is thermodynamically favourable only if the binding energy of O_{ads} on the surface is smaller than the bond strength: $E_d(O_{ads}) < D(O-NO)=3.1$ eV. From the other hand we detect only sufficiently stable atoms having the lifetime on the surface of the order of 10^3 s. This determines the lower limit of the binding energy of probed O_{ads} of the order of 1 eV (see § 1.1.1.2). Thus, only a fraction of adsorbed oxygen atoms with the binding energy lying in the range $1 \text{ eV} \leq E_a \leq 3.1 \text{ eV}$ can be probed by titration with NO. According to the notation introduced in § 1.7, O_{ads} that are reactive towards NO will be denoted O_{ads}^* .

4.3.1 Experimental details

The experimental procedure is shown schematically in Figure 4. 8. First, the inner surface of the discharge tube was pretreated by a flowing rf discharge in O_2 in standard conditions during 60 minutes. Then the reactor was pumped for 10 minutes in order to remove molecular oxygen and let the surface cool down to room temperature. And finally a mixture containing 1% of NO diluted in argon was rapidly injected in the reactor from the buffer volume at a pressure of 0.045 – 5.3 mbars using fast pneumatic valves. So the concentration of introduced NO was in the range $10^{13} - 10^{15} \text{ cm}^{-3}$.

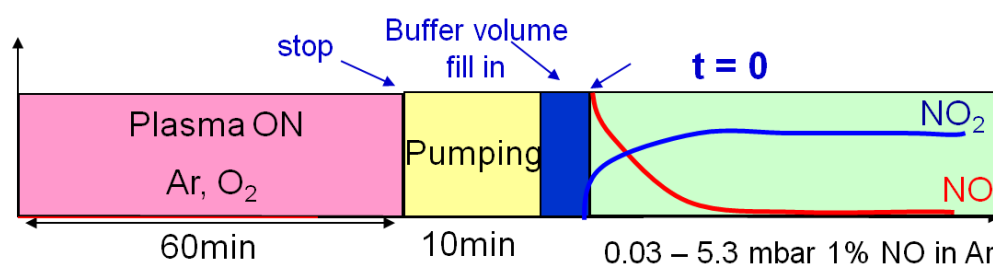


Figure 4. 8 Schematics of the experimental procedure.

Trial experiments have shown that NO kinetics is significantly altered by the presence of any metallic parts in direct contact with the plasma. Therefore, the measurements were performed in a specially designed discharge tube having no dc electrodes and no removable sections. So, the discharge was in contact only with Pyrex surface.

Adsorption and reactivity of O atoms

Typically, time evolution of NO and NO₂ concentrations was followed *in-situ* using laser absorption spectroscopy. Concentration of both species were measured one by one in identical experiments using the TDLAS spectrometer capable of detecting one molecule at a time. The reproducibility of successive measurements was better than 10%, therefore we could compare the kinetics of NO losses and NO₂ production obtained in separate experiments (in identical conditions). Results obtained with TDLAS were confirmed by a series of measurements with a 2-channel QCL spectrometer in which the evolution of NO and NO₂ concentrations was followed simultaneously.

The limit of NO₂ detection with TDLAS was 10^{12} cm^{-3} ; if we assume that one NO₂ correspond to one O_{ads}^{*} picked up from the surface, that corresponds to the surface density of O_{ads}^{*} $\sim 5 \cdot 10^{11} \text{ cm}^{-2}$. Therefore, titration with NO allows detection of the coverage of adsorbed oxygen species the order of 10^{-4} of a monolayer.

4.3.2 Evidence of NO oxidation by adsorbed O atoms

A series experiments with different initial concentration of injected NO was performed. In Figure 4. 9 TDLAS measurements of NO and NO₂ concentrations in Pyrex reactor pretreated by O₂ plasma are shown. One can see that NO is lost and NO₂ is produced after the introduction of the 1%NO-Ar mixture. The total concentration (NO+NO₂) represents the balance of N atoms in the system. When the amount of introduced nitric oxide is small ($\leq 3 \cdot 10^{13} \text{ cm}^{-3}$), NO is converted completely into NO₂. At higher initial concentrations of NO the balance of N atoms is incomplete; a decrease of the total concentration (NO+NO₂) with time can be seen.

Test experiments were performed in order to prove that the observed NO→NO₂ conversion is indeed catalyzed by O atoms adsorbed on Pyrex surface under O₂ plasma exposure.

First, the discharge tube was cleaned by a flowing rf discharge in argon in standard conditions during 60 minutes and then NO was introduced in the reactor. No significant decrease of the NO concentration was observed, and the concentration of NO₂ was always below the detection limit.

In the second test experiment we have verified if NO can be oxidized by adsorbed O₂ molecules. The surface was exposed to a flow of molecular oxygen after 60 min long argon plasma cleaning. No losses of NO and no production of NO₂ could be detected in this case.

Described experiments prove that:

- NO is not lost due to the adsorption neither on Pyrex discharge tube nor on the metallic vacuum connections between the reactor and the vacuum system.
- After argon discharge treatment there is no reactive O atoms on the surface of Pyrex. Therefore, possibility “activation” of O atoms of the material by argon plasma may be excluded.
- Adsorbed O₂ do not contribute to NO→NO₂ conversion on the surface.

We can conclude that stable and at the same time reactive towards NO oxygen atoms are adsorbed on the surface of Pyrex under O₂ plasma exposure.

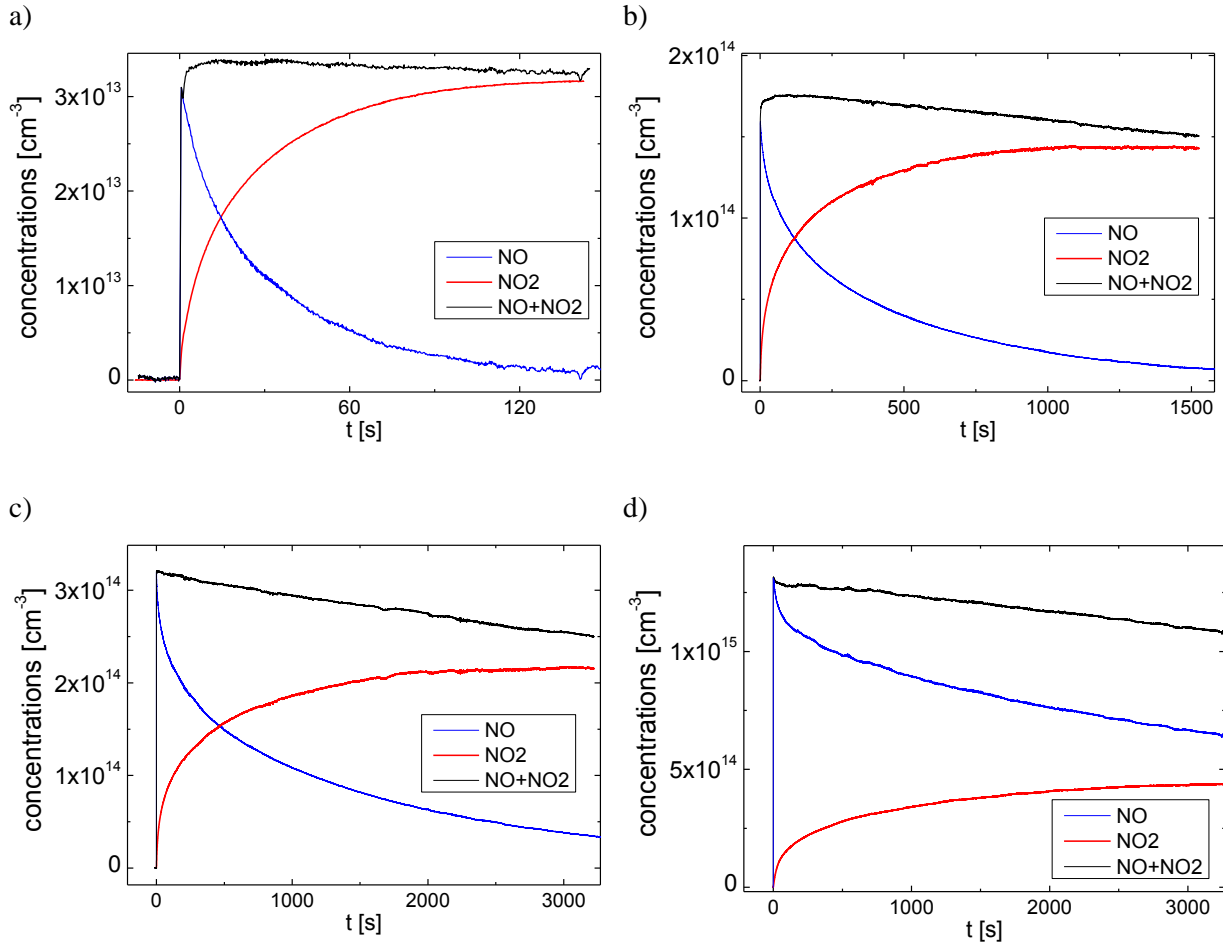


Figure 4. 9 Time evolution of NO and NO₂ concentrations measured by TDLAS. Pyrex discharge tube was pretreated by a capacitive rf discharge in O₂ and then a mixture of 1% NO in Ar was introduced at a pressure a) p = 0.13 mbar b) p = 0.65 mbar c) p = 1.3 mbar, d) p = 5.3 mbar.

4.3.3 Determination of the surface coverage of adsorbed O atoms

The maximum detected concentration of NO₂ may be used to estimate the coverage of O_{ads}^{*}. Assuming that the production of NO₂ stops when all the available O_{ads}^{*} participate in the reaction and taking into account the surface to volume ratio of the discharge tube we have calculated the initial density [O_{ads}^{*}] = 2.5 · 10¹⁴ cm⁻². This value corresponds to the geometrical surface of the tube without taking into account surface roughness.

The non-conservation of the initial value of the concentration of (NO+NO₂) is probably due to the adsorption of NO₂ on the reactor walls or formation of other NO_x that are not measured in this study. Thus, probably not all the O_{ads}^{*} that react on the surface end up as NO₂ molecules in the gas phase. Therefore, obtained value should be considered as the lower boundary of the coverage of [O_{ads}^{*}].

Adsorption and reactivity of O atoms

4.3.4 Evidence of a distribution of reactivity adsorbed O atoms

In Figure 4. 9 we can see that the characteristic time of NO_2 production increases with increasing the amount of introduced NO. It goes from about 60 s for initial concentration $[\text{NO}] = 3 \cdot 10^{13} \text{ cm}^{-3}$ to 1500 s for $[\text{NO}] = 1.3 \cdot 10^{15} \text{ cm}^{-3}$. This points to a complex kinetics of oxidation of NO on the surface. For high concentrations of injected NO we may expect poisoning of the surface by adsorbed reaction products (NO_2 for example), which is supported by observed decrease of the total concentration of $(\text{NO} + \text{NO}_2)$. This complicates the analysis of the kinetics of $\text{NO} \rightarrow \text{NO}_2$ conversion.

According to our results shown in Figure 4. 9, when the initial density of NO is small ($\sim 3 \cdot 10^{13} \text{ cm}^{-3}$) a complete oxidation of NO into NO_2 is achieved. This means that the contribution of adsorbed by-products to the balance of N atoms and poisoning of the surface are negligible. Here we analyse the kinetics of NO oxidation on the surface by further reducing the number of injected NO molecules.

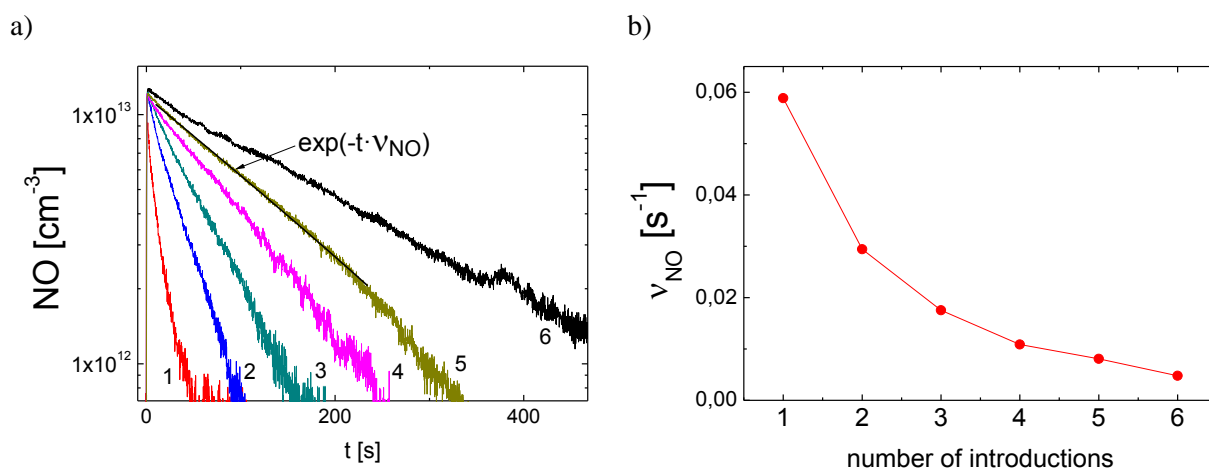


Figure 4. 10 a) Time evolution of NO concentration in successive injections of 1%NO in Ar at $p = 0.045$ mbar after **single** O_2 plasma pretreatment of the surface. The reactor was evacuated after each introduction of the gas mixture. b) Characteristic frequency of NO losses v_{NO} is obtained by fitting the curves from the left panel with $f \sim \exp(-t \cdot v_{\text{NO}})$. An example of the fit is shown in the left panel.

Figure 4. 10 shows the time evolution of NO concentration in successive injections of a 1%NO/Ar gas mixture at 0.045 mbar after a **single** O_2 plasma pretreatment of Pyrex discharge tube. The right panel in Figure 4. 10 shows the characteristic frequency of NO losses calculated using single-exponential fit of curves from the left panel. One can see that the rate of NO oxidation on the surface drops by a factor of 10 between the 1st and the 6th injection of NO.

The number of O_{ads}^* that are used for NO oxidation in 6 successive injections is only $\sim 4 \cdot 10^{13} \text{ cm}^{-2}$, i.e. about 15% of the estimated total coverage of O_{ads}^* . A simple reduction of the density of available reactive oxygen atoms upon injections of NO cannot explain the 10 fold decrease of the v_{NO} . Poisoning of the surface with adsorbed NO_2 has been also excluded. The only

plausible explanation for the observed reduction of the value of v_{NO} is the existence of different groups of adsorbed oxygen atoms that have different reactivity towards NO. Therefore similarly to N_{ads} on SiO_xN_y , O_{ads}^* exhibit a **distribution** of reactivity. Probably, this distribution is related to a distribution of **binding energies** of adsorbed O atoms on a real inhomogeneous surface.

Based on the NO loss frequency shown in Figure 4. 10, the value of the effective loss probability of NO on pretreated surface can be estimated using the well known expression

$$\gamma_{NO \rightarrow NO_2} = \frac{2v_{NO}r}{v_{th}} \quad (3. 10)$$

Where r is the tube radius and v_{th} is the average thermal velocity of molecules. This calculation gave a variation of $\gamma_{NO \rightarrow NO_2} = 2 \cdot 10^{-7} - 2 \cdot 10^{-8}$ between the 1st and the 6th injection respectively. For comparison, the value of $\gamma_{NO \rightarrow NO_2} = 2 \cdot 10^{-7}$ on stainless steel surface in a hollow cathode discharge in air was found in [31].

4.3.5 Conclusions on the study of O_{ads} reactivity on Pyrex

In this section we have shown that:

- Stable and reactive towards NO oxygen atoms are grafted to Pyrex surface under continuous low pressure O_2 plasma exposure. Reaction $NO + O_{ads}^* \rightarrow NO_2$ may be used to titrate O_{ads}^* .
- An important finding is that like in the case of N_{ads} , there exists a distribution of reactivity of O_{ads}^* . We suggest that this distribution is related to the spectrum of binding energies of adsorbed atoms.

The lower limit of the density of O_{ads}^* was found to be $[O_{ads}^*] = 2.5 \cdot 10^{14} \text{ cm}^{-2}$. We don't know yet if these atoms are active for surface recombination of O. New experiments with ^{18}O isotopes employing short dc discharge pulses should be performed in order to probe the reactivity of O_{ads}^* towards ^{18}O . Isotopic exchange $^{16}O_{ads}^* \leftrightarrow ^{18}O$ will be then probed by oxidation of $N^{16}O$ on the surface with the TDLAS detection of $^{16}ON^{16}O$ and $^{16}ON^{18}O$ products in the gas phase.

4.4 On the role of O_{ads} for VOC oxidation

In the previous sections we have proven that under O_2 plasma exposure reactive oxygen atoms may be adsorbed and used for oxidation of stable molecules on silica-like surfaces. In this section we will investigate the reactivity of O_{ads} in connection with air pollution control. In the PhD work of O. Guaitella [64] it has been shown that introduction of high specific surface SiO_2 or SiO_2/TiO_2 catalysts in a DBD discharge improves the efficiency and

Adsorption and reactivity of O atoms

selectivity of C_2H_2 destruction. Stabilization of reactive atomic oxygen on the catalyst surface has been proposed as one of the possible explanations for observed synergetic effects. Similarly, other authors have demonstrated that O adsorbed on the catalyst surface under plasma exposure participate in the VOC destruction [13][115].

The aim of this section is to investigate the potential of O_{ads} for oxidation of C_2H_2 .

4.4.1 Context of the study: influence of the chemical nature of the surface on the reactivity of O_{ads}

The first experiment on C_2H_2 oxidation by catalytic materials pretreated by low pressure plasma was performed at LPP by Olivier Guaitella and Claudia Lazzaroni. Here we will summarize the main results of this work and give the interpretation that became possible after the study of the reactivity of O_{ads} on Pyrex. The details of this work can be found in [116]. The catalysts used in this study were all made of silica fibres coated or not with SiO_2 and TiO_2 nano-particles:

- Silica fibers
- Fibres with $40g/m^2$ of SiO_2 particles (referenced as “Si40”)
- Fibres with $20g/m^2$ of SiO_2 particles and $20g/m^2$ of TiO_2 particles (“Si20Ti20”)

Figure 4. 11 shows a microscopic image of the Si20Ti20 material. With different magnification one can see the fibres and the impregnated particles. Strips of catalytic tissue were placed on the inner surface of the discharge tube and pretreated by a pulsed dc discharge in Ar, O_2 , N_2 or synthetic air at a pressure 1.3 mbar for 30 minutes. Discharge current was 30 mA, frequency 25 Hz and pulse duration 4 ms. Then a mixture containing 950 ppm of C_2H_2 in air was injected in the reactor at $p=1.3$ mbar and the kinetics of C_2H_2 was monitored in-situ using laser absorption spectroscopy. In order to avoid photo catalytic degradation of C_2H_2 the reactor was covered from the external light.

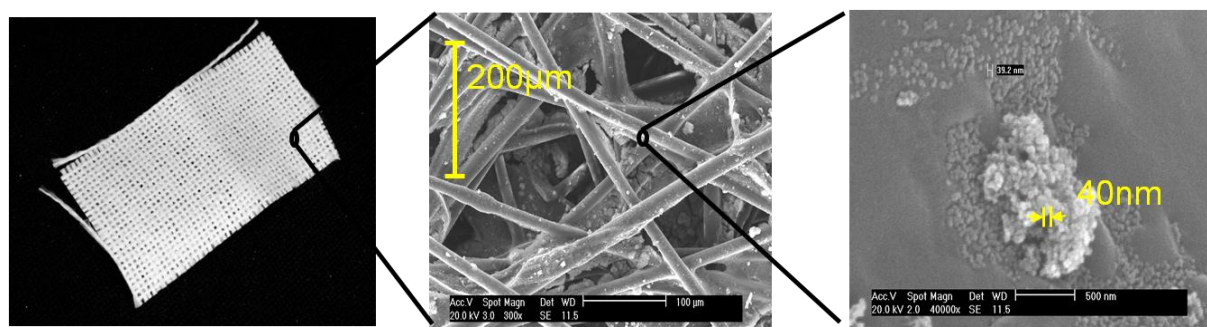


Figure 4. 11 A microscopic image of Si20Ti20 material. With different magnification one can see fibres and impregnated particles.

In Figure 4. 12 the time evolution of C_2H_2 concentration after different plasma pretreatment of Si40 and Si20Ti20 materials is shown. One can see that $[C_2H_2]$ with Si40 material stays constant for all pretreatments, same result was observed with empty Pyrex reactor and reactor filled with just silica fibres. Losses of C_2H_2 were observed *only* when material containing

TiO₂ was pretreated by plasmas containing O₂. In [116] it has been concluded that C₂H₂ molecules can be destroyed by O atoms adsorbed on TiO₂.

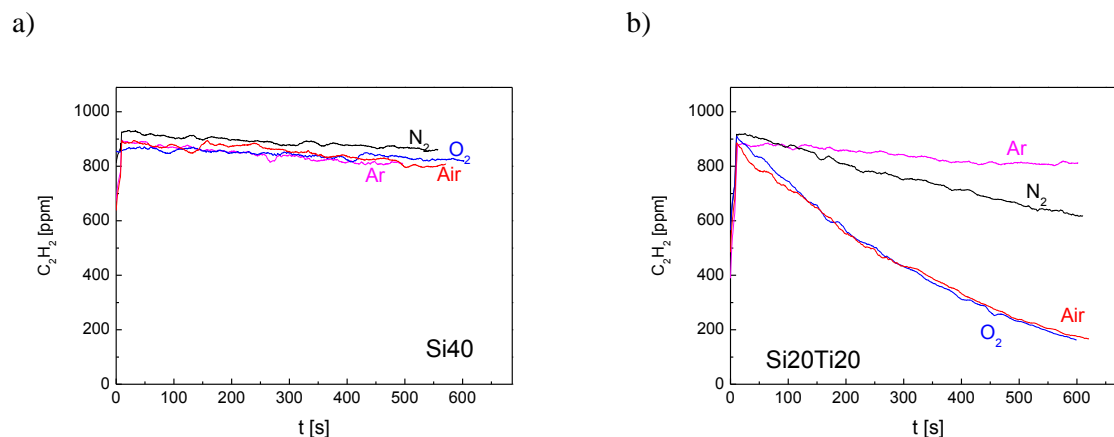


Figure 4.12 Evolution of C₂H₂ concentration after different plasma pretreatment of a) Si40 material b) Si20Ti20 material.

Based on the results of previous sections we know that under O₂ plasma exposure adsorbed O atoms would be found on silica and Pyrex as well. However, these atoms are not reactive towards C₂H₂. In order to explain this difference of the reactivity of O atoms adsorbed on SiO₂ and TiO₂ it was suggested in [116] that the binding energy of O_{ads} on these materials is different. This hypothesis is supported by recent *ab-initio* study of O adsorption on TiO₂ rutile [117] and β -cristobalite SiO₂ [39]. Calculations have shown that the binding energy of O on SiO₂ (E_{ads}=5.9 eV) is considerably higher than on TiO₂ (E_{ads}=1-1.5 eV).

Comparison between different surfaces (TiO₂, SiO₂, Pyrex) and different target molecules (NO, C₂H₂) brings us to the conclusion that the reactivity of adsorbed oxygen atoms depends on *both* the nature of the **surface** and reacting **molecules**.

Experiments described above gave the first evidence of the specific reactivity of O_{ads} on TiO₂. The main problem of using tissue-like materials was a huge (almost 100 m²) total surface of the catalyst inserted in the discharge tube. In addition TiO₂ particles were distributed inside the tissue as one can see in Figure 4.11 and different particles received completely different plasma exposure. This made difficult the control of the state of the surface and the results were not reproducible. In addition, for understanding of the mechanism of C₂H₂ removal by O_{ads}, possible oxidation products such as CO₂ and CO should be measured. Therefore, a new experiment was set up.

4.4.2 C₂H₂ oxidation by adsorbed oxygen atoms on TiO₂

4.4.2.1 Experimental details

In this study TiO₂ catalyst was deposited on the inner surface of silica discharge tube using sol-gel technique as in [118]. The coating was impregnated with Degussa P25 TiO₂ particles containing anatase and rutile phases in a ratio of about 3:1 [119]. The specific surface of such

Adsorption and reactivity of O atoms

impregnated coating ($38 \text{ m}^2/\text{g}$) was somewhat lower than of non-deposited P25 powder ($48 \text{ m}^2/\text{g}$). Typically, the mass of deposited catalyst was 0.1 g and hence the total surface area of TiO_2 in the reactor was about 4 m^2 .

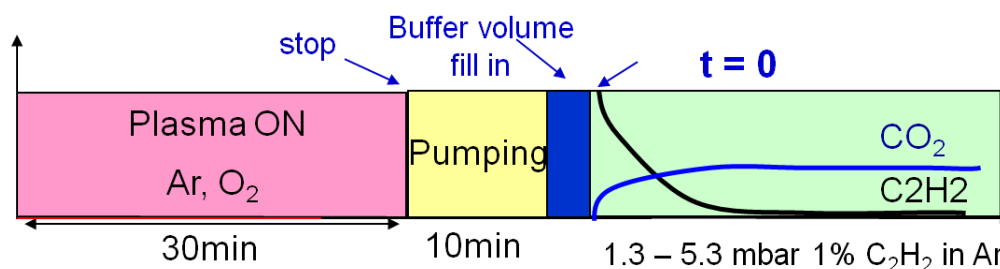


Figure 4. 13 Schematics of the experimental procedure.

Schematically the experimental procedure is shown in Figure 4. 13. The surface was pretreated during 30 min by a rf capacitive discharge in O_2 at a pressure of 0.53 mbar , the discharge power was $P_{\text{pl}}=16 \text{ W}$. Then a mixture of $1\% \text{ C}_2\text{H}_2$ in Ar was introduced in the reactor in static conditions. The reactor was covered from the external light in order to avoid photo catalytic degradation of C_2H_2 . A 3-channel QCL spectrometer was used for simultaneous *in-situ* measurements of C_2H_2 , CO_2 and CO .

4.4.2.2 Kinetics of C_2H_2 destruction on pretreated TiO_2 surface

Figure 4. 14 shows the time evolution of C_2H_2 and CO_2 concentrations after the introduction of a mixture containing 1% of C_2H_2 in argon at $p=2.7 \text{ mbar}$. The number density of C_2H_2 decreases after the introduction and disappears almost completely after 30 min. Upon the removal of C_2H_2 only a small amount of CO_2 is produced ($\sim 2 \cdot 10^{13} \text{ cm}^{-3}$). The concentration of CO was always below the limit of detection ($\sim 10^{13} \text{ cm}^{-3}$).

Observed losses of C_2H_2 may be explained by two mechanisms:

- Adsorption on TiO_2 .
- Chemical reactions on the pretreated surface.

To check if C_2H_2 is simply adsorbed on TiO_2 , a test experiment was performed. The surface was treated during 30 min by argon plasma and in this case no decrease of C_2H_2 concentration was observed. This proves that acetylene is not adsorbed on clean TiO_2 and the removal of C_2H_2 after O_2 plasma pretreatment is catalyzed by adsorbed O atoms.

In order to determine the maximum amount of C_2H_2 that can be removed by the pretreated catalyst, experiments with different pressures of injected acetylene were performed. The saturation was found at the total number $\sim 2 \cdot 10^{17}$ of C_2H_2 molecules in the reactor. Taking into account the surface area of TiO_2 (4 m^2), this corresponds to approximately $\sim 5 \cdot 10^{12} \text{ C}_2\text{H}_2$ molecules lost per cm^2 . This value is much smaller than the density of O_{ads}^* found on Pyrex ($\sim 2 \cdot 10^{14} \text{ cm}^{-2}$) after similar O_2 plasma treatment. The coverage of adsorbed oxygen atoms on TiO_2 after O_2 plasma pretreatment is not known; therefore we are unable to conclude if they

are all reactive towards C_2H_2 or what we observe is only a small fraction of O_{ads} . Very low coverage of O_{ads} reactive towards C_2H_2 points to the fact that only atoms adsorbed on some specific active sites are capable of oxidizing C_2H_2 .

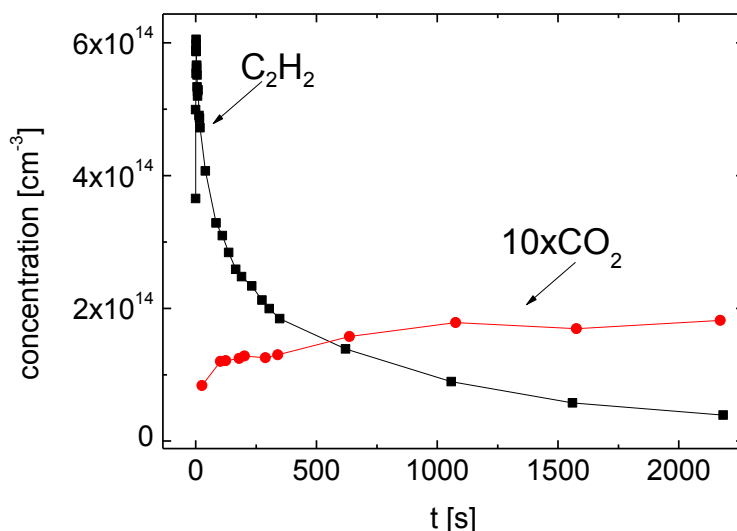


Figure 4. 14 Time evolution of C_2H_2 and CO_2 concentrations measured using QCLAS. A mixture of 1% C_2H_2 in Ar was introduced in the reactor at $p=2.7$ mbar in static conditions after O_2 plasma pretreatment of TiO_2 .

Production of CO_2 shown in Figure 4. 14 represents only 2% of the carbon balance. In order to check if some other products containing C are released upon the destruction of C_2H_2 , mass spectrometric analysis of the gas phase was performed. Mass spectra of the initial mixture (1% C_2H_2 in Ar) and of the gas mixture in the reactor 30 min after the introduction are shown in Figure 4. 15. No new peaks could be detected in the range 1 – 100 a.m.u. (the graph shows only a zoom on 10 – 50 a.m.u.). Slight increase of peak intensities corresponding to N_2 and O_2 may be ascribed to the leak in the vacuum system. Being unable to detect important gas phase products of C_2H_2 oxidation on the surface, we conclude the major products of the reaction ($O_{ads} + C_2H_2$) $_{TiO_2}$ stay adsorbed on the surface.

4.4.2.3 Oxidation of adsorbed reaction intermediates

The products of C_2H_2 oxidation by O_{ads} stay on the surface of TiO_2 . We have tried to recover adsorbed species by activating the catalyst in closed reactor with simultaneous detection of C_2H_2 , CO_2 and CO. Figure 4. 16 shows the evolution of C_2H_2 and CO_2 concentrations in the conditions of the experiment demonstrated in Figure 4. 14. Approximately 30 minutes after the introduction of C_2H_2 , the reactor was pumped out, filled with argon at 1.3 mbar and the catalyst was activated in two possible ways:

- Heating at 200 °C or 350 °C.
- Exposure with UV lamps (we should not forget that TiO_2 is a photo-catalyst).

Adsorption and reactivity of O atoms

One can see that CO_2 is released upon heating or UV exposure but no desorption of C_2H_2 or CO is detected. The absence of C_2H_2 desorption when the catalyst is heated is yet another proof of the reactive adsorption mechanism. If acetylene was just molecularly adsorbed, we would expect to observe thermal desorption of C_2H_2 .

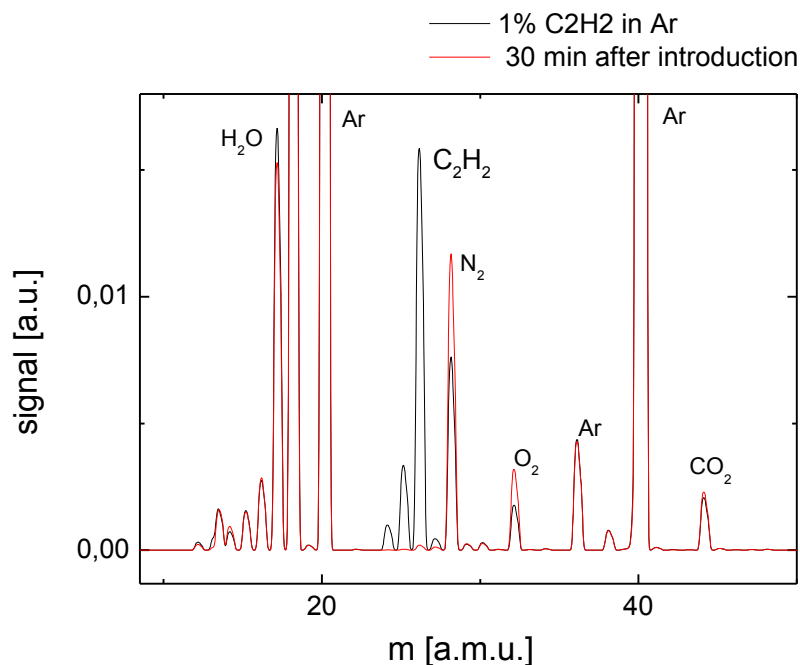


Figure 4. 15 Mass spectra of the initial mixture 1% C_2H_2 in Ar in the beginning and 30 min after the introduction in the reactor. TiO_2 surface was pretreated by O_2 plasma.

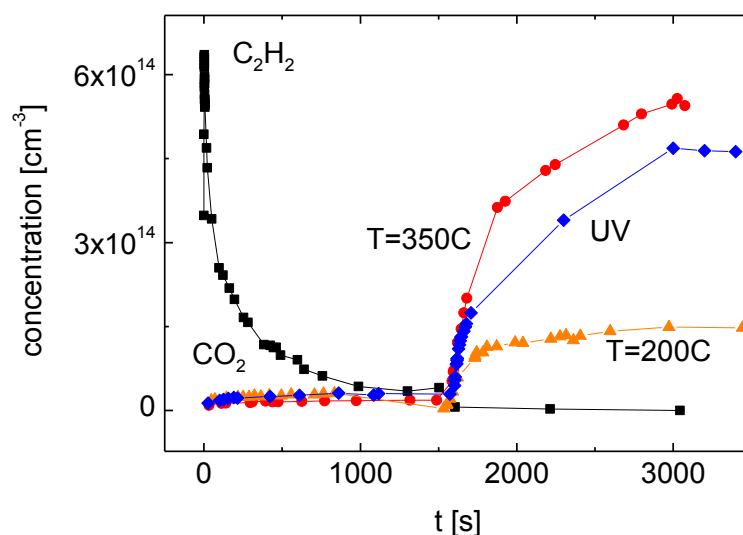


Figure 4. 16 Time evolution of C_2H_2 and CO_2 concentrations measured using QCLAS. A mixture of 1% C_2H_2 in Ar was introduced at $p=2.7$ mbar in static conditions after O_2 plasma pretreatment. After 30 min, the reactor was pumped out and heated at 200°C or 350°C under Ar atmosphere or exposed to UV light. Concentration of CO was always below the detection limit.

Our results demonstrate that reaction $(O_{ads} + C_2H_2)_{TiO_2}$ produces some adsorbed intermediates that can be thermally or photo-oxidized into CO_2 . In other words, oxidation of C_2H_2 by adsorbed oxygen atoms at room temperature is incomplete and O_{ads} ensure only the first step of oxidation. At present we can only make some hypotheses based on the analogy with the mechanism of the gas phase reaction $C_2H_2 + O$. Oxidation of C_2H_2 into CO_2 is a multistep process. It is known that there exist two major mechanisms of the first attack of C_2H_2 by O [120]:

- (i) $C_2H_2 + O \rightarrow CO + CH_2$
- (ii) $C_2H_2 + O \rightarrow HCCO + H$

It would be reasonable to suggest that oxidation of C_2H_2 on the surface proceeds via similar bond breaking pathways. Reaction (i) is less probable because CO production wasn't observed experimentally. Resulting fragments may stay adsorbed on the surface. In-situ analysis of adsorbed species (for example transmission FTIR) is required in order to get a deeper insight into the mechanism of C_2H_2 oxidation by O_{ads} on TiO_2 .

4.4.3 Discussion and conclusions on the study of O_{ads} reactivity on TiO_2

In this section we have shown that in general the reactivity of O atoms adsorbed on oxide surfaces depends on both the nature of the surface and reacting molecules. For example, O atoms adsorbed on Pyrex and reactive towards NO are not useful for oxidation of C_2H_2 . Whereas O atoms adsorbed on TiO_2 are capable of oxidizing C_2H_2 . Probably, the difference in the reactivity of O_{ads} is related to the difference in their binding energy: atoms that are less bonded to the surface are more reactive. In order to further compare the reactivity of O_{ads} on Pyrex and TiO_2 it would be desirable to investigate NO oxidation on pretreated TiO_2 surface. But we haven't performed such experiments because it is known from the literature [121] that NO_2 is adsorbed on TiO_2 and analysis of NO oxidation kinetics is complicated in this case.

The maximum number of C_2H_2 lost on the TiO_2 surface pretreated by O_2 plasma was $\sim 5 \cdot 10^{12}$ molecules per cm^2 . It was found that C_2H_2 is oxidized only partially by O_{ads} leaving some reaction intermediates adsorbed on the surface. Further oxidation of these adsorbed species into CO_2 can be reached by heating or UV activation of the catalyst.

Speaking about the role of O_{ads} in plasma-catalyst systems for VOC abatement, we have proven that O_{ads} can be used for oxidation of organic molecules. But we have employed low pressure discharge in order to graft stable O_{ads} to the surface. In real applications, atmospheric pressure discharges are used. It is evident that conditions on the surface and especially ion fluxes differ strongly at low and atmospheric pressure. Can we expect the adsorption of oxygen atoms on the catalyst surface in contact with atmospheric pressure discharge?

Recently, Kim *et al.* [115] have performed isotopic exchange experiments in an atmospheric pressure DBD reactor packed with TiO_2 . Authors used a procedure similar to the one that is shown in Figure 4. 1. The surface of TiO_2 was first exposed to a discharge in the mixture $He/^{36}O_2$ and then $^{16}O^{18}O$ production on the surface was observed when the discharge feed gas

Adsorption and reactivity of O atoms

was switched to He/ $^{32}\text{O}_2$. This proves that O_{ads} can be grafted to the surface of TiO_2 even under atmospheric pressure plasma exposure. Therefore our results are relevant to the real systems used for pollution control. And O_{ads} identified in this study may be responsible for improved efficiency and selectivity of plasma- TiO_2 combination reported in the literature.

So far we have studied the properties of strongly bonded O_{ads} on oxide surfaces, in the following section we will investigate the properties of weakly bonded atoms O^{weak} .

4.5 Investigation of ozone formation on surfaces

In Chapter 3 we have seen that strongly bonded N atoms on SiO_xN_y are not the main sites for N recombination on the surface. Therefore, recombination of N atoms takes place on some weakly bonding active sites. We haven't yet come to similar conclusions for O recombination on silica-like surfaces. But it would be reasonable to suggest that weakly bonded O may participate in surface recombination of oxygen atoms.

Our aim is to get insight into the reactivity of O^{weak} species on silica surface. Experimental procedures employed so far are appropriate for investigation of adsorbed atoms having the lifetime on the surface of the order of several minutes and more. In order to follow the recombination of unstable adsorbed atoms, fast in-situ diagnostics is required. For example, the spinning wall technique developed by Donnelly *et al.* [54] is suitable for investigation of adsorbed atoms with the lifetime of the order of 1 ms.

In case of O recombination on the surface one of the possible pathways is the production of ozone:



As we have discussed in § 1.1.3, ozone may be produced only in reactions of atoms having the binding energy on the surface inferior to 1.04 eV. Therefore, detection of O_3 produced on the walls may provide an insight onto the reactivity of O^{weak} .

It is interesting to note that reaction (4.2) is very efficient at LN2 temperature. For example in [122], reaction (4.2) has been used for collection of atomic oxygen in the post-discharge of a dc glow discharge in O_2 on a LN2 trap. Concentration of produced ozone was used as a measure of the dissociation fraction of O_2 in the discharge. However, reaction (4.2) is completely overlooked in atomic oxygen recombination studies not only at intermediate but also at low surface temperatures [28]. Only recently, ozone formation on the surface has attracted a considerable interest [107] due to an unusual isotopic effect of heterogeneous O_3 production in comparison to the gas phase mechanism. Lately, Lopaev *et al.* [111] have also found that reaction (4.2) is an important O_3 production pathway in O_2 dc discharge at intermediate pressures (10 – 50 torr).

4.5.1 Experimental details

So far ozone production on silica surface has been reported in continuous O_2 discharges at pressures $p=1 - 65$ mbar [107] [111]. In cw discharges, due to the presence of electrons and high concentrations of excited species ozone formation is balanced by fast destruction processes what strongly complicates ozone kinetics. In this study we use pulsed dc discharge with short pulse duration of the order of 1 ms. The discharge creates some initial concentration of active species and ozone production takes place in the afterglow. Thus, much smaller number of processes has to be taken into account. In addition, valuable information which is accessible with pulsed discharge technique is the time evolution of species concentrations.

Experiments have been performed in silica discharge tube. In some experiments in order to enhance the role of surface reactions a material made of silica fibres (Si40 material presented in § 4.4.2.1) was placed on the inner surface of the discharge tube. Time resolved measurements of absolute concentrations of O and O_3 were performed using TALIF and broad-band UV absorption.

4.5.2 Ozone production in bare silica tube

The first step required for ozone production in plasmas is the dissociation of molecular oxygen. The number of O_2 dissociations increases with increasing the energy injected in the discharge and one may expect that ozone production will also increase. However, as it was shown in [109] with increasing the injected energy, ozone destruction in reactions with atomic oxygen, $O_2(a^1\Delta)$ and $O_2(b^1\Sigma)$ metastables and due to heating of the gas also increases. This leads to a complex dependence of the resulting concentration of O_3 on the energy injected in the gas. Therefore, an optimum energy input should be found in order to maximize production of O_3 .

First, we have performed UV absorption measurements of ozone production in a pulsed discharge in flowing O_2 at a pressure $p=6.7$ mbar. Residence time of the gas in the reactor was equal to 2 second. Pulse repetition frequency was 0.25 Hz so complete gas renewal between discharge pulses was achieved. The amplitude of the applied high voltage was kept constant $U_{HV}=8.3$ kV. Pulse duration was varied between 0.5 and 10 ms. The concentration of ozone was measured 300 ms after the end of the discharge pulse. As it will be shown later, this delay corresponds to the steady state of O_3 concentration in the post discharge. Energy injected in the gas was calculated from current-voltage waveforms taking into account the cathode fall voltage $U_{cath} \approx 300$ V[68]. Figure 4. 17 shows current and voltage waveforms of 10 ms discharge pulse in O_2 at $p=6.7$ mbar.

Adsorption and reactivity of O atoms

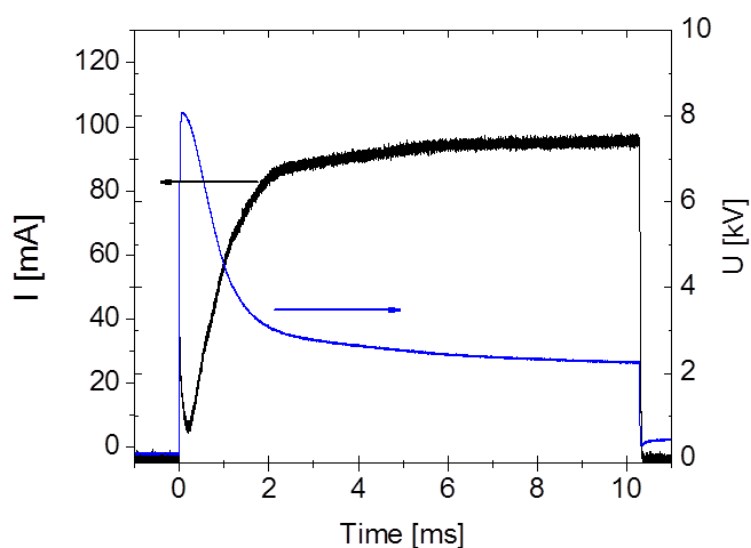


Figure 4. 17 Current and voltage waveforms, 10 ms discharge pulse in O_2 at $p=6.7$ mbar.

In Figure 4. 18, the dependence of ozone concentration on the injected energy is shown. One can see that $[O_3]$ increases for $E \leq 0.5$ J/pulse and then it starts to decrease. In order to maximize ozone production, for further experiments we have selected $E=0.16$ J/pulse.

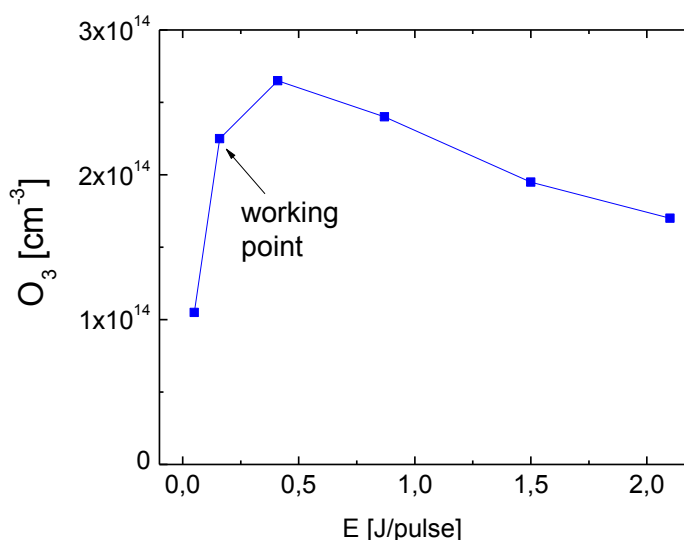


Figure 4. 18 Dependence of O_3 concentration on the energy injected per discharge pulse. Measurements are performed 300 ms after the end of the discharge pulse at $p=6.7$ mbar.

When the working point was selected, the measurements of ozone production kinetics in the pressure range $p=1.3 - 6.7$ mbar have been performed while keeping injected energy close to $E \approx 0.16$ J/pulse. Applied high voltage was kept $U_{HV}=8.3$ kV and discharge pulse duration was varied in the range $\tau=0.5-2$ ms. Chosen discharge parameters are listed in Table 4. 1 (see below).

In Figure 4. 19 the kinetics of ozone production is shown. One can see that ozone is formed in the post discharge with the characteristic time is in the range $\tau_{O_3}=60 - 100$ ms. At $p=1.3$ mbar maximum measured concentration of O_3 was $7 \cdot 10^{12} \text{ cm}^{-3}$ which is close to the limit of detection of UV absorption technique ($2 \cdot 10^{12} \text{ cm}^{-3}$). With a 5 fold increase of the pressure, the maximum ozone concentration increases by a factor of about 30.

Kinetics of ozone is coupled to the kinetics of O atoms. Figure 4. 20 shows the results of TALIF measurements of the absolute concentration of atomic oxygen at the end of the discharge pulse and kinetics of O losses in the post discharge. Discharge conditions were identical to those used for ozone measurements shown Figure 4. 19. Concentration of atomic oxygen is found in the range $[O]=(4-10) \cdot 10^{14} \text{ cm}^{-3}$. One can see that $[O]$ in the post discharge follows a single-exponential decay with characteristic time $\tau_O = 70 - 140$ ms. Similar to the characteristic ozone production time τ_{O_3} , the value of τ_O decreases with increasing O_2 pressure.

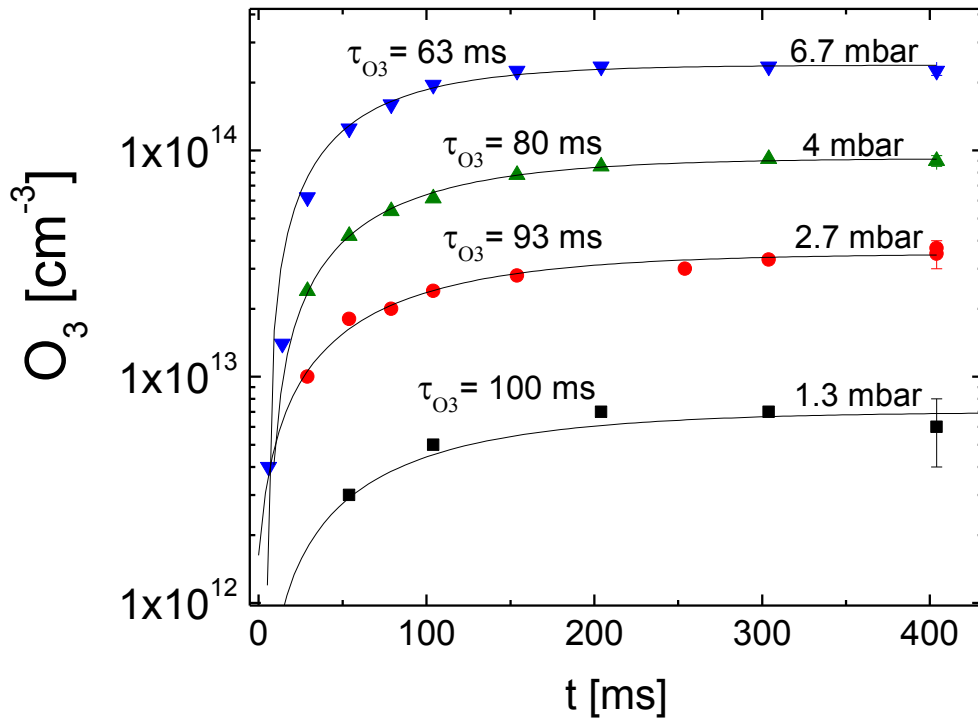


Figure 4. 19 Kinetics of ozone production in pulsed dc discharge at $p=1.3 - 6.7$ mbar, $t=0$ corresponds to the end of the discharge pulse. Energy injected in plasma was in the range $0.14 - 0.22$ J/pulse. The characteristic time of ozone production was obtained by fitting experimental data with $f=a(1-\exp(-t/\tau_{O_3}))$.

Adsorption and reactivity of O atoms

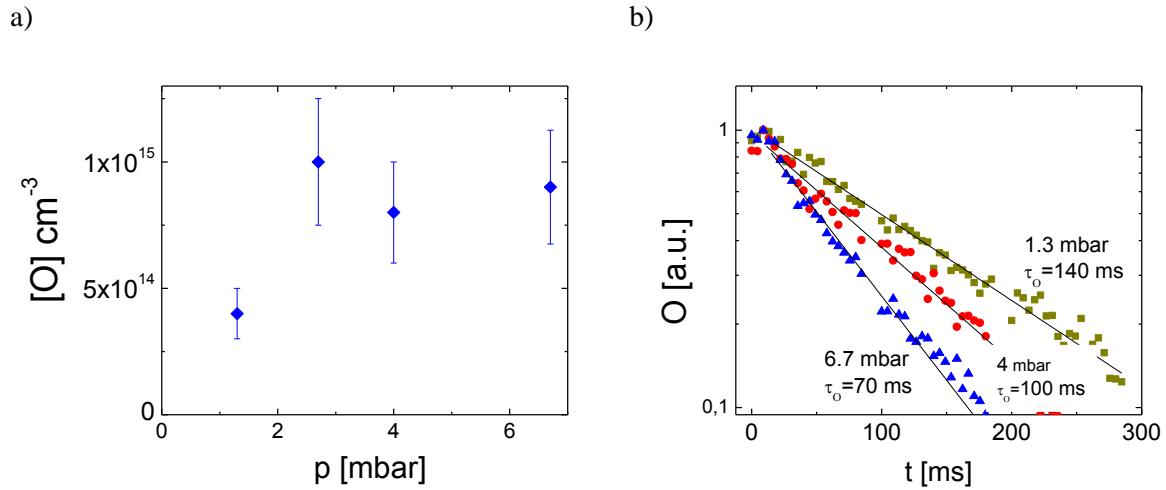
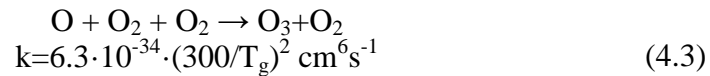


Figure 4. 20 a) Absolute concentration of atomic oxygen measured by TALIF at $p=1.3 - 6.7$ mbar. Energy injected in plasma was in the range $0.14 - 0.22$ J/pulse. b) TALIF measurements of the lifetime of atomic oxygen in the same conditions.

p (mbar)	t (ms)	E (J/pulse)	[O ₃] (cm ⁻³)	[O] (cm ⁻³)
1.3	2	0.18	$7 \cdot 10^{12}$	$4 \cdot 10^{14}$
2.7	1	0.22	$3.7 \cdot 10^{13}$	$1 \cdot 10^{15}$
4	0.5	0.14	$9 \cdot 10^{13}$	$8 \cdot 10^{14}$
6.7	1	0.16	$2.4 \cdot 10^{14}$	$9 \cdot 10^{14}$

Table 4. 1 Parameters of pulsed dc discharge in O₂ and results of O and O₃ concentration measurements.

Our objective is to detect ozone produced on the surface. But even at low pressures ozone may be formed in a 3-body reaction (4.3). In order to estimate relative contribution of surface and gas phase mechanisms of ozone formation, let's first compare characteristic times of relevant processes. The rate of ozone formation in 3-body reaction in the gas phase is well known [111]:



In Table 4. 2, experimentally measured lifetime of atomic oxygen τ_O is compared with a calculation of the characteristic time of O losses in reaction (4.3), $\tau_{k1} = (k \cdot [\text{O}_2] \cdot [\text{O}_2])^{-1}$. We can see that at $p=1.3$ mbar atomic oxygen is lost mainly on the surface due to recombination into O₂ and **probably** O₃. When the pressure is increased to $p=6.7$ mbar, the characteristic time of ozone formation in reaction (4.3) becomes comparable with the measured lifetime of atomic oxygen. This means that in our conditions recombination of atomic oxygen in the gas phase reaction (4.3) is not negligible compared to O losses on the surface. Quadratic increase of the rate of (4.3) as a function of the gas pressure may explain experimentally observed decrease of τ_O and τ_{O_3} when the gas pressure is increased.

p (mbar)	τ_O (ms)	τ_{kl} (ms)
1.3	140	1460
2.7	140	364
4	100	162
6.7	70	58

Table 4. 2 Comparison between experimentally measured lifetime of atomic oxygen τ_O and the characteristic lifetime of atomic oxygen τ_{kl} with respect to the reaction (4.3).

We can conclude that in bare silica reactor the lifetime of atomic oxygen with respect to surface recombination is very long and gas phase reaction (4.3) may significantly contribute to the production of ozone. Therefore, we cannot unambiguously determine the fraction of ozone produced on the surface from experimental measurements of $[O_3]$. In such conditions kinetic modelling is required in order to determine the role of different ozone formation mechanisms. In the following we will perform a simple modelling of ozone kinetics in silica reactor. But an alternative way to identify the role of ozone formation on the surface is to change the nature of the material in contact with the plasma.

4.5.3 Ozone production in the presence of high specific surface material

In order to enhance the role of heterogeneous processes, a high specific surface material made of silica fibres coated with SiO_2 particles (Si40 material defined in § 4.4.1) was placed on the inner surface of the discharge tube. In Figure 4. 21 results of TALIF measurements of the lifetime of atomic oxygen in the presence of catalyst are shown. One can see that the decay of $[O]$ is much faster than in bare tube. Obtained values of τ_O at $p=1.3$ and 6.7 mbar are approximately equal to the characteristic time of radial diffusion of oxygen atoms to the tube walls. The diffusion coefficient of O atoms decreases with increasing the pressure what explains why the lifetime of atomic oxygen is higher at $p=6.7$ mbar.

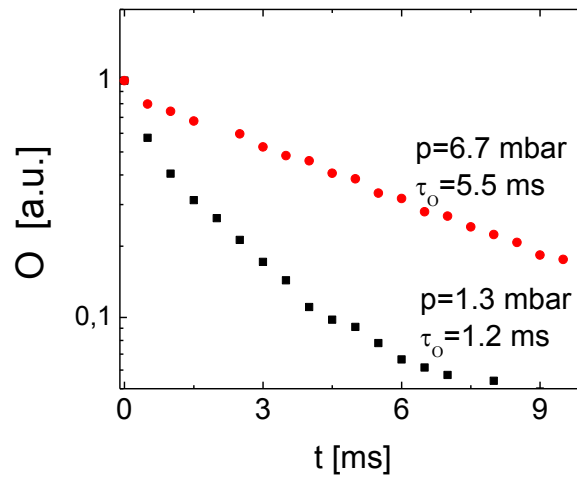


Figure 4. 21 Decay of the atomic oxygen density in the presence of Si40 fibres measured by TALIF, $t=0$ corresponds to the end of the discharge pulse.

Adsorption and reactivity of O atoms

Listed in Table 4. 2 characteristic times of ozone production in the reaction (4.3) are much longer than the lifetime of O in the presence of the catalyst. Thus, O atoms simply don't have enough time to form ozone in the gas phase when fibres are introduced. However, absorption measurements demonstrate significant ozone production even in this case. In Figure 4. 22, time evolution of $[O_3]$ at $p=6.7$ mbar and injected energy $E=0.16$ J/pulse with and without catalyst is shown.

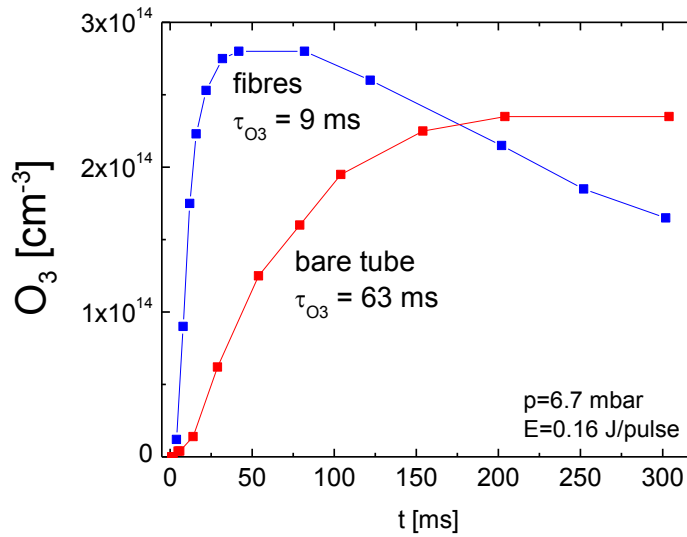


Figure 4. 22 Comparison of ozone production in pulsed dc discharge at $p=6.7$ mbar with and without catalytic material inside the reactor. The injected energy was kept the same $E=0.16$ J/pulse.

One can see that regardless fast losses of O on the surface of silica fibres, even greater amount of ozone is produced in identical discharge conditions. In addition, with the catalyst the characteristic time of ozone production is much smaller than in bare reactor ($\tau_{O_3}=9$ ms with catalyst and $\tau_{O_3}=63$ ms in bare tube). Observed fast ozone formation cannot be explained by any gas phase reaction, and, therefore, it necessarily comes from the **surface**.

We have directly demonstrated that ozone can be formed on silica surface in recombination reaction (4.2). What is the efficiency of the atomic oxygen loss channel $(O+O_2)_w$ in comparison with usual recombination into O_2 and adsorption of O on the surface? In order to answer this question we should compare the number of O atoms produced in the discharge with the measured concentration of ozone. We haven't performed TALIF measurements of atomic oxygen in reactor with introduced catalyst. But fibres were placed on the inner surface of the discharge tube and didn't significantly modify the geometry of the discharge. We assume that at fixed pressure and injected energy the number of O_2 dissociations with and without the catalyst is the same. Therefore, for further estimations we use absolute [O] measurements performed in bare tube.

Seeing that in the presence of Si40 material losses of atoms and production of ozone take place exclusively on the surface, the ratio $\eta=[O_3^{max}]/[O^{initial}]$ represents the fraction of lost

atoms that recombine producing ozone. In conditions shown in Figure 4. 22, $\eta \approx 0.3$. This means that at $p=6.7$ mbar production of ozone accounts for **30%** of O losses on the surface!

4.5.3.1 Influence of gas pressure and surface pretreatment

We have studied how the value of η depends on the O_2 pressure and on the state of the SiO_2 surface. Concentration of ozone was measured 50 ms after the end of the discharge pulse at different gas pressures ($p=1.3 - 6.7$ mbar) in the conditions identical to bare tube experiment (see Table 4. 1). Two different types of catalyst surface pretreatment were compared. Normally, fibres were just introduced in the reactor and exposed for few hours to a pulsed dc discharge in O_2 ("fibres"). "Clean fibres" stands for pretreatment of the surface with a flowing capacitive rf discharge in O_2 in standard conditions for 1 hour.

In Figure 4. 23, the value of η is plotted as a function of the gas pressure for two types of catalyst preparation. For comparison, results obtained in empty reactor are also shown. As one can see, the value of η in the presence of fibres increases linearly with the pressure. This means that recombination of O and O_2 on the surface is the first order process with respect to $[O_2]$. In other words, catalyst surface plays the role of the 3rd body for recombination. In the empty reactor the value of η increases as a square of the pressure. This indicates that ozone is produced mainly in the 3 body reaction (4.3).

One can see that after pretreatment of fibres, ozone production is about 3 times less efficient. The same effect was observed when the catalyst was heated at $350^\circ C$ under O_2 atmosphere for 1 hour. After cleaning, the efficiency of O_3 production was recovered to the normal level if the catalyst was left under continuous pumping for several hours.

It is known that water molecules and some hydroxyl groups are efficiently removed from silica surface upon heating or under O_2 plasma exposure [123][124]. The removal of adsorbed water and/or surface hydroxyls by O_2 rf discharge (in standard conditions) has been evidenced by optical emission spectroscopy. In Figure 4. 24, emission spectra of the discharge in the beginning and at the end of the cleaning procedure are shown. One can see that after 60 min of plasma exposure the intensity of OH emission band at 310 nm is strongly reduced. Therefore, the most likely explanation for the reduced efficiency of ozone production on clean fibres is the dehydroxylation of the surface. Observed slow recovery of ozone formation efficiency under pumping may be explained by the re-adsorption of water molecules coming from leaks in the vacuum system.

We conclude that the presence of OH and/or adsorbed H_2O on silica surface favours recombination channel $(O+O_2)_w \rightarrow O_3$ with respect to $(O+O)_w \rightarrow O_2$. The presence of OH and H_2O_{ads} on the surface may have a double effect, from the one hand they may play a role of active sites for O_3 productions and from the other hand they may inhibit the recombination into O_2 .

Adsorption and reactivity of O atoms

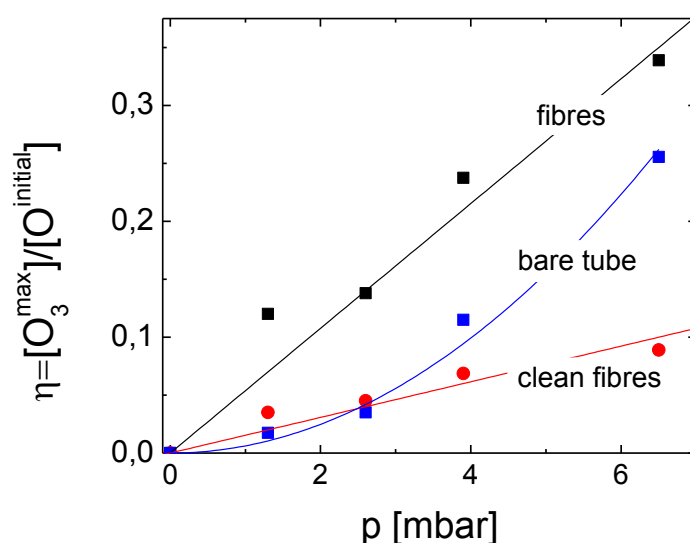


Figure 4. 23 Efficiency of surface recombination with production of ozone η as a function of the gas pressure. Discharge conditions are the same as listed in Table 4. 1. “Clean” fibres were treated by a capacitive rf discharge during 60 minutes.

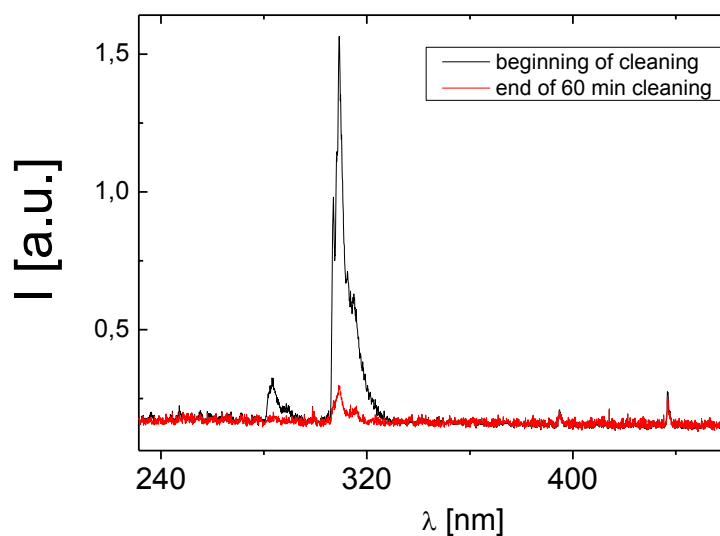


Figure 4. 24 Emission spectra of rf discharge in O_2 used for cleaning of silica fibres. A strong reduction of the intensity of OH band at 310 nm is seen after 60 min of cleaning.

4.5.4 Modelling of ozone production in bare silica tube

In bare silica tube, surface reactions are slow and gas phase processes significantly contribute to the production of O_3 . In order to determine the fraction of ozone that comes from the surface, a simple kinetic model was developed. The rates of gas phase reactions are supposed to be known with a good precision. Thus, ozone production on the surface may be evidenced

if gas phase reactions are not able to reproduce experimentally observed kinetics of O_3 . The processes that were taken into account in the model are listed in Table 4. 3.

Following [111] we suppose that only 1/3 of ozone is formed in vibrationally ground state and 2/3 of produced ozone molecules are excited into asymmetric stretching mode. As in [125] we consider only one effective vibrational level O_3^* . One can see that destruction of O_3^* in collisions with O and $O_2(a^1\Delta)$ is much faster than for ground state O_3 .

	Reaction	Rate constant	Ref.
R1	$O + O_2 + O_2 \rightarrow O_3 + O_2$	$\frac{1}{3} \cdot 6.3 \cdot 10^{-34} \cdot (300/T_g)^2 \text{ cm}^6 \text{ s}^{-1}$	[111]
R2	$O + O_2 + O_2 \rightarrow O_3^* + O_2$	$\frac{2}{3} \cdot 6.3 \cdot 10^{-34} \cdot (300/T_g)^2 \text{ cm}^6 \text{ s}^{-1}$	[111]
R3	$O + O_3 \rightarrow O_2 + O_2$	$8 \cdot 10^{-12} \cdot \exp(-2060/T_g) \text{ cm}^3 \text{ s}^{-1}$	[109]
R4	$O_2(a^1\Delta) + O_3 \rightarrow O + O_2 + O_2$	$5.2 \cdot 10^{-11} \cdot \exp(-2840/T_g) \text{ cm}^3 \text{ s}^{-1}$	[109]
R5	$O_3^* + O \rightarrow O_2 + O_2$	$8 \cdot 10^{-12} \cdot \exp(-480/T_g) \text{ cm}^3 \text{ s}^{-1}$	[111]
R6	$O_3^* + O_2(a^1\Delta) \rightarrow O + O_2 + O_2$	$5.2 \cdot 10^{-11} \cdot \exp(-1260/T_g) \text{ cm}^3 \text{ s}^{-1}$	[111]
R7	$O_3^* + O_2 \rightarrow O_3 + O_2$	$3 \cdot 10^{-15} \text{ cm}^3 \text{ s}^{-1}$	[111]
R8	$O_3^* + O \rightarrow O_3 + O$	$2 \cdot 10^{-13} \text{ cm}^3 \text{ s}^{-1}$	[111]
R9	$O_3^* + \text{wall} \rightarrow O_3 + \text{wall}$	$\gamma = 0.1$	[111]
R10	$O + \text{wall} \rightarrow \frac{1}{2}O_2 + \text{wall}$	$\gamma_O = 2 \cdot 10^{-4}$	measured
R11	$O_2(a^1\Delta) + \text{wall} \rightarrow O_2 + \text{wall}$	$\gamma = 1.8 \cdot 10^{-4}$	[109]

Table 4. 3 The list of reactions that were taken into account in the kinetic model.

The recombination probability of O atoms on the surface was determined from the τ_O measurements at $p=1.3$ mbar shown in Figure 4. 20 b). At this low pressure O losses due to ozone formation in the gas phase are negligible according to Table 4. 2. At $p=1.3$ mbar ozone formation on the surface is much less efficient than recombination into O_2 as it follows from the measurements shown in Figure 4. 23. Therefore, γ_O can be calculated directly from τ_O using the well known expression [63]:

$$\gamma_O = \frac{2r}{\tau_O v_{th}} \quad (4.4)$$

where v_{th} is the average thermal velocity of O atoms. Calculation with (4.4) gives $\gamma_O = 2 \cdot 10^{-4}$ which is in a good agreement with literature data for silica [110]. In the model, we suppose that γ_O is independent of the gas pressure.

An important quencher of ozone in the post discharge is singlet oxygen. The concentration of $O_2(a^1\Delta)$ hasn't been measured, so it has to be estimated. According to [109], $O_2(a^1\Delta)$ in oxygen plasmas is produced mainly by electron impact excitation of ground state O_2 molecules. In conditions similar to ours [109], it was shown that the lifetime of $O_2(a^1\Delta)$ with respect to quenching by neutral species and de-excitation in collisions with electrons is of the order 100 ms. This means that in our experiments quenching of $O_2(a^1\Delta)$ may be neglected on

Adsorption and reactivity of O atoms

the timescale of the discharge pulse which is always shorter than 2 ms. Thus, the concentration of $O_2(a^1\Delta)$ at the end of the discharge pulse is equal $[O_2(a^1\Delta)] = k_{O_2a}n_e[O_2]\tau$. Where n_e is the electron density, k_{O_2a} is the electron impact excitation coefficient and τ is the pulse duration. Similarly, one can express the concentration of atomic oxygen as $[O] = 2k_{diss}n_e[O_2]\tau$ because the measured value of τ_0 is always much longer than the pulse duration. Therefore, at the end of the discharge pulse $[O_2(a^1\Delta)]/[O] = k_{O_2a}/2k_{diss}$. Assuming $E/N = 60\text{--}100$ Td which is typical for our conditions according to [67] and using Bolsig EEDF solver, the ratio $k_{O_2a}/2k_{diss}$ was found to be in the range 0.5 – 0.2. In the following we will assume that at the end of the discharge pulse $[O_2(a^1\Delta)]/[O] = 0.5$ in order to estimate the maximum possible contribution of $O_2(a^1\Delta)$.

Calculations were performed for the discharge afterglow. Experimentally measured atomic oxygen concentration $[O]$ and the estimated value of $[O_2(a^1\Delta)]$ were used as an input parameter. In the first instance ozone production on the surface was discarded in the model. The gas temperature was supposed to be equal to the room temperature.

Comparison between experimental results and modelling of ozone kinetics is shown in Figure 4. 25. Two different simulations were performed. In the first case (model 1) we neglected vibrationally excited ozone and assumed that all the O_3 molecules are produced in the vibrationally ground state. In the second case (model 2) a complete reaction set from Table 4. 3 was used.

One can see that model 1 strongly overestimates production of O_3 in the post discharge. Agreement obtained with the model 2 is somewhat better especially for $p = 6.7$ mbar. But for lower pressures the discrepancy with the experiment is still strong. This means that some important reactions of O_3^* are still missing even in the model 2. Probably, multilevel vibrational kinetics of O_3^* should be taken into account as in [111]. However, at present the vibrational level-dependent reaction rates of excited ozone are not known with sufficient precision, and reliability of such detailed modelling would be questionable.

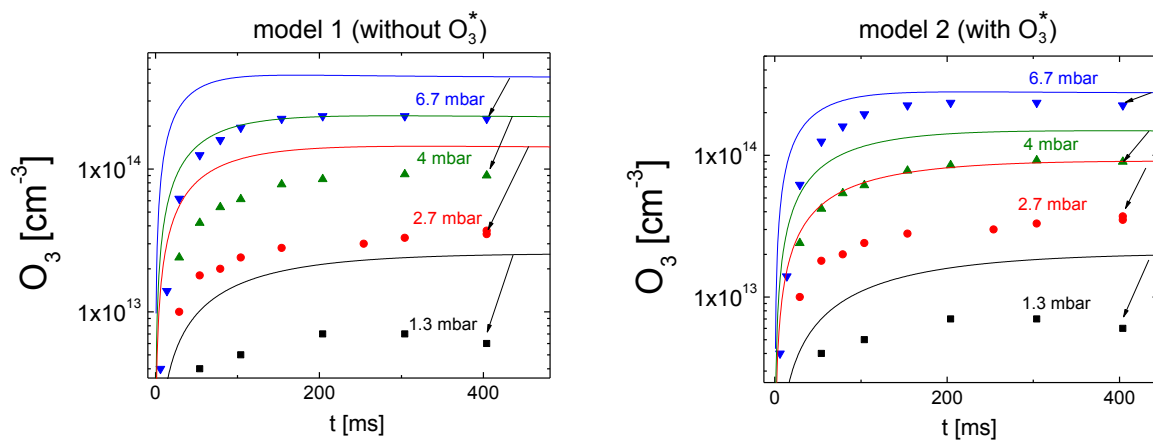


Figure 4. 25 Comparison between experimental and calculated time evolution of $[O_3]$. Model calculations shown in the left panel were performed assuming that ozone is formed in vibrationally ground state. Right panel shows results of a complete model.

Based on this attempt of kinetic modelling of ozone production we can conclude that:

- In the conditions of our study, the kinetics of **vibrationally excited** ozone is of primary importance for correct description of O_3 production.
- But even taking O_3^* into account, the model overestimates production of ozone compared to the experiment. Thus in the model, there is no need for an additional (surface) O_3 formation term in order to reproduce experimentally measured values of ozone concentration. This means that with the actual knowledge of reaction rates of O_3^* it is impossible to assess the probability of ozone formation on the surface in our experiments.

An estimation of the ozone yield from surface recombination in case of bare silica tube can be made based on the results shown in Figure 4. 23. The efficiency of heterogeneous ozone production depends on the hydroxylation of silica surface. In contrast to highly porous Si40 material in which a great part of the surface is shadowed, the surface of bare discharge tube is exposed to uniform ion and atomic fluxes. We may, therefore, expect that under pulsed dc discharge conditions the surface of the discharge tube is free from OH and adsorbed water. Similarly in [57], Cartry following the recombination model of Jumper [41] supposed that under pulsed dc discharge in O_2 , silica surface is covered by oxygen atoms double bonded to Si atoms of the substrate. In other words, experiments in bare tube correspond to the case “clean” shown in Figure 4. 23. Thus, ozone production on the surface of silica discharge tube represents at maximum 10% of the heterogeneous losses of O in the pressure range $p = 1.3 - 6.7$ mbar. The experimentally obtained value of γ_O is of the order of 10^{-4} , and hence the probability of ozone formation on silica surface should be of the order of 10^{-5} in the studied pressure range.

4.5.5 Conclusions on the ozone production study

- In this section we have shown that silica surface may play a role of the third body for ozone formation. Experiments with high specific surface silica fibres have shown that formation of ozone accounts for 30% of surface losses of atomic oxygen at $p=6.7$ mbar. Ozone can be formed only in recombination of weakly bonded O with molecular oxygen; hence our results prove the importance of O^{weak} for surface processes in oxygen. The possibility of recombination process $(O^{weak}+O_2)_w$ indicates that $(O^{weak} + O^{weak})_w$ or $(O^{weak} + O^{gas})_w$ may also contribute to surface losses of O.
- The presence of adsorbed water and/or hydroxyl groups increases the efficiency of ozone formation on the surface.
- Coming back to experiments in bare silica tube, we have found that in this case surface recombination is not likely to be the dominant source of ozone. This is explained by the fact that in bare tube, the lifetime of atomic oxygen with respect to surface recombination is long and gas phase production of ozone is important even at low pressures.

Adsorption and reactivity of O atoms

Kinetic modelling has revealed a very important role of vibrationally excited ozone as an intermediate in the formation of O_3 in the gas phase. Destruction of vibrationally excited ozone in collisions with O atoms and $O_2(a^1\Delta)$ molecules is much faster compared to the ground state O_3 . Therefore, introduction of O_3^* in the model reduces the resulting O_3 production. Due to the lack of reliable data on the reaction rates of O_3^* , ozone production was overestimated by the model. As a consequence, determination of the fraction of ozone produced on the surface from comparison between the model and the experiment was not possible.

Results of this section are a good illustration to the fact that quantification of molecule production on the surface using a combination of kinetic modelling and experiment is not always an easy task. Even in such a simple system as an O_2 afterglow, the gas phase kinetics is rather complex and still not fully understood.

4.6 Conclusions

In this chapter we have studied interaction between O_2 plasma and three oxide surfaces – silica, Pyrex and TiO_2 . Many similarities with the results of the previous chapter dealing with N-SiO₂ system have been observed. Namely, the exchange of the atoms of the crystalline network under direct plasma exposure, the distribution of the reactivity of adsorbed atoms and the importance of weakly bonded atoms for surface recombination. Below we summarize the main results of this chapter:

- Under direct O_2 plasma exposure, oxygen atoms that compose the outmost layer of silica and Pyrex are continuously exchanged with oxygen atoms and ions from the gas phase. Typically, in our standard pretreatment conditions $(5-6) \cdot 10^{15}$ O atoms per cm^2 are replaced during 500 s of plasma exposure.
- We have found that under O_2 plasma exposure reactive O atoms are adsorbed on Pyrex or TiO_2 . The reactivity of O_{ads} towards stable molecules depends on the nature of the surface and the target molecule.
- Oxygen atoms adsorbed on Pyrex surface are reactive towards NO (we denote these atoms O_{ads}^*). Titration of O_{ads}^* using the reaction $NO + O_{ads}^* \rightarrow NO_2$ allowed determination of the lower limit of the coverage $[O_{ads}^*] = 2.5 \cdot 10^{14} cm^{-2}$.
- A distribution of reactivity of O_{ads}^* towards NO have been observed. We suggest that this distribution is related to a spectrum of binding energies of adsorbed atoms. The maximum rate of NO oxidation on the surface corresponds to the effective surface reaction probability $\gamma_{NO \rightarrow NO_2} = 2 \cdot 10^{-7}$.
- Oxygen atoms adsorbed on TiO_2 are reactive towards C_2H_2 . The maximum number of C_2H_2 lost on the TiO_2 surface pretreated by O_2 plasma was $\sim 5 \cdot 10^{12}$ molecules per cm^2 . It was found that C_2H_2 is oxidized only partially by O_{ads} leaving some reaction intermediates on the surface. Further oxidation of these adsorbed species into CO_2 can be reached by heating or UV activation of the catalyst.

- We have found that ozone may be formed from surface recombination $(\text{O}+\text{O}_2)_w$ on silica surface. The presence of adsorbed water and surface OH groups favours ozone production on the surface. At $p=6.7$ mbar ozone production accounts for 30% of losses of O atoms on silica surface. This result demonstrates the importance of weakly bonded O^{weak} for surface catalyzed reactions in oxygen plasmas.
- Modelling of O_3 production in bare silica reactor has revealed a very important role of the kinetics of vibrationally excited ozone.

5. Chapter V: Study of surface vibrational relaxation of N₂

5.1 Introduction

Above we have seen that in low pressure N₂/O₂ plasmas surface processes play a key role in plasma chemical kinetics. Another aspect of surface interactions in molecular plasmas is heterogeneous vibrational relaxation. Relaxation of vibrationally excited molecules on reactor walls is often the dominant mechanism of losses of vibrational energy in laboratory plasmas at pressures in the mbar range [126]. Due to a low energy threshold, vibrational excitation by electron impact is very efficient and it controls the electron energy distribution function. Therefore, the knowledge of the rate of vibrational relaxation on the surface is important for understanding of the overall energy balance in bounded molecular plasmas.

In this work we investigate heterogeneous relaxation of vibrationally excited nitrogen molecules. There are only few published works devoted to the study of N₂(*v*) relaxation on surfaces [127][128][129] and they all deal with flowing post-discharge systems. So at present the number of studied surfaces is very limited and very little is known about the effect of plasma exposure on the probability of vibrational relaxation of N₂(*v*) on the surface. In this chapter we develop a new experimental technique for in-situ investigation of vibrational relaxation of N₂(*v*) in plasmas. We use the idea of titrating vibrationally excited N₂ by an admixture of infrared (IR) active molecules (CO₂, N₂O or CO). Gas mixtures containing 0.05 – 1 % of CO₂ (CO or N₂O) in N₂ were excited by a pulsed dc discharge and time resolved quantum cascade laser absorption spectroscopy was used to follow the relaxation kinetics of titrating molecules *in-situ*. Due to a very efficient vibrational coupling between nitrogen and CO₂(N₂O, CO), the excitation of titrating molecules reflects the degree of vibrational excitation of N₂. In this chapter we apply infrared titration technique to study the quenching of N₂(*v*) on different catalytic surfaces exposed to low pressure N₂/O₂ containing plasmas.

5.2 Kinetics of vibrationally excited nitrogen

5.2.1 Role played by N₂(*v*) in nitrogen containing plasmas

Vibrationally excited nitrogen molecules have been recognized as an important product of plasma-chemical processes in nitrogen in the 1950s due to their chemical activity [130] and high energy storage capacity [131]. In the afterglow of a flowing microwave discharge in N₂ at a pressure of 3-8 mbar [132], the energy associated with vibrationally excited nitrogen (about 0.25 eV/molecule) was found to be much higher than the kinetic energy of N₂ molecules. During the subsequent 50 years of research a very important and sometimes

Study of surface vibrational relaxation of N₂

mysterious role of N₂(*v*) in N₂ containing plasmas and afterglows was revealed experimentally and by means of kinetic modelling.

It is almost impossible to cite all the discovered and suggested reactions of vibrationally excited nitrogen molecules in plasmas. Here we will name only few processes:

- Vibration to dissociation (V-D) [97]
$$\text{N}_2(\text{X}, 10 < v < 25) + \text{N}_2(\text{X}, 10 < v < 25) \rightarrow \text{N}_2(\text{X}) + 2\text{N}$$
- Vibration to electronic (V-E) [133]
$$\text{N}_2(\text{X}, v > 39) + \text{N}({}^4\text{S}) \rightarrow \text{N}_2(\text{A}) + \text{N}({}^2\text{D})$$
- Vibration to ionization (V-I) [99]
$$\text{N}_2(\text{X}, v > 29) + \text{N}_2(\text{X}, v > 29) \rightarrow \text{N}_4^+ + \text{e}$$
- Chemical reactions [63]
$$\text{N}_2(\text{X}, v > 12) + \text{O} \rightarrow \text{NO} + \text{N}$$
- Collisions with electrons
$$\text{N}_2(\text{X}, v) + \text{e} \leftrightarrow \text{N}_2(\text{X}, w) + \text{e}$$

One can see that vibrationally excited nitrogen molecules influence directly or indirectly all the important processes in nitrogen containing plasmas. Therefore, understanding of the kinetics of N₂(*v*) is indispensable for a correct description of physical-chemical processes in discharges in N₂ and N₂ containing mixtures.

Vibrational kinetics of N₂ may be split into three groups of processes:

- Electron impact excitation and super-elastic collisions with electrons.
- Gas phase vibrational relaxation and vibrational exchange.
- Surface vibrational relaxation.

In subsequent sections we will briefly discuss the actual state of our knowledge of the mechanisms of these processes.

5.2.2 Electron impact excitation/de-excitation of N₂(*v*)

Let's first imagine that N₂ molecule consists of two N atoms connected by an elastic spring and let's suppose that an electron collides with one of the atoms. As it follows from the conservation of momentum and energy, the part of the kinetic energy of the electron that can be transferred to the atom is of the order of $m_e/M_N \sim 10^{-4}$, where m_e is the electron mass and M_N the mass of N atom. The vibrational quantum of N₂ is ≈ 0.25 eV; therefore, vibrational excitation in such direct impact with a heavy N atom can be efficient only for very high collision energies. However, it is known from the experiment that low-energy (having few eV) electrons are very efficient for excitation of vibrations of N₂ [134].

Thus, in order to excite N₂ vibrations, colliding electrons have to interact with the molecular electronic shell. In [135] and later theoretical works [136] it was shown that the incoming electron forms with N₂ molecule an unstable compound state, a so-called resonance. Then this negative ion decays and may leave the molecule in a vibrationally excited state. Schematically

this two-step excitation mechanism is illustrated in Figure 5. 1. In Figure 5. 2 the $N_2(v=1)$ electron impact excitation cross section measured in [134] is shown.

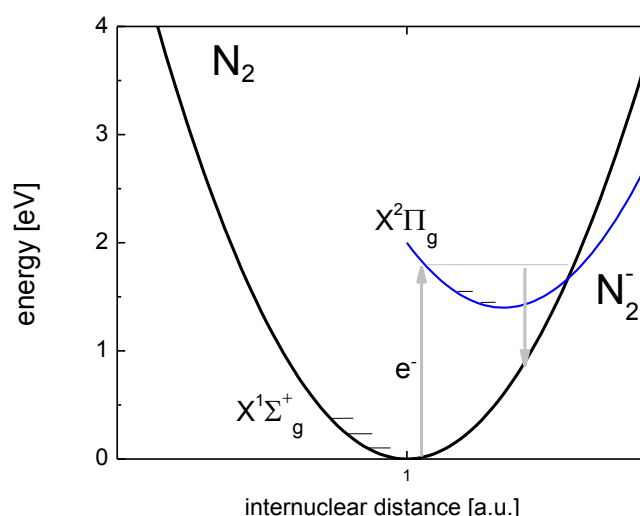


Figure 5. 1 Illustration of the mechanism of electron-impact excitation of N_2 .

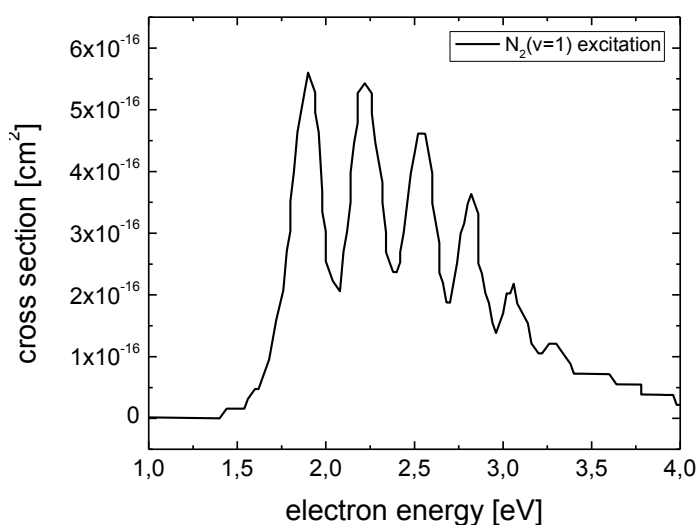


Figure 5. 2 Electron-impact excitation cross-section of $N_2(v=1)$.

The threshold energy 1.4 eV for $N_2(v=1)$ excitation is much higher than the vibrational quanta of N_2 and it corresponds to the energy of the negative ion state. The peaks on the cross section may be explained by the interference with different vibrational levels of N_2^- . The lifetime of N_2^- is of the order of few molecular vibrations ($\sim 10^{-14}$ s) and it determines the width of the N_2^- energy levels and hence the width of the peaks on the cross section shown in Figure 5. 2. The existence of these relatively broad peaks makes vibrational excitation of N_2 so efficient in

Study of surface vibrational relaxation of N₂

plasmas. In contrast, molecules that have a stable negative ion state (O₂ for example) exhibit very narrow resonance peaks on the cross-section of electron-impact vibrational excitation. Excitation of these molecules by plasma electrons that have continuum energy spectrum is rather inefficient.

When the density of vibrationally excited N₂ molecules is high, the inverse process of electron impact de-excitation of molecular vibrations starts to play a significant role. Especially superelastic collisions are important in the absence of other electron-heating sources. For example in [137] it was demonstrated that in the N₂ afterglow, the electron temperature is controlled by de-excitation of N₂(v). The mechanism of N₂(v) de-excitation is similar to the direct process and its rate can be obtained from the detailed balance principle.

5.2.3 Vibrational relaxation of N₂(v) in the gas phase

Redistribution of vibrational energy between different degrees of freedom in collisions of N₂(v) with different species has been studied intensively over the past century. It was found that the most important processes that govern N₂(v) vibrational distribution are the following [126]:

- Vibrational – translational/rotational relaxation (V-T/R)
$$\text{N}_2(v, J_1) + \text{M} \rightarrow \text{N}_2(w, J_2) + \text{M}$$
- Vibrational – vibrational relaxation in N₂ (V-V)
$$\text{N}_2(v_1) + \text{N}_2(w_1) \rightarrow \text{N}_2(v_2) + \text{N}_2(w_2)$$
- Vibrational – vibrational relaxation with other molecules (V-V')
$$\text{N}_2(v_1) + \text{M}(w_1) \rightarrow \text{N}_2(v_2) + \text{M}(w_2)$$

Nitrogen possesses 60 [138] vibrational levels and in order to model its vibrational kinetics the knowledge of the reaction rates for all the levels is required. Of course, experimental determination of the whole set of relaxation rates (especially for high vibrational levels) is not possible. Typically, the measurements are performed for a few lower levels and the complete dataset is obtained using analytical theoretical scaling laws or by means of numerical modeling.

The most widely used analytical treatment of vibrational relaxation is Schwartz, Slawsky and Hertzfeld (SSH) theory [139]. In SSH theory, the collision is supposed to be one dimensional and only repulsive forces between colliding molecules are considered. In addition, for relaxation processes listed above only single-quantum ($\Delta v=1$) exchange processes are considered. The $\Delta v=1$ selection rule is rigorous for harmonic oscillators and it is valid with a good precision for real anharmonic molecules. All above simplifications allow analytical solution of the problem that gives vibrational number dependence of V-T and V-V rates. Usually, the absolute values of relaxation rates are not well reproduced by simplified analytical theories and a normalization to experimental data is required. The SSH scaling laws for V-T and V-V relaxation of anharmonic oscillators are the following [126]:

$$P_{v+1,v} = P_{1,0}(v+1)e^{\delta_{VT}v} \quad (5.1)$$

$$Q_{v+1,v}^{w,w+1} = Q_{1,0}^{0,1}(v+1)(w+1)e^{\delta_{VV}|v-w|} \left(\frac{2}{3} - \frac{1}{2}e^{-\delta_{VV}|v-w|} \right) \quad (5.2)$$

Parameters δ_{VT} and δ_{VV} depend on the anharmonicity of the colliding species. In the case of harmonic oscillator, these parameters are equal to zero and the scaling laws transform into a simple linear dependence on the vibrational quantum number.

The most detailed theoretical investigation of the mechanisms of vibrational energy transfer in N_2 - N_2 collisions has been recently performed in [140]. Authors used a semi-classical method in which the translational and rotational motion of molecules was treated classically, whereas the molecular vibrations were treated quantum mechanically. This technique allowed accurate calculation of the V-T and V-V rates in a broad temperature range. In contrast to analytical models, semi-classical calculations give absolute reaction rates which are in good agreement with the experimental values. Moreover, probabilities of multi-quantum transitions are calculated in [140].

5.2.4 Vibrational relaxation on surfaces: motivation of the study

Based on the previous discussion we conclude that the gas phase vibrational kinetics of N_2 containing plasmas is well established. However, in bound laboratory plasmas the relaxation of molecular vibrations on the reactor walls becomes important and it should be taken into account. According to [126] V-T relaxation in N_2 is extremely slow and quenching of $N_2(v)$ on the reactor walls may be the dominant vibrational quanta loss mechanism for pressures up to several tens mbars. At present, understanding of the mechanisms of gas-surface interactions with vibrationally excited molecules is rather limited.

Historically, one of the most studied gas-surface interaction process is the relaxation of $NO(v)$ on LiF, Ag and graphite single crystals [141][142][143] in molecular beam experiments. Nitrogen oxide molecules were prepared in a specific quantum state (v, J) with a tunable infrared laser and then vibrational, rotational and translational distributions of the scattered molecules were measured by state-specific multiphoton ionization using a tunable UV laser. On atomically smooth surfaces the vibrational quanta loss probability was found to be 0.1 – 0.25. It was concluded that the most plausible mechanism of vibrational relaxation is the interaction between physisorbed $NO(v)$ and surface phonons. Experimentally observed increase of the deactivation probability with decreasing the temperature of the surface supported this hypothesis; at lower temperature physisorbed molecules spend more time on the surface before being desorbed. Coupling between vibrational and rotational/translational degrees of freedom as well interaction with the electrons of the solid were found to be inefficient for vibrational deactivation. The roughness of the surface was also a very crucial parameter, measured deactivation probability on rough (although optically polished) LiF surface was almost 1 in contrast to ~0.1 on a cleaved surface.

Study of surface vibrational relaxation of N₂

To the best of our knowledge with N₂ no detailed beam studies have been performed so far. As a matter of fact, the number of experimental studies devoted to the determination of N₂(ν) loss probabilities on different surfaces is rather limited. The main difficulty in such experiments is the detection of vibrationally excited nitrogen that does not exhibit dipole allowed transitions in emission and has absorption features only in VUV. Therefore, calorimetric methods [132], spontaneous or coherent Raman scattering[127][129] or infrared titration with CO₂ [128] were used in the past. Typically, all the experiments were carried out in a flowing discharge system and the concentration of N₂(ν) was measured as a function of the distance in the post discharge. The probability of vibrational quanta loss in collisions with the wall (γ_{N_2}) was determined from the measured decay of N₂(ν) concentration. Typically, the value of γ_{N_2} for the first vibrational level on different surfaces lies in the range $10^{-4} - 10^{-2}$. In [127][128] the results of γ_{N_2} measurements on glass were interpreted in terms of the two step mechanism similar to one proposed for NO(ν) relaxation on LiF. Vibrationally excited N₂(ν) were supposed to physisorb on the surface and then to transfer the vibrational energy to surface phonons. Low relaxation probability of N₂(ν) was explained in [127] by the very short residence time of N₂(ν) on the surface and by the poor coupling of energy transfer involving phonon excitation.

In real plasma conditions the surface may be covered by a layer of adsorbed molecules. Vibrational energy transfer between impinging N₂(ν) and this surface layer may represent an efficient pathway for heterogeneous vibrational relaxation [144].

One of the shortcomings of the techniques described above is that the relaxation of N₂(ν) was studied in a flowing post-discharge zone. First, the values of γ_{N_2} in the post-discharge may differ from those under direct plasma exposure as it was demonstrated for atomic recombination on surfaces [21]. Second, the state of the surface under post-discharge exposure is not well controlled and it may evolve in time. Indeed, authors [127][129] pointed out drifts in measured values of γ_{N_2} with increasing exposure time to the afterglow.

We can conclude here that at present the modeling of vibrational kinetics in N₂ containing plasmas, very elaborated and exhaustive in what concerns gas phase kinetics, is limited by the knowledge of the rates of surface vibrational relaxation. Plasma simulations for new emerging applications such as material processing [145] or plasma-catalyst technology [11] require the knowledge of γ_{N_2} for a number of surface materials.

The development of a simple and reliable technique for in-situ γ_{N_2} determination was therefore our main motivation.

In addition, the following questions require a thorough investigation:

- How does plasma exposure modify the probability of N₂(ν) quenching on surfaces?
- How do molecular admixtures influence the value of γ_{N_2} ?

5.3 Study of $N_2(v)$ relaxation using infrared titration

5.3.1 Principles of the infrared titration technique

The basic idea of the infrared titration technique consists in the addition of a small amount of infrared active molecules (CO_2 , N_2O , CO) into N_2 . As it can be seen in the

Table 5. 1, titrating molecules have vibrational levels that are very close to the first level of nitrogen $N_2(v=1)$. When N_2 undergoes vibrational excitation, a fast resonant vibrational energy exchange tends to equilibrate vibrational distributions of $N_2(v)$ and IR active admixtures. Therefore, the degree of vibrational excitation of titrating molecules is an image of the degree of vibrational excitation of N_2 . The described method was first proposed and applied in [128] for $N_2(v)$ surface deactivation studies; CO_2 was added in the flowing nitrogen post-discharge and vibrationally excited CO_2 molecules were detected using their IR emission.

	ν_1, cm^{-1}	ν_2, cm^{-1}	ν_3, cm^{-1}
N_2	2331		
CO	2143		
CO_2	1388	667	2349
N_2O	1285	589	2224

Table 5. 1 Wave numbers of the fundamental vibrational modes of N_2 , CO , CO_2 and N_2O .

In our case, we wish to develop an *in-situ* diagnostics inside the plasma zone but not in the post-discharge. Therefore, IR active molecules are added to N_2 and then the mixture is excited by a pulsed DC discharge. Quantum cascade laser absorption spectroscopy is used to monitor kinetics of titrating molecules.

5.3.2 Experimental procedure

Figure 5. 3 illustrates the experimental procedure. First, the discharge tube is pre-treated by a flowing RF discharge in argon, N_2 or O_2 . Then a mixture of N_2 containing 0.05-1% of CO_2 (N_2O , CO) is introduced in the reactor and a single-pulse DC discharge is ignited in static conditions. Time evolution of up to 3 species is followed in situ using the 3-channel QCLAS spectrometer with time resolution 5-200 μs .

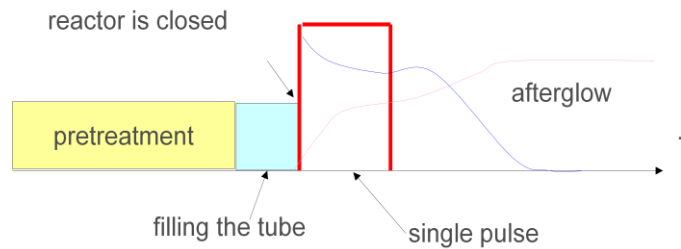


Figure 5. 3 Experimental sequence.

Study of surface vibrational relaxation of N₂

After each discharge pulse the reactor is refilled with a new gas mixture. The standard experimental conditions are the following:

- gas pressure $p=1.33$ mbar
- discharge current $I=50$ mA
- pulse duration $\tau=5$ ms

Several discharge tubes made of different materials (silica, Pyrex, anodized aluminum) or silica with a sol-gel film of TiO₂ or Al₂O₃ deposited on its inner surface are studied.

5.3.3 Validity of the diagnostics

In Figure 5. 4, results of the relaxation measurements in N₂ – CO₂ (N₂O, CO) mixtures in standard conditions with silica-made discharge tube. The concentration of admixtures was in the range (0.05 – 0.5)%. Before the measurements, the reactor was treated by argon RF plasma at a pressure of 0.3 mbar during 30 minutes. It should be noted that the acquisition is done in a single pulse without data accumulation.

First of all let us discuss the particularity of quantum cascade laser absorption measurements in the conditions of non-equilibrium vibrational excitation. According to expression (2. 2), the measured absorbance is proportional to the difference between the lower and the upper roto-vibrational level populations n_i and n_k . Taking into account the Boltzmann relation between n_i and n_k and the total density of molecules on the lower (N_0) and the upper (N_1) vibrational levels (2. 2) and (2. 3) is expressed as follows

$$\int \ln \left(\frac{I_v(L)}{I_v(0)} \right) dv = - \frac{h\nu_{ik}}{c} \frac{g_i B_{ik} e^{-\frac{E_i}{kT}}}{Q_{rot}} \left(N_0 - e^{\frac{E_i - E_k}{kT}} N_1 \right) LK \quad (5. 3)$$

where E_i and E_k correspond to the rotational energy of the lower and the upper levels respectively, Q_{rot} is the rotational partition function, K is a calibration factor that accounts for the absorption line distortion due to the rapid passage effect. Effectively (5. 3) may be rewritten

$$\int \ln \left(\frac{I_v(L)}{I_v(0)} \right) dv = -\alpha(N_0 - \beta N_1) \quad (5. 4)$$

where α is found from the calibration and β depends on the chosen transition and can be calculated using the known molecular parameters. Typically $\beta \sim 1$ because the statistical weights and the rotational energies of the levels connected by allowed dipole transitions ($\Delta J=0, \pm 1$) are close. The values of β at 300K for the absorption lines used in this study:

- $\beta=1.145$ for P28 CO₂(00⁰1←00⁰0) transition at 2324.976 cm⁻¹
- $\beta=1.135$ for P18 N₂O(00⁰1←00⁰0) transition at 2207.62 cm⁻¹
- $\beta=0.67$ for R18 CO(1←0) transition at 2209.508 cm⁻¹

Therefore, we conclude that the measured absorption signal is proportional to the population difference ($N_0 - \beta N_1$) of the lower and the upper vibrational levels. This is reflected in the y-axis labels in Figure 5. 4 (an further in this chapter).

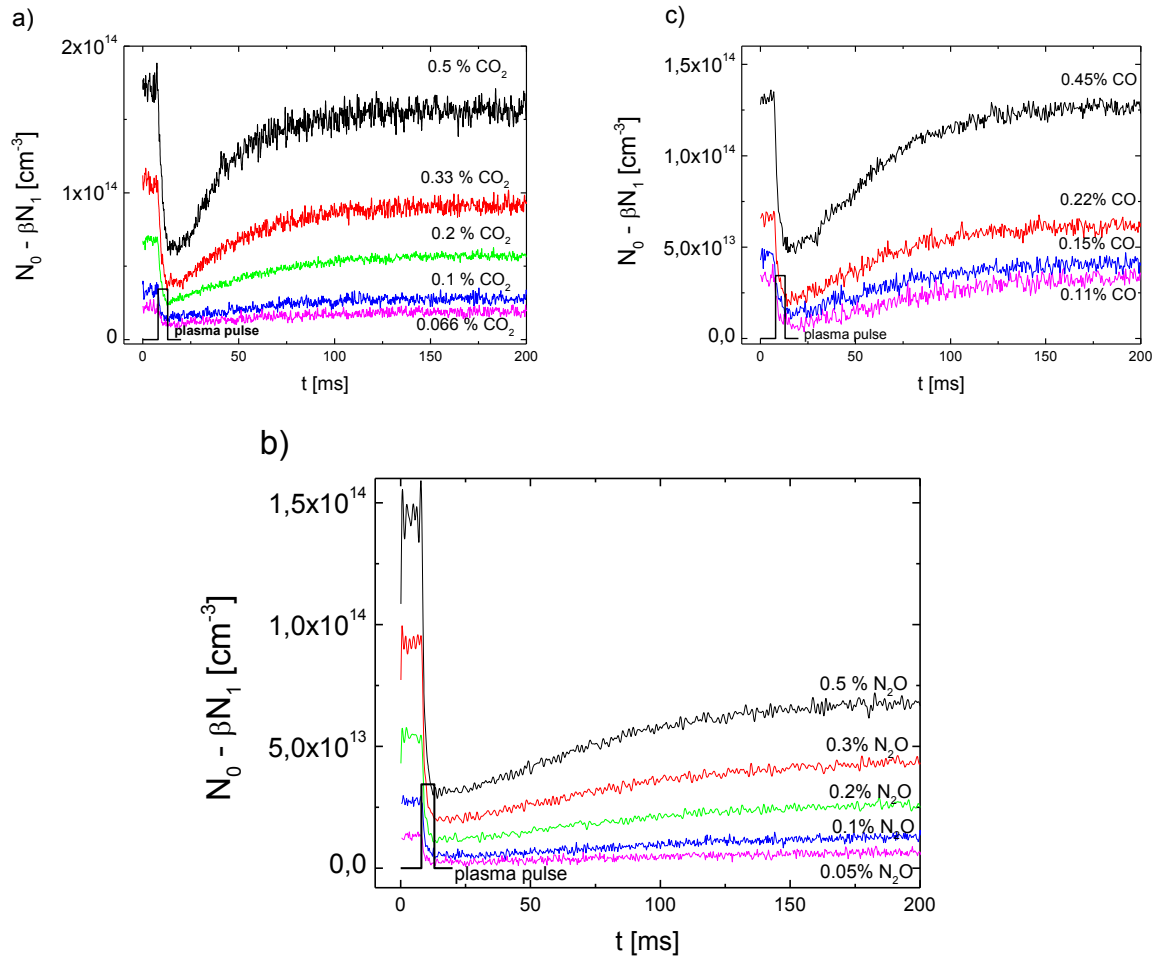


Figure 5. 4 a)-c) Relaxation measurements in $\text{N}_2 - \text{CO}_2$ (N_2O , CO) mixtures at $p=1.33$ mbar, $I=50$ mA, $\tau=5$ ms in silica tube pretreated by argon RF plasma.

In Figure 5. 4 all the titrating molecules exhibit the same behavior. The value of ($N_0 - \beta N_1$) drops rapidly during the discharge pulse and then relaxes to a stationary level in the afterglow on the timescale of few tens milliseconds. Typically, the stationary level of ($N_0 - \beta N_1$) in the afterglow is lower than the initial value which can be explained by the dissociation of the probe molecules in the discharge.

The fast decrease of the measured value of ($N_0 - \beta N_1$) when the discharge pulse is applied may be caused by 3 principal processes:

1. Variation of the rotational distribution due to the gas heating.
2. Dissociation.
3. Vibrational excitation.

Here we will discuss the role of these processes under the conditions of this study.

Study of surface vibrational relaxation of N₂

5.3.3.1 Gas temperature and its influence on the relaxation measurements

As it was shown in [78], in the discharge an increase of the gas temperature may alter significantly the laser absorption measurements of species concentrations. In this work we have independently measured the temporal variation of the gas temperature in the discharge active phase and in the afterglow using optical emission spectroscopy of the N₂ 2⁺ band at 337 nm as described in Chapter 2. In Figure 5. 5 the time evolution of the T_g in a 10 ms discharge pulse with $I=50 - 150$ mA is shown.

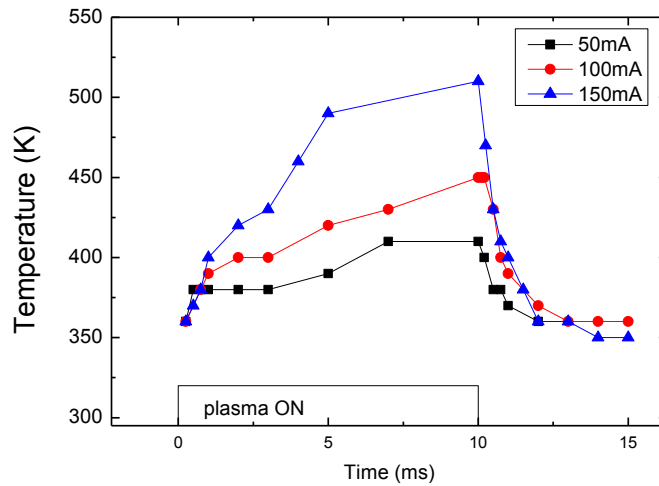


Figure 5. 5 Evolution of the gas temperature determined by OES in N₂ pulsed DC discharge at 1.33 mbar. Discharge current is $I=50 - 150$ mA, pulse duration $\tau=10$ ms.

As it was discussed in Chapter 2, OES measurements tend to slightly overestimate the value of T_g for low gas temperatures. In addition, in the presence of radial temperature gradients, the measured T_g is an effective average over the discharge cross section. Therefore, the absolute values of T_g obtained using OES under conditions of this study should be used with care. Nevertheless, the measured characteristic times of gas heating and cooling are meaningful. One can see that after 2-3 ms in the post discharge the value of T_g is indistinguishable from T_g measured in the beginning of the main discharge pulse when the gas is cold ($T_g=300$ K). The relaxation of the value of $(N_0 - \beta N_1)$, shown in Figure 5. 4 is much slower and therefore it cannot be related to the temperature effects. Moreover, one can note that curves plotted in Figure 5. 4 exhibit no fast changes when the discharge is stopped as it would be expected if the variation of the gas temperature had a strong influence on the absorption measurements [78]. In the further discussion we will be interested in relaxation processes that take place on the timescale of several tens of milliseconds when the gas temperature is already in equilibrium with reactor walls.

5.3.3.2 Dissociation and re-association of titrating molecules

Dissociation of CO_2 (N_2O , CO) in the discharge with the subsequent recombination of produced fragments at reactor walls may also influence time evolution of the absorption signals. Special test experiments have been performed in order to evaluate the efficiency of dissociation/re-association reactions in the case of CO_2 and N_2O .

The main dissociation products of CO_2 are O and CO [146]. Recombination of these fragments may result in the production of CO_2 or $1/2\text{O}_2$ and a CO molecule. It is known that surface association of oxygen atoms with carbon monoxide on silica surface ($\text{O}+\text{CO}|_{\text{w}}$) is inefficient [147] compared to the recombination of oxygen atoms ($\text{O}+\text{O}|_{\text{w}}$) [21]. Therefore it is unlikely that dissociation products recombine back into CO_2 .

In order to confirm the low efficiency of $\text{O}+\text{CO}|_{\text{w}}$ recombination process under the conditions of the present study a test experiment was done. A single discharge pulse with $\tau=5$ ms and $I=50$ mA was applied in a mixture of $\text{CO}/\text{Ar}/\text{O}_2=0.5/49.5/50$ at $p=1.33$ mbar under static conditions in silica discharge tube. The concentration of CO_2 measured after the discharge pulse was about $1 \cdot 10^{13}$ molecules cm^{-3} . A simple estimation shows that the density of atomic oxygen at the end of the pulse was in the order of 10^{15} cm^{-3} . The density of CO was $1.5 \cdot 10^{14}$ molecules cm^{-3} . Thus even with an excess of atomic oxygen recombination into CO_2 doesn't exceed 10% of the initial CO concentration. It is evident that in the experimental conditions shown in Figure 5. 4 a), the density of CO and O available for recombination are approximately equal and they are always smaller than in the experiment with the $\text{CO}/\text{Ar}/\text{O}_2$ mixture. Hence we conclude that surface re-association of CO and O has only a minor role in the conditions of this study. Therefore the $\sim 15\%$ depletion of the CO_2 concentration measured at the end of the post discharge, shown in Figure 5. 4 a), is the true value of the dissociation degree of CO_2 in the discharge.

Similar experiments were performed for the case of N_2O . According to [148] the main dissociation products of N_2O in the discharge are N_2 and O . In order to determine the efficiency of N_2O production from the recombination of O and N_2 , a DC discharge pulse with $\tau=5$ ms, $I=50$ mA in $\text{N}_2/\text{O}_2=4/1$ at $p=1.33$ mbar was applied in static conditions in silica discharge tube. The concentration of N_2O measured after the discharge pulse was only $[\text{N}_2\text{O}]_{\text{pulse}} = 4 \cdot 10^{12}$ cm^{-3} . This proves that production of N_2O in the postdischarge in the conditions of the experiment shown in Figure 5. 4 b) is negligible. The $\sim 50\%$ difference between the initial and the final concentrations of N_2O is due to the dissociation in the discharge.

Compared to CO_2 and CO , N_2O has the smallest bond dissociation energy $D(\text{NN-O})=1.67$ eV (for comparison $D(\text{C-O})=11.1$ eV and $D(\text{OC-O})=5.45$ eV). Hence, the dissociation of CO and CO_2 in the discharge is less pronounced, as it can be seen in Figure 5. 4.

Study of surface vibrational relaxation of N₂

5.3.3.3 Vibrational excitation of titrating molecules

We conclude here that 2-3 ms after the end of the discharge pulse temperature and dissociation effects do not influence the relaxation measurements. Therefore, the evolution of the value of $(N_0 - \beta N_1)$ is determined by **vibrational excitation** of titrating molecules.

During the discharge ON phase gas mixtures N₂ – CO₂ (CO or N₂O) are excited by plasma electrons. Depletion of the value of $(N_0 - \beta N_1)$ is caused by the decrease of the population of the ground state (N_0) and the increase of the population of the upper level (N_1). In the case of CO₂ and N₂O laser absorption measurements are performed in the asymmetric stretching mode ν_3 . As it follows from

Table 5. 1, this mode is in resonance with N₂(ν) and we will show later that it has the highest population compared to other vibrational modes. Excitation of ν_1 and ν_2 modes of CO₂ and N₂O reduces the value of N_0 and contributes as well to the depletion of the measured absorption signals.

When the discharge is stopped, relaxation of the mixture as a whole takes place. Vibrationally excited nitrogen molecules play the role of energy reservoir and their quenching on the reactor walls and in the gas phase determine the characteristic relaxation time of the system.

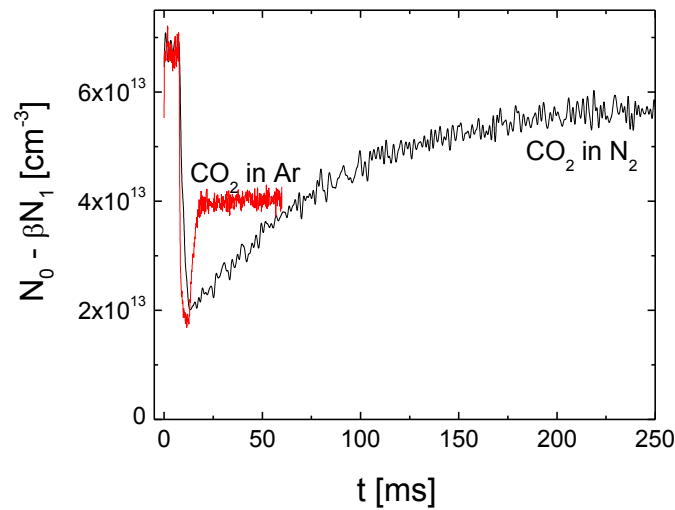


Figure 5. 6 Comparison of CO₂ relaxation measurements in mixtures with Ar and N₂. Pulse duration $\tau=5$ ms, $I=50$ mA, $p=1.33$ mbar, silica discharge tube.

In order to illustrate the role of N₂(ν) for vibrational relaxation of titrating molecules in the afterglow, a test experiment has been performed. A mixture containing 0.2% of CO₂ in Ar was excited by a $\tau=5$ ms, $I=50$ mA discharge pulse at $p=1.33$ mbar in static conditions. In Figure 5. 6 time evolution of $(N_0 - \beta N_1)$ in case of CO₂ diluted in Ar and N₂ is shown. One can see that in argon mixture the characteristic relaxation time is $\tau_{\text{relax}} \sim 2$ ms while with N₂ $\tau_{\text{relax}} \sim 70$ ms. This proves that in the afterglow, N₂(ν) is the main source of the vibrational

excitation of CO₂. The degree of vibrational excitation of CO₂ literally follows the excitation of N₂.

5.4 Modeling of vibrational kinetics in N₂-CO₂

In order to interpret the result shown in Figure 5. 4 and to get the information on surface relaxation processes a numerical model of the vibrational kinetics in N₂ – CO₂ (CO or N₂O) has to be developed. From the modeling viewpoint, the simplest case would be the N₂-CO mixture because CO has only one vibrational mode and reliable data on the vibrational relaxation rates in this system are available in the literature [149]. However, from the experimental viewpoint, the line of CO at 2209.508 cm⁻¹ (Hitran intensity 7.5·10⁻²⁰ cm⁻¹/(molecules·cm⁻²)) is much weaker than the lines of CO₂ (2.08·10⁻¹⁸ cm⁻¹/(molecules·cm⁻²)) and N₂O (9.07·10⁻¹⁹ cm⁻¹/(molecules·cm⁻²)). Therefore, measurements in wider concentration ranges, especially towards lower concentrations, have been performed with CO₂ and N₂O.

For kinetic modeling we have chosen CO₂ because of the existence of detailed information on the rates of vibrational relaxation in N₂-CO₂ [150][151][152] due to the development of CO₂ laser in 1960s [153] and due to the atmospheric relevance of this system [154][155]. Thus, a detailed model of vibrational kinetics in N₂-CO₂ was created and applied to the experimental conditions of this work. Using the insight into the relaxation kinetics gained with the combined experimental/modeling approach we will propose a simplified data interpretation procedure for measurements with CO and N₂O.

5.4.1 Relevant relaxation processes

Let us briefly consider the processes that are important for the relaxation kinetics shown in Figure 5. 4. During the 5 ms plasma ON phase vibrations of both CO₂ and N₂ are efficiently excited by electron impact. In the afterglow, vibrational energy is exchanged between different modes of CO₂ and N₂ and the reactor walls.

Results shown in Figure 5. 6 prove that vibrational excitation of CO₂ persists in the afterglow. As is shown in [128], excitation of CO₂ in the post discharge takes place in the V-V' exchange process.

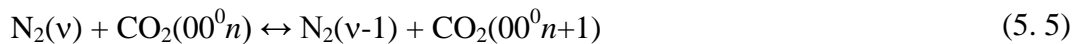


Figure 5. 7 shows the diagram of the vibrational levels of N₂ and CO₂, the vibrational state notation is taken from [154]. For the first excited levels N₂(ν=1) and CO₂(00⁰1) the process (5. 5) is almost resonant and as a consequence it is rather fast, $k_{\text{N}_2\text{-CO}_2}=7 \cdot 10^{-13} \text{ cm}^3\text{s}^{-1}$ at 300 K [155]. We will show later, that the high efficiency of (5. 5) leads to the equalization of the vibrational temperatures of N₂(ν) and the CO₂(00⁰ν₃).

Study of surface vibrational relaxation of N₂

For a correct description of the vibrational kinetics in the N₂ subsystem the V-V and V-T processes for all the vibrational levels of N₂ should be considered in the model. In nitrogen V-T relaxation at room temperature is very slow, for N₂($\nu=1$) $k_{VT}=7 \cdot 10^{-22} \text{ cm}^3 \text{ s}^{-1}$ [140]. Thus, the relaxation of the low lying vibrational levels is controlled by impurities and by quenching on the reactor walls [63] [126]. Under the conditions of the present study in pure N₂, surface relaxation is dominant due to the low level of impurities in the N₂ gas used. According to [156] V-T quenching by atomic nitrogen may be an important process of N₂(ν) relaxation. However in our conditions at room temperature and with the typical degree of dissociation of 1% [97] the V-T relaxation by N atoms is negligible. Relaxation caused by CO₂ becomes increasingly important upon the addition of CO₂.

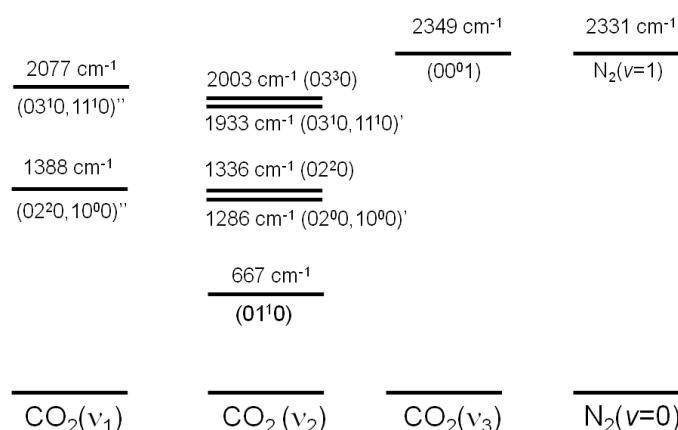


Figure 5. 7 Diagram of the vibrational levels of N₂ and CO₂.

The modeling of the CO₂ subsystem requires consideration of the vibrational energy transfer from N₂(ν). Apart from the excitation of ν_3 mode in the reaction (5. 5) other vibrational levels of CO₂ may be in principle excited in collisions with N₂(ν). However, as it is shown in [157] these processes are very inefficient due to either substantial energy mismatch or the necessity of multi-quantum excitation. Therefore, reaction (5. 5) is the only efficient process of the vibrational energy exchange between CO₂(00⁰ ν_3) and N₂. Other CO₂ vibrational modes (ν_1 , ν_2) are populated in so-called intramolecular vibrational exchange reactions (as for example CO₂(00⁰1)+M→ CO₂(ij^k 0)+M). Typically, exchange between the levels having the smallest energy gap is the most efficient [150][157].

As one can see from Figure 5. 6, without the vibrational pumping by N₂(ν) the relaxation time in CO₂ is of the order of 2 ms. Such a fast relaxation is explained by a very efficient surface quenching and spontaneous emission (radiative lifetime of CO₂(00⁰1) is 2.4 ms [150]). It is known from a number of works [127][158] that the deactivation probability of CO₂(010) and CO₂(001) on glass surfaces is found to be in the range of $\gamma_{CO_2} \sim 0.18 - 0.4$. To the best of our knowledge there is no data available for the ν_1 mode, but it would be reasonable to suggest that the deactivation probability of this mode is also relatively high. In our conditions, for $\gamma_{CO_2} \geq 0.1$ the lifetime of the vibrationally excited CO₂ is limited by the diffusion towards the wall and does not exceed 2 ms.

5.4.2 Model description

5.4.2.1 Gas phase processes

We used the approach to the modeling of vibrational kinetics similar to a number of published works [63] [159]. The model is zero dimensional and it incorporates excitation of vibrations by electronic impact (e-V), V-V and V-T exchange in the N₂ subsystem as well as the V-V' exchange (5. 5) between N₂ and CO₂ and intramolecular vibrational relaxation in CO₂. Relaxation in collisions between two CO₂ molecules was neglected due to the low concentration of admixed CO₂. Electron impact excitation of CO₂ was also ignored because we are interested only in the afterglow phase where CO₂ is excited in collisions with N₂(v). The system of kinetic equations can be written in a symbolic form:

$$\frac{dN_2(i)}{dt} = \left(\frac{dN_2(i)}{dt}\right)_{e-V} + \left(\frac{dN_2(i)}{dt}\right)_{VV}^{N_2-N_2} + \left(\frac{dN_2(i)}{dt}\right)_{VT} + \left(\frac{dN_2(i)}{dt}\right)_{R1}^{N_2-CO_2} + \left(\frac{dN_2(i)}{dt}\right)_W \quad (5. 6)$$

$$\frac{dCO_2(k)}{dt} = \left(\frac{dCO_2(k)}{dt}\right)_{R1}^{CO_2-N_2} + \left(\frac{dCO_2(k)}{dt}\right)_{VT} + \left(\frac{dCO_2(k)}{dt}\right)_{intra}^{CO_2-N_2} + \left(\frac{dCO_2(k)}{dt}\right)_W + \left(\frac{dCO_2(k)}{dt}\right)_{RD} \quad (5. 7)$$

where W accounts for wall losses, RD is the spontaneous radiative decay term and R1 is the contribution of reaction (5. 5).

The system of equations was solved for 0 - 45 vibrational levels of N₂ and 6 levels of CO₂ ((00⁰0), (00⁰1), (00⁰2), (01¹0), [(02⁰0,10⁰0)',(02⁰0,10⁰0)",(02²0)], [(03¹0,11¹0)',(03¹0,11¹0)",(03³0)]). The groups of 3 levels in square brackets have close energies and they are affected by the Fermi resonance therefore these levels were treated as a single effective level [154] (100)_{eff} and (110)_{eff} respectively.

The e-V rates in N₂ were found from the solution of Boltzmann equation using the EEDF solver developed by Dyatko *et al* [160] taking into account superelastic collisions between electrons and vibrationally excited N₂ molecules. The average electron density was calculated based on the discharge current (*I*) and the electron drift velocity (*v_{dr}*) obtained from the Boltzmann equation solution.

$$n_e = \frac{I}{ev_{dr}S} \quad (5. 8)$$

Where *e* is the electron charge and *S* is the discharge tube cross section. The electron density was assumed to be constant during the pulse in accordance with the experimentally measured current waveforms. The value of the reduced electric field in pure N₂ was taken from [99] [159] E/N=80Td and it was assumed to be constant during the pulse as it was done by Pintassilgo *et al* [149] under similar conditions in N₂/O₂ pulsed DC discharge. Upon the addition of CO₂ the sustaining discharge voltage was gradually increased, 10% rise compared to pure N₂ was measured for 0.5% CO₂ in N₂. We neglected the influence of CO₂ addition on the cathode fall voltage and therefore the increase of the E/N proportional to the discharge

Study of surface vibrational relaxation of N₂

voltage was assumed taking into account a correction for the literature value $U_c=210$ V of the cathode fall [68]. It is worth noting that e-V rates are not very sensitive functions of E/N because of the low energy threshold of vibrational excitation. Typically, variation of E/N from 70 to 90 Td leads to less than 20 % increase in the electron excitation rate of the first vibrational level of N₂.

We used the most recent set of V-V and V-T rates in N₂ calculated in [140][161] using a semiclassical trajectory method. Only single-quantum transitions were taken into account. The rates of the V-V' exchange between N₂ and CO₂ as well as V-T and intramolecular relaxation rates in CO₂ were taken from [150] [151] [152] [154]. Exchange reaction (5. 5) was considered for 45 levels of N₂ and 3 levels of CO₂(00⁰v₃). The dependence of the rate of (5. 5) on the vibrational quantum number of N₂ and CO₂ is not known. In the present study it was assumed to follow the analytical scaling of SSH theory [126]. Einstein coefficients for spontaneous emission in CO₂ were taken from [150].

5.4.2.2 Heterogeneous processes

Rigorous consideration of surface relaxation requires solution of a 1D problem that takes into account radial diffusion of species with appropriate boundary conditions. However, for the sake of simplicity surface processes are usually considered as volume ones with an effective frequency that can be written as [63]:

$$\nu_w = \left(\frac{\Lambda^2}{D} + \frac{2r}{\gamma v_{th}} \right)^{-1} \quad (5. 9)$$

where $\Lambda=(r/2.4)$ is the characteristic diffusion length, r is the tube radius, D is the diffusion coefficient, v_{th} is the average thermal velocity of the molecules and γ is the probability of deactivation in a single collision with the surface.

For CO₂ it was assumed that $\gamma_{CO_2}=0.2$ for all the vibrational levels of CO₂ [127], moreover a complete accommodation of vibrational energy was supposed. This lead to the characteristic surface relaxation time of CO₂ of the order of 2 ms, which is consistent with the results shown in Figure 5. 6.

In principle, different vibrational levels of N₂ may have different quenching probability in collision with the surface. At present there is no clear understanding of the dependence of γ_{N_2} on the vibrational quantum number v . Usually in the literature, γ_{N_2} is assumed to be either constant for all vibrational levels or proportional to the vibrational quantum number:

- i. $\gamma_{N_2}(v)=\gamma_1$
- ii. $\gamma_{N_2}(v)=\gamma_1 \cdot v$

In both cases only single vibrational quantum is supposed to be lost. Although quite often employed in the literature [63][159], the first hypothesis has no theoretical ground. The

second assumption is similar to the scaling of the gas phase quenching of harmonic oscillators and consequently it seems to be more physical. We will, therefore, adopt this hypothesis as working one. The influence of the choice of the γ_{N_2} scaling on the resulting value of γ_1 deduced from the experiment will be discussed in subsequent sections.

The *only* tuning parameter of the model was the probability of the vibrational deactivation of N_2 on the surface γ_1 . It was determined from the best agreement between the model and the experiment.

5.4.2.3 Numerical solution

The system of 52 differential equations (5. 6)-(5. 7) was solved numerically using Maple software package. Special solver for stiff ODEs was used. Pulsed discharge was simulated by introducing a time dependent discharge current which was set to zero in the afterglow. This allowed modeling of both plasma ON and plasma OFF phases in one run.

5.4.3 Validation of the model

The model developed in this work takes into account only kinetics of the vibrational levels of N_2 and completely omits other important plasma species, such as ions, atoms and electronically excited molecules. In order to verify the feasibility of our model (at least the part describing the vibrational kinetics of the N_2 subsystem) and to prove that the most important processes are well described, results of our calculations were compared with a complete self-consistent modeling performed by Vasco Guerra [159] for the same conditions ($p=1.33$ mbar, $I=50$ mA, $\tau=5$ ms). The model of V. Guerra has been applied for numerous experimental conditions and has proved its validity.

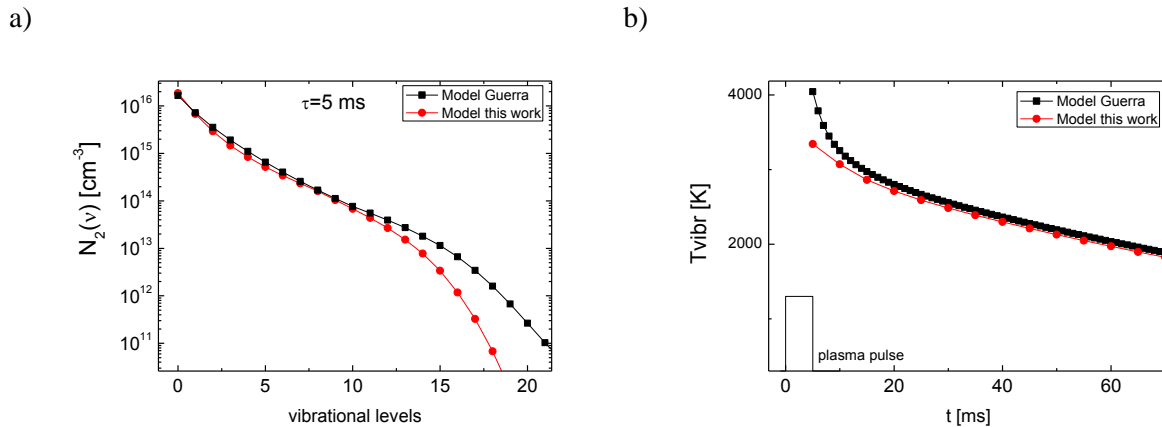


Figure 5. 8 Comparison between the results of our simplified model and a complete self-consistent simulation of V. Guerra for the same conditions ($p=1.33$ mbar, $I=50$ mA, $\tau=5$ ms). a) VDF at the end of the discharge pulse. b) Evolution of the effective vibrational temperature in the post-discharge.

In Figure 5. 8 the VDF at the end of the discharge pulse and time evolution of the vibrational temperature $T_v = E_1 / \left(\ln \left(\frac{N_2(v=0)}{N_2(v=1)} \right) \right)$ in the post discharge are shown. One can see that the

Study of surface vibrational relaxation of N₂

results of the simplified modeling are in reasonable agreement with the complete simulation, especially taking into account that different sets of e-V, V-V and V-T rates have been used.

In addition to the verification of our model for lower vibrational levels we have performed calculations for the conditions of the work [162] where the density of N₂($\nu=18$) in a dc discharge in N₂ (p=2.3 torr, I=100 mA) was measured using CRDS. To the best of our knowledge [162] it is the only experimental determination of the vibrational population of N₂ in the so-called plateau part of the VDF. In Figure 5. 9 the measured concentration [N₂($\nu=18$)]= $(9\pm 3.5)\cdot 10^{13}$ cm⁻³ is compared with our calculated VDF; an excellent agreement is obtained.

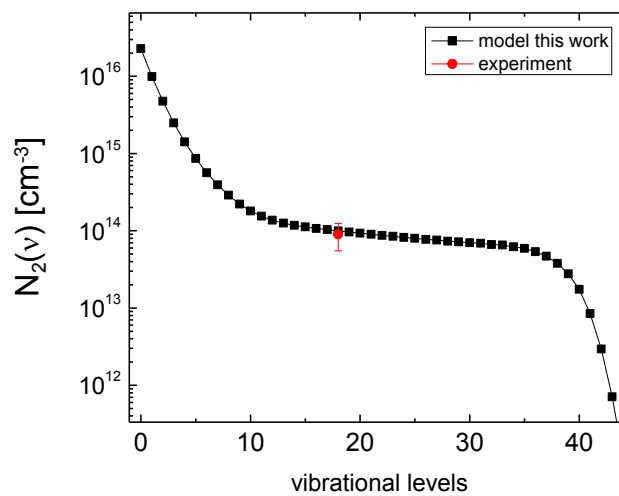


Figure 5. 9 Calculation for the conditions of [162] where [N₂($\nu=18$)] was measured in a continuous DC discharge in N₂, I=100 mA, p=2.3 torr.

We conclude that our model is correct and it gives a good description of N₂ vibrational kinetics in low pressure DC discharges.

5.4.4 On the possibility of experimental determination of γ_{N_2} dependence on ν

Before we start the analysis of experimental results let us first discuss the principle possibility of experimental determination of γ_{N_2} dependence on ν in discharge experiments. The titration technique developed in this work allows time resolved measurements of the degree of vibrational excitation of N₂ (vibrational temperature). This information is not detailed enough, so some hypothesis concerning $\gamma_{N_2}(\nu)$ has to be introduced for data analysis.

The most detailed information on the kinetics of vibrational relaxation of lower vibrational levels of N₂ may be obtained using Coherent Antistokes Raman Scattering (CARS) measurements. For example, in [129] concentrations up to $\nu=5$ were measured in a flowing N₂

discharge. We have calculated the time evolution of $[N_2(v)]$ for $v=0-5$ in the standard experimental conditions as in Figure 5. 4.

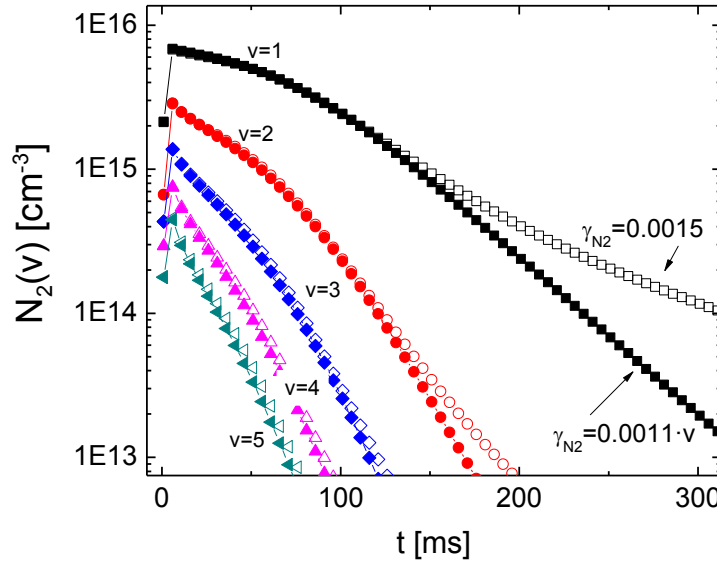


Figure 5. 10 Calculated time evolution of $[N_2(v)]$ for $v=1-5$ in a pulsed DC discharge in N_2 at $p=1.33$ mbar, $I=50$ mA, $\tau=5$ ms. Filled symbols correspond to $\gamma_{N_2(v)}=0.0011 \cdot v$, open symbols correspond to $\gamma_{N_2(v)}=0.0015$.

Two assumptions concerning $\gamma_{N_2(v)}$ dependence were tested:

- i. $\gamma_{N_2(v)}= 0.0011 \cdot v$ (we will see later that these values correspond to the relaxation on silica surface).
- ii. $\gamma_{N_2(v)}= 0.0015$ (this value was found by an adjustment to verify if the same result may be obtained with both hypotheses).

One can see that both hypotheses result in almost the same behavior of $[N_2(v)]$. Even for the $v=5$ level for which $\gamma_{N_2(v)}= \gamma_1 \cdot v$ hypothesis gives 4 times faster surface relaxation rate. The only minor difference is observed for $N_2(v=1)$ in the late afterglow. Slower relaxation of the first level with $\gamma_{N_2(v)}= 0.0015$ is caused by slower quenching of high vibrational levels which were populated by non-resonant VV exchange.

Apparent independence of the relaxation kinetics on the individual quenching probabilities of different vibrational levels is explained the fast V-V exchange that establishes a Treanor VDF on lower vibrational levels [126]. As a result, all the levels are coupled and the relaxation of the system as a whole takes place with the individual rates greatly masked.

Linear increase of γ_{N_2} with v suggests that for high vibrational levels surface relaxation may be much faster than for $v=1$. In order to check if the hypothesis concerning the scaling of γ_{N_2} may influence the populations on higher vibrational levels (and keeping in mind possible measurements of $[N_2(v=18)]$), we have calculated VDFs in a continuous dc discharge in N_2 at

Study of surface vibrational relaxation of N₂

p=1.33 mbar, I=50 mA with the same assumptions concerning γ_{N_2} as in Figure 5. 10. As one can see in Figure 5. 11, VDFs exhibit only a minor difference for levels up to $v=30$.

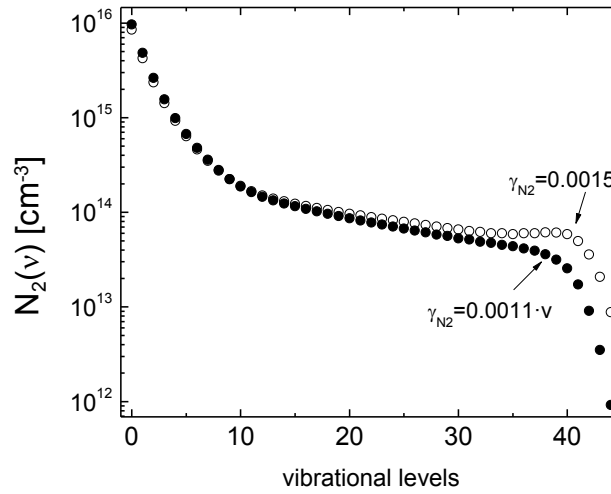


Figure 5. 11 Calculated VDF in a continuous DC discharge in N₂ at p=1.33 mbar, I=50 mA. Filled symbols correspond to $\gamma_{N_2}(v)=0.0011 \cdot v$, open symbols correspond to $\gamma_{N_2}(v)=0.0015$.

We conclude here that in typical low pressure discharge conditions, even detailed measurements of $N_2(v)$ would not allow an unambiguous determination of γ_{N_2} dependence on v . The reason for this is the fast vibrational exchange in the gas phase. Therefore, in order to determine γ_{N_2} for individual vibrational levels, experimental conditions should be specially selected to keep surface relaxation faster than the gas phase exchange processes.

Based on the above discussion we can state that regardless less detailed measurements, the titration technique for γ_{N_2} determination in low pressure discharge conditions is not less informative than CARS.

5.4.5 Modeling results in N₂ – CO₂ mixtures

Figure 5. 12 and Figure 5. 13 show the typical output of the model for experimental conditions as in Figure 5. 4. In Figure 5. 12, the vibrational distribution function (VDF) of N₂ is shown for different delays after the ignition of the discharge pulse. For times inferior to 1 ms the VDF is governed by the electron impact excitation which is efficient for $v=1-9$ and VDFs reflect the excitation pattern. With increasing the degree of the excitation, V-V exchange tends to establish a Treanor distribution on low-lying vibrational levels. The population of high vibrational levels takes place in the ladder-like V-V exchange and it is delayed compared to the evolution of the VDF on lower levels. In the post discharge (delays longer than 5 ms), the relaxation of the VDF is determined by population of higher vibrational levels of N₂ and the loss of the vibrational energy on the reactor walls and in collisions with CO₂.

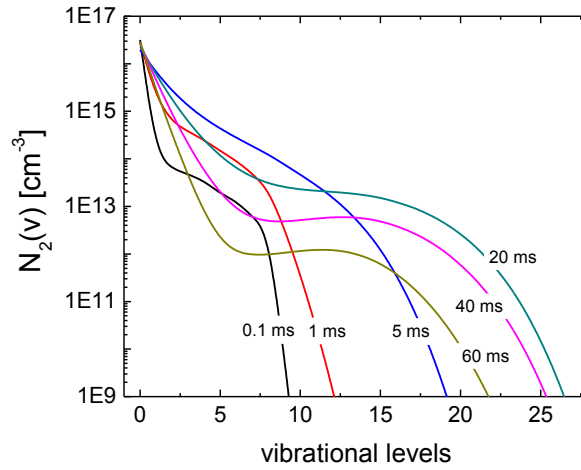


Figure 5. 12 Time evolution of the N_2 vibrational distribution function in a single discharge pulse with $\tau=5$ ms, $I = 50$ mA and $p=1.33$ mbar in a 0.2% CO_2 - N_2 mixture. The beginning of the discharge pulse corresponds to $t=0$.

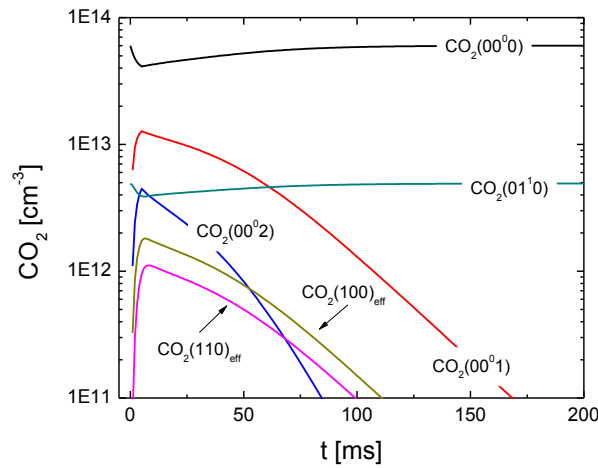


Figure 5. 13 Time evolution of the population of the vibrational levels of CO_2 . Discharge conditions are the same as in Figure 5. 12.

Figure 5. 13 depicts the time evolution of the CO_2 vibrational level population. During the 5 ms discharge pulse, one can see a depletion of the $CO_2(00^0_0)$ concentration and the appearance of the molecules in the excited states due to the vibrational transfer from $N_2(v)$. In the afterglow, the vibrational distribution of CO_2 relaxes to thermal equilibrium following the relaxation of the VDF of $N_2(v)$. The analysis of the simulation results shows that $N_2(v)$ and $CO_2(00^0_{v_3})$ are strongly coupled because the V-V' exchange (5. 5) is much faster than the quenching of $CO_2(00^0_{v_3})$. It was found that vibrational temperatures of N_2 and $CO_2(00^0_{v_3})$ are very close and obey the well known analytical relation [126]:

$$\frac{E_1^{CO_2}}{T_1^{CO_2}} - \frac{E_1^{N_2}}{T_1^{N_2}} = \frac{E_1^{CO_2} - E_1^{N_2}}{T_{gas}} \quad (5. 10)$$

Study of surface vibrational relaxation of N₂

where $T_1^{CO_2}$ ($T_1^{N_2}$) and $E_1^{CO_2}$ ($E_1^{N_2}$) correspond to the effective temperature and the energy of the first vibrational level of CO₂ (N₂), T_{gas} is the gas temperature (equal to 300K).

Vibrational modes other than CO₂(00⁰v₃) are weakly populated and do not contribute to the depletion of the value of $(N_0 - \beta N_1)$. The overpopulation of CO₂(kl^m0) after the discharge pulse compared to the 296 K level doesn't exceed 5% of the total CO₂ concentration. The low population of CO₂ modes, which are not directly coupled to N₂(v), can be explained by a relatively slow intramolecular exchange in CO₂ compared to surface losses and spontaneous emission. For example at a pressure of 1.33 mbar using the relaxation rates from [154] we estimate the total quenching frequency of CO₂(00⁰1) → CO₂(kl^m0) by N₂ to be $\nu_{intra} \sim 130 \text{ s}^{-1}$ while the frequency of surface losses of each individual level CO₂(kl^m0) is $\nu_W \sim 600 \text{ s}^{-1}$.

5.4.6 Determination of γ_{N_2} for silica. The influence of CO₂ admixture

In order to determine the probability of N₂(v) quenching on silica surface, the value of γ_1 ($\gamma_{N_2} = \gamma_1 \cdot v$ scaling was adopted) in the simulations was varied to achieve the best fit with the experimental data shown in Figure 5. 4. Experimental and simulated curves for 0.2% CO₂ are shown in Figure 5. 14. The best fit value $\gamma_1 = 1.6 \cdot 10^{-3}$ was found. Calculated curves with $\gamma_1 = 1.4 \cdot 10^{-3}$ and $1.8 \cdot 10^{-3}$ illustrate the sensitivity of the model to the γ_1 variation and allow one to estimate the relative error of the γ_1 to be $\pm 15\%$.

One can note that the magnitude of the measured relaxation signals is well reproduced in the simulation. Depletion of the value of $(N_0 - \beta N_1)$ is determined by the degree of vibrational excitation of N₂ after the discharge. Therefore we conclude that electron impact excitation of N₂ is correctly treated in the model.

Calculations with different concentrations of added CO₂ were performed. The agreement between the experiment and the model was achieved by varying the value of γ_1 for every given CO₂ admixture. It was found that the best fit value of γ_1 increases systematically with increasing CO₂ concentration. Figure 5. 15 shows the obtained dependence, an increase of γ_1 by a factor of 2 over the studied range of the CO₂ concentration can be seen.

From the calculation viewpoint the increase of the best fit value of γ_1 as a function of the CO₂ concentration signifies that gas phase processes of N₂(v) quenching by CO₂ that were taken into account in the model are not sufficient to reproduce experimentally observed relaxation kinetics. In the model, we have included all the known gas phase processes of N₂(v) quenching by CO₂. Therefore, we believe that the obtained increase of the surface quenching probability of N₂(v) upon the addition of CO₂ is a real physical effect and it is not related to the incompleteness of the model.

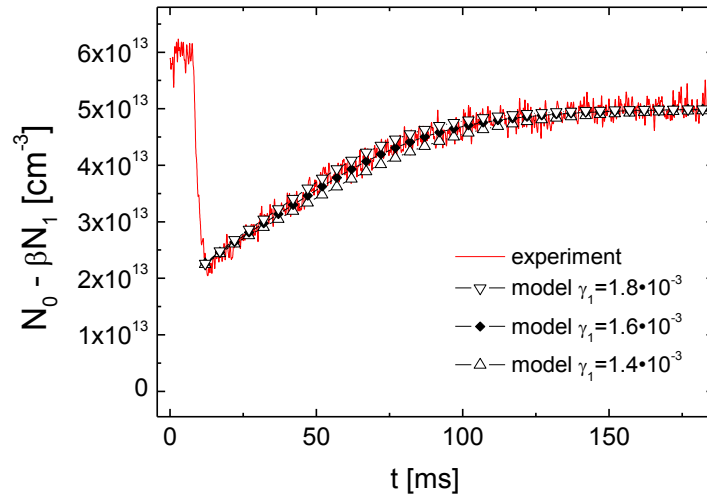


Figure 5. 14 Experimental relaxation curve with 0.2% of CO₂ (—), silica discharge tube. Results of calculations with $\gamma_1 = 1.4 \cdot 10^{-3}$ (— ∇ —), $\gamma_1 = 1.6 \cdot 10^{-3}$ (— \blacklozenge —) $\gamma_1 = 1.8 \cdot 10^{-3}$ (— \triangle —) (γ_{N_2} is supposed to increase linearly with the vibrational quantum number $\gamma_{N_2}(v) = \gamma_1 \cdot v$).

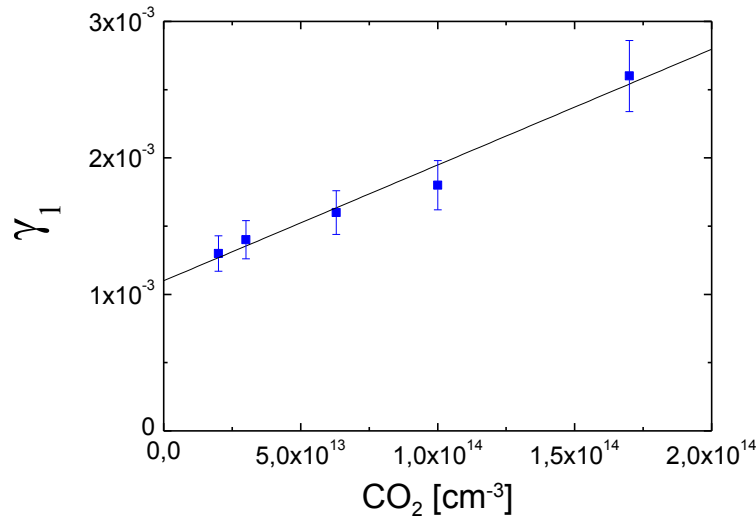


Figure 5. 15 Wall deactivation probability of N₂(v=1) as a function of the added CO₂ concentration (■). Linear fit with $\gamma_1 = 0.0011 + 8 \cdot 10^{-18} [\text{CO}_2]$ (—).

To support this statement let us consider the most important mechanisms of N₂(v) vibrational relaxation in the presence of CO₂. According to [154] V-T quenching of N₂(v) by CO₂ is very inefficient ($k_{VT} = 1 \cdot 10^{-22} \text{ cm}^3 \text{ s}^{-1}$). The effective mechanism of N₂ vibrational quanta losses in N₂-CO₂ mixture proceeds via the fast transfer N₂(v) ↔ CO₂(00⁰v3) followed by the quenching of CO₂(00⁰v3). Therefore, the “leakage” of N₂ vibrational quanta is proportional to the CO₂ concentration. Taking into account that CO₂(00⁰v3) is nearly in equilibrium with N₂(v) the characteristic frequency of N₂ quanta losses in such two-step process can be written as follows:

Study of surface vibrational relaxation of N₂

$$\varphi = [\text{CO}_2] \frac{\nu_{\text{intra+W+RD}}}{[\text{N}_2]} \quad (5.11)$$

where $\nu_{\text{intra+W+RD}}$ is the quenching frequency of $\text{CO}_2(\nu 3)$, $[\text{N}_2]$ and $[\text{CO}_2]$ is the concentration of N_2 and CO_2 respectively. Calculation using (5.11) for CO_2 concentration ranging between $2 \cdot 10^{13} - 2 \cdot 10^{14} \text{ cm}^{-3}$ yields $\varphi = 0.8 - 8 \text{ s}^{-1}$. At the same time the characteristic frequency of surface relaxation of $\text{N}_2(\nu=1)$ calculated using (5.9) with the γ_1 values from Figure 5.15 is found in the range $25 - 60 \text{ s}^{-1}$. Therefore, the relaxation induced by the presence of CO_2 in the gas phase is far too slow to explain the experimental results from Figure 5.4. Using model calculations we have found that in order to reproduce experimentally observed time evolution of $(N_0 - \beta N_1)$ at different levels of added CO_2 with a fixed value of γ_1 , the total quenching frequency of $\text{CO}_2(00^0\nu 3)$ has to be increased by a factor of 10. In previous sections it was shown that the quenching of $\text{CO}_2(00^0\nu 3)$ is dominated by the diffusion limited surface vibrational deactivation and spontaneous emission. Therefore, the value of $\nu_{\text{intra+W+RD}}$ is known with a sufficient accuracy and its underestimation by a factor of 10 is very unlikely. Hence we conclude that the strong increase of the $\text{N}_2(\nu)$ relaxation frequency with increasing CO_2 concentration is likely due to a modification of the surface state by the presence of CO_2 .

The physical mechanism of the CO_2 induced enhancement of γ_1 may consist in the transfer of the vibrational energy between $\text{N}_2(\nu)$ and CO_2 molecules adsorbed on the quartz surface. In [163] a similar mechanism was proposed to explain the experimentally measured surface relaxation rates in pure CO_2 .

In Figure 5.15 the data points are approximated by a linear function $\gamma_1 = 0.0011 + 8 \cdot 10^{-18} [\text{CO}_2]$ where $[\text{CO}_2]$ is the concentration of carbon dioxide in molecules cm^{-3} . The intercept value $\gamma_1^0 = (1.1 \pm 0.15) \cdot 10^{-3}$ can be considered as the wall deactivation probability of $\text{N}_2(\nu=1)$ on fused silica in pure nitrogen. In contrast to γ_1 values shown in Figure 5.15, it was found that the value of γ_1^0 does not depend on the rates of CO_2 relaxation that were used in the model.

The value of γ_1^0 obtained in this study is in reasonable agreement with the literature data which are found in the range $(2 - 7) \cdot 10^{-4}$ [127] [129] depending on surface pretreatment history. One should note that any comparison between different experimental data is not straightforward due to the differences in the surface preparation; surface roughness may also vary depending on the specific materials supplier and it is almost never specified. Therefore, we consider the agreement between the results of this work and the available literature data to be generally good.

The influence of the assumption concerning the γ_{N_2} dependence on the vibrational quantum number.

The obtained value of γ_1 depends on the assumption made regarding the vibrational quantum number dependence of γ_{N_2} . As it was mentioned above, the $\gamma_{\text{N}_2} = \gamma_1 \cdot \nu$ hypothesis is justified by the similarity with the ν -scaling of gas phase quenching processes. Nevertheless, other dependences cannot be excluded. For example, assuming γ_{N_2} to be constant for all the

vibrational levels of N_2 , we obtain the best fit value of $\gamma_1^0 = (1.5 \pm 0.2) \cdot 10^{-3}$. Therefore, the choice of the vibrational level dependence of γ_{N_2} may introduce an additional systematic error of γ_1 determination.

However, the dependence of γ_{N_2} on ν is an unknown input parameter of any vibrational kinetics model of N_2 . If in the future values of γ_1 obtained in this work are used for kinetic modeling, the ν scaling of γ_{N_2} employed in the model should be the same as we used to deduce γ_1 . This will reduce the effect of the systematic error of γ_1 determination.

5.4.7 Conclusions on the study of the $N_2 - CO_2$ system

In this section we have obtained quite a detailed picture of the vibrational relaxation in the N_2 - CO_2 system. Here we will briefly summarize the most important points.

- Temperature and dissociation/re-association effects are not important for the relaxation measurements of $(N_0 - \beta N_1)$ starting from 2-3 ms in the post discharge. The behavior of the measured signals is determined exclusively by the vibrational relaxation.
- Due to the fast vibrational exchange, almost equal (governed by (5. 10)) vibrational temperatures of $N_2(\nu)$ and $CO_2(\nu_3)$ are established at any moment in the post discharge.
- Vibrational modes of CO_2 other than ν_3 exhibit very weak overpopulation because of the fast quenching on the walls and insufficient intramolecular exchange in CO_2 . As a result the depletion of the measured value of $(N_0 - \beta N_1)$ is governed exclusively by the excitation of the ν_3 mode.
- The value of γ_1 obtained from comparison between model and experiment for silica is in a good agreement with available literature data.
- The relaxation rate of $N_2(\nu)$ increases upon the addition of CO_2 due to the gas phase quenching and notably due to the increase of the value of γ_{N_2} .

A detailed analysis of the measurements and determination of the value of γ_{N_2} from the best fit condition in $N_2 - N_2O$ and $N_2 - CO$ would require creation of a dedicated kinetic model for each case. This is rather time consuming task and in addition the relaxation rates in N_2O are known with less precision than in CO_2 . A simplified data treatment procedure for γ_{N_2} determination is therefore desirable.

5.4.8 Data analysis using characteristic relaxation times

In fact, the value of γ_{N_2} influences the relaxation time of $(N_0 - \beta N_1)$ in the afterglow. The characteristic time may be introduced by fitting the experimental curves with an appropriate analytical function. We have found that the function

Study of surface vibrational relaxation of N₂

$$f(t) = \frac{A}{1 + \alpha \cdot \exp(-(t - t_0)/\tau_{eff})} \quad (5.12)$$

perfectly describes the experimental time evolution of $(N_0 - \beta N_1)$ in a wide range of conditions.

The proposed data treatment procedure is the following (we will apply it to the case of N₂ – CO₂ to check if it gives the same results as the detailed modeling). First, the relaxation curves are fitted with (5.12) and then the value of the “characteristic relaxation frequency” $\varphi=1/\tau_{eff}$ is plotted as a function of the CO₂ concentration. The result of this operation for data depicted in Figure 5. 4 a) is shown in Figure 5. 16. Then using a linear fit, an extrapolation towards [CO₂]=0 is performed. The intercept value corresponds to the relaxation frequency in pure N₂.

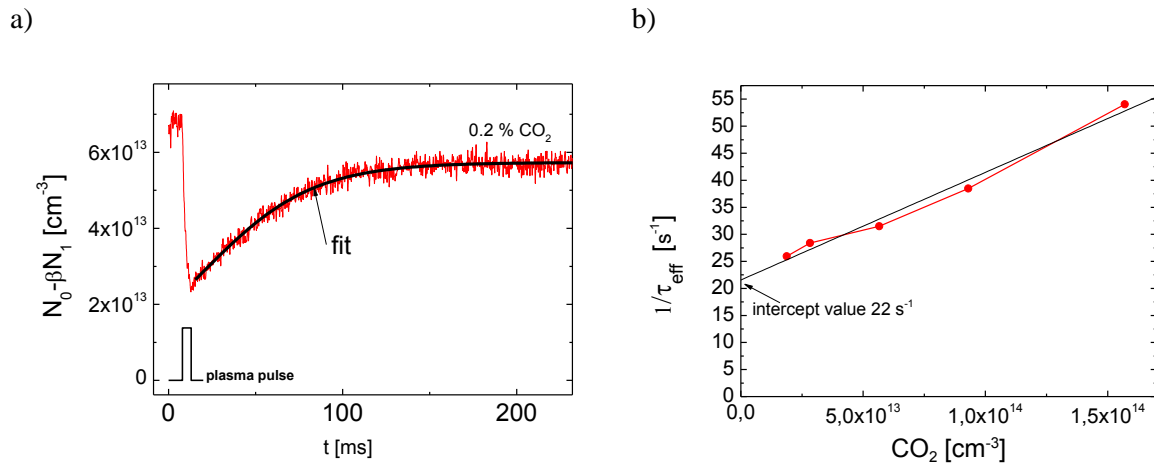


Figure 5. 16 a) An example of the analytical fit using (5.12). b) The characteristic relaxation frequency as a function of the CO₂ concentration left after the discharge pulse. Data points are fitted with a linear function. Conditions are the same as in Figure 5. 4 a).

In order to obtain γ_{N_2} from the extrapolated value of $(1/\tau_{eff})_{CO_2=0}$ the kinetic model should be used. But in this case we can deal with the kinetics in pure N₂ without taking into account the addition of IR active molecules. The value of $(N_0 - \beta N_1)$ is constructed for N₂($v=0$) and N₂($v=1$). This operation is justified because N₂(v) is all the time in equilibrium with CO₂ (CO or N₂O). Then a set of relaxation curves is calculated with different values of γ_1 (assuming that $\gamma_{N_2}=\gamma_1 \cdot v$) for the experimental conditions. And finally calculated relaxation curves are fitted with (5.12) in order to obtain the calibration curve of γ_1 as a function $(1/\tau_{eff})$.

In Figure 5. 17 a) a set of calculated relaxation curves for standard experimental conditions with different values of γ_1 is shown. One can see that simulated results may be also fitted with (5.12). The resulting calibration curve for $\gamma_1(1/\tau_{eff})$ is shown in Figure 5. 17 b). Coming back to the results depicted in Figure 5. 16, with the described calibration we obtain that the intercept value $(1/\tau_{eff})_{CO_2=0}=22 \text{ s}^{-1}$ corresponds to $\gamma_1=0.0011$. Therefore, the simplified data treatment procedure for CO₂-N₂ gives exactly the same resulting value of γ_1 (extrapolated to [CO₂]=0) as the complete kinetic modeling.

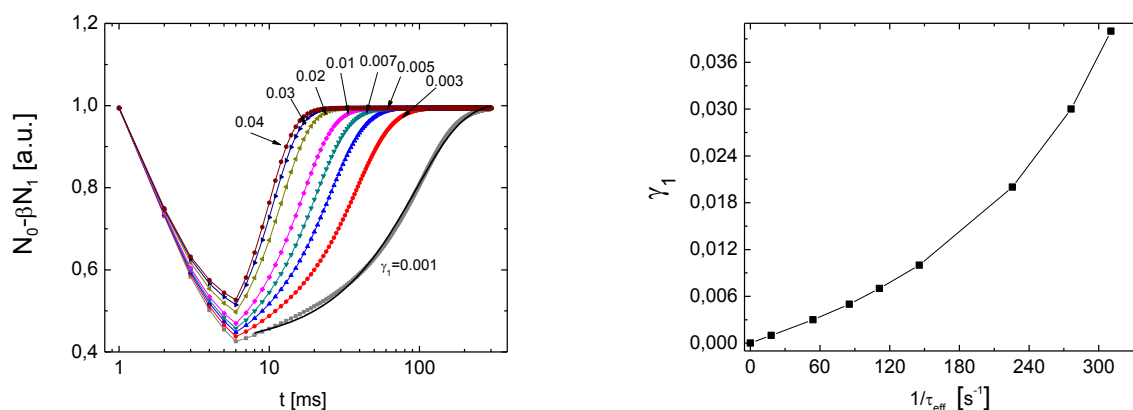


Figure 5. 17 a) Calculation of the time evolution of $(N_0 - \beta N_1)$ in pure N_2 at $p=1.33$ mbar, $I=50$ mA, $\tau=5$ ms, $\gamma_1=0.001 - 0.04$. Fitting with (5.12) is shown for $\gamma_1=0.001$. b) Calibration curve γ_1 as a function of $1/\tau_{\text{eff}}$ obtained using the simulated curves shown in the right panel.

If τ_{eff} is a good characteristic of the relaxation process?

The procedure described in this section may be directly applied to any IR active admixture. However, it is important to verify that τ_{eff} is a universal characteristic of the relaxation process and it is independent of the type of the titrating molecule employed. In order to check if different titrating molecules give the same value of τ_{eff} in *exactly the same* conditions we used the multi-species detection capability of the TRIPLE Q spectrometer. A mixture containing $[\text{CO}_2]=[\text{N}_2\text{O}]=4.5 \cdot 10^{13} \text{ cm}^{-3}$ in N_2 at 1.33 mbar was excited by a pulsed DC discharge ($I=50$ mA, $\tau=5$ ms). Both species were measured simultaneously. In Figure 5. 18 one can see that CO_2 and N_2O yield the same value of τ_{eff} . Similar measurements were performed in a mixture containing CO and CO_2 (Figure 5. 19) and it was found that τ_{eff} for both species is the same within 15% uncertainty. It should be noted that the difference of the relaxation times shown in Figure 5. 18 and Figure 5. 19 is due to different pretreatment history of the reactor.

Therefore, we conclude that τ_{eff} is a good characteristic of the vibrational relaxation process in $N_2 - \text{CO}_2$ (CO , N_2O) and the same data treatment may be applied to all the studied mixtures.

Study of surface vibrational relaxation of N₂

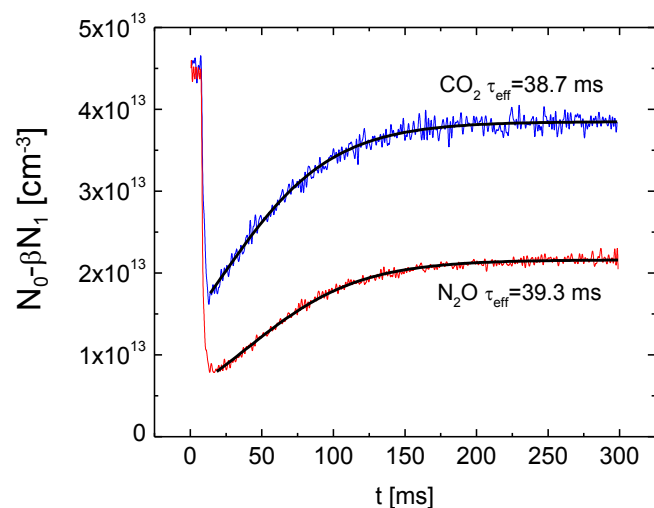


Figure 5. 18 Time evolution of the absorption signals of CO₂ and N₂O measured simultaneously in a pulsed DC discharge at p=1.33 mbar, I=50 mA, τ =5ms. Fitting with (5.12) is shown by black solid line.

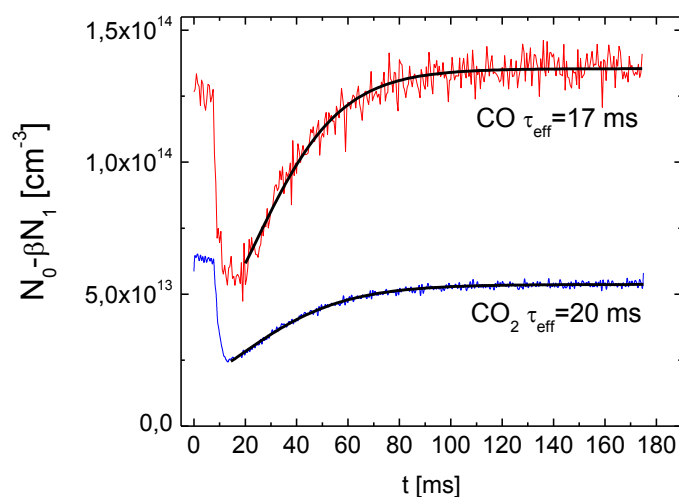


Figure 5. 19 Time evolution of the absorption signals of CO₂ and CO measured simultaneously in a pulsed DC discharge at p=1.33 mbar, I=50 mA, τ =5ms. Fitting with (5.12) is shown.

5.5 Application of the IR titration for γ_{N_2} determination on catalytic and plasma-pretreated surfaces

Now, when the IR titration technique is established and tested on a well studied silica surface, we can apply it to the investigation of other materials. The possibility of single pulse operation gives a unique opportunity to study surfaces pretreated by reactive plasmas.

In this section we will compare the utilization of three tracers CO_2 , N_2O and CO for γ_{N_2} determination on different surfaces (SiO_2 , Pyrex, TiO_2 , Al_2O_3 , anodized aluminum) pretreated by low pressure plasma (Ar , N_2 , O_2). We will also investigate the effect of O_2 addition in the discharge.

5.5.1 The effect of plasma pretreatment

A series of experiments with silica discharge tube was performed in order to study the role of plasma exposure on the probability of surface vibrational relaxation of $N_2(v)$. First, the reactor was pretreated by a flowing RF discharge in N_2 , O_2 or argon during 30 min at a pressure $p=53$ Pa. Then single pulse experiments in $N_2 - CO_2$ (N_2O or CO) mixtures were performed with varying admixture concentrations. The discharge conditions were the standard ones ($p=1.33$ mbar, $I=50$ mA, $\tau=5$ ms).

Typically, measurements with six different concentrations were done (in the range of 0.05-0.5%) in order to perform extrapolation towards zero admixture. A series of experiments consisted in a pretreatment followed by relaxation measurements with one tracer. Even short discharge pulses may alter the state of the pretreated surface due to the exposure to the species produced in the plasma (ions, N , O , CO , NO). However, we have verified that this effect is rather small and the value of γ_{N_2} stays constant during more than 10 dc discharge pulses after the pretreatment.

Figure 5. 20 shows the dependence of $1/\tau_{eff}$ on the concentration of CO_2 (N_2O or CO) for three different pretreatments of the surface. Data points are fitted by linear function in order to obtain the intercept value which is used for γ_{N_2} determination. One can see that three molecules give similar results. The highest relaxation frequency is obtained after N_2 plasma pretreatment, Ar gives intermediate values and the slowest relaxation is after O_2 plasma. However, the intercept values of $1/\tau_{eff}$ are slightly different. In Table 5. 2, deduced values of γ_1 are summarized. After O_2 plasma treatment results obtained with CO_2 , N_2O and CO are fairly close. After Ar plasma, CO gives γ_1 which is 60% higher than the measurements with CO_2 and N_2O . After N_2 pretreatment the strongest discrepancy between three tracers can be seen. Therefore, the measured values of γ_1 depend on both pretreatment procedure and employed IR tracer.

Observed variation with the type of the tracer for the same pretreatment procedure cannot be attributed to the irreproducibility of the measurements. The same experiments were performed over a period of several months and results were reproducible within 25%. For example,

Study of surface vibrational relaxation of N₂

$\gamma_1=1,1\cdot 10^{-3}$ presented in § 5.4.6 and $\gamma_1=8,8\cdot 10^{-4}$ from Table 5. 2 were measured using CO₂ titration after Ar plasma cleaning in the same silica discharge tube with 12 month elapsed between 2 measurements. The fact that with different tracers different values of γ_1 are obtained even after extrapolation to zero admixture signifies that the state of the surface may be irreversibly modified by the presence of titrating molecules. Upon the first introduction of the mixture in the reactor chemisorption (or reactive adsorption) of IR active molecules on surface active sites may take place. The contribution of these irreversibly adsorbed species cannot be corrected by the extrapolation procedure.

Pretreatment	N ₂ O	CO ₂	CO
N ₂	$1,05\cdot 10^{-3}$	$1,5\cdot 10^{-3}$	$2,3\cdot 10^{-3}$
Ar	$8,2\cdot 10^{-4}$	$8,8\cdot 10^{-4}$	$1,4\cdot 10^{-3}$
O ₂	$5,7\cdot 10^{-4}$	$5,2\cdot 10^{-4}$	$6,5\cdot 10^{-4}$

Table 5. 2 The values of γ_1 obtained using three titrating molecules after different plasma pretreatment of silica tube.

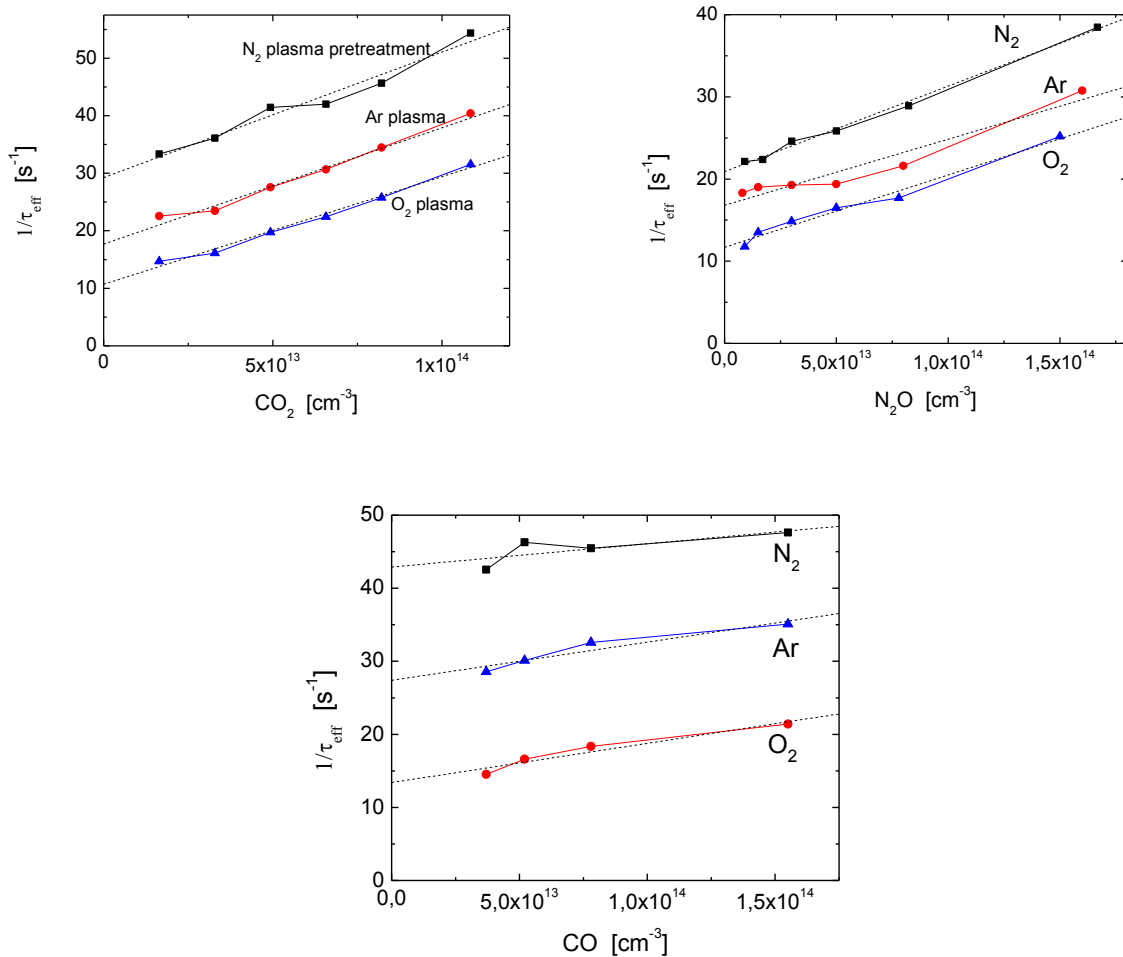


Figure 5. 20 Dependence of $1/\tau_{\text{eff}}$ on the concentration of IR tracers in silica reactor pretreated by N₂, O₂ and argon plasmas. Standard DC discharge conditions. IR tracer is CO₂ (upper left panel), N₂O (upper right panel) or CO (lower panel).

Let's consider separately three types of plasma pretreatment and try to understand what is the contribution due to the introduction of IR tracers (diagnostics artifact) and what is the contribution of plasma pretreatment (real effect) in the measured values of γ_1 .

N₂ plasma treatment

The highest relaxation probability was measured with CO after N₂ plasma exposure. In order to confirm the possibility of surface state modification by CO molecules in this case, a test experiment was performed. The reactor was treated by N₂ plasma for 30 minutes and then it was exposed to a flow of CO molecules (0.45% CO in N₂ at p=1.33 mbar) during 10 minutes followed by 10 min of pumping. Then the relaxation measurements were done with N₂O. Figure 5. 21 shows the dependence of $1/\tau_{\text{eff}}$ on the concentration of N₂O after N₂ plasma pretreatment with and without the exposure to CO flow. One can see that the exposure to CO increases the rate of vibrational relaxation. This proves that interaction of CO molecules with N₂ plasma treated silica may irreversibly change the probability of N₂(ν) quenching on the surface.

From the results presented in Chapter 3 we know that under N₂ plasma exposure a silicon oxynitride (SiO_xN_y) layer with chemically active adsorbed N atoms is formed on silica surface. It is known from the literature [164] that CO may react with N atoms on V₂O₅/Al₂O₃ forming adsorbed NCO species; similar reaction may take place with N atoms on SiO_xN_y in our case. Less is known about the reactivity and chemisorption of CO₂ and N₂O on SiO_xN_y and in principle we cannot exclude the possibility of chemisorption of these tracers and their influence on γ_1 measurements.

Therefore, high values of γ_1 measured after N₂ plasma exposure are caused by two effects:

- The increased N₂(ν) relaxation probability on SiO_xN_y compared to SiO₂
- The interaction of the titrating molecules with SiO_xN_y surface.

At present we are not able to separate these two contributions. The value of γ_1 measured with N₂O is the smallest one. Therefore, it is less disturbed by N₂O adsorption effects and it gives the best approximation for the true value of N₂(ν) quenching probability on SiO_xN_y.

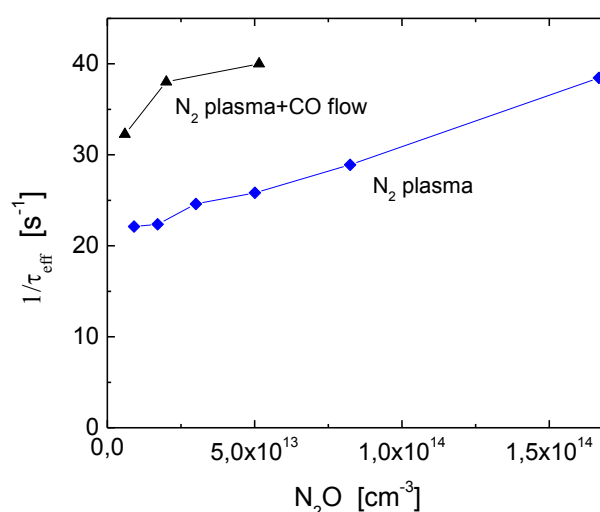


Figure 5. 21 Dependence of the $1/\tau_{\text{eff}}$ on the concentration of N₂O in silica reactor pretreated by N₂ plasma with and without the exposure to CO. Standard DC discharge conditions.

Study of surface vibrational relaxation of N₂

Argon plasma treatment

After argon plasma pretreatment a clean SiO₂ surface is expected according to the results of Chapter 3 and Chapter 4. However, due to argon plasma exposure some new surface active sites may be formed [110] which can explain the increased values obtained using CO titration. Carbon monoxide may occupy these active sites and enhance surface vibrational relaxation of N₂. Results obtained with CO₂ and N₂O are identical within experimental uncertainty what let us assume that in this case chemisorption effects are negligible. And we suppose that the true value of γ_1 on argon plasma treated SiO₂ is obtained with CO₂ and N₂O after extrapolation to zero tracer admixture.

Oxygen plasma treatment

Pretreatment by O₂ plasma results in the SiO₂ surface saturated with adsorbed O atoms as we have shown in Chapter 4. Apparently, there is no significant adsorption of titrating molecules on this surface because identical result of measurements with 3 different tracers. The true value of γ_1 is obtained with all tracers.

Among three molecules used in this study, N₂O is known to be the most inert from the viewpoint of adsorption on catalytic surfaces [164]. In catalysis studies it is often employed as a non-reactive IR tracer [118]. Therefore, we expect that the values of γ_1 obtained using N₂O are less perturbed by chemisorption effects. Looking at the γ_1 values measured with N₂O we conclude that depending on plasma pretreatment the relaxation probability of N₂(ν) on silica surface may be changed by a factor of 2. This is a new effect, and its observation was possible only because of the single-pulse operation mode of the IR titration technique.

5.5.2 Vibrational relaxation on TiO₂.

Titanium dioxide is a promising material for air pollution control using plasma-catalyst technology [11]. To the best of our knowledge, there is no literature data available for the relaxation probability of N₂(ν) on TiO₂. In this study we used a silica discharge tube with a TiO₂ sol-gel coating on its inner surface.

Measurements with three different tracers and three different plasma pretreatments were performed with TiO₂ coating in the same way as it was described in the previous section for SiO₂. In Figure 5. 22 the dependencies of $1/\tau_{\text{eff}}$ on the concentration of IR tracers left after the discharge pulse for different pretreatments are presented. The resulting values of γ_1 are summarized in Table 5. 3. One can see that with CO₂ somewhat higher values of γ_1 are obtained. This may be explained by the modification of the TiO₂ surface by the chemisorption of CO₂ as it was discussed above for silica surface.

As in the case of SiO₂, the lowest (and hence the most precise) values of γ_1 are measured with N₂O indicating the inert nature of this tracer. Results obtained with N₂O are almost independent on plasma pretreatment.

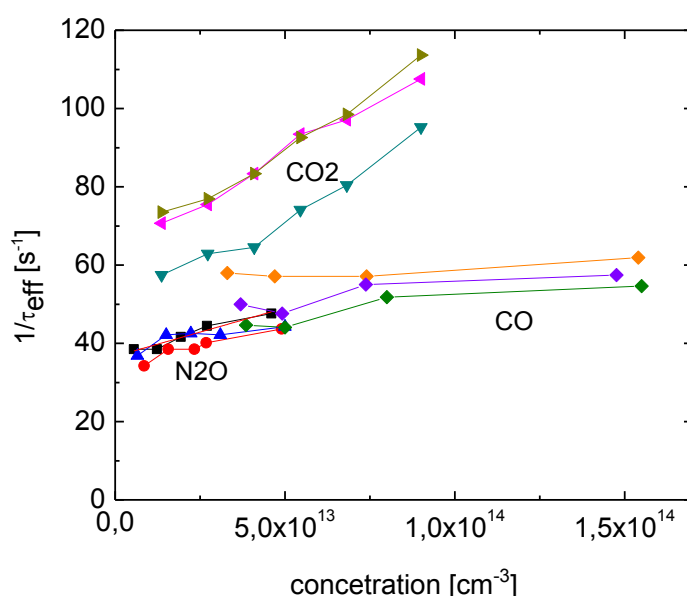


Figure 5. 22 Dependence of the $1/\tau_{\text{eff}}$ on the concentration of IR tracers with TiO_2 coating pretreated by N_2 , O_2 and argon plasmas. Standard dc discharge conditions.

Pretreatment	N_2O	CO_2	CO
N_2	$1,9 \cdot 10^{-3}$	$3,6 \cdot 10^{-3}$	$3,1 \cdot 10^{-3}$
Ar	$2 \cdot 10^{-3}$	$2,6 \cdot 10^{-3}$	$2,2 \cdot 10^{-3}$
O_2	$1,8 \cdot 10^{-3}$	$3,6 \cdot 10^{-3}$	$2,5 \cdot 10^{-3}$

Table 5. 3 The values of γ_1 obtained using three titrating molecules after different plasma pretreatment of TiO_2 coating.

The studied sol-gel coating was smooth and it had a specific surface approximately equal to the geometric surface of the reactor. In real applications high specific surface catalytic materials are usually used [11]. We have performed relaxation measurements with a TiO_2 coating impregnated with Degussa P25 TiO_2 particles identical to one used in § 4.4.2.1. Compared to the smooth coating, the impregnated sol-gel film was rough having the total surface of approximately 4 m^2 . Figure 5. 23 shows the time evolution of the absorption signal measured in 0.3% $\text{CO}_2 - \text{N}_2$ mixture in standard DC discharge conditions. Fitting of the experimental curve with (5.12) gives $\tau_{\text{eff}} = 2.4 \text{ ms}$, which is comparable with the characteristic diffusion time of $\text{N}_2(\nu)$ in our conditions. As it was discussed before, τ_{eff} is weakly dependent on the value of γ_1 when it approaches the characteristic diffusion time (when surface relaxation is limited by the diffusion). Therefore, only the lower boundary of the value of γ_1 can be determined in this case. From the results shown in Figure 5. 23 we have found that $\gamma_1 \geq 0,04$ on impregnated TiO_2 . Faster relaxation on the impregnated film may be caused by the increase of the surface area due to the presence of TiO_2 particles. In addition to this geometric effect, TiO_2 particles may possess an enhanced efficiency for quenching of $\text{N}_2(\nu)$ due to the presence of different active sites compared to the sol-gel film.

This example demonstrates that IR titration allows measurements of $\text{N}_2(\nu)$ vibrational relaxation times in the conditions ranging from diffusion-limited to surface step limited heterogeneous vibrational relaxation.

Study of surface vibrational relaxation of N₂

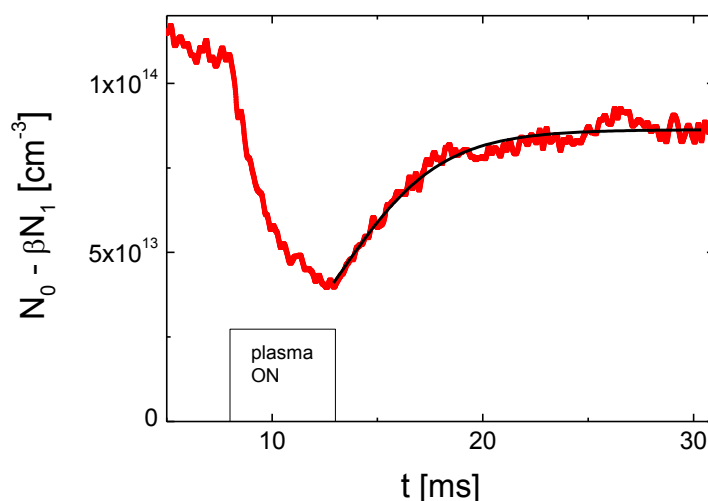


Figure 5. 23 Time evolution of the absorption signals of CO₂ measured in a pulsed DC discharge at p=1.33 mbar, I=50 mA, τ =5ms in a 0.3%CO₂ – N₂ mixture. The reactor with impregnated TiO₂ coating was used. Fitting of experimental data with (5.12) is shown.

5.5.3 Vibrational relaxation on other catalytic surfaces

Above we have seen that N₂O is the most inert tracer that gives the most reliable values of γ_1 . In contrast to CO₂, N₂O may be used with Al₂O₃ which is known for its CO₂ trapping properties [165]. Thus, experiments with different materials of the reactor inner surface pretreated by low pressure plasma were performed using N₂O as a titrating molecule. As before, for each material a series of measurements with different concentrations of N₂O was done in order to obtain the extrapolation of $1/\tau_{\text{eff}}$ at [N₂O]→0. The value of γ_1 was then determined using the calibration curve from Figure 5. 17. The results of all the measurements done with N₂O are summarized in Table 5. 4 and compared with available literature data. One can see that our results are in good general agreement with already published data.

Surface	γ_1 this work	literature values	Ref.
Silica (O ₂ plasma pretr.)	$5,7 \cdot 10^{-4}$	$(1,8-7) \cdot 10^{-4}$	[127]
Silica (N ₂ plasma pretr.)	$10,5 \cdot 10^{-4}$		
Silica (Ar plasma pretr.)	$8,2 \cdot 10^{-4}$		
Pyrex (O ₂ plasma pretr.)	$6 \cdot 10^{-4}$	$(2,3-10) \cdot 10^{-4}$	[127]
Pyrex (N ₂ plasma pretr.)	$11 \cdot 10^{-4}$		[129]
Al ₂ O ₃ (O ₂ plasma pretr.)	$15 \cdot 10^{-4}$	$(11-14) \cdot 10^{-4}$	[127]
Anodized Al (O ₂ plasma pretr.)	$29 \cdot 10^{-4}$	no	
TiO ₂ sol gel film (N ₂ , O ₂ , Ar plasma pretr.)	$19 \cdot 10^{-4}$	no	

Table 5. 4 Summary of all the γ_1 measurements done using N₂O titration. Comparison with available literature data is shown.

5.5.4 Vibrational relaxation on silica surface in air plasma.

We have seen in previous sections that molecular admixtures may change the probability of $N_2(v)$ vibrational quenching on the surface. In air discharge, substantial amounts of NO and NO_2 are formed [16]. Usually in kinetic models of low pressure air plasmas, the value of γ_{N_2} is taken the same as in pure N_2 . To the best of our knowledge, no measurements in N_2 - O_2 mixtures have been done so far.

A series of measurements in $N_2/O_2=4/1$ with CO_2 and N_2O admixtures was performed. The discharge conditions were the same as before ($p=1.33$ mbar, $I=50$ mA, $\tau=5$ ms), silica and Pyrex tubes were used. The surface was exposed to a pulsed dc discharge in air for 10 minutes. The value of $\gamma_1=(8\pm3)\cdot 10^{-4}$ was found for both materials. The relatively high uncertainty of the measurements is due to the unknown contribution of the VT quenching by atomic oxygen. The upper limit of γ_1 was calculated by completely neglecting the contribution of VT quenching by O. The lower limit was estimated by assuming a constant concentration $[O]=10^{15} \text{ cm}^{-3}$ [149] in the post discharge with the VT relaxation constant taken from [166] $k_{VT} = 4.5 \cdot 10^{-15} \text{ cm}^3 \text{ s}^{-1}$.

We conclude here that the presence of O_2 and NO_x doesn't significantly modify the quenching probability of $N_2(v)$ on silica and Pyrex and the use of values of γ_1 measured in pure N_2 discharges is justified.

5.6 Infrared titration as a plasma diagnostics tool: determination of the vibrational temperature of N_2

We have shown that the depletion of the measured value of $(N_0 - \beta N_1)$ in the afterglow is caused by the vibrational excitation of the titrating molecules which is in turn determined by the vibrational excitation of N_2 . In this section we will show how the time evolution of the vibrational temperature of N_2 , $T_v = E_1 / \left(\ln \left(\frac{N_2(v=0)}{N_2(v=1)} \right) \right)$, can be directly obtained from laser absorption measurements. First, we will consider the $N_2 - CO_2$ system because it is better characterized and then we will apply the same treatment to N_2 - N_2O and N_2 -CO.

5.6.1 Formulation of the method and its application to the $N_2 - CO_2$ system

As it has been shown in § 5.4.5, in standard pulsed DC discharge conditions, only the $CO_2(00^0v_3)$ mode has a significant population. This means that the amplitude of the depletion of $(N_0 - \beta N_1)$ can be related to the vibrational temperature of this mode. Assuming Boltzmann distribution of $CO_2(00^0v_3)$, the normalized value of $(N_0 - \beta N_1)$ can be expressed as follows:

$$(N_0 - \beta N_1)_{\text{norm}} = ((1 - \theta) - \beta(1 - \theta)\theta) \quad (5.13)$$

Study of surface vibrational relaxation of N₂

where $\theta = e^{-\frac{E_1}{T_v}}$. Only the relative variation of the value of $(N_0 - \beta N_1)$ is significant, so it is normalized to the stationary post discharge level. The vibrational temperature of CO₂(00⁰v₃), which is related to the vibrational temperature of N₂ by (5. 10), can be calculated by solving (5. 13) at any time point. The measurements are free from the distortion by the variation of the gas temperature starting from the ~ 3 ms in the post discharge. In Figure 5. 24 evolution of the vibrational temperature of N₂ calculated using (5. 10) and (5. 13) in a mixture containing 0.2% CO₂ in N₂ at 1.33 mbar in Pyrex discharge tube is shown. The discharge current was 50 mA, pulse duration was 1 ms and 5 ms. A good agreement between the model and the experiment proves the feasibility of the proposed method for T_v determination. It is important to note, that the complete time evolution of T_v in the afterglow is obtained in a *single* discharge pulse.

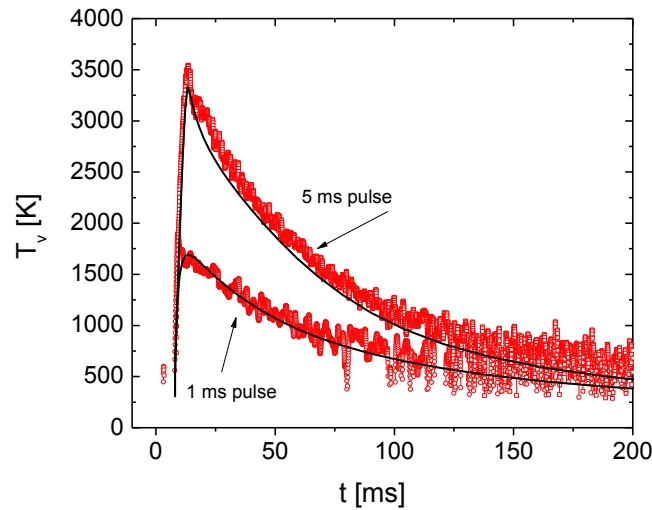


Figure 5. 24 Evolution of the vibrational temperature of N₂ in the afterglow of a discharge pulse with I=50 mA in a 0.2% CO₂ – N₂ gas mixture at p=1.33 mbar. Pyrex discharge tube. Pulse durations were 1 ms (—○—) and 5 ms (—□—). Simulation results are shown by solid lines.

5.6.2 On the vibrational temperature measurements in N₂ - N₂O and N₂ - CO

As it has been shown for CO₂, the deduction of the vibrational temperature of N₂ from the absorption measurements in N₂-CO₂ relies on the fact that only the v₃ mode has a significant population. If v₁ and v₂ were strongly involved, the depletion of $(N_0 - \beta N_1)$ signals would be determined by the population of the whole vibrational manifold of CO₂, and the direct determination of T_v would be impossible. The low population of v₁ and v₂ under the conditions of this study is due to the fast surface quenching and slow intra molecular vibrational exchange. Another important condition is the applicability of the relation (5. 10). It was derived based on the assumption that V-V' exchange between N₂(v) and titrating molecules is much faster than other relaxation processes. In principle, a complete kinetic

model is required to check the possibility of direct T_v determination under the conditions of this study for N_2 - N_2O and N_2 -CO mixtures.

At present, we tentatively apply the same treatment as has been developed for N_2 - CO_2 to relaxation measurements in N_2 -CO and N_2 - N_2O . For tests we use the experimental data shown in Figure 5. 18 and Figure 5. 19. Simultaneous measurements allow direct comparison of T_v evolution determined using two different tracers in exactly the same conditions.

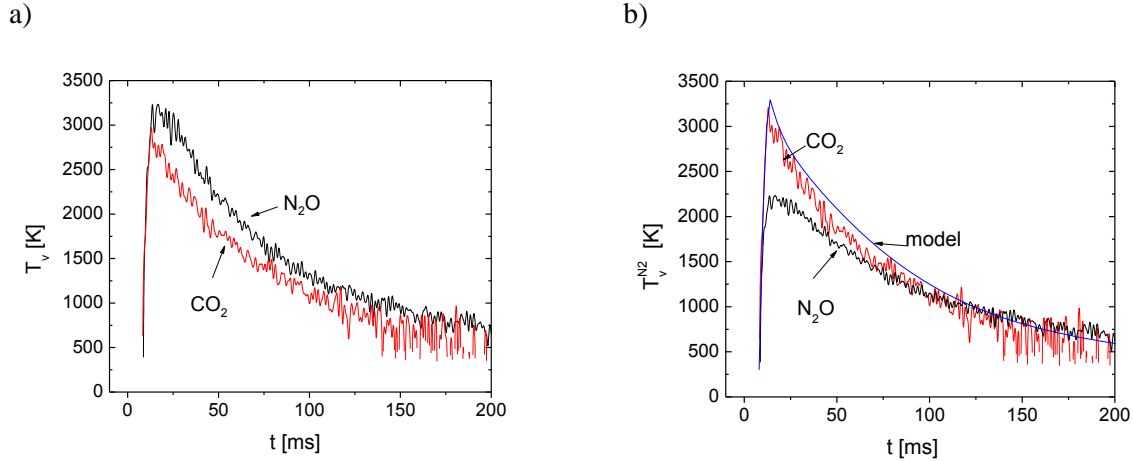


Figure 5. 25 a) Evolution of the vibrational temperature of $CO_2(00v3)$ and $N_2O(00v3)$ obtained by applying (5. 13) in the conditions shown in Figure 5. 18. b) Vibrational temperature of N_2 calculated using (5. 10) for T_v from the left panel. Result of the model calculation of the vibrational temperature of N_2 is also shown.

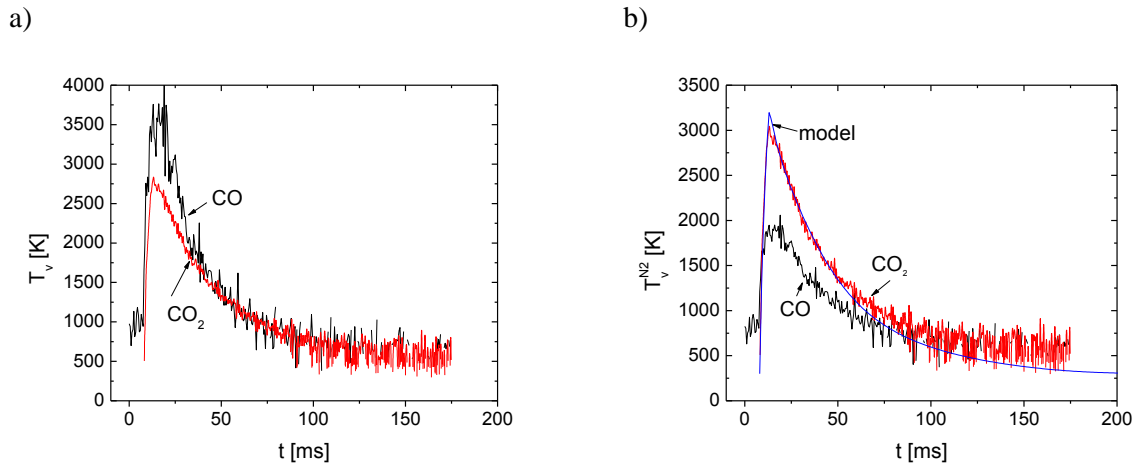


Figure 5. 26 a) Evolution of the vibrational temperature of $CO_2(00v3)$ and CO obtained by applying (5. 13) in the conditions shown in Figure 5. 19. b) Vibrational temperature of N_2 calculated using (5. 10) for T_v from the left panel. Result of the model calculation of the vibrational temperature of N_2 is also shown.

First we have calculated the vibrational temperature of IR tracers using (5. 13) based on the experimental data. Figure 5. 25 a) and Figure 5. 26 a) show time evolution of the vibrational temperatures of couples of tracers [$CO_2(00v3)$ and $N_2O(00v3)$] and [$CO_2(00v3)$ and CO] respectively. Then (5. 10) was used (with corresponding vibrational quanta of N_2O and CO) to calculate the evolution of T_v of nitrogen in each case. The results of calculation are shown in Figure 5. 25 b) and Figure 5. 26 b). One can see that results obtained with CO and N_2O differ from those obtained with CO_2 (which are in good agreement with the model).

Study of surface vibrational relaxation of N₂

The possible reason of this discrepancy is an unjustified application of (5. 10) which yields too low vibrational temperatures of N₂. As is shown in

Table 5. 1, CO₂(00⁰v3) is almost in perfect resonance with N₂(v) (the difference is of only 18 cm⁻¹). This leads on the one hand to faster vibrational exchange between two species, and on the other hand the correction introduced by (5. 10) is very small. The departure of CO and N₂O(00⁰v3) from the resonance is much stronger (187 cm⁻¹ and 106 cm⁻¹ respectively) what may lead to underestimation of the vibrational temperature of N₂. More detailed analysis of the vibrational kinetics is required in order to get a correct interpretation of the relaxation measurements in N₂-CO and N₂-N₂O mixtures.

5.7 Conclusions

In this chapter we have developed a method for *in-situ* investigation of relaxation of vibrationally excited nitrogen molecules on different surfaces. This method uses a combination of quantum cascade laser absorption measurements in mixtures N₂-CO₂(N₂O or CO) excited by a pulsed dc discharge and modeling of vibrational kinetics.

Laser diagnostics

We have used a novel type of tunable solid state lasers – quantum cascade lasers which are specially designed for fast kinetics measurements. The main challenges in using quantum cascade lasers in intra-pulse mode are associated with their extremely fast chirp rate (~ 0.02 cm⁻¹/ns in the QCL used for CO₂ detection) so the laser is swept across the absorption line in few nanoseconds. Apart from technical difficulties, associated with the use of very fast detectors and acquisition systems (~ 1 GHz bandwidth), fast tuning of QCLs induce non-linear (rapid passage) effect in absorption of laser light. Interpretation of QCL absorption spectra distorted by the rapid passage effect in equilibrium conditions is well documented [75]. In this study QCLs were used for the first time for measurements in vibrationally excited gases.

In order to account for stimulated emission from upper vibrational levels of molecular transitions probed with the laser we used expression (5. 3) which is not justified *a-priori* in case of absorption lines distorted by rapid passage effect. Excellent agreement between measured and modeled depletion signals obtained in § 5.4.6 prove the validity of our treatment of laser absorption measurements. Validity of (5. 3) is a prerequisite condition for measurements of vibrational temperature of N₂ that were performed in § 5.6.1.

Another important point is the high time resolution achievable with the QCL lasers. With maximum time resolution of 5 μ s we were able to follow relaxation kinetics even when the characteristic time of vibrational relaxation was of the order of 1 ms (as in Figure 5. 23).

Kinetic modeling

A 0-dimensional model of vibrational kinetics in pure N₂ and N₂ – CO₂ mixtures has been developed in order to give interpretation of experimental relaxation measurements and determine vibrational relaxation probability of N₂(v) on the surface. With a small number of

input parameters (discharge tube radius, gas pressure, discharge current and pulse duration) the model predicts the time evolution of coupled VDFs of N_2 and CO_2 . The model is based on a reduced set of processes that are relevant to vibrational kinetics only and it contains 52 coupled equations for 0 – 45 levels of N_2 and 6 levels of CO_2 . The validity of our model for pure N_2 was confirmed by comparison with more detailed self-consistent simulations performed by V. Guerra for our conditions. The predictions of our model were found to be in excellent agreement with the experimental measurements of population of $N_2(v=18)$ measured in [162].

Unknown parameter in simulations is the probability of vibrational relaxation of $N_2(v)$ on the surface (γ_{N_2}) and its dependence on the vibrational quantum number. We have chosen linear scaling law $\gamma_{N_2} = v \cdot \gamma_1$ as more physical and γ_1 was used as the only tuning parameter in the model. The value of γ_1 for various surfaces was obtained from comparison between characteristic times of vibrational relaxation measured experimentally and calculated by the model for a set of different γ_1 .

Surface vibrational relaxations of $N_2(v)$

All the experiments have been performed in a *single* discharge pulse without data accumulation. This excluded uncontrollable drifts of the state of the surface due to long plasma exposure and allowed measurements with specially prepared surfaces. The validity of IR titration technique has been confirmed by measurements of γ_1 for well studied surfaces - Pyrex and silica. A good agreement with literature values has been obtained. The values of γ_1 have been also measured for different materials – TiO_2 , Al_2O_3 , anodized aluminium.

We have found that the value of γ_1 depends on a number of factors:

- Chemical nature of the surface
- Surface morphology
- Plasma pretreatment of the surface
- Presence of physisorbed and chemisorbed molecules

The influence of plasma exposure on silica surface has been thoroughly investigated. It has been shown that depending on the pretreatment by low pressure plasma (N_2 , Ar or O_2) the value of γ_1 may be changed by a factor of 2. Typically the highest relaxation probability has been obtained after N_2 pretreatment, i.e. when silicon oxynitride layer is formed on the surface. The lowest value of γ_1 has been measured on silica surface pretreated by O_2 plasma. As we know, in this case grafted O atoms are present on SiO_2 . This result demonstrates that O and N atoms chemisorbed on SiO_2 are not only involved in surface reactivity but also influence mechanisms of vibrational relaxation of $N_2(v)$ on the surface.

We have observed for the first time that molecular admixtures in N_2 increase the value of γ_1 on silica surface. This effect was explained by vibrational energy transfer between adsorbed molecules and $N_2(v)$. It is interesting that both physisorbed and chemisorbed molecules can be involved in $N_2(v)$ relaxation on the surface. It has been found that N_2O is the most reliable

Study of surface vibrational relaxation of N₂

titrating molecule and it can be used for γ_1 measurements on different catalytic surfaces without significant distortion effects due to the chemisorption.

6. Chapter VI: General conclusions and outlook

6.1 General conclusions

In the beginning of this work the only “image” of recombination of O and N atoms on silica-like materials was the one developed in the mesoscopic models of Kim&Boudart [5] and Jumper [41]. The investigation of the mechanism of $N_2(v)$ vibrational relaxation on the surface was limited to few studies in the flowing post-discharge[127] [128]. Our results provide new information on the modification of the state of the surface under low pressure plasma exposure and give an insight into the mechanisms of chemical reactions and relaxation processes on the surface. We can outline three principle findings of this work which are generic for surface interactions in reactive molecular plasmas.

The role of plasma exposure

Under low pressure plasma exposure atoms of the material are replaced by atoms and/or ions from the gas phase. Therefore, the surface is not static, it is constantly restructured and modified. In such conditions the notion of chemisorption has to be redefined; surface atoms belonging to the crystalline network of the material are indistinguishable from atoms grafted to the surface under plasma exposure.

The distribution of reactivity of adsorbed atoms

Due to the inhomogeneous nature of real surfaces adsorbed atoms exhibit a distribution of reactivity which is most probably related to the spectrum of their binding energies. Weakly bonded atoms are more reactive and play an important role for surface catalyzed reactions.

The role of adsorbed atoms and molecules in the relaxation of vibrational energy on the surface

In addition to the vibrational relaxation mechanisms that are typical for clean surfaces (as for example interaction with phonons and electrons of the solid) in real plasma conditions new pathways of vibrational quenching on the surface become possible. We have found that the presence of adsorbed atoms and molecules may significantly modify the probability of vibrational relaxation on the surface.

Experimental technique developed in this study allowed us to isolate and investigate elementary surface reactions (for example $NO + O_{ads}^* \rightarrow NO_2$ or $O + N_{ads}^* \rightarrow NO$). In the future this approach may be used for investigation of reactions catalyzed by different adsorbed atoms on various surfaces.

General conclusions and outlook

6.2 Summary of the main results

Here we give a list of the most important results of this work:

Adsorption and reactivity of N

- Under N_2 plasma exposure silicon oxynitride layer is formed on the surface of silica discharge tube. Nitridation is driven by ion bombardment and it takes place only under direct N_2 plasma exposure. When silica surface is exposed to a flowing post-discharge nitridation is negligible.
- Formation of SiO_xN_y layer is very sensitive to the presence of O_2 admixtures in N_2 plasma. Addition of 0.1% of O_2 into N_2 reduces the number of grafted N atoms by a factor of 10.
- Under N_2 plasma exposure N_{ads} are continuously exchanged with N atom and ions from the gas phase. We have found two groups of N_{ads} : i) first with a characteristic turnover time ~ 10 s in our standard rf discharge conditions ii) second having the characteristic replacement time ~ 300 s. The first group was assigned to N on the outmost surface layer and the second one to atoms distributed in the SiO_xN_y layer.
- Nitrogen atoms on the surface of SiO_xN_y exhibit a distribution of reactivity. We have found a small fraction of N_{ads} (having a coverage $[N_{ads}^*]=3.5 \cdot 10^{13} \text{ cm}^{-2}$) that can recombine with atomic oxygen producing NO molecules.
- N_{ads} participate in recombination of N on the surface, but recombination with these atoms cannot explain the rate of N losses on the surface. We suppose therefore that recombination of N atoms takes place on weakly bonding active sites.

Adsorption and reactivity of O

- Under direct O_2 plasma exposure, oxygen atoms that compose the outmost layer of silica and Pyrex are continuously exchanged with oxygen atoms and ions from the gas phase. Typically, in our standard pretreatment conditions $(5-6) \cdot 10^{15}$ O atoms per cm^2 are replaced during 500 s of plasma exposure.
- We have found that under O_2 plasma exposure reactive O atoms are adsorbed on Pyrex or TiO_2 . The reactivity of O_{ads} towards stable molecules depends on the nature of the surface and the target molecule.
- Oxygen atoms adsorbed on Pyrex surface are reactive towards NO (we denote these atoms O_{ads}^*). Titration of O_{ads}^* using the reaction $NO + O_{ads}^* \rightarrow NO_2$ allowed determination of the lower limit of the coverage $[O_{ads}^*] = 2.5 \cdot 10^{14} \text{ cm}^{-2}$.
- A distribution of reactivity of O_{ads}^* towards NO have been observed. We suggest that this distribution is related to a spectrum of binding energies of adsorbed atoms. The maximum rate of NO oxidation on the surface corresponds to the effective surface reaction probability $\gamma_{NO \rightarrow NO_2} = 2 \cdot 10^{-7}$.
- Oxygen atoms adsorbed on TiO_2 are reactive towards C_2H_2 . The maximum number of C_2H_2 lost on the TiO_2 surface pretreated by O_2 plasma was $\sim 5 \cdot 10^{12}$ molecules per cm^2 . It was found that C_2H_2 is oxidized only partially by O_{ads} leaving some reaction

intermediates on the surface. Further oxidation of these adsorbed species into CO_2 can be reached by heating or UV activation of the catalyst. Observed adsorbed oxygen atoms may be responsible for reported in the literature improved pollutant destruction by plasma- TiO_2 combination.

- We have found that ozone may be formed from surface recombination $(\text{O}+\text{O}_2)_w$ on silica surface. The presence of adsorbed water and surface OH groups favours ozone production on the surface. At $p=6.7$ mbar ozone production accounts for 30% of losses of O atoms on silica surface. This result demonstrates the importance of weakly bonded O^{weak} for surface catalyzed reactions in oxygen plasmas.

Vibrational relaxation of $\text{N}_2(v)$ on surfaces

- A new infrared titration technique has been developed for determination of $\text{N}_2(v)$ relaxation probability on the surface (γ_{N_2}) at mbar pressures.
- A 0-dimensional modeling of vibrational kinetics in pure N_2 and $\text{N}_2 - \text{CO}_2$ mixtures has been performed in order to give interpretation of experimental relaxation measurements and determine vibrational quenching probability of $\text{N}_2(v)$ on the surface. Results of our simplified kinetic model are in a good agreement with more sophisticated complete self-consistent simulations. In the model we have assumed the linear scaling of the quenching probability with the vibrational quantum number $\gamma_{\text{N}_2} = v \cdot \gamma_1$. The value of γ_1 was determined from the best agreement between the experiment and the simulations.
- The validity of IR titration technique has been confirmed by measurements of γ_1 for well studied surfaces - Pyrex and silica. Our results ($\gamma_1=(5-10) \cdot 10^{-4}$) are in good agreement with literature values. Using the new technique the values of γ_1 have been determined for different materials – TiO_2 , Al_2O_3 , anodized aluminium.
- The influence of plasma exposure on silica surface has been thoroughly investigated. It has been shown that depending on the pretreatment by low pressure plasma (N_2 , Ar or O_2) the value of γ_1 may be changed by a factor of 2. Typically the lowest value of γ_1 is obtained after O_2 plasma treatment and the highest after N_2 plasma.
- We have observed for the first time that molecular admixtures in N_2 increase the value of γ_1 on silica surface. This effect was explained by vibrational energy transfer between adsorbed molecules and $\text{N}_2(v)$.

6.3 Implication for modelling of surface recombination

Mesosopic modelling

We have shown in this work that losses of N atoms on the surface cannot be described by recombination on one type of chemisorption sites and there exists a distribution of active sites with different binding energies. This means that separation of surface atoms into two groups – physisorbed (mobile) and chemisorbed (stable) which is usually used for mesoscopic

General conclusions and outlook

description of atomic recombination is very schematic. The existence of a distribution of adsorption energies literally bridges the gap between physisorption and chemisorption.

It is clear that distribution of adsorption energies (including weakly bonded atoms) has to be considered in the models for correct description of atomic recombination on surfaces. Recently, only by assuming a broad distribution of binding energies of atoms on anodized aluminium surface Donnelly *et al.* [54] have been able to reproduce the kinetics of LH recombination of O and Cl atoms in spinning wall experiments. At present similar effort has never been done for modelling of atomic recombination on silica-like surfaces.

Microscopic modelling

Recent studies of O and N recombination on model SiO₂ surfaces [35][38] take into account only strongly bonded atoms. Our results demonstrate that weakly bonded atoms are active for recombination and, therefore, they have to be included in *ab-initio* simulations of surface catalyzed recombination of atoms.

6.4 Future work

Surface reactivity

Based on the new results on surface reactivity in N₂ and O₂ plasmas obtained in this work we suggest the following direction for further research:

- We have found that O and N atoms composing the material of the surface (SiO₂ or SiO_xN_y) are continuously replaced under plasma exposure. The role of ions in the exchange process is still not clear. Experiments with independent atomic and ion beams should be performed in order to separate the contribution of charged and neutral species.
- In this thesis we have revealed that weakly bonded N and O atoms on silica-like surfaces play a very important role for surface catalyzed reactions. The nature and properties of these unstable species have to be further investigated. This will require application of different surface diagnostics techniques, capable of detecting species having short lifetime on the surface.
- We have separately investigated interaction between plasmas in pure O₂ and N₂ and different oxide surfaces. The next step would be the understanding of surface processes that take place under air plasma exposure. We have already obtained some valuable results as, for example, suppression of SiO_xN_y layer formation when O₂ is added into N₂ plasma.

Application of isotopic techniques developed in this work may be very useful for understanding of complex chemical kinetics of surface catalyzed reactions in N₂/O₂ plasmas. For example, utilization of N₂ isotopes with time resolved ¹⁴NO and ¹⁵NO detection allows distinction between gas phase and surface mechanisms of NO production. In Figure 6. 1 production of NO in a pulsed dc discharge in ³⁰N₂/O₂ = 4/1 mixture in silica reactor pretreated

by $^{28}\text{N}_2$ plasma is shown. One can see that ^{15}NO is formed only during the discharge pulse while ^{14}NO that comes from the surface is produced predominantly in the afterglow. This experiment demonstrates different time scales of surface and volume mechanisms of NO production in N_2/O_2 pulsed discharges.

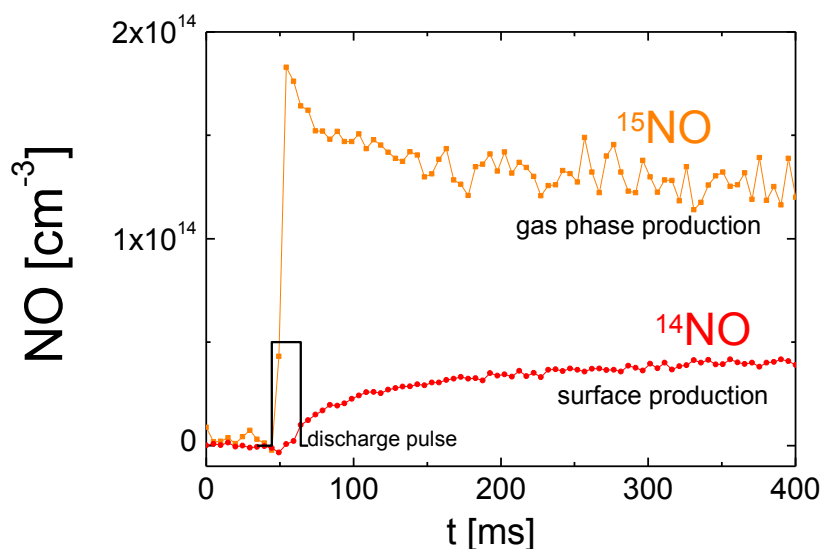


Figure 6. 1 Production of NO isotopologues in a pulsed dc discharge (10 ms, 100 mA pulse) in $^{30}\text{N}_2/\text{O}_2 = 4/1$ mixture at 1.3 mbar. Silica discharge tube was pretreated by a rf discharge in $^{28}\text{N}_2$.

Surface vibrational relaxation

The work on the investigation of surface vibrational relaxation using IR titration may be continued in the following way:

- Investigation of the **temperature dependence** of γ_{N_2} which may give a deeper insight in the mechanism of $\text{N}_2(v)$ relaxation on surfaces. So far there exists only one example in the literature where the variation of γ_{N_2} with the temperature have been measured [128]. In addition it would be interesting to investigate the effect of molecular additions at different temperatures. We have supposed that the enhancement of the value of γ_{N_2} upon the addition of CO_2 is caused by the vibrational transfer between $\text{N}_2(v)$ and physisorbed CO_2 molecules. The coverage of physisorbed CO_2 should be very sensitive to the variations of the temperature of the wall.
- Study of the **pressure dependence** of γ_{N_2} . Similarly to the role of the wall temperature, data on the γ_{N_2} dependence on the gas pressure are very scarce.

General conclusions and outlook

6.5 New diagnostic techniques

In this work we have developed and validated several new diagnostics techniques for investigation of surface and gas phase processes in N_2/O_2 containing plasmas. They are all based on the combination of pulsed discharge excitation with the measurements of gas phase species concentrations.

Mass-spectrometric measurements of N_2 dissociation

Using the QMS measurements of the isotopic exchange upon dissociation in $^{30}N_2/^{28}N_2$ mixtures we have determined the dissociation fraction of N_2 in a pulsed dc or rf discharges. This technique has been applied at one particular pressure and discharge current (or injected power). A very interesting result obtained using this new technique is that in studied conditions the dissociation and surface recombination of different nitrogen isotopologues is identical.

In the future this technique may be used for parametric investigation of N_2 dissociation at different pressures and discharge currents. According to [97] at pressures of the order of few mbars, processes with vibrationally excited N_2 (V-D processes) contribute significantly to N_2 dissociation. Due to the difference in the vibrational quanta of different isotopologues, V-D processes are isotopologue-dependent. Therefore, the rate of isotopic exchange is expected to be different in different $^{28}N_2/^{30}N_2$ mixtures when V-D processes are important.

In principle, isotopic exchange technique may be applied to investigation of dissociation in different diatomic gases. An important parameter that has to be verified for each gas is the rate of isotopic exchange in collisions between atoms and molecules in the gas phase. For example in the case of O_2 , a very efficient exchange in $O - O_2$ collisions make impossible dissociation measurements using isotopic exchange.

IR titration of vibrationally excited molecules

The IR titration technique developed in this work allows simultaneous measurements in a **single** discharge pulse of the value of γ_{N_2} and the time evolution of the vibrational temperature of N_2 . It may be used for diagnostics of pulsed discharges in N_2 with different molecular admixtures.

7. References

- [1] I Langmuir, *Proc. Natl Acad.Sci. USA*, vol. 14, pp. 627-637, 1928.
- [2] R W Wood, "An Extension of the Balmer Series of Hydrogen and Spectroscopic Phenomena of Very Long Vacuum Tubes," *Proc. R. Soc.Lond. A*, vol. 97, pp. 455-470, 1920.
- [3] W V Smit, "The Surface Recombination of H Atoms and OH Radicals," *J. Chem. Phys.*, vol. 11, p. 110, 1943.
- [4] K E Shuler and K J Laidler, "The Kinetics of Heterogeneous Atom and Radical Reactions. I. The Recombination of Hydrogen Atoms on Surfaces," *J. Chem. Phys.*, vol. 17, p. 1212, 1949.
- [5] Y C Kim and M Boudart, "Recombination of O, N and H Atoms on Silica: Kinetics and Mechanism," *Langmuir*, vol. 7, pp. 2999 - 3005, 1991.
- [6] J W Coburn and H F Winters, "Ion- and electron-assisted gas-surface chemistry—An important effect in plasma etching ," *J. Appl. Phys.*, vol. 50, p. 3189, 1979.
- [7] A Keudell and W Jacob, "Elementary processes in plasma surface interaction: H-atom and ion-induced chemisorption of methyl on hydrocarbon film surfaces," *Progress in Surface Science*, vol. 76, pp. 21-54, 2004.
- [8] U Roland, F Holzer, and F-D Kopinke, "Improved oxidation of air pollutants in a non-thermal plasma," *Catalysis Today*, vol. 73, pp. 315 - 323, 2002.
- [9] J V Durme, J Dewulf, C Leys, and H V Langenhove, "Combining non-thermal plasma with heterogeneous catalysis in waste gas treatment: a review," *Applied Catalysis B: Environmental*, vol. 78, pp. 324-333, 2008.
- [10] H-H Kim, "Nonthermal Plasma Processing for Air-Pollution Control: A historical Review, Current Issues, and Future Prospects," *Plasma Process. Polym.*, vol. 1, pp. 91-110, 2004.
- [11] O Guaitella, F Thevenet, E Puzenat, C Guillard, and A Rousseau, "C₂H₂ oxidation by plasma/TiO₂ combination: Influence of the porosity, and photocatalytic mechanisms under plasma exposure," *Appl. Catal. B: environmental*, vol. 80, pp. 296-305, 2008.
- [12] T Oda, "Non-thermal plasma processing for environmental protection:decomposition of dilute VOCs in air," *Journal of Electrostatics*, vol. 57, pp. 293-311, 2003.
- [13] F Thevenet et al., "Comparioson of plasma-photocatalyst synergy at low and atmospheric pressure," *PEST*, vol. 1, no. 1, pp. 52 - 56, 2007.

References

- [14] L Gatilova et al., "NO formation mechanisms studied by infrared laser absorption in a single low pressure pulse," *Plasma Sources Sci. Technol.*, vol. 16, pp. S107–S114, 2007.
- [15] O Guaitella, L Gatilova, and A Rousseau, "Plasma-photocatalyst interaction: Production of oxygen atoms in a low pressure discharge," *Appl. Phys. Lett.*, vol. 86, 2005.
- [16] Y Ionikh, A Meshchanov, J Roepke, and A Rousseau, "A diode laser study and modeling of NO and NO₂ formation in a pulsed dc air discharge," *Chem. Phys.*, no. 322, pp. 411-422, 2006.
- [17] T Seino, T Matsuura, and J Murota, "Atomic-order nitridation of SiO₂ by nitrogen plasma," *Surf. Interface Anal.*, vol. 34, pp. 451 - 455, 2002.
- [18] R Reuter, D Ellerweg, A von Keudell, and J Benedikt, "Surface reactions as carbon removal mechanism in deposition of silicon dioxide films at atmospheric pressure," *Appl. Phys. Lett.*, vol. 98, 2011.
- [19] C Riccardi et al., "Surface modification of poly(ethylene terephthalate) fibers induced by radio frequency air plasma treatment," *Appl. Surf. Sci.*, vol. 211, no. 1-4, pp. 386 - 397, 2003.
- [20] M Balat-Pichelin, J Badie, R Berjoan, and P Boubert, "Recombination coefficient of atomic oxygen on ceramic materials under earth re-entry conditions by optical emission spectroscopy," *Chem. Phys.*, vol. 291, pp. 181-194, 2003.
- [21] G Cartry, X Duten, and A Rousseau, "Atomic Oxygen Surface Loss Probability on Silica in Microwave Plasmas Studied by a Pulsed Induced Fluorescence Technique," *Plasma Sources Sci. Technol.*, vol. 15, no. 3, pp. 479-488, 2006.
- [22] B Gordiets et al., "Surface kinetics of N and O atoms in N₂-O₂ discharges," *J. Phys. D: Appl. Phys.*, vol. 29, pp. 1021 - 1031, 1996.
- [23] G Bond, *Heterogeneous catalysis principles and applications 2nd ed.* Oxford: Clarendon Press, 1987.
- [24] R Barrer, *J Appl Phys*, vol. 5, p. s41, 1954.
- [25] V P Zhdanov, J Pavlicek, and Z Knor, "Preexponential factors for elementary surface processes," *Catal. Rev. Sci.-Eng.*, no. 30(4), pp. 501-517, 1988.
- [26] V Guerra, "Analytical Model of Heterogeneous Atomic Recombination on Silicalike Surfaces," *IEEE Trans on Plasma Science*, vol. 35, no. 5, 2007.
- [27] G Cartry, L Magne, and G Cernogora, "Atomic oxygen recombination on fused silica: modelling and comparison to low-temperature experiments (300 K)," *J. Phys. D: Appl.*

- Phys*, vol. 33, pp. 1303 - 1314, 2000.
- [28] P Macko, P Veis, and G Cernogora, "Study of oxygen atom recombination on a Pyrex surface at different wall temperatures by means of time resolved actinometry in a double pulse discharge technique," *Plasma Sours. Sci. Technol*, vol. 13, pp. 251 - 262, 2004.
- [29] J Hirschfelder, "Semi-empirical calculations of activation energies," *J. Chem. Phys.*, vol. 9, pp. 645 - 653, 1941.
- [30] J Dean, *Lange's Handbook of chemistry (15th edition)*.: McGraw-Hill , 1999.
- [31] M Castillo, V Hererro, I Mendez, and I Tanarro, "Spectrometric and kinetic study of a modulated glow air discharge," *Plasma Sources Sci. Technol*, vol. 13, pp. 343-350, 2004.
- [32] M Castillo, V Herrero, and I Tanarro, "Characterization and modelling of the steady state and transients of modulated hollow cathode discharges of nitric oxide," *Plasma Sources Sci. Technol.*, vol. 11, pp. 368 - 376, 2002.
- [33] D Pejacovic, J Marschall, L Duan, and M Martin, "Nitric oxide production from surface recombination of oxygen and nitrogen atoms," *J. Thermophys. Heat Transfer*, vol. 22, p. 178, 2008.
- [34] L Bedra and M Balat-Pichelin, "Comparative modeling study and experimental results of atomic oxygen recombination on silica-based surfaces at high temperature," *Aerospace Science and Technol.*, vol. 9, pp. 318 - 328, 2005.
- [35] L Bedra, M Rutigliano, M Balat-Pichelin, and M Cacciatore, "Atomic oxygen recombination on quartz at high temperature: experiments and molecular dynamic simulation," *Langmuir*, vol. 22, pp. 7208 - 7216, 2006.
- [36] W Seward and E Jumper, "Model of oxygen recombination on silicon dioxide surfaces," *J. Thermophys. Heat Transf.*, vol. 5, pp. 284-291, 1991.
- [37] V Guerra and J Loureiro, "Dynamical Monte Carlo simulation of atomic recombination," *Plasma Sources Sci. Technol.*, vol. 13, pp. 85-94, 2004.
- [38] M Rutigliano, A Pieretti, M Cacciatore, N Sanna, and V Barone, "N atoms recombination on a silica surface: A global theoretical approach," *Surface Science*, vol. 600, pp. 4239 - 4246, 2006.
- [39] M Rutigliano et al., "Oxygen Adsorption on beta-Cristobalite Polymorph: Ab Initio Modeling and Semiclassical Time-Dependent Dynamics," *J. Phys. Chem. A*, vol. 113, pp. 15366 - 15375, 2009.

References

- [40] C Arasa, P Gamallo, and R Sayos, "Adsorption of Atomic Oxygen and Nitrogen at beta-Cristobalite (100): A Density Functional Theory Study," *J. Phys. Chem B*, vol. 109, pp. 14954 - 14964, 2005.
- [41] E Jumper, "Recombination of oxygen and nitrogen on silica-based thermal protection surfaces: mechanism and implications," in *Molecular physics and hypersonic flows.*: Kluwer, 1996, pp. 181-191.
- [42] T Kurotaki, "Catalytic Model on SiO₂-Based Surface and Application to Real Trajectory," *Journal of Spacecraft and Rockets*, vol. 38, no. 5.
- [43] R Zijlmans, "Molecule conversion in recombining plasmas," Technische Universiteit Eindhoven, Eindhoven, PhD 2008.
- [44] M Lieberman and A Lichtenberg, *Principles of plasma discharges and materials processing.*: Wiley, 1994.
- [45] R Dovesi, C Pisani, C Roetti, and B Silvi, "The electronic structure of alpha-quartz: A periodic Hartree-Fock calculation," *J. Chem. Phys.*, vol. 86, 1987.
- [46] A Diamy, J Legrand, and J Al Andari, "Atomic oxygen titration in dioxygen microwave plasma," *New. J. Chem.*, vol. 21, pp. 177-185, 1997.
- [47] S Wichramanayaka, N Hosokawa, and Y Hatanaka, "Variation of the recombination coefficient of atomic oxygen on pyrex glass with applied Rf power," *Jap. J. Appl. Phys.*, vol. 30, no. 11, pp. 2897 - 2900, 1991.
- [48] J Greaves and J Linnett, "Recombination of atoms at surfaces, Part 6 - recombination of oxygen atoms on silica from 20 C to 600 C ," *Trans. Faraday Soc.*, vol. 55, pp. 1355-1361, 1959.
- [49] T Belmonte, L Lefevre, T Czerwicz, H Michel, and A Ricard, "Measurements of the loss probability of N atoms versus temperature on various surfaces," *Thin Solid Films*, no. 341, pp. 27 - 30, 1999.
- [50] L Lefevre, T Belmonte, and H Michel, "Modeling of N atoms recombination on Pyrex: influence of the vibrationally excited N₂ molecules on the loss probability of N," *J. Appl. Phys.*, vol. 87, no. 10, pp. 7497 - 7507, 2000.
- [51] L Magne, H Coitout, G Cernogora, and G Gousset, "Atomic oxygen recombination at the wall in a time afterglow," *J. Phys. III*, vol. 3, pp. 1871 - 1889, 1993.
- [52] D Lopayev, E Malykhin, and S Zyryanov, "Surface recombination of oxygen atoms in O₂ plasma at increased pressure: I. The recombination probability and phenomenological model of surface processes," *J. Phys. D: Appl. Phys.*, vol. 44, 2011.

- [53] D Pagnon, J Amorim, J Nahorny, M Touzeau, and M Vialle, "On the use of actinometry to measure the dissociation in O₂ DC glow discharges: determination of the wall recombination probability," *J. Phys. D: Appl. Phys.*, vol. 28, pp. 1856 - 1868, 1995.
- [54] V Donnelly, J Guha, and L Stafford, "Critical review: Plasma-surface reactions and the spinning wall method," *J. Vac. Sci. Technol. A*, vol. 29, no. 1, 2011.
- [55] J Guha et al., "Effect of Cu contamination on recombination of O atoms on a plasma-oxidized silicon surface," *J. Appl. Phys.*, vol. 105, 2009.
- [56] A Vesel, "Heterogeneous surface recombination of neutral nitrogen atoms," *Materials and Technology*, vol. 46, pp. 7-12, 2012.
- [57] Gilles Cartry, "Etude par spectroscopie de la cinetique des decharges electriques dans les melanges N₂-O₂," Universite de Paris Sud, Orsay, These de doctorat 1999.
- [58] D Schram, "Is plasma unique? The presence of electrons and the importance of charge," *Plasma Sources Sci. Technol.*, vol. 18, 2009.
- [59] J H van Helden, R A B Zijlmans, D Schram, and R Engeln, "Resemblance in gas composition of Ar-N₂-O₂ plasmas and Ar-NO plasmas," *Plasma Sources Sci. Technol.*, vol. 18, 2009.
- [60] M Castillo, V Hererro, I Mendez, and I Tanarro, "Time resolved diagnostics and kinetic modelling of a modulated hollow cathode discharge of NO₂," *Plasma Sources Sci. Technol.*, vol. 13, pp. 39 - 47, 2004.
- [61] T de los Arcos et al., "Diagnostics and Kinetic Modeling of a Hollow Cathode N₂O Discharge," *J. Phys. Chem. A*, vol. 102, pp. 6282 - 6291, 1998.
- [62] D Pejacovic, J Marschall, L Duan, and M Martin, "Direct detection of NO produced by high-temperature surface-catalyzed atom recombination," *J. Thermophys. Heat Transf.*, vol. 24, no. 3, 2010.
- [63] B Gordiets et al., "Kinetic model of a low-pressure N₂-O₂ flowing glow discharge ," *IEEE Trans. Plasma Sci.*, vol. 23 , pp. 750-767, 1995.
- [64] Olivier Guaitella, "Nature de la synergie plasma-photocatalyseur pour la destruction d'un composé organique volatil type : l'acétylène ," Palaiseau, 2006.
- [65] Lina Gatilova, "Etude de la cinétique de formation de NO_x dans une décharge impulsionnelle à basse pression par spectroscopie d'absorption infrarouge. Influence d'une surface catalytique," Orsay, 2006.
- [66] V Guerra and J Loureiro, "Electron and heavy particle kinetics in a low-pressure

References

- nitrogen glow discharge," *Plasma Sources Sci. Technol.*, vol. 6, pp. 361–372, 1997.
- [67] G Gousset, P Panafieu, M Touzeau, and M Vialle, "Experimental study of a D.C. oxygen glow discharge by VUV absorption spectroscopy," *Plasma Chem. Plasma Proc.*, vol. 7, no. 4, 1987.
- [68] Y P Raizer, *Gas Discharge Physics*. Berlin: Springer, 1991.
- [69] V Godyak, R Piejac, and B Alexandrovich, "Electrical characteristics of parallel-plate rf discharge in argon," *IEEE Trans. On Plasma Science*, vol. 19, no. 4, 1991.
- [70] J Ropcke, G Lombardi, A Rousseau, and P Davies, "Application of mid-infrared tuneable diode laser absorption spectroscopy to plasma diagnostics: a review," *Plasma Sources Sci. Technol.*, vol. 15, 2006.
- [71] S Welzel et al., "Quantum Cascade Laser Absorption Spectroscopy as a Plasma Diagnostic Tool: An Overview," *Sensors 2010*, vol. 10, no. 7, pp. 6861-6900, 2010.
- [72] L Rothman, "The HITRAN 2008 molecular spectroscopic database," *Journal of Quantitative Spectroscopy & Radiative Transfer*, vol. 110, pp. 533–572, 2009.
- [73] R Suris and R Kazarinov, "POSSIBILITY OF THE AMPLIFICATION OF ELECTROMAGNETIC WAVES IN A SEMICONDUCTOR WITH A SUPERLATTICE," *Sov. Phys. Semicond.*, vol. 5, no. 4, pp. 707-709, 1971.
- [74] J Faist et al., "Quantum Cascade Laser," *Science*, vol. 264, pp. 553-556, 1994.
- [75] M Hubner et al., "TRIPLE Q: A three channel quantum cascade laser absorption spectrometer for fast multiple species concentration measurements," *REVIEW OF SCIENTIFIC INSTRUMENTS*, vol. 82, p. 093102, 2011.
- [76] G Duxbury, N Langford, and K Hay, "Delayed rapid passage and transient gain signals generated using a chirped 8 km quantum cascade laser," *Journal of Modern Optics*, vol. 55, no. 19-20, pp. 3293–3303, 2008.
- [77] J H van Helden, S Horrocks, and G Ritchie, "Application of quantum cascade lasers in studies of low-pressure plasmas: Characterization of rapid passage effects on density and temperature measurements," *Appl. Phys. Lett.*, vol. 92, p. 081506, 2008.
- [78] S Welzel, L Gatilova, J Ropcke, and A Rousseau, "Time-resolved study of a pulsed dc discharge using quantum cascade laser absorption spectroscopy: NO and gas temperature kinetics," *Plasma Sources Sci. Technol.*, vol. 16, pp. 822-831, 2007.
- [79] D Mavor, O Guaitella, A Rousseau, and Y Ionikh, "Production of molecules on a surface under plasma exposure: example of NO on pyrex," *J. Phys. D: Appl. Phys.*, vol.

- 43, 2010.
- [80] V Ochkin, *Spectroscopy of Low Temperature Plasma*.: WILEY, 2009.
- [81] B Lavrov, "Determination of the gas temperature of a low-pressure plasma from the intensities of the H₂ and D₂ molecular bands. Relationship between the intensity distribution in a band and the gas temperature," *Optics and Spectroscopy*, vol. 48, no. 4, pp. 375-380, 1980.
- [82] S Zyryanov and D Lopaev, "Measurements of the Gas Temperature in an Oxygen Plasma by Spectroscopy of the O₂(b) → O₂(X) transition," *Plasma Physics Reports*, vol. 33, no. 6, pp. 563 - 574, 2007.
- [83] V Ochkin and S Savinnov, "Measurements of Gas Temperature in Glow Discharge from Electronic- Vibrational - Rotational Spectra of Molecules," *Zhurnal Prikladnoi Spektroskopii*, vol. 28, no. 3, pp. 408 - 412, 1978.
- [84] A Goyette, J Peck, Y Matsuda, L Anderson, and J Lawler, "Experimental comparison of rotational and gas kinetic temperatures in N₂ and He–N₂ discharges," *J. Phys. D: Appl. Phys.*, vol. 31, pp. 1556–1564, 1998.
- [85] P Bruggeman et al., "Optical emission spectroscopy as a diagnostic for plasmas in liquids: opportunities and pitfalls," *J. Phys. D: Appl. Phys.*, vol. 43, 2010.
- [86] C Laux, T Spence, C Kruger, and R Zare, "Optical diagnostics of atmospheric pressure air plasma," *Plasma Sources Sci. Technol.*, vol. 12, pp. 125 - 138, 2003.
- [87] B Gordiets, A Osipov, and L Shelepin, *Kinetic Processes in Gases and Molecular Lasers*.: Gordon and Breach Science Publishers, 1988.
- [88] P Bruggeman et al., "Electronic quenching of OH(A) by water in atmospheric pressure plasmas and its influence on the gas temperature determination by OH(A–X) emission," *Plasma Sources Sci. Technol.*, vol. 19, p. 015016, 2010.
- [89] Yu Golubovskii et al., "Dynamics of gas heating in a pulsed microwave nitrogen discharge at intermediate pressures," *J. Phys. D: Appl. Phys.*, vol. 37, pp. 868–874, 2004.
- [90] Laux C, "Radiation and nonequilibrium collisional-radiative models," Rhode-Saint-Genese: Von Karman Institute Publishing, 2002.
- [91] J Malicet, D Daumont, J Charbonnier, and C Parisse, "Ozone UV spectroscopy. II. Absorption cross-sections and temperature dependence," *J. Atmos. Chem.*, vol. 21, pp. 263 - 273, 1995.

References

- [92] K Niemi, V Schulz-von der Gathen, and H F Dobeles, "Absolute atomic oxygen density measurements by two-photon absorption laser-induced fluorescence spectroscopy in an RF-excited atmospheric pressure plasma jet," *Plasma Sources Sci. Technol.*, vol. 14, pp. 375–386, 2005.
- [93] K Niemi, V Schulz-von der Gathen, and H F Dobeles, "Absolute calibration of atomic density measurements by laser-induced fluorescence spectroscopy with two-photon excitation," *J. Phys. D: Appl. Phys.*, vol. 34, 2001.
- [94] J Amorim, G Baravian, M Touzeau, and J Jolly, "Twophoton laser induced fluorescence and amplified spontaneous emission atom concentration measurements in O₂ and H₂ discharges," *J. Appl. Phys.*, vol. 76, p. 1487, 1994.
- [95] R Gottscho and T Miller, "Optical Techniques in Plasma Diagnostics," *Pure and Appl. Chem.*, vol. 56, no. 2, pp. 189 - 208, 1984.
- [96] A Tserepi, E Wurzburg, and T Miller, "Two-photon-excited stimulated emission from atomic oxygen in rf plasmas: detection and estimation of its threshold," *Chem. Phys. Lett.*, vol. 265, pp. 297 - 302, 1997.
- [97] V Guerra, E Galiaskarov, and J Loureiro, "Dissociation mechanisms in nitrogen discharges," *Chem Phys Lett*, no. 371, pp. 576-581, 2003.
- [98] T Yamashita, "Rate of recombination of nitrogen atoms," *J. Chem. Phys.*, vol. 70, p. 4248, 1979.
- [99] D I Slovetskii, *Mechanisms of Chemical Reactions in Nonequilibrium Plasmas*. Moscow: Nauka, 1980.
- [100] V Markovic, Z Petrovic, and M Pejovic, "Surface recombination of atoms in a nitrogen afterglow," *J. Chem. Phys.*, vol. 100, no. 11, 1994.
- [101] I Borovikova and E Galiaskarov, "Kinetic Characteristics of Production and Loss of Nitrogen Atoms in N₂ Plasma," *High Temperature*, vol. 39, no. 6, 2001.
- [102] Y Kim et al., "Nitrogen bonding structure in ultrathin silicon oxynitride films on Si(100) prepared by plasma nitridation," *Phys. Rev B*, vol. 70, 2004.
- [103] Y Chung, J C Lee, and H Shin, "Direct observation of interstitial molecular N₂ in Si oxynitrides," *Appl. Phys. Lett.*, vol. 86, 2005.
- [104] C Powell, "Elemental binding energies for X-ray photoelectron spectroscopy," vol. 89, pp. 141-149, 1995.
- [105] P Citrin and D Hamann, "Measurement and calculation of polarization and potential-energy effects on core-electron binding energies in solids: X-ray photoemission of rare

- gases implanted in noble metals," *Phys. Rev. B*, vol. 10, no. 12, 1974.
- [106] R Back and J Mui, "The reactions of active nitrogen with N¹⁵O and 30N₂," *J. Phys. Chem.*, vol. 66, no. 7, pp. 1362-1364, 1962.
- [107] C Janssen and B Tuzson, "Isotope Evidence for Ozone Formation on Surfaces," *J. Phys. Chem. A*, vol. 114, pp. 9709–9719, 2010.
- [108] G Cernogora, L Hochard, M Touzeau, and C Ferreira, "Population of N₂(A metastable states in a pure nitrogen glow discharge," *J. Phys. B At. Mol. Phys.*, vol. 14, pp. 2977-2987, 1981.
- [109] O Braginskiy et al., "Singlet oxygen generation in O₂ flow excited by RF discharge: I. Homogeneous discharge mode: α -mode," *J. Phys. D: Appl. Phys.*, vol. 38, pp. 3609–3625, 2005.
- [110] G Cartry, L Magne, and G Cernogora, "Atomic oxygen recombination on fused silica: experimental evidence of the surface state influence.," *J. Phys. D: Appl. Phys.*, no. 32, 1999.
- [111] D Lopayev, E Malykhin, and S Zyryanov, "Surface recombination of oxygen atoms in O₂ plasma at increased pressure: II. Vibrational temperature and surface production of ozone," *J. Phys. D: Appl. Phys.*, vol. 44, 2011.
- [112] K Tatsumura et al., "Reactions and diffusion of atomic and molecular oxygen in the SiO₂ network," *Phys. Rev. B*, vol. 72, p. 045205, 2005.
- [113] A Eletskii and B Smirnov, "Dissociation of molecules in plasma and gas: the energy," *Pure and Appl. Chem.*, vol. 57, no. 9, pp. 1235-1244, 1985.
- [114] J-J Kim, H-H Park, and S-H Hyun, "The effects of plasma treatment on SiO₂ aerogel film using various reactive (O₂, H₂, N₂) and non-reactive (He, Ar) gases," *Thin Solid Films*, vol. 377-378, pp. 525-529, 2000.
- [115] H-H Kim, A Ogata, M Schiorlin, E Marotta, and C Paradisi, "Oxygen Isotope (¹⁸O₂) Evidence on the Role of Oxygen in the Plasma-Driven Catalysis of VOC Oxidation," *Catal. Lett.*, vol. 141, pp. 277-282, 2011.
- [116] O Guaitella, C Lazzaroni, D Marinov, and A Rousseau, "Evidence of atomic adsorption on TiO₂ under plasma exposure and related C₂H₂ surface reactivity," *Appl. Phys. Lett.*, vol. 97, 2010.
- [117] Z Qu and G Kroes, "Theoretical Study of Adsorption of O(³P) and H₂O on the Rutile TiO₂(110) Surface," *J. Phys. Chem. B*, vol. 110, pp. 23306 - 23314, 2006.

References

- [118] S Loganathan, F Thevenet, P Gravejat, and A Rousseau, "Plasma regeneration of TiO₂ surface saturated with IPA: influence of air relative humidity," in *International Workshop on Plasma Spectroscopy*, Giens, 2012.
- [119] T Ohno, K Sarukawa, K Tokieda, and M Matsumura, "Morphology of a TiO₂ Photocatalyst (Degussa, P-25) Consisting of Anatase and Rutile Crystalline Phases," *Journal of Catalysis*, vol. 203, pp. 82 - 86, 2001.
- [120] J Peeters, W Boullart, and I Langhans, "Branching Ratio of the C₂H₂+O Reaction at 290 K from Kinetic Modelling of Relative Methylene Concentration versus Time Profiles in C₂H₂/O/H Systems," *Int. J. Che. Kin.*, vol. 26, pp. 869-886, 1994.
- [121] U Diebold, "The surface science of titanium dioxide," *Surf. Sci. Reports*, vol. 48, pp. 53-229, 2003.
- [122] H Sabadil and S Pfau, "Measurements of the Degree of Dissociation in Oxygen DC Discharges: Comparison of the Ozone Method with the Wrede-Harteck Method ," *Plasma Chemistry and Plasma Processing*, vol. 5, no. 1, 1985.
- [123] O Sneh and S George, "Thermal Stability of Hydroxyl Groups on a Well-Defined Silica Surface ," *J. Phys. Chem.*, vol. 99, pp. 4639 - 4647, 1995.
- [124] L Zhuravlev, "The surface chemistry of amorphous silica," *Colloids and Surfaces A*, vol. 173, pp. 1 - 38, 2000.
- [125] B Eliasson, M Hirth, and U Kogelschatz, "Ozone synthesis from oxygen in dielectric barrier discharges," *J. Phys.D: Appl. Phys.*, vol. 20, pp. 1421-1437, 1987.
- [126] B F Gordiets, A I Osipov, and L A Shelepin, *Kinetic Processes in Gasas and Molecular Lasers*. New York: Gordon and Breach, 1986.
- [127] G Black, H Wise, and S Schechter, "Measurements of vibrationally excited molecules by Raman scattering. II. Surface deactivation of vibrationally excited N₂," *J. CHem. Phys.*, vol. 60, no. 9, pp. 3526-3536, 1974.
- [128] V I Egorov, Y M Gershenzon, V B Rozenshtein, and S Ya Umanskii, "On The Mechanism of Heterogeneous Relaxation of Vibrationally Excited Nitrogen Molecules," *Chem. Phys. Lett.*, vol. 20, no. 1, pp. 0-3, 1973.
- [129] P Yanney and J Parish, "Studies of Surface Deactivation of Vibrationall-Excited Homonuclear Molecules in Gaseous Discharge Media Using Coherent Anti-Stokes Raman Spectroscopy (CARS)," 1999.
- [130] H Evans and C Winkler, "THE REACTIVE COMPONENTS IN ACTIVE NITROGEN AND THE ROLE OF SPIN CONSERVATION IN ACTIVE NITROGEN

- REACTIONS," *Can. J. Chem.*, vol. 34, pp. 1217-1231, 1956.
- [131] F Kaufman and J Kelso, "Vibrationally Excited Ground State Nitrogen in Active Nitrogen," *J. Chem. Phys.*, vol. 28, p. 510, 1958.
- [132] J Morgan and H Schiff, "The Study of Vibrationally Excited N₂ Molecules With the Aid of an Isothermal Calorimeter," *Can. J. Chem.*, vol. 41, pp. 903-912, 1963.
- [133] P A Sa, V Guerra, J Loureiro, and N Sadeghi, "Self-consistent kinetic model of the short-lived afterglow in flowing nitrogen," *J. Phys. D: Appl. Phys.*, vol. 37, pp. 221-231, 2004.
- [134] M Allan, "Excitation of vibrational levels up to $v=17$ in N₂ by electron impact in the 0-5 eV region," *J. Phys. B: At. Mol. Phys.*, no. 18, pp. 4511-4517, 1985.
- [135] Chen J, "Theory of Subexcitation Electron Scattering by Molecules. I. Formalism and the Compound Negative-Ion States," *The Journal of Chemical Physics*, vol. 40, no. 12, p. 3507, 1964.
- [136] D Birtwistle and A Herzenberg, "Vibrational excitation of N₂ by resonance scattering of electrons," *J Phys. B: At. and Mol. Phys.*, vol. 4, pp. 53-70, 1971.
- [137] V Guerra, P Sa, and J Loureiro, "Relaxation of the electron energy distribution function in the afterglow of a N₂ microwave discharge including space-charge field effects," *Phys. Rev. E*, vol. 63, no. 4, pp. 1-13, 2001.
- [138] R Le Roy, Y Huang, and J Calvin, "An accurate analytic potential function for ground-state N₂ from a direct-potential-fit analysis of spectroscopic data," *J. Chem. Phys.*, vol. 125, p. 164310, 2006.
- [139] R N Schwartz, Z I Slawsky, and K F Herzfeld, "Calculation of Vibrational Relaxation Times in Gases," *J. Chem. Phys.*, vol. 20, no. 10, pp. 1591-1599, 1952.
- [140] M Cacciatore, A Kurnosov, and A Napartovich, "Vibrational energy transfer in N₂-N₂ collisions: a new semiclassical study," *J. Chem. Phys.*, vol. 123, p. 173315, 2005.
- [141] J Misewich and M. M. T. Loy, "Single quantum state molecular beam scattering of vibrationally excited NO from Ag(111) and Ag(110)," *J. Chem. Phys.*, vol. 84, no. 3, p. 1939, 1986.
- [142] J Misewich, H Zacharias, and M Loy, "State-to-state molecular-beam scattering of vibrationally excited NO from cleaved LiF (100) surfaces," *Phys.Rev.Lett.*, vol. 55, no. 18, pp. 1919-1922, 1985.
- [143] H Vach, J Hager, and H Walther, "Energy transfer processes during the scattering of vibrationally excited no molecules from a graphite surface," *Chem. Phys. Lett*, vol. 133,

References

- no. 4, pp. 279-282, 1987.
- [144] M Kovacs, D Ramachandra Rao, and A Javan, "Study of Diffusion and Wall Deexcitation Probability of $00^{\circ}1$ State in CO_2 ," *J. Chem. Phys.*, vol. 48, p. 3339, 1968.
- [145] A Khandelwal, H Niimi, G Lucovsky, and H Lamb, "Low temperature Ar- N_2 remote plasma nitridation of SiO_2 thin film," *J. Vac. Sci. Technol. A*, vol. 20, no. 6, pp. 1989-1996, 2002.
- [146] L Polak and D Slovetsky, "Electron Impact Induced Electronic Excitation and Molecular Dissociation," *Int. J. Radiat. Phys. Chem.*, vol. 8, pp. 257-282, 1976.
- [147] W Choi and M Leu, "Kinetics of the heterogeneous reaction $\text{CO} + \text{O} = \text{CO}_2$ on inorganic oxide and water ice surfaces: Implications for the Martian atmosphere," *Geophys. Research Lett.*, vol. 24, no. 23, pp. 2957-2960, 1997.
- [148] T de los Arcos, C Domingo, V Herrero, M Sanz, and I Tanarro, "Diagnostics and Kinetic Modeling of the Ignition and the Extinction Transients of a Hollow Cathode N_2O Discharge," *J. Phys. Chem. A*, vol. 104, pp. 3974-3983, 2000.
- [149] C Pintassilgo, O Guaitella, and A Rousseau, "Heavy species kinetics in low-pressure dc pulsed discharge in air," *Plasma Sources Sci. Technol.*, vol. 18, p. 025005, 2009.
- [150] J Blauer and G Nickerson, "A survey of vibrational relaxation rate data for processes important to CO_2 - N_2 - H_2O infrared plume radiation," 1973.
- [151] R Taylor and S Bitterman, "Survey of vibrational relaxation data for processes important in the CO_2 - N_2 laser system," *Reviews of Modern Physics*, vol. 41, no. 1, pp. 26-47, 1969.
- [152] V Nevdakh, L Orlov, and N Leshenyuk, "Temperature dependence of the vibrational relaxation rate constants of CO_2 (001) in binary mixtures," *J. Appl. Spectr.*, vol. 70, no. 2, pp. 276-284, 2003.
- [153] C K Patel, *Phys. Rev.*, vol. 136, pp. 1187-1193, 1964.
- [154] V Joly and A Roblin, "Vibrational relaxation of $\text{CO}_2(m,n,l,p)$ in a CO_2 - N_2 mixture. Part1: survey of available data.," *Aerospace Sci. Technol.*, no. 4, pp. 229-238, 1999.
- [155] V Joly, C Marmignon, and P Jacquet, "Vibrational relaxation of $\text{CO}_2(m,n,l,p)$ in a CO_2 - N_2 mixture. Part2: application to one dimensional problem.," *Aerospace Sci. Technol.*, no. 5, pp. 313-322, 1999.
- [156] F Esposito, I Armenise, and M Capitelli, " $\text{N}-\text{N}_2$ state-to-state vibrational relaxation and dissociation rates based on quasiclassical calculations," *Chem. Phys.*, vol. 331, pp. 1-8,

- 2006.
- [157] K Herzfeld, "Deactivation of vibrations in collisions in the presence of Fermi resonance," *J. Chem. Phys.*, vol. 47, no. 2, 1967.
 - [158] M Margottin-Maclou, L Doyennette, and L Henry, "Relaxation of vibrational energy in CO, HCl, CO₂ and N₂O," *Appl. Optics*, vol. 10, no. 8, 1971.
 - [159] V Guerra and J Loureiro, "Electron and heavy particle kinetics in a low-pressure nitrogen glow discharge," *Plasma Sources Sci. Technol.*, vol. 6, pp. 361-372, 1997.
 - [160] N Dyatko, I Kochetov, A Napartovich, and A Sukharev, "EEDF: the software package for calculations of the electron energy distribution function in gas mixtures, <http://www.lxcat.laplace.univ-tlse.fr/software/EEDF>".
 - [161] A Kurnosov, A Napartovich, S Shnyrev, and M Cacciatore, "A database for V-V state-to-state rate constants in N₂-N₂ and N₂-CO collisions in a wide temperature range: dynamical calculations and analytical approximations," *Plasma Sources Sci. Technol.*, vol. 19, p. 045015, 2010.
 - [162] P Macko, G Cunge, and N Sadeghi, "Density of N₂(v=18) molecules in a dc glow discharge measured by cavity ringdown spectroscopy at 227 nm; validity domain of the technique," *J. Phys. D: Appl. Phys.*, vol. 34, pp. 1807-1811, 2001.
 - [163] M Kovacs, D Ramachandra Rao, and A Javan, "Study of Diffusion and Wall Deexcitation Probability of 00°1 State in CO₂," *J. Chem. Phys.*, vol. 48, p. 3339, 1968.
 - [164] K Hadjiivanov, "Identification of neutral and charged N_xO_y surface species by IR spectroscopy," *Catal. Rev. - Sci. Eng.*, vol. 42, no. 1&2, pp. 71-144, 2000.
 - [165] Z Yong, V Mata, and A Rodrigues, "Adsorption of carbon dioxide on basic alumina at high temperatures," *J. Chem. Eng. Data.*, vol. 45, pp. 1093 - 1095, 2000.
 - [166] N Popov, "Fast gas heating in a nitrogen-oxygen discharge plasma: I. Kinetic mechanism," *J. Phys. D: Appl. Phys.*, no. 44, 2011.

Related publications

Chapter II

«TRIPLE Q: A three channel quantum cascade laser absorption spectrometer for fast multiple species concentration measurements»

Hübner M, Welzel S, Marinov D, Guaitella O, Glitsch S, Rousseau A and Röpcke J 2011 *Rev. Sci. Instr.* **82** 093102

Chapter III

«Production of molecules on surface under plasma exposure: Example of NO on pyrex»
D. Marinov, O. Guaitella, A. Rousseau, Y. Ionikh *J. Phys. D : Appl. Phys.*, Vol 43 (2010) 115203

Chapter IV

«Evidence for surface oxidation on Pyrex of NO into NO₂ by adsorbed O atoms»
O Guaitella, M Hübner, S Welzel, D Marinov, J Röpcke and A Rousseau *Plasma Sources Sci. Technol.*, 19 (2010) 045026

«Evidence of atomic adsorption on TiO₂ under plasma exposure and related C₂H₂ surface reactivity»
O. Guaitella, C. Lazzaroni, D. Marinov, and A. Rousseau *Appl. Phys. Lett.*, 97, (2010) 011502

Chapter V

«Surface vibrational relaxation of N₂ studied by CO₂ titration with time resolved quantum cascade laser absorption spectroscopy»

D. Marinov, D. Lopatik, O. Guaitella, M. Hübner, Y. Ionikh, J. Röpcke and A. Rousseau 2012 *J. Phys. D: Appl. Phys.* **45** 175201